Differential scanning fluorometry analysis of antibodies, *P. falciparum* proteins and assessing two copper-based assays to detect *P. falciparum* Histidine Rich Protein-2

by

Sheldon Sookai
BSc. *(Hons)* Biochemistry

Pietermaritzburg

Submitted in fulfilment of the academic requirements for the degree of Master of Science in Biochemistry

School of Biochemistry, Microbiology and Genetics

College of Agriculture, Engineering and Science

University of KwaZulu-Natal

Pietermaritzburg

South Africa

January 2019

1 ABSTRACT

Malaria is an endemic disease across sub-Saharan Africa. *P. falciparum* is the most lethal species of the parasite and is responsible for over 400 000 deaths in the region. There is no effective vaccine for malaria. Early diagnosis remains key to ensure that the correct treatment for the disease can be administrated. Rapid diagnostic tests (RDT's) are an attractive alternative to light microscopy for the diagnosis of a malaria infection. RDT's have weaknesses such as the reagents are not stable. Therefore, this study looked at ways to improve RDT's.

Differential scanning fluorimetry (DSF) was used to study the thermal stability of recombinant *Plasmodium falciparum* glyceraldehyde-3-phosphate dehydrogenase (r*Pf*GAPDH), lactate dehydrogenase (r*Pf*LDH) and Histidine Rich Protein-2 (r*Pf*HRP-2) and found that r*Pf*GAPDH had the highest melting temperature (T_m; 55°C), while a T_m could not be obtained for r*Pf*HRP-2. Chloroquine and quinine were shown to interact with r*Pf*LDH and r*Pf*GAPDH using DSF. The drug-protein interactions were also shown *in silico* with docking studies. Anti-r*Pf*LDH IgY and anti-r*Pf*HRP-2 IgY antibodies were evaluated using DSF in the presence of the respective antigens. A higher T_m was obtained in the presence of the antigen, indicating binding of antigen to the antibody at pH 4.

RDT's are often exposed to high ambient temperatures which can cause the antibodies to degrade. Cold chain storage facilities are not always available to store RDT's. Heat stable antibodies may aid in improving the stability of RDT's. The thermodynamic parameters of antibodies from chickens, mice, rabbits and crocodiles were compared . Chicken IgY was found to be the most stable having a ΔμG of 71.48 $Kjmol^{-1}$ (±0.32); ΔμS = 1.47 (± 0.01) $Kj.mol^{-1}.K^{-1}$; ΔμH = 508 $Kj.mol^{-1}$ (2.08) and T_m 73.75°C (±0.2). The T_m of freshly isolated chicken IgY and IgY stored from 1990 were compared and found to have similar a T_m confirming the IgY molecule is a stable molecule.

Different conjugating methods were compared for the conjugation of HRPC to chicken anti-rabbit serum albumin IgY and the glutaraldehyde method was found to be the most efficient conjugating method. The conjugate detected 20 ng of rabbit serum albumin.

Storage of low concentrations of HRPC was found to lose activity in a short period of time. Therefore, an aqueous-organic solvent buffer with methanol and Ca^{2+} was developed and was able to store HRPC for three months with 70% activity.

The second part of the study was to develop a diagnostic test for a *P. falciparum* infection by detecting r*Pf*HRP-2. Two Copper-based assays were developed based on the high affinity histidine residues in *Pf*HRP-2 have for copper (Cu). The first assay depends on reducing Cu^{2+} to Cu^{+} which inhibits horseradish peroxidase activity. The presence of r*Pf*HRP-2 binds to and removes Cu^{+} allowing HRPC to maintain high activity. This assay detected 100 ng of r*Pf*HRP-2 in solution. The second assay involves Cu^{2+} catalysing the oxidation of tetramethylbenzidine (TMB). The Presence of r*Pf*HRP-2 prevents TMB oxidation by binding and removing Cu^{2+}, leading to a suppressed oxidised TMB signal. Neither assay worked in an ELISA based format.

Graphical abstract

Part 1

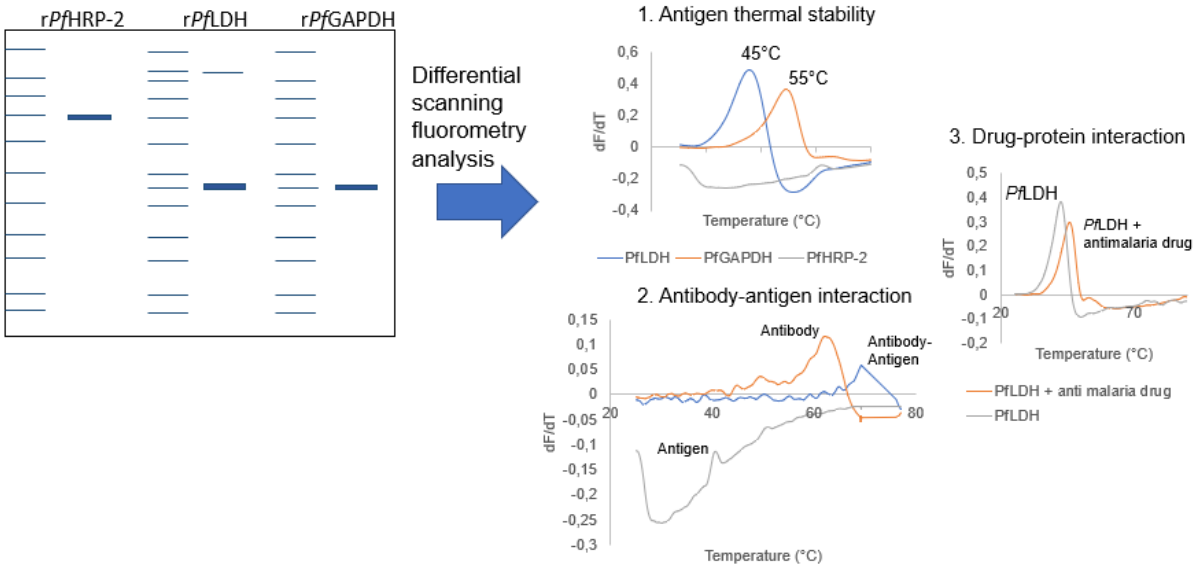

Part 2

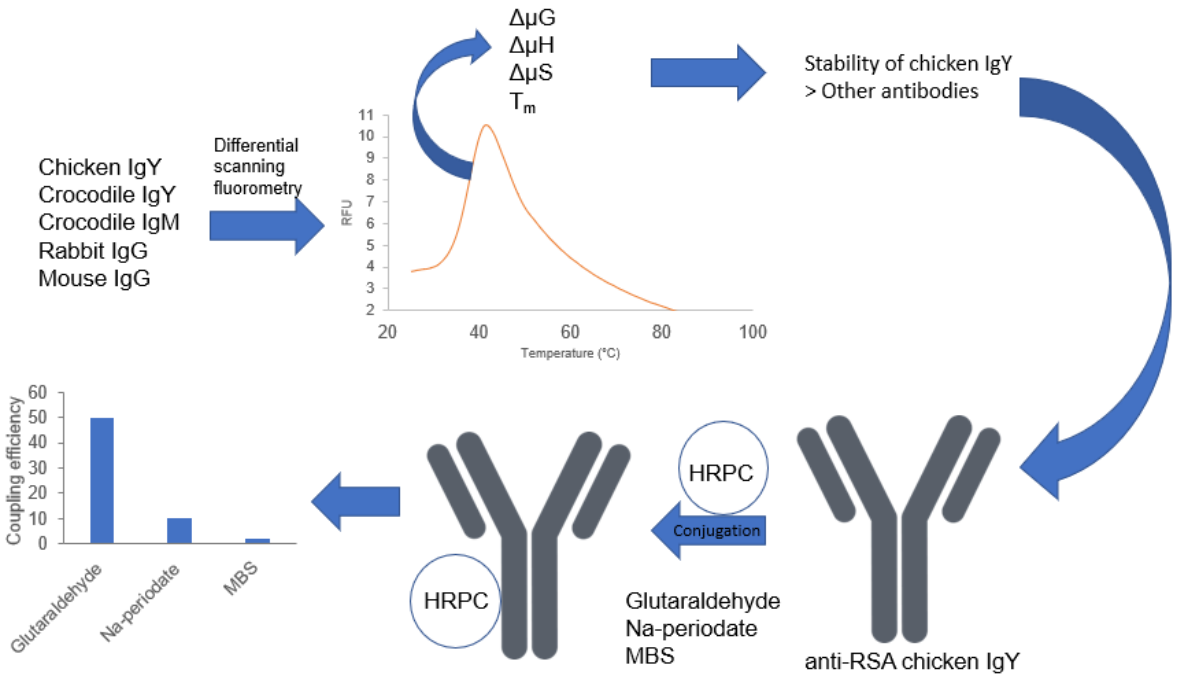

Part 3

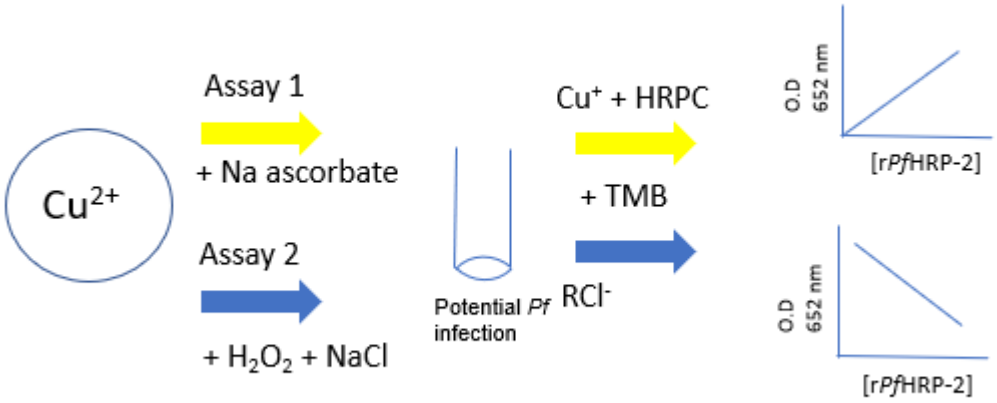
Cu2+
Assay 1
+ Na ascorbate
Assay 2
+ H2O2 + NaCl
Potential Pf infection
Cu+ + HRPC
+ TMB
RCl-
O.D 652 nm
[rPfHRP-2]
O.D 652 nm
[rPfHRP-2]

2 PREFACE

The research contained in this dissertation was completed by the candidate while based in the Discipline of Biochemistry, School of Biochemistry, Microbiology and Genetics of the College of Agriculture, Engineering and Science, University of KwaZulu-Natal, Pietermaritzburg, South Africa. The research was financially supported by the National Research Foundation.

The contents of this work have not been submitted in any form to another university and, except where the work of others is acknowledged in the text, the results reported are due to investigations by the candidate.

_____

Signed: Professor J.P.D Goldring

Date: January 2019

3 DECLARATION 1: PLAGIARISM

Note that two declaration sections are required if there are papers emanating from the dissertation. The first (obligatory) declaration concerns plagiarism and the second declaration specifies your role in the published papers.

I, Sheldon Sookai, declare that:

(i) the research reported in this dissertation, except where otherwise indicated or acknowledged, is my original work;

(ii) this dissertation has not been submitted in full or in part for any degree or examination to any other university;

(iii) this dissertation does not contain other persons' data, pictures, graphs or other information, unless specifically acknowledged as being sourced from other persons;

(iv) this dissertation does not contain other persons' writing, unless specifically acknowledged as being sourced from other researchers. Where other written sources have been quoted, then:

a) their words have been re-written but the general information attributed to them has been referenced;

b) where their exact words have been used, their writing has been placed inside quotation marks, and referenced;

(v) where I have used material for which publications followed, I have indicated in detail my role in the work;

(vi) this dissertation is primarily a collection of material, prepared by myself, published as journal articles or presented as a poster and oral presentations at conferences. In some cases, additional material has been included;

(vii) this dissertation does not contain text, graphics or tables copied and pasted from the Internet, unless specifically acknowledged, and the source being detailed in the dissertation and in the References sections.

_____

Signed: Sheldon Sookai

Date: January 2019

4 ACKNOWLEDGMENTS

I would like to express many thanks to:

- Professor Goldring my supervisor, for his mentoring, time and patience, reading through my writing which was at times “hieroglyphics” and most of all affording me the opportunity to work in his laboratory.
- Professor THT Coetzer for allowing me to use the ELISA plate reader, Dr Hewer for allowing me to use the Schrodinger (2018-2) software, Dr Krause for his patients and assistance while working in the laboratory, Mark Chambers for assisting me with the Schrodinger (2018-2) software and finally to my laboratory.
- To the biochemistry department, administrative staff and the ‘malaria lab’ for always being ready to assist.
- The National Research Foundation of South Africa (NRF) for a scholarship. The Medical Research Council (MRC), the University of KwaZulu-Natal for their financial assistance and the University of KwaZulu-Natal for allowing my first year of study to be free , without which my postgraduate studies would not have been possible.
- Finally, thank you to all of my friends and family for all their support, but above all I would like to dedicate this dissertation to Yashin and (parents) Herman and Asha.

“Science means constantly walking a tightrope between blind faith and curiosity; between expertise and creativity; between bias and openness; between experience and epiphany; between ambition and passion; and between arrogance and conviction - in short, between an old today and a new tomorrow.” Heinrich Rohrer

5 TABLE OF CONTENTS

Contents

6 LIST OF TABLES

Table **Page**

7 LIST OF FIGURES

Figure Page

8 ABBREVIATIONS

2 x YT	2 x yeast extract, tryptone
2D	Two dimensional
3D	Three dimensional
AMT	Acetic acid, MES, Tris buffer
ALP	Alkaline phosphatase
BBB	Blood brain barrier
BFC	BODIPY FL L-cystine
BSA	Bovine serum albumin
CM	Cerebral malaria
CH/L	Constant heavy/ constant light domain
CPM	N-[4-(7-diethylamino-4-methyl-3-coumarinyl)phenyl] maleimide
dF/dT	First derivative (Change in fluorescence/ change in time)
dH_2O	Distilled H_2O
DMSO	Dimethyl sulfoxide
DNA	Deoxyribonucleic acid
DSC	Differential scanning calorimetry
DSF	Differential scanning fluorometry
DTT	Dithiothreitol
ECL	Enhanced chemiluminescence
ECVAM	European centre for the validation of alternate methods
EDTA	Ethylenediaminetetra-acetic acid
ELISA	Enzyme-linked immunosorbent assay
EMP-1	Erythrocyte membrane protei-1
EtOH	Ethanol
F	Fluorescence
Fab	Fragment antigen binding domain
Fc	Fragment crystallizable group
g	Centrifugal force
GAPDH	Glyceraldehyde-3-phosphate dehydrogenase
h	Hour
HEPES	4-(2-hydroxyethyl)-1-piperazineethanesulfonic acid)
HMP	Higher melting partner
HRP-2	Histidine rich protein-2
HRPC	Horseradish peroxidase isozyme C
Ig	Immunoglobulin
IMAC	Immobilised metal affinity chromatography
IPTG	Isopropyl-β -D-thiogalactopyranoside
kDa	kilodalton
Kμ	Protein unfolding constant
LB	Lysogeny Broth
LDH	Lactate dehydrogenase
LMP	Lower melting partner

LOD	Limit of detection
MBP	Maltose binding protein
MBS	M-maleimidobenzoyl acid N-hydroxy succinimide ester
MeOH	Methanol
MES	2-(N-Morpholino)ethanesulfonic acid
MWCO	Molecular weight cut off
min	Minute
Mr	Molecular mass
N.D	Not determined
NADPH	Nicotinamide adenine dinucleotide phosphate
NTA	Nitrotriacetic acid
O_2^-	Super oxide anion
O.D	Optical density
OH•	Hydroxy radical
PBS	phosphate buffered saline
PCR	Polymerase chain reaction
PEG	polyethylene glycol
Pf	Portion of folded protein
Pμ	Portion unfolded protein
RBC	Red blood cell
RCl^-	Reactive chloride species
RDT	Rapid diagnostic test
RFU	Relative fluorescence units
ROS	Reactive oxide species
RSA	Rabbit serum albumin
RT	Room temperature
S.D	Standard deviation
SDS-PAGE	Sodium dodecyl sulphate polyacrylamide gel electrophoresis
TB	Terrific Broth
TBS	Tris buffer saline
T_m	melting temperature
TMB	Tetramethyl benzidine
Tris	2-amino-2-(hydroxymethyl)-1,3-propandiol
μG	unfolding Gibbs energy
μH	Unfolding enthalpy
μS	Unfolding entropy
UV	Ultra violet
VH/L	Variable heavy/ variable light domain
WBC	White blood cell
WHO	World health organisation

CHAPTER 1: Literature review

1.1. Introduction of malaria related to humans

There are five species of malaria parasite that infect humans they are*; Plasmodium falciparum, vivax, ovale, malariae* and *knowlsei* (Snow *et al*., 2005). The infection from *Plasmodium falciparum* is the most lethal and is responsible for the largest number of deaths (Geleta and ketema, (2016). Malaria parasites are transmitted by the female Anopheles mosquito to a human with a single bite. The World Health Organisation (WHO) predicts that 3.3 billion people are at risk of contracting the disease across the globe. Areas with the highest malaria burden are Southeast Asia, South America and Africa. In 2015 there were 214 million malaria cases of which over 80% (171.2 million) were from Africa and 438 000 deaths of which, over 90% (394 200) were from Africa (WHO, 2015b).

1.2. The life cycle of the malaria parasite

The malaria life cycle occurs in two hosts, the female Anopheles mosquitos and humans (Figure 1.1). A human host is infected when a female Anopheles mosquito carrying a *Plasmodium* malaria infection bites a human for a blood meal, the sporozoites are injected into the human (Kebaier *et al*., 2009). The sporozoites migrate through the lymphatic system or by the blood system usually via active gliding motility whereby the sporozoites move towards the liver, pass through the Kuppfer cells and enter hepatocytes. This marks the beginning of the liver stage of the malaria infection (Kebaier *et al.,* 2009; Cowman and Crabb, 2006).

Within hepatocytes, sporozoites differentiate and divide into mature hepatic schizonts which burst open and release thousands of merozoites. Merozoites invade red blood cells (RBC) via protein-protein interaction called the actin-myosin motor (Keeley and Soldati, 2004), to start the blood stage of the malaria life cycle. Within RBC asexual reproduction occurs whereby the merozoites go through a 48-hour replication cycle, going through ring, trophozoite, and schizont stages that finally lead to the formation of 16-32 daughter merozoites that are released when the RBC ruptures. Uninfected RBC can be infected by the daughter merozoites (Cowman and Crabb, 2006). During RBC rupture, a malaria patient's symptoms are headaches, sore muscle and joints and fatigue, which develops into fever and vomiting. A *P. falciparum* infection may worsen to severe and cerebral malaria (Reyburn, 2010).

The sexual stage of *P. falciparum* occurs in the blood of the human host, where male and female gametocytes are formed. The gametocytes are ingested by a female Anopheles mosquito when it feeds for a blood meal (Cowman and Crabb, 2006). Gametocytes develop into gametes in the mosquito's gut, then into a zygote which moves into the mosquito's midgut and develops into an ookinete and finally into an oocyst which releases sporozoites that can enter into the salivary gland of the mosquito.

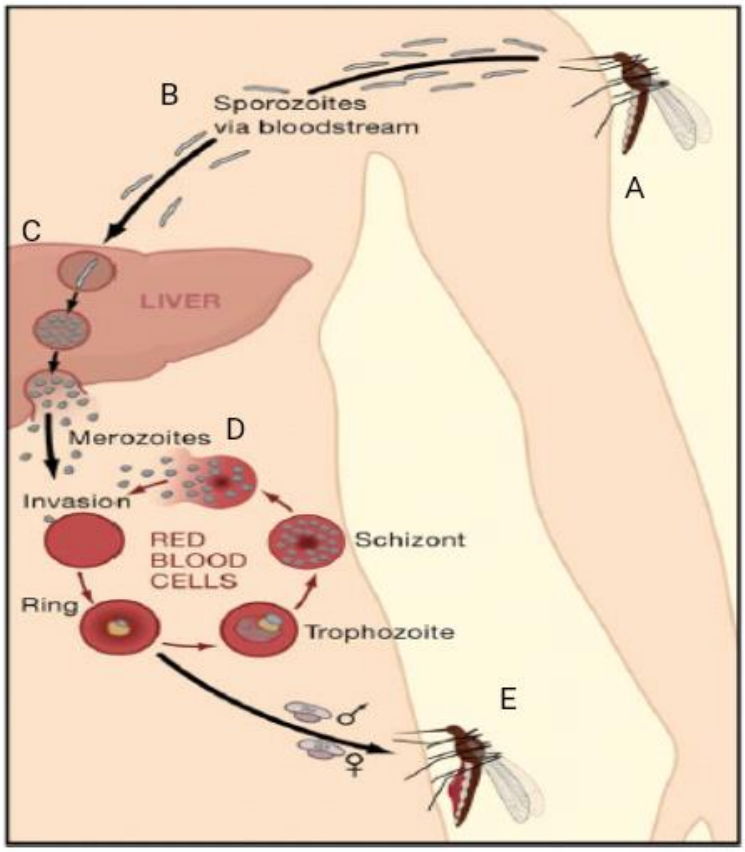

Figure 1.1: A cartoon representation of a *P. falciparum* malaria infection in a human host. The human host is infected with sporozoites from a female Anopheles mosquito **(A)**. Sporozoites migrate to the liver via the blood or lymphatic system **(B)**. Sporozoites invading the hepatocytes (beginning of the liver stage) differentiation into merozoites **(C)**. Merozoites infecting RBC mark the beginning of the parasites asexual life cycle **(D)**. Following sexual stage of the life cycle in the blood a female anopheles mosquito feeds on a blood meal containing male and female gametes **(E)**. (Figure adapted from Cowman and Crabb, 2006).

1.3. Malaria in South Africa

In South Africa the number of malaria cases are much lower than neighbouring countries, with 20 malaria infections per 100 000 individuals. Most of the infections are from *P. falciparum* malaria (Manana *et al*., 2018). The disease is an endemic in three of South Africa's nine provinces (Limpopo, Mpumalanga, and KwaZulu-Natal) and higher transmission is associated with rainy weather. In the 2015/2016 season, there were 6 385 reported cases of malaria with 58 deaths, which increased in the 2016/2017 season to 9 478 infections and 76 deaths (Malaria in South Africa, http://www.nicd.ac.za/wp-content/uploads/2017/05/Malaria-update.pdf). The primary defence in households in malaria-endemic areas is the use of long-lasting residual insecticides.

However, there has been insecticide resistance to deltamethrin (pyrethroid), DDT (organochlorine) and bendiocarb (carbamate) (Brooke *et al*., 2015).

An alternative approach to aid in eradicating malaria from South Africa that is currently being considered is the use of the sterile insect technique (Manana *et al*., 2018; Munhenga *et al*., 2011). Until there is a vaccine developed against malaria infections, RDT's and correct anti-malaria drugs remain critical to saving lives.

1.4. Cerebral malaria

Cerebral malaria is the most lethal form of malaria and caused by a *P. falciparum* infection which is responsible for the most malaria deaths globally. Around 20% of CM infected patients do not survive and children under the age of five, living in sub-Saharan Africa are at highest risk (Ghazanfari *et al.,* 2018; Christensen and Eslick, 2015). About 25% of patients who survive a CM infection often have neurological disorders such as epilepsy, attention deficit hyperactivity disorder (ADHD), lower intelligence quotient (IQ) and other neurodisabilities (Christensen and Eslick, 2015).

The exact mechanism for CM is not entirely understood and ideas of the CM mechanism are based on post-mortem studies on the brains of CM victims. One of the ideas was that the sequestration of the parasites were due to parasitized red blood cells (pRBC) adhering to the erythrocyte cell surface by *P. falciparum* erythrocytes membrane protein-1 (*Pf*EMP-1) binding to ligands on CD36 cells (Craig and Scherf, 2001; Kraemer and Smith, 2006), endothelial protein C receptor (EPCR; Newbold *et al.,* 1997), or intercellular adhesion molecule 1 (ICAM-1; Chakravorty and Craig, 2005). The adherence of pRBC leads to the infected RBC's blocking blood vessels which results in reduced blood flow, which may result in the patient going into a coma or death. Some studies have reported a positive correlation between the number of pRBC and patients going into a coma (Silamut *et al*., 1999; Ponsford *et al*., 2011). However, in a review by Ghazanfari *et al.,* (2018) it was argued that several factors must be involved for developing CM.

P. falciparum is the only species of malaria that produces histidine rich protein-2 (*Pf*HRP-2) and this has led to speculation that *Pf*HRP-2 may be involved in the progression of *P. falciparum* malaria to CM. Various studies have reported that higher concentrations of *Pf*HRP-2 is associated with a malaria progression to CM (Park *et al.,* 2017; Fox *et al.,* 2013; Rubach *et al*., 2012; Seydel *et al.,* 2012). The ranges of *Pf*HRP-2 concentrations from patients in the different studies were 2684 ng/ml (1092 – 5537 ng/ml) for CM and 929 ng/ml (379 – 2735 ng/ml) severe malaria anaemia (Park *et al.,* 2017); 7833 ng/ml (± 2.5 ng/ml) for CM and 421 ng/ml (± 9 ng/ml) for an uncomplicated malaria infection (Fox *et al*., 2013); 1008 ng/ml (342 – 2572 ng/ml Interquartile range (IQR)) for CM, 465 ng/ml (36 -1432 ng/ml IQR) for uncomplicated infections and 4000 ng/ml (1194.5 – 5287.3 ng/ml) for victims of CM

(Rubach *et al.,* 2012); 12 800 ng/ml (± 7057 ng/ml) from CM infected patients; 1028 ng/ml (±2970 ng/ml) for malaria infected patients; 6367 ng/ml (± 3862 ng/ml) for retinopathy

CM positive patients and 1539 ng/ml (± 2032 ng/ml) retinopathy CM negative patients (Seydel *et al.,* 2012).

It could be argued that the increased concentrations of *Pf*HRP-2 may be due to a higher parasite biomass, however, Seydel *et al*., (2012) showed that even though a CM patient has a 5-fold higher *Pf*HRP-2 concentration, the parasites had a concentration of 2.03 fg/ml for CM retinopathy negative patients, while parasites for CM retinopathy positive patients were 2.46 fg/ml. This therefore indicated that even though the parasite biomasses were similar, the higher concentration of *Pf*HRP-2 was associated to patients with CM.

All these studies have highlighted the correlation between *Pf*HRP-2 and the development of CM. However, some of the studies had conflicting results. Manning *et al.,* (2011) reported *Pf*HRP-2 concentrations for uncomplicated malaria infections (77 – 1114 ng/ml) were at a similar range to severe malaria (113 – 1113 ng/ml). It is important to note that CM patients were not compared, and the study was conducted in Papa New Guinea (PNG), while studies mentioned prior were all done in sub-Saharan Africa where CM is most prominent.

Further evidence suggesting *Pf*HRP-2 may play a role in the development of CM was provided by Pal *et al., (*2016) in an *in vitro* and in an *in vivo* model (Pal *et al.,* 2017). The *in vitro* model used the human cerebral microvascular endothelial cell line (hCMEC/D3) and measured its transendothelial electric resistance (TEER) in the presence of *P falciparum* 3D7 parasitized RBC (HRP-2 positive); Dd2 parasitized RBC (HRP-2 negative); Dd2 parasitized RBC (supplemented with HRP-2). Results showed 3D7 RBC and Dd2 HRP-2 supplemented RBC caused the TEER resistance to decrease while the Dd2 RBC showed no substantial change in resistance. Poly L-His and the two main *Pf*HRP-2 fragments were supplemented with Dd2 and there was no significant change in the resistance of the TEER. The result was due to the triggering of the endothelial cell inflammasome causing junctional protein rearrangement, which makes the endothelial cell more permeable causing leakage and decrease resistance showed by the TEER. Furthermore, r*Pf*HRP-2 treatment of hCMEC/D3 upregulated ICAM-1 and vascular cell adhesion protein-1 (VCAM-1) which have been shown to bind *Pf*EMP-1. *Pf*EMP-1 is thought to play a role in the development of CM (Craig and Scherf, 2001). Pal *et al.,* (2017) showed when *Pf*HRP-2 was spiked into *P. berghei* infected mice, *Pf*HRP-2 was able to pass the blood brain barrier (BBB) and the mice died six days earlier when *Pf*HRP-2 was present compared to mice infected with *P. berghi* and spiked with BSA.

There is some evidence suggesting *Pf*HRP-2 may play a role in the progression of an uncomplicated malaria infection to a CM infection. To date, there is no reliable diagnosis for a CM infection.

Currently, if a patient is living in a malaria endemic area and goes into a coma, they are diagnosed with CM and diagnosis is revaluated if the antimalaria drug treatment does not work.

The gold standard for confirming a CM infection is if a post-mortem on the brain tissue of an infected patient shows sequestration of parasites (Seydel *et al*., 2012). Therefore, if a rapid, low cost, reliable detection system could be optimised for determining *Pf*HRP-2 concentrations, one could potentially diagnose the likelihood of a patient's infection progressing to a CM infection.

1.5. Malaria diagnosis methods:

1.5.1. Light microscopy to diagnose a malaria infection

Light microscopy is a common method used to diagnose malaria and there are two types of samples used: a thick or thin blood film. Thick blood film should be used first to diagnose if a patient is infected.

Thick blood films use 1 – 2 drops of blood smeared (20 – 30 layers thick) over 1.5 to 2 cm in diameter. A hypotonic solution is used to lyse the erythrocytes, and the cell contents are released including different stages of the malaria parasite stain. Thick blood film is more sensitive for detecting a malaria infection. An infection is determined by counting either 500 parasites or 1000 white blood cells (WBC). If the WBC count is not previously determined, assume 8000 WBC per µl of blood (Garcia and Isenberg, 2007; Mathinson and Pritt, 2017).

In a thin blood film, erythrocytes are stained in and fixed with absolute methanol and it can be used to diagnose the species of malaria (Garcia and Isenberg, 2007; Mathinson and Pritt, 2017).

Typical stain dyes are used for both thick and thin blood films are Giemsa, Wright stain or a Giemsa-Wright stain, all the stains, stain DNA. The Giemsa stain is recommended as all cytoplasmic material is stained and can be viewed easily, making malaria species identification possible (Moody, 2002). Examination of slides is recommended at 100 x magnification with oil immersion of 100 – 300 fields depending on the area, as more fields should be viewed where the disease is less prevalent (Ochola *et al*., 2006).

Light microscopy remains the gold standard to diagnose a malaria infection due to advantages such as sensitivity, species identity and low cost. The drawbacks are that sensitivity depends on the microscopist or that mixed infections can be missed (*P. knowlesi*; Singh and Daneshvar, 2013).

Fluorescence microscopy is an alternative to light microscopy, however, only offers a qualitative measure of the parasite progression, therefore %parasitaemia cannot be calculated. The two main fluorophores of fluorescence microscopy used are acridine orange and benzothiocarboxypurine both work by staining DNA.

Acridine orange stains DNA of living and dead parasites and is toxic, therefore may overestimate the severity of an infection. Benzothiocarboxypurine can stain only living parasite DNA since it is actively adsorbed (Moody, 2002).

1.5.2. Nucleic acid method to detect malaria

The Polymerase chain reaction (PCR) is used to determine a malaria infection in a laboratory environment. Two commonly used PCR methods are quantitative PCR and nested PCR. Typically, the technique works by obtaining a suspected patient's blood sample, after which, nucleic acids are extracted. Reagents are added including the primers to amplify the target nucleic acid sequence. The targeted genes are the 18s small subunit ribosomal gene. The amplicon is then visualised by fluorescence, the turbidity of the solution or UV visualisation of the band on an agarose gel (Vasoo and Pritt, 2013; Buppan *et al.,* 2010).

The advantages of PCR are: its sensitivity, as 0.02 to 20 parasites per µl of blood can be identified; nested-PCR can identify different species of infection; a mixed malaria infection and is less subjective than light microscopy (Vasoo and Pritt, 2013; Mathinson and Pritt, 2017). The drawbacks of PCR are: its cost factor as a laboratory is required and the method requires skilled personnel (Mathinson and Pritt, 2017).

1.5.3. Aptamers used to diagnose a malaria infection

Aptamers are biorecognition oligonucleotide chains (made up of either DNA or RNA) that are used for the capture of specific molecules depending on their properties (Ragavan *et al*., 2018). The method is used to find aptamers that are systematic evolution of ligands by exponential enrichment (SELEX) which screen between 10^{12}-10^{15} nucleotide random regions from a library. Jain *et al*., (2016) reported the use of an aptamer (P38) conjugated to gold nanoparticles that were used to diagnose a malaria *P. falciparum* infection by detecting *Pf*LDH. The P38 aptamer was shown to detect *Pf*LDH and none of the human LDH (hLDHA and hLDHB). The K_d was 0.35 µM and a *Pf*LDH limit of detection 281 ± 11 pM. Other studies that have looked at aptamers as a diagnostic tool for malaria were reported by Lee *et al*., (2012); Cheung *et al.,* (2013) and Frith *et al*., (2018).

1.5.4. Serology to detect malaria

Serology is the detection of antibodies. Serology is not used for malaria diagnosis as antibodies take at least a week after the infection to be detected and may last up to 12 months post infection. Therefore, past and current infections cannot be differentiated. Serology is used is in the screening of blood donors and testing febrile patients (Mathinson and Pritt, 2017).

1.5.5. Biosensors and optical assays for malaria diagnosis

Biosensors include electrochemical sensors, immunosensors, and optical sensors, colorimetric biosensors, fluorescence sensors, surface plasmon resonance sensors, surface-enhanced Raman spectroscopy, quartz crystal microbalance sensors, lab-on-a-chip

and microfluidic devices, paper-based sensors, cell phone-based sensors, optical imaging and miscellaneous sensors. Even though these are beyond the scope of the current review, a review by Ragavan *et al*., (2018) covered these malaria diagnostic assays.

1.5.6. Malaria rapid diagnostic tests to detect malaria

Malaria rapid diagnostic tests (MRDT's) are a popular alternative to light microscopy in remote malaria endemic areas (Cheng *et al*., 2014). The technique is simple to perform, and low level of expertise needed. The basic concept of an RDT is shown in Figure 1.2.

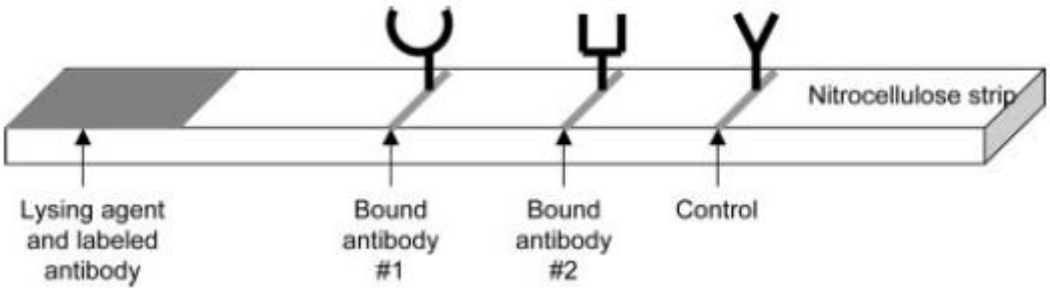

Figure 1.2: A cartoon representation of an RDT. (Figure adapted from Murray et al., 2008).

An RDT utilises a lateral flow immunochromatographic system on a nitrocellulose-based platform. A blood spot is added to the lysing agent. The lysed parasite material flows through the nitrocellulose via capillary action and passes a set of capture antibodies (represented by 1 and 2; Figure 1.2). Within an RDT a second set of antibodies are present, known as detector antibodies and usually have gold nano particles conjugated to them. If the parasite's antigen is present the detector antibodies will bind to the antigens and once the parasite antigen is captured at positions 1 or 2, a coloured line will form, indicating a positive infection. A control line shows the RDT is working and typically the most commonly used antigens are *Pf*HRP-2 for *P. falciparum* and LDH and aldolase to diagnose different infections or pan infections depending on the RDT (Murray *et al*., 2008).

For RDT *Pf*HRP-2 is the antigen most commonly detected (WHO, 2015b; Cheng *et al*., 2014). Generally, *Pf*HRP-2 based RDT are more stable and have higher sensitivity than RDT's detecting LDH and aldolase (WHO, 2015b). RDT's are easy to use, and personnel require minimum training, results are available in under 30 minutes and a laboratory is not necessary.

RDT's are less sensitive compared to light microscopy and the WHO recommends RDT's to be used in combination with a separate diagnostic method like light microscopy (Mathinson and Pritt, 2017).

Another major problem with RDT's is its variation in sensitivity and selectivity due to batch variation and the antibodies on the nitrocellulose strip degrade when exposed to high ambient temperatures in areas where the RDT's are stored (Jimenez *et al*., 2017).

1.5.7. Diagnosis of cerebral malaria

To date, there is no rapid diagnosis method for CM. Reports have stated about 25% of deaths initially diagnosed with CM were due to other causes (Taylor *et al.,* 2004). Retinopathy is been looked at as a possible technique which can be used for the diagnosis of CM infection. This is due to CM infected patients having retinal whitening, and retinal vessels appear orange rather than red due to parasite infected erythrocytes, which cause polymerisation of hemoglobin into hemozoin (Beare *et al*., 2006). However, Seydel *et al.,* (2012) highlighted that retinopathy is relatively challenging and is not appropriate for use in remote locations.

1.6. An alternative to retinopathy for CM rapid diagnosis

Due to the complexity and lack of understanding of CM, a rapid diagnostic is difficult to develop. To date, a possible marker for severe malaria or a CM infection is tracking HRP-2 concentrations in the blood (Seydel *et al*., 2012; Dvorin, 2017; Sinha *et al*., 2015). Dvorin, (2017) suggested a two-part diagnosis method based on the detection of HRP-2 and endothelial protein C receptor binding transcripts using PCR. The current most common method used to quantify *Pf*HRP-2 concentrations is ELISA, but reagents and equipment are not readily available in the remote malaria endemic areas (Desakorn *et al*., 1997; Kim *et al.,* 2016). Sinha *et al*., (2015) evaluated the use of RDT's as semi quantitative HRP-2 detectors, Paracheck® was found to work best, although the plasma had to be separated from the sample as the threshold of HRP-2 was reached below the HRP-2 limit of detection. There is a need for a diagnostic method to detect and quantify HRP-2 as a potential indicator of severe malaria.

1.7. The structure of HRP-2

P. falciparum Histidine rich protein-2 is a 30 kDA water soluble protein that was first discovered by Wellems and Howard, (1986). HRP-2 is only expressed by *P. falciparum* malaria where it is expressed in two stages, the blood stage and the gametocyte stage (Howard *et al.,* 1986; Hayward *et al.,* 2000). Some HRP-2 is released into the blood when the blood stage schizont is developing, and most is released when the infected erythrocyte ruptures (Howard *et al.,* 1986). HRP-2 can be present in concentrations greater than 1 µg/ml in the blood and may persist for up to a month after a *P. falciparum* malaria infection has been resolved (Dondorp *et al.,* 2005).

HRP-2 has an unusual amino acid composition where 87% of the protein consists of histidine (35%), alanine (40%) and aspartic acid (12%) (Wellems and Howard, 1986). A 3D crystal structure has not been resolved for HRP-2.

The AHHAAD repeats occurring throughout the amino acid sequence of the protein and the 309 amino acid sequence is shown in Figure 1.3.

```
10                  20                  30                  40                  50
MVSFSKNKVL  SAAVFASVLL  LDNNNSAFNN  NLCSKNAKGL  NLNKRLLHET
      60                  70                  80                  90                 100
QAHVDDAHHA  HHVADAHHAH  HAADAHHAHH  AADAHHAHHA  ADAHHAHHAA
     110                 120                 130                 140                 150
DAHHAHHAAY  AHHAHHAADA  HHAHHASDAH  HAADAHHAAY  AHHAHHAADA
     160                 170                 180                 190                 200
HHAHHASDAH  HAADAHHAAY  AHHAHHAADA  HHAADAHHAT  DAHHAHHAAD
     210                 220                 230                 240                 250
ARHATDAHHA  ADAHHATDAH  HAADAHHAAD  AHHATDAHHA  ADAHHATDAH
     260                 270                 280                 290                 300
HAADAHHAAD  AHHATDAHHA  HHAADAHHAA  AHHATDAHHA  TDAHHAAAHH

EAATHCLRH
```

Figure 1.3: The amino acid sequence of *Pf*HRP-2. (P90582-1).

1.8. Function of HRP-2

The exact function of HRP-2 is unknown. Benedetti *et al.,* (2003) showed HRP-2 is similar to hisactophilin in the sense that both proteins can bind actin at acidic pH (Shown using circular dichroism spectra). HRP-2 also binds phosphatidyl- inositol 4,3 biphosphate (PIP_2) in an α- helical conformation, which is typical to an actin binding protein. By binding actin, the secondary structure formed stabilises actin-filaments, and this could stabilise infected erythrocytes and aid in the cytoskeleton changes during knob formation.

Das *et al.,* (2006) showed HRP-2 might play a role in the supersession of the host's immune system by binding to T-cells and B-cells. Sullivan *et al*., (1996) and Choi *et al.,* (1999) demonstrated HRP-2 aids in heme binding (50 molecules of heme per molecule of HRP-2) and polymerization of toxic heme into non-toxic hemozoin. However, Nakatani *et al*., (2014) suggested heme detoxification protein aids the parasite with heme detoxification.

Ndonwi *et al*., (2011) showed HRP-2 acts as a procoagulant by binding heparin with high affinity, therefore, preventing antithrombin activity. Interestingly when HRP-2 was in the presence of Zn^{2+}, or Cu^{2+} HRP-2 had a higher binding affinity for heparin. The 51 His-His-Ala repeat regions on HRP-2 allow the protein to bind to metal cations. HRP-2 affinity for metal ions was first reported by Panton *et al.,* (1989). Panton *et al*., (1989) showed *Pf*HRP-2 needed 450 mM imidazole to be removed off a Cu^{2+} matrix, while only 300 mM imidazole was needed to elute *Pf*HRP-2 of a Zn^{2+} matrix. This indicated *Pf*HRP-2 binds with higher affinity to Cu^{2+}.

According to Bauer *et al*., 2017; Co^{2+} and Zn^{2+} had the highest K_{ON} but the lowest K_D, whereas Cu^{2+} had the lowest K_{ON} and the highest K_D, therefore the proteins affinity is higher for Co^{2+} and Zn^{2+} than for Cu^{2+}.

1.9. *P. falciparum* isolates lacking the HRP-2 gene

Even though most RDT's rely on the detection of HRP-2 to diagnose a *P. falciparum* malaria infection (Lee *et al.,* 2006), isolates lacking HRP-2 have recently been reported.

The first reported area affected was the Peruvian Amazon basin (Gamboa *et al*., 2010). Several studies have since then reported HRP-2 and HRP-3 deletions in isolates from India (Kumar *et al*., 2013), Brazil and Bolivia (Viana *et al*., 2017), Mali (Koita *et al*., 2012); Senegal (Wurtz *et al*., 2013) and Kenya (Beshir *et al.,* 2017).

The genes for HRP-2 and HRP-3 are located on chromosomes 8 (HRP-2) and 13 (HRP-3) therefore, gene deletions are assumed to be due to independent events. In Brazil and Bolivia HRP-3 gene deletions are more common (Viana *et al*., 2017).

1.10. Current state of malaria diagnosis

Light microscopy is the gold standard for diagnosing a malaria infection, however, it cannot diagnosed if a *P. falciparum* infected patients malaria infection will progress to CM. Many biosensors and optical assays are being developed for the rapid detection and quantification of HRP-2 but none of them are recommended by WHO.

1.11. Copper binding to histidine residues

A study done by Zhao and Waite, (2006) showed histidine residues of the Mcfp-4-sequence peptide (a histidine rich protein) bound more Cu ions than any other metal ion tested using mass spectroscopy (Figure 1.4).

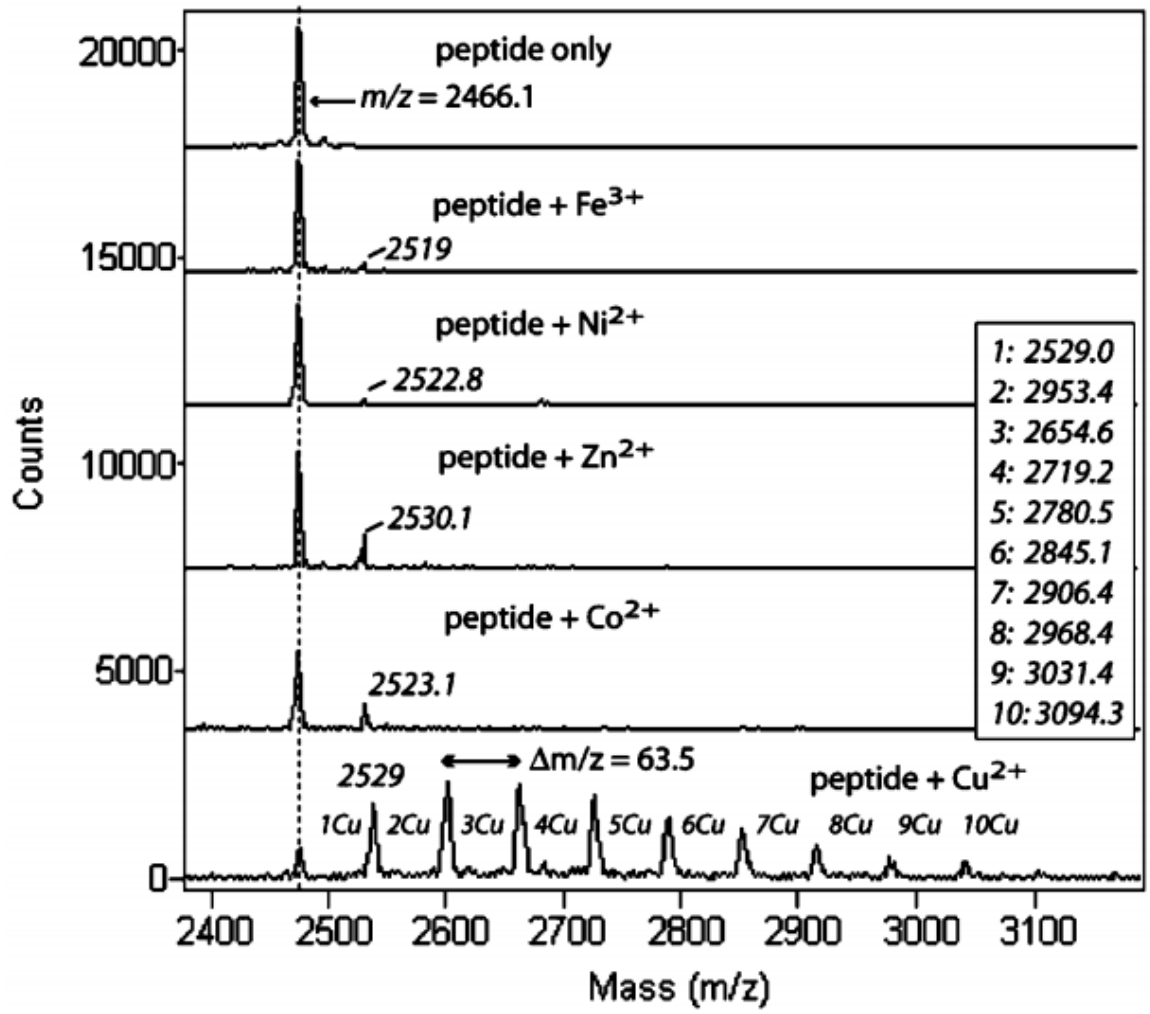

Figure 1.4: A mass spectrum illustrating the binding of Fe^{3+}, Ni^{2+}, Zn^{2+}, Co^{2+} and Cu^{2+} to Mcfp-4-. The result of showed 11 Cu^{2+} bound per 8 histidine residues. Knowing HRP-2 has a high affinity for Cu, an assay could potentially be developed and used to detect and quantify HRP-2 based on its high affinity for Cu ions. (Figure adapted from Zhao and Waite, 2006).

1.12. Introduction of HRPC

Horseradish peroxidase (HRP; E.C1.11.1.7) is a plant peroxidase which is present in the roots of the horseradish plant (*Armoracia Rusticana*). There are at least 15 peroxidase isoenzymes with isoenzyme C (HRPC) being the most abundant and widely studied (Hoyle, 1977; Veitich, 2004). HRPC is part of the type 3 peroxidase superfamily of heme containing oxidoreductases enzymes. The oxidoreductases catalyse the oxidation of various chromogenic organic compounds usually with high enzyme activity in the presence of hydrogen peroxide (H_2O_2) or sodium perborate (Zhao *et al*., 2015). HRPC is used in various fields like, biotechnology (Azevedo *et al*., 2003), immunodiagnostics (Krieg and Halbhuber, 2003), biomedical applications such as aiding in cancer treatment (Wardman, 2002), wastewater treatment (Alemzadeh and Nejati, 2009) and detection of Cu in water samples (Xianyu *et al*., 2013).

1.13. Structure of HRPC

HRPC is made up of 308 amino acids and a total molecular weight of 44 kDa. Gajhede *et al*., (1997) resolved the X-ray crystal structure of HRPC at 2.15Å (Figure 1.5). The main features of the HRPC molecule indicate most of the protein is made up of α- helices, the blue circles represent the Ca^{2+} ions in the distal and proximal region and the iron (III) protoporphyrin IX or heme group is indicated in red.

There are 13 α-helices, and α-helices A-J are common in most peroxidases, while there is an additional three a-helices D', F' and F" unique to HRPC. The function of the additional 3 α-helices is not understood but it is suspected that helices D', F' and F" may aid the catalytic efficiency of HRPC by keeping reactive intermediates within the hemes active site, therefore aiding in the oxidation of substrates.

HRPC is a glycoprotein with a total carbohydrate content of between 18 – 22%. The carbohydrates are in the form of glycans (mannose, xylose, fucose, and N-acetylglucosamine) that are bound to the loops of the α- helices distributed across the protein (Gajhede *et al*., 1997). HRPC has nine potential glycosylation sites of which eight are glycosylated via N-linked amide bonds to asparagine residues.

The amide bond motif is Asn-X (any amino acid)-Ser/Thr (Asn13, Asn57, Asn158, Asn186, Asn198, Asn214, Asn255 and Asn268; Veitch, 2004; Welinder, 1979). The glycans point away from HRPC and their role is to aid the enzyme to maintain its conformation and improve solubility. Smith *et al*., (1990) found that glycans were removed from HRPC, the enzyme precipitated in aqueous-saline buffer. This further confirmed the importance of the glycans for HRPC.

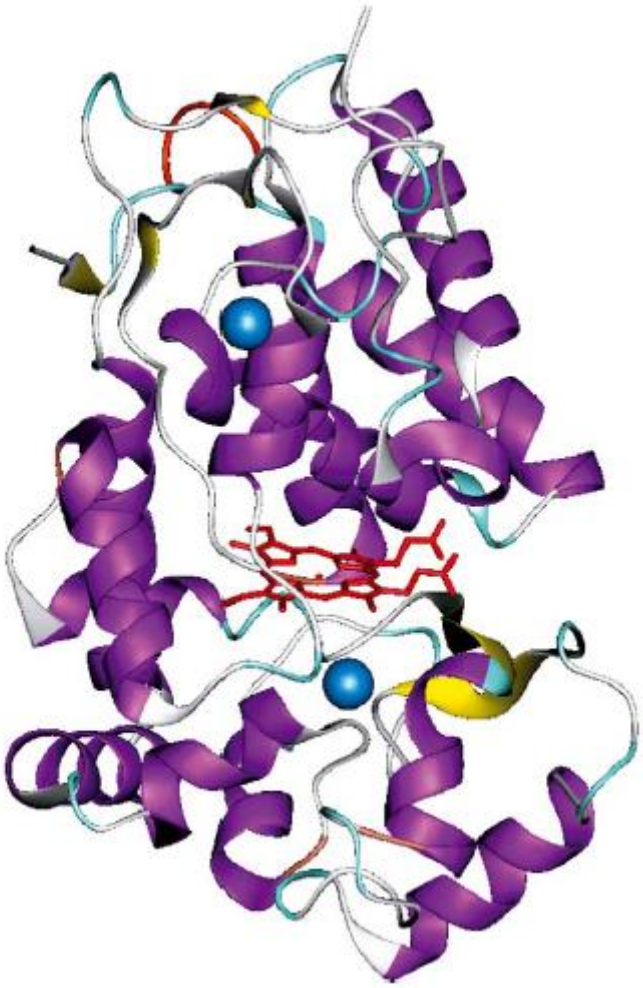

Figure 1.5: The 3D X-ray structure of horseradish peroxidase done at 2.15 Å using x-ray crystallography. The 3D structure shows a stick model in red that represents the heme, above the heme is a distal domain and below the heme is the proximal domain, both contain a calcium atom shown as a blue sphere. The α helices are shown by purple ribbons and the β sheets are shown in yellow. (Brookhaven accession code 1H5A). (Veitch, 2004).

The active site of HRPC houses two metal ions, Ca^{2+} and a Fe^{3+} in the heme centre. There are two Ca^{2+} atoms per HRPC molecule. They are situated on either side of the heme in the distal region (above the heme) and proximal region (below the heme) respectively.

The distal calcium atom is in a seven-coordinate state and is formed with an oxygen ligand set. The oxygen ligand set is formed by Asp43, Asp50, Ser52 side chains and Asp43, Val46 and Gky48 carbonyl groups (Gajhede *et al.,* 1997).

The proximal calcium atom has seven-coordinate bonds with Asp222, Asp230, Thr171, Thr225 side chains and Thr171, Thr225 and Ile225 carbonyl groups. Ca^{2+} helps maintain the heme pocket structure (Gajhede *et al.,* 1997; Veitch, 2004). Howes *et al*., (2001) showed that the proximal Ca^{2+} atom is more often lost resulting in a conformational change in HRPC active site, therefore, substrates bind less efficient in the heme pocket. The Fe^{3+} centre plays a role in the oxidation of substrates.

The solvent access channel is located toward the right side of the heme edge and has a hydrophobic outer edge because of three Phe68, Phe142 and Phe179 residues and a C18 methyl group. The inner layer of the solvent channel is positively charged, and this is due to the distal Arg38. Of the Phe residues, Phe179 is the most important of the three Phe due to its position (closest to the heme) that allows stereoselectivity of substrates entering the active site. This helps with rapid transfer of electrons to oxidise a substrate (Gajhede *et al*., 1997; Azevedo *et al*., 2003).

Important amino acids in the catalytic mechanism are summarised in Table 1.1.

Table 1.1: Amino acids important to the catalytic mechanism of HRPC.

Amino acid	Function
Arginine 38	● Found in the distal region ● Helps to maintain the reactive intermediate from compound 1, by promoting H^+ and stabilise reactive intermediates.
Phenylalanine 41	● Prevents substrates from binding to compound 1
Histidine 42	● Found in the distal region ● Binds the first substrates H^+ in compound 1 formation ● Provides 1 H^+ for the formation of H_2O, when heme regenerated
Asparagine 70	● Binds to His42 to maintain its alkaline nature, when participating in compound 1 formation.
Proline 139	May assist proton transfer when forming compound 2

Gajhede *et al*., (1997); Azevedo *et* al., (2003); Veitich, (2004)

1.14. HRPC mechanism

The reaction mechanism of HRPC is important to look at in order to understand how HRPC functions and is explained in Figures 1.6-1.8.

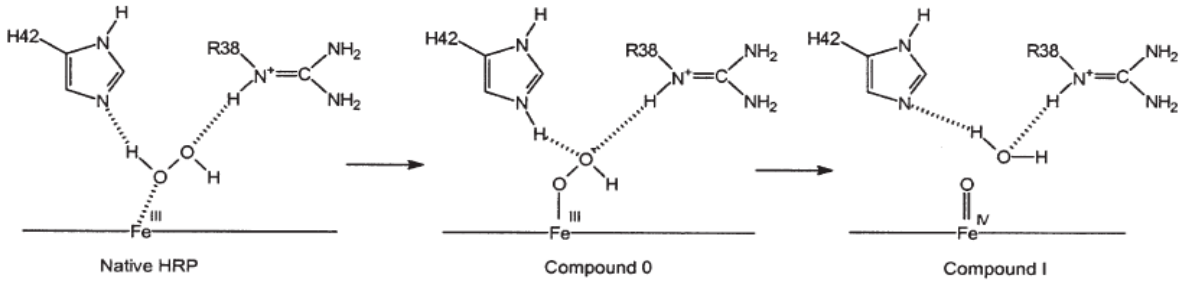

Figure 1.6: The mechanism formation of compound 1, Fe^{4+}- oxoferryl. The Fe^{3+} in HRPC active site is oxidised by H_2O_2 with the aid of His42 and Arg38 (Veitch and Smith, 2000).

An H_2O_2 molecule enters the HRPC active site through the solvent access channel and binds to Fe^{3+} by the α-oxygen while the distal His42 abstracts a H^+ from the H_2O_2 and the distal Arg38 stabilises the reactive β-oxygen. A highly reactive intermediate form called compound 0 that through hetroclyclic cleavage becomes compound 1 (Figure 1.6). The result is Fe^{3+} is now Fe^{4+}=O which is reactive to substrates (phenol represents the substrate in the mechanism).

Phenol enters the active site and is oxidised, firstly B: removes an H^+ from the OH group of the phenol. The H^+ is then attached to the distal His42 (intermediate not shown), and the now reactive phenolic substrate radical is stabilised by distal Arg38. The His42 donates the abstracted H^+ to the oxyferryl heme and compound 2 is formed (Figure 1.7).

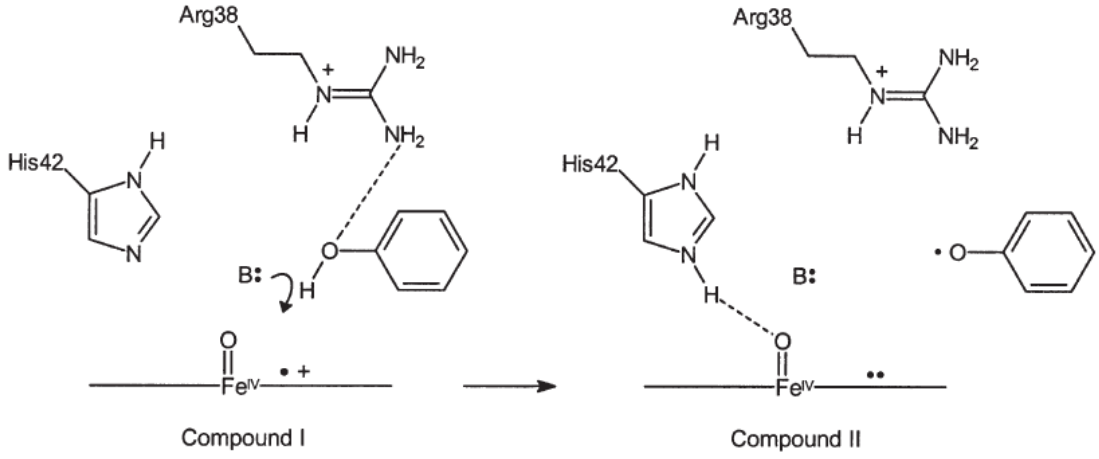

Figure 1.7: The reduction of compound 1 by phenol into compound 2. B represents a protein that abstracts H^+ from phenol that will be taken up by distal His42 (Veitch and Smith, 2000).

Finally, a second phenol can enter and is oxidised (Figure 1.8).

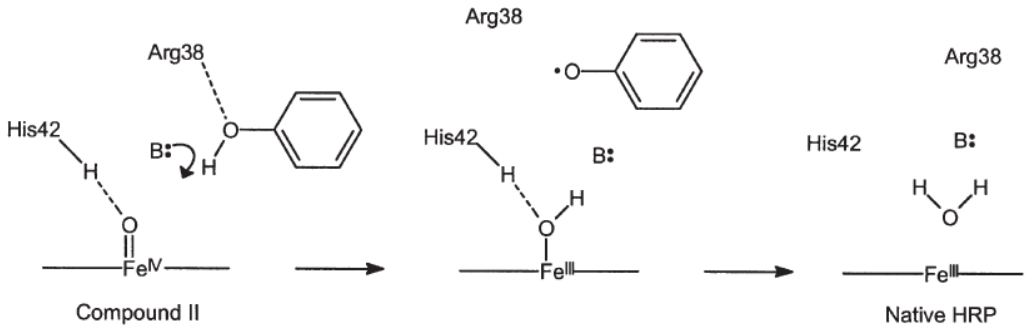

Figure 1.8: A new phenol substrates H^+ is abstracted by B. There is formation of H_2O and regeneration of the active site (Veitch and Smith, 2000).

The distal His42 binds to the α- O on the oxyferryl heme, which then has two H^+ bound forming a H_2O molecule displaced by the heme.

The heme centre returns to the original state with after the oxidation of two phenols and two H_2O molecules from the H_2O_2. The overall reaction can be summarised as:

$$H_2O_2 + 2AH_2 \xrightarrow{HRP\ C} 2H_2O + 2AH^{\bullet} \quad (1)$$

Whereby the AH represents any chromogenic substrate. The overall reaction illustrates a single HRPC molecule oxidises two molecules of a substrate.

1.15. HRPC substrates

HRPC oxidises a large range of chromogenic and fluorometric substrates including 2,20-Azino-di(3-ethylbenzothiazolin-6-sulfonate (ABTS); Benzidine (4,40-Diaminobiphenyl); 3,30-Diaminobenzidine (DAB); Guaiacol (2-Methoxyphenol) Pyrogallol (1,2,3-Trihidroxybenzene); Phenol; 3,3,5,5-Tetramethylbenzidine (TMB), to just name a few (Veitch and Smith, 2000). Of all substrates, the focus in the study was on TMB. TMB is an endpoint chromogenic substrate used in several biochemical techniques. The substrate is hydrophobic therefore it needs to be dissolved in an organic solvent like DMSO. TMB is popular due to its low toxicity and high sensitivity (Bos *et al*., 1981). Spectrophotometric analysis of TMB shows it has two peaks at 370 nm and 650 nm, this is where the diamine forms (oxidised TMB and is bright blue in colour; Figure 1.9) if a concentrated acid is added a second H^+ from TMB is lost and the diamine becomes a diimine that absorbs at 450 nm (Figure 1.9; Josephy *et al.,* 1982). Assays using metal ions like Cu^{2+} and nanoparticles use TMB as the chromogen of choice (Shi *et al.,* 2016; Fu *et al*., 2018).

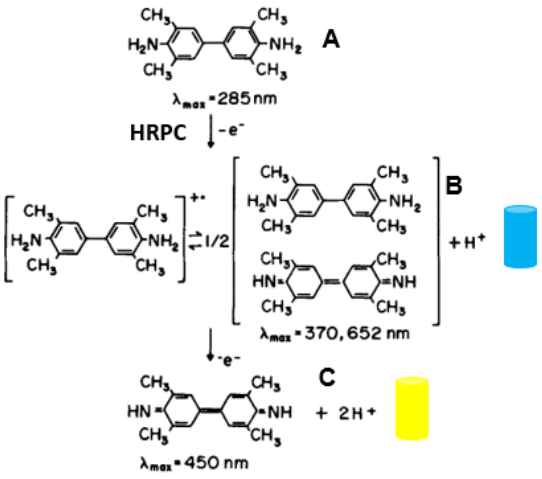

Figure 1.9: Resulting products for the oxidation of TMB. The TMB molecule before oxidation **(A)**. Diamine form of TMB after it has been oxidised by HRPC **(B)**. The addition of a concentrated acid leads to formation of Diimine **(C)**. **(**Figure adapted from Josephy *et al.,* 1982).

1.16. Inhibitors of HRPC

There are several known inhibitors of HRPC such as L-cysteine and other thiol-based compounds (Sariri *et al.,* 2006), EDTA, sodium azide (Ortiz de Montellano *et al*., 1988) and several metal ions. Keyhani *et al.,* (2003) and (2005) has reported the inhibitory effects of Cd^{2+} and Ni^{2+} on HRPC activity. This was of environmental importance as both heavy metals are released from pollutants and interact with plant life. Ni^{2+} and Cd^{2+} both showed kinetic inhibition of peroxidase activity. Han *et al.,* (2008) reported the inhibition of HRPC by Co^{2+} in a dose dependent manner and Moyo, (2014) reported the use of HRPC as a biosensor for the detection of Zn^{2+}, based on the inhibition of HRPC by Zn^{2+}. The most potent of the inhibitors reported was Cu^{+}. Detection of Cu was used in an assay to detect Cu concentrations in water (Xianyu *et al.,* 2013). Of all the metal ions reported, none were competitive inhibitors of HRPC.

1.17. Advances of HRPC in biotechnology

There are several assays which use HRPC as a reporter enzyme and the uses of the enzyme in biotechnology was reviewed by Azevedo *et al.,* (2003). A potential new method in which HRPC could be used for the detection of compounds or other proteins could be based on their binding affinities to metal ions. One such assay has been described by Shi *et al*., (2016) whereby Cu^{+} was incubated in a sample with pyrophosphate. Pyrophosphate binds Cu^{+}. Therefore, if HRPC was inhibited, it meant the absence of pyrophosphate and the amount of HRPC activity correlated to pyrophosphate concentration.

1.18. Peroxidase like activity of Cu^{2+} and Fe^{3+}

Nanotechnology is evolving and developing. Nanoparticles with peroxidase- like activity is an avenue researched to potentially replace enzymes (Gao *et al.,* 2007; Wang *et al*., 2017).

Wu *et al*., (2014) reported that Fe^{3+} ions possess peroxidase- like activity indicating that within nanoparticles the peroxidase like activity was not only due to the nature of the nanoparticle but the Fe^{3+} ions as well. Similarly, Cu^{2+} has also been shown to possess peroxidase like activity (Shan *et al*., 2016). Interestingly both metal ions are involved in Fenton chemistry.

Fenton chemistry involves a metal ion transferring an electron (e^{-}) to an oxidant like H_2O_2. This breaks up H_2O_2 into two OH• molecules that are highly reactive. The OH• can attack and oxidise chromogenic substrates like TMB into a diamine (Figure 1.9). The addition of NaCl to a H_2O_2 mixture forms more reactive intermediates called reactive chloride species (RCl^{-}; Wardman and Candeias, 1996; Shan *et al*., 2016). This well characterised interaction has since been used for the detection of molecules which bind Fe^{3+} and Cu^{2+} such as L-cysteine and L-histidine in urine (Wu *et al*., 2014; Xu *et al*., 2015); Uric acid (Lu *et al;* 2017) and dopamine (Wang *et al*., 2017). These assays indicate that there is promise around the peroxidase- like activity metal ion assays and this could potentially be used in a diagnostic assay.

1.19. Introduction to differential scanning fluorometry

Differential scanning calorimetry (DSC) is commonly used to determine the thermal and thermodynamic stability of proteins in the field of life sciences (Bruylants *et al*., 2005). Methods such as surface plasma resonance (SPR) and isothermal calorimetry are methods used in determining protein-protein interactions and drug-protein interactions. However, a shortfall of these techniques is that they do not have high throughput capability for screening drug and fragment-based libraries. Therefore, the screening of small molecules is labour intensive, and the techniques require expensive machinery (Lo *et al*., 2004; Redhead *et al*., 2017).

An assay was developed by Pantoliano *et al*., (2001) to reduce the labour required for drug discovery screening while still remaining economical. The assay was called the thermal shift assay which is now more commonly referred to as differential scanning fluorometry (DSF). For DSF a protein sample is heated at a constant temperature in the presence and absence of a drug molecule. A hydrophobic dye, known as a fluorophore which is usually SYPRO Orange is present in the mixture. The fluorophore binds specifically to hydrophobic amino acid residues and fluoresces upon binding.

From the fluorescence signal the proteins melting temperature (T_m) is extrapolated. The T_m is an indication of when 50% of a protein has unfolded and higher T_m values generally correlates to more stable protein (Pantoliano *et al*., 2001 Niesen *et al*., 2007).

If the drug molecule present in the mixture binds to the protein the drug can stabilise the protein and increase the proteins T_m. Generally, a 2°C increase in T_m for a protein in the presence of a drug is considered a protein-drug interaction. A drug may sometimes bind to a protein and reduce its stability. The drug is then not regarded as a potential drug to study further, since the drug may be binding non-specifically to the protein (Niesen *et al*., 2007; McMahon *et al*., 2014; Huynh and Partch, 2015).

DSF has become a widely used biophysical technique due to its various applications in drug discovery (McMahon *et al*., 2014); extraction of thermodynamic properties of proteins (Wright *et al.,* 2017); optimising of buffers for protein stability and protein purification (Crowther *et al*., 2010; Huynh and Partch, 2015); Measure of protein-protein interactions (Douse *et al*., 2015). DSF can be used to screen hundreds of compounds in a single day, the reagents are inexpensive, low concentrations of proteins are used 1 – 5 µM (Niesen *et al*., 2007) and the equipment required is an RT-qPCR machine. DSF has been applied to be used in cultured cells and tissue samples to show *in vivo* drug-protein interactions, the assay is called cellular thermal shift assay (CETSA; Jafari *et al.,* 2014).

DSF has some shortfalls when determining a protein T_m and drug-protein interactions. Not all proteins are suitable candidates for analysis using DSF, different transition curves of proteins unfolding are illustrated in Figure 1.10.

The green line is an indication of a protein well suited for DSF analysis, the initial fluorescence is low, and denaturation is indicated by a sharp transition with increasing temperature. The yellow line indicates an intermediate thermodenaturation curve, the initial fluorescence is high, but a transition still occurs. Typically, an intermediate transition is present for proteins that are in sub-optimal buffer conditions, are partially denatured or may have surface hydrophobic patches, which leads the fluorophore binding at lower temperatures (before the protein unfolds due to an increased temperature) and fluorescence. The red line shows the absence of a transition and from the profile a T_m cannot be obtained, generally this is due to a completely denatured protein, a buffer containing surfactants, or the protein is an enzyme with a large solvent access, therefore allowing the dye to enter the hydrophobic core (Niesen *et al*., 2007; Crowther *et al*., 2010; Reinhard *et al*., 2013).

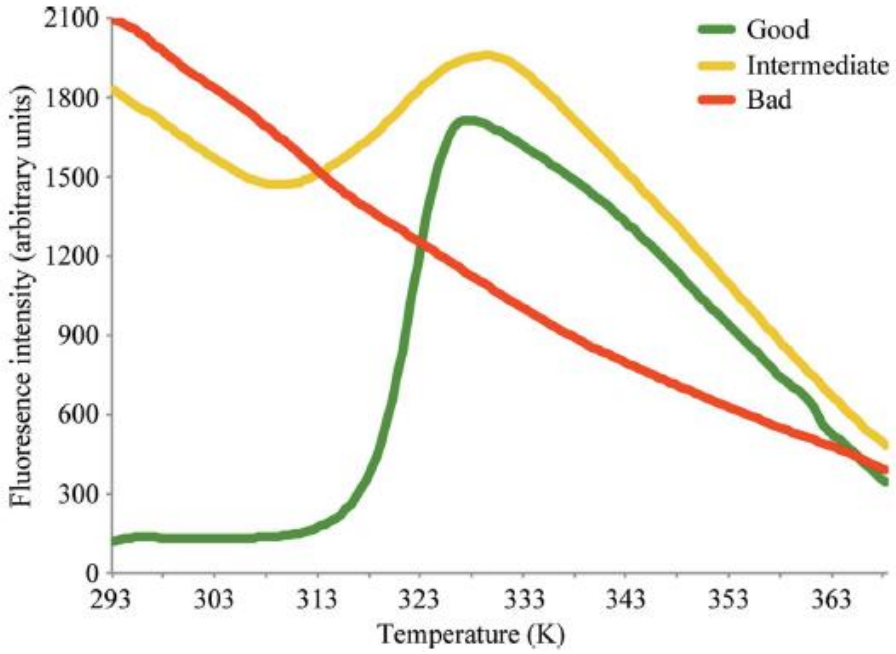

Figure 1.10: An arbitrary DSF fluorescence curve showing the transition of thermal denaturation of a good, intermediate and bad protein candidate. (Figure adapted from Reinhard *et al*., 2013).

It is suspected about 20% of recombinant proteins do not produce transitions when evaluated using DSF, due to the nature of the protein or incorrect purification conditions. A concern raised by Redhead *et al*., (2017) and Wright *et al*., (2017) was that by only measuring the protein's T_m as a parameter to determine the protein's stability or to determine if a small molecule can be considered a potential drug is just a qualitative measure. Both studies suggested using DSF data but by using ΔμG energy rather than T_m as a more quantitative measure.

Some studies have successfully used DSF as a primary fragment-based drug discovery screening tool with success.

Major and Smith, (2011) screened a 600 compound FBDD library against myoinositol-3-phosphate synthase form *Trypanasoma brucei* and had a 6% hit rate. Hudson *et al.,* (2012) screened a 665 compound FBDD library and had 66 matches of which 40% were validated by NMR. Redhead *et al*., (2015) showed SPR and DSF had a good correlation of results when identifying small molecules against kinase p38a. Even though some compounds may interfere with DSF screening due to the interactions with the fluorophore, DSF should be considered as a primary or secondary screen for interrogating small molecules for drug discovery (McMahon *et al*., 2014). Well established methods such as NMR and electro paramagnetic resonance (EPR) have also been shown to have conflicting data when interrogating small molecules for drug discovery (McMahon *et al*., 2014).

Several studies have used DSF as a method to screen monoclonal antibodies to find the most stable antibody. An interesting observation from these studies was that DSF had a good correlation with DSC when determining the T_m of the proteins (He *et al.,* 2010; Menzen and Friess, 2013; King *et al.,* 2011). In summary a protein's T_m has been shown to successfully identify drug candidates and has been used successfully to determine a proteins stability.

1.20. Using DSF as a method to determine the thermal stability of proteins that could be used as malaria diagnostic reagents

Currently, RDT's are an attractive alternative to light microscopy but should be used in conjunction with other malaria diagnostic methods like light microscopy (Jimenez *et al.,* 2017). This is due to limitations such as variance in sensitivity per batch of RDT. Sometimes RDT's give false positive results due to the antibodies on the test strip losing activity because of high ambient temperatures in areas where the RDT's are stored. Mouse monoclonal antibodies are used in the tests which can cross react with rheumatoid factor giving false positive (Iqbal *et al*., 2000). If RDT's could detect below 100 parasites per µl, this will aid in the diagnosis of malaria infected patients and will allow individuals to receive treatment faster, resulting in more lives being saved.

1.21. Advantages of polyclonal chicken IgY antibodies in biotechnology

Polyclonal chicken IgY antibodies are often used in biochemical techniques. Chicken IgY is cheap to produce, the antibodies can be obtained and purified using non-invasive methods (Schade *et al*., 1996), there is very little cross reactivity with mammalian IgG and IgY does not recognise rheumatoid factor. Chicken IgY is stable up to 60°C and 70°C in the presence of sugars (30% sucrose, trehalose or lactose; Jaradat and Marquardt, 2000). The advantage of chicken IgY has been recognised by the European Centre for the Validation of Alternate Method (ECVAM). They suggested that chicken IgY antibodies should be looked at to replace the use of mouse monoclonal IgG antibodies (Schade *et al*., 1996; Terzolo *et al.,* 2003).

These benefits suggest chicken IgY antibodies have the potential to be used in RDT's and should be further investigated as an avenue to address the limitations of RDT's.

1.22. *Pf*GAPDH as a potential biomarker for diagnosis a *P. falciparum* malaria infection

Since some malaria isolates are lacking *Pf*HRP-2 (Gamboa *et al*., 2010), protein diagnostic markers are being analysed for their potential. Krause *et al*., (2017) showed *Pf*GAPDH has the potential to be used a *P. falciparum* diagnostic marker as the protein exists in a 4 -6-fold higher concentration than *Pf*LDH in parasite lysate.

Detection of malaria biomarkers that are more stable and are present in higher concentrations in infected patients would overcome the limitation of *Pf*LDH, which it is found in low concentrations and RDT's detecting *Pf*LDH lack sensitivity. However, further research still needs to be conducted.

1.23. Problem statement

Malaria related deaths have decreased in the last decade through vector control strategies like long-lasting insecticidal nets and indoor residual spraying, and the use of RDT's allowing patients to receive appropriate treatment. More work still needs to be done to reduce the number of malaria related deaths. There is no rapid diagnosis method for a CM infection and CM results in 20% of infected patients dying and a further 25% with permanent neurological disorders. There is a link between a *P. falciparum* infection leading to CM and the concentration of the *Pf*HRP-2 protein.

Malaria RDT's do not need skilled personnel to diagnose an infection and are economical. However, due to HRP-2 gene deletions and antibodies degrading under high ambient storage temperatures, RDT's are recommended to be used in conjunction with a second diagnostic method like light microscopy.

Hypothesis:

Chicken IgY antibodies are more stable than the more commonly used mammal IgG molecules. Therefore, chicken IgY should be studied for its potential as diagnostic reagent.

The second hypothesis was to show that *Pf*HRP-2 can be detected by measuring its ability to bind Cu ions.

1.24. Aims

The first aim was to measure the thermal stability of common diagnostic target proteins r*Pf*HRP-2 and r*Pf*LDH and compare them to the thermal stability of r*Pf*GAPDH (a potential diagnostic protein). DSF will also be used to show protein-protein interactions (*Pf*HRP-2 and r*Pf*LDH interaction with their respective antibodies) and r*Pf*LDH and r*Pf*GAPDH interaction with anti-malaria drugs.

In silico methods will be used to show the interaction of anti-malarial drugs with r*Pf*LDH and r*Pf*GAPDH. This can show the amino acids interacting with anti-malarial drugs and provide insight into important functional groups new anti-malarial drugs require.

The second aim was to determine the thermal stability of chicken IgY antibodies and compare it to the antibodies from other species (Chapter 3). The third aim was to develop a detection and quantification method for *Pf*HRP-2 by creating two competition assays with Cu and *Pf*HRP-2.

The first assay is based on a competition assay between HRPC and Cu^{+} for r*Pf*HRP-2 and the second assay is based on Cu^{2+} Fenton chemistry (Chapter 4).

2. CHAPTER 2: Recombinant expression and purification of *P. falciparum* HRP-2, LDH and GAPDH; differential scanning fluorometry analysis of recombinant protein, chicken IgY antibodies; r*Pf*LDH and r*Pf*GAPDH with anti-malarial drugs

2.1. Introduction

Recombinant protein expression is by far the most widely used technique to obtain high (mg) yields of a protein, which avoids the need to continuously purify proteins from large amounts of animal or plant based material (Rosano and Ceccarelli, 2014). Recombinant protein expression has the added advantage of producing large quantities of proteins that would otherwise be difficult to obtain due to their low concentrations in nature (Rosano and Ceccarelli, 2014). There are various expression hosts such as plant (Krainer and Glieder, 2015); fish (Davidson *et al*., 2003); filamentous fungi; yeast and, bacteria (Demain and Vaishnav, 2009). All expression hosts have their own advantages and disadvantages and an ideal host is selected according to experimental needs. The bacteria host *Escherichia coli* (*E. coli*) BL21 DE3 is the most widely used expression host (Rosano and Ceccarelli, 2014).

There are numerous advantages that favour using *E. coli* (BL21) DE3 as an expression host such as: Its rapid growth rate kinetics resulting in high-density cell cultures in short periods of time. The media used to grow the bacterial cultures are economical (Sezonov *et al*., 2007). Competent *E. coli* (BL21) cells can be transformed with plasmid vectors in just 5 minutes (Pope and Kent, 1996). The host bacteria have the lacUV5 promoter which controls T7 RNA polymerase expression and this controls expression of genes coded for by the T7 promoter. The *E.coli* BL21 (DE3) strain is deficient in the Lon protease and ompT proteases. (Gottesman, 1996; Grodberg and Dunn, 1988), therefore, protease inhibitors are not required.

The two plasmid vectors used here were the pET(15b) and pKK223-3, which express fusion proteins with a hexa-his tag. The hexa-his tag allows for a single purification step of recombinant protein (≥ 95%) from a cell lysate. The recombinant protein can be used for immunisation of animals to raise antibodies. Chicken IgY antibodies are an attractive source of antibodies as high yields can be purified using non-invasive techniques (Schade *et al*., 1996).

Differential scanning fluorometry (DSF) is a popular assay used to determine the biophysical properties of proteins (Niesen *et al*., 2007). DSF measures the melting temperature (T_m) of a protein with the aid of a fluorescent dye typically SYPRO Orange (Niesen *et al*., 2007). The T_m value is an indication of when 50% of a protein has unfolded.

The principle of the DSF assay is a protein sample is heated at a ramp temperature from 25°C to 90°C (Pantoliano *et al*., 2001; Matulis *et al*., 2005). As a protein is heated the protein's stability decreases and it begins to unfold, it causes the hydrophobic core amino acids to be exposed, which in turn interacts with the fluorescent dye (Pantoliano e*t al.*, 2001).

DSF has been used in various studies and protocols. The studies range from looking at various biophysical properties of proteins, such as their thermodynamic properties (Wright *et al*., 2017) to high throughput thermal scanning (HTTS; Lavinder *et al*., 2009). HTTS uses DSF to screen if ligands bind to a protein as is often used as a primary screen in the field of drug discovery. The theory is that if a drug binds to a protein, the protein is stabilised, and there will be a shift in the T_m. However, DSF can show if a drug destabilises the protein, then, the T_m is reduced (Cimmperman *et al*., 2008; Lavinder *et al*., 2009 McMahon *et al*., 2014). Other studies looked at calculating the binding constant of ligands to proteins (Vivoli *et al*., 2014), screening for optimal buffers (Vedadi *et al*., 2006; Ericsson *et al*., 2006; Crowther *et al*., 2010) and protein-protein interactions (Layton and Hellinga, 2011).

DSF has several advantages, such as equipment and reagents are economical (Lo *et al*., 2004), and the assay has a short run time (McMahon *et al*., 2014). The disadvantages of DSF are that some proteins do not produce melt curves that show transitions, therefore a T_m cannot be determined (Crowther *et al*., 2010). Attempts have been made to get around this by using thiol-specific fluoroprobes (Vedadi *et al.*, 2010; Hofmann *et al*., 2016).

P. falciparum HRP-2, LDH, GAPDH were recombinantly expressed and affinity purified. DSF analysis was performed on the three antigens to determine their stability and interactions with different drugs *in silico*.

2.2. Materials and Methods

2.2.1. Materials (Chemicals and equipment)

All common reagents, buffers, salts and SDS-PAGE reagents were purchased from Sigma and Merck. Recombinant protein expression reagents (Yeast extract, tryptone) were purchased from Sigma-Aldrich-Fluka (Steinheim, Germany). Antibodies purchased from Novagen (Damstadt, Germany; excluding chicken IgY antibodies). Protein molecular weight marker, containing: 116 kDa β-galactosidase; 66.2 kDa bovine serum albumin; 45 kDa ovalbumin; 35 kDa lactate dehydrogenase; 25 kDa REase Bsp981; 18.4 kDa β-lactoglobulin and 14.4 kDa lysozyme (Vilinius, Lithuania). SYPRO Orange (Sigma).

Bovine serum albumin (BSA) was purchased from Roche (Mannheim, Germany). Maxi Sorp™ 96-well ELISA plates were from Nunc products (Roskilde, Denmark). PCR-X clear tubes (Star labs; Germany). Ni^{2+}-NTA agarose (Qiagen).

AvantiTM J-26 XPI and AllegraTM X-22R centrifuges from Beckman Coulter (California, USA); UV-1800 Shimadzu spectrophotometer from Shimadzu corporation (Kyoto, Japan); pH meter from HANNA instruments; Corbett Research PCR Rotorgene 6000 and VersaMax™ ELISA plate reader was purchased from Molecular Devices Corporation (California, USA).

2.2.2. Recombinant expression and purification of *Pf*HRP-2; *Pf*LDH and *Pf*GAPDH

Glycerol stocks of *E*. *coli* (BL21) DE3 bacterial cells transformed with either the pET-15(b) vector coding for r*Pf*HRP-2 or r*Pf*GAPDH or the pKK223-3 vector coding for r*Pf*LDH, were used. The glycerol stocks were used to 3-way streak a LB agar plate (1% (w/v) tryptone; 0.5 % (w/v) yeast extract; 85 mM NaCl; 11 mM glucose; 1.5% (w/v) bacto-agar prepared in dH_2O and autoclaved) which was incubated overnight at 37°C. A single colony was used to inoculate 10 ml of 2 x YT (1.6% (w/v) Tryptone; 1.0% (w/v) bacto yeast; 0.5% NaCl; 50 µg/ml ampicillin) and grown overnight at 37°C with agitation (200 RPM).

A sample of the culture was diluted 1:100 in fresh terrific broth (TB media; 1.2% (w/v) tryptone, 2.4% (w/v) yeast extract, 0.4% (v/v) glycerol, 0.17 M KH_2PO_4, 0.72 M K_2HPO_4; 50 µg/µl ampicillin) and grown at 37°C with agitation (200 RPM) until the cultures reached an O.D of 0.5-0.6 for r*Pf*HRP-2. The culture was then supplemented with 1 mM lactose (lactose was used since it has previously been shown inhouse to increase the expression of r*Pf*HRP-2) and grown overnight at 37°C with agitation (200 RPM). For r*Pf*LDH and r*Pf*GAPDH cultures were grown overnight at 37°C.

2.2.3. Ni^{2+}-NTA affinity purification of r*Pf*HRP-2, r*Pf*LDH and r*Pf*GAPDH

After expression of all three proteins, the cells were harvested by centrifugation (5000 x g; 10 min; 4°C), the supernatant was decanted, and the pellet was resuspended in wash buffer (50mM NaH_2PO_4; 300 mM NaCl; 20 mM imidazole) at 20% of the original cell cultures volume. The cells were lysed by sonication (6 x 45 sec at 20% amplitude).

The insoluble cell material was pelleted by centrifugation (12 000 x g; 20 min; 4°C) and the supernatant contained the recombinant protein. A Ni^{2+}-NTA resin was equilibrated with wash buffer and used to affinity purify recombinant proteins. The supernatant fraction was incubated with the resin for an hour at RT on an end over end rotor.

The lysates and Ni^{2+}-matrices were poured into a 10 ml Bio-Rad affinity matrix column. For r*Pf*LDH and r*Pf*GAPDH *E. coli* (BL21) DE3 proteins were washed away with wash buffer (50mM NaH_2PO_4; 300 mM NaCl; 20 mM imidazole) and the recombinant protein was eluted with elution buffer (50mM NaH_2PO_4; 300 mM NaCl; 250 mM imidazole).

For r*Pf*HRP-2, two wash steps were required, buffer 1 (50mM NaH_2PO_4; 300 mM NaCl; 20 mM imidazole) and wash buffer 2 (50mM NaH_2PO_4; 300 mM NaCl; 250 mM imidazole). r*Pf*HRP-2 was eluted with 500 mM imidazole.

2.2.4. SDS-PAGE

The protein samples purity was determined by running the samples on a 12.5% reducing SDS-PAGE gels that were stained with Coomassie brilliant blue R-250 for analysis (Laemmli, 1970). The gels were run at 20 mA.

2.2.5. Western blotting

The western blotting procedure was followed as per Towbin *et al*., (1979). In brief, electrophoresis on an SDS-PAGE gel, the protein was transferred to the nitrocellulose paper overnight at 20 mA and proteins were visualised by staining with Ponceau S (0.1% (w/v) Ponceau S, 15% (v/v) acetic acid).

The nitrocellulose membrane was blocked with (5% (w/v) low fat milk powder in TBS-Tween-20 (20 mM Tris-HCl buffer; 200 mM NaCl; pH 7.4); 0.1% Tween-20)) for an 1 h at RT. Primary antibody solutions (either monoclonal mouse anti-His-tag IgG (1/6000) or polyclonal chicken ant-r*Pf*HRP-2 IgY (1 µg/ml); made up in 0.5%(w/v) BSA-PBS) were added and incubated at RT for 2 h. A secondary antibody (either goat anti-mouse IgG-HRPO (1/6000) or rabbit anti-chicken IgG-HRPO (1/10 000) in 0.5%(w/v) BSA-PBS) was added and incubated at RT for 1 h. After each incubation the nitrocellulose was washed (3 x 5 min) using TBS-Tween 20 (0.1% (w/v)). Finally, proteins recognised by the antibodies were visualised using 4-chloro-1-naphthol·H2O2 substrate (0.06% (w/v) 4-chloro-1-naphthol, 0.1% (v/v) methanol and 0.0015% (v/v) H2O2 in TBS) in the dark.

2.2.6. Bradford protein determination

The Bradford method was used to determine protein concentration (Bradford, 1976). Concentrations of unknown protein samples were calculated from a BSA (Bradford standard curve) standard curve 0 -50 µg and was measured at 595 nm.

2.2.7. Isolation of anti-r*Pf*HRP-2 IgY from chicken eggs

Eggs from chickens immunised with antigen were collected and stored at 4°C. Anti-r*Pf*HRP-2 IgY was purified by the method described by Polson *et al*., (1985).

2.2.8. Affinity purification of anti-r*Pf*HRP-2 IgY

Anti-r*Pf*HRP-2 IgY was affinity purified using an r*Pf*HRP-2-AminoLink^{Tm} matrix (Qoronfleh *et al.,* 2003).

2.2.9. Indirect ELISA for determining the LOD of r*Pf*HRP-2 detected using anti-r*Pf*HRP-2

r*Pf*HRP-2 was diluted in PBS (pH 7.0) at various concentrations and pipetted into wells of Nunc Maxi Sorp^{Tm} 96 well ELISA plates and incubated overnight at 4°C. All steps were done at 37°C. Wells were blocked with 150 µl BSA-PBS 0.5% (w/v) for 1 h.

r*Pf*HRP-2 (75 ng in BSA-PBS 0.5%(w/v) was added to each well and incubated for 2 h, (100 µl) rabbit anti-chicken IgG-HRPO (1/10 000 in BSA-PBS 0.5%(w/v) was added for 1 h. Wash steps were performed before each incubation step using PBS-Tween 20 (0.1%(v/v)). 150 µl of substrate (TMB (426 µM); H_2O_2 (1.176 mM in citrate-phosphate buffer (150 mM; pH 5.0)). After an hour the plates were read at 652 nm (Versamax^{Tm} microplate reader).

The controls were: no r*Pf*HRP-2 coat, no blocking, no anti-r*Pf*HRP-2 IgY coat and no rabbit anti-chicken IgY coat. All results were corrected for background by subtracting the relevant controls.

2.2.10. Standard protein thermodenaturation differential scanning fluorometry assay to measure the T_m of proteins

The assay described by Niesen *et al*., (2007) with minor modifications was followed. Protein at 2.5 µg was typically used unless otherwise stated in 7.5 µl AMT buffer (200 mM Na-acetate buffer; 200 mM MES and 400 mM Tris-HCl; pH 4-9), 7.5 µl dH_2O and 10x SYPRO Orange.

The assay was run in xtra-clear qPCR tubes (Star labs) in a Rotor-Gene 6000 RT-PCR machine (Corbett). The condition parameters set were high resolution melt (HRM) which has an ƛexcitation = 460 nm and an ƛemission at 510 nm, which was used to measure the SYPRO Orange fluoresce probe. A temperature range of 25°C to 95°C was used with a ramp temperature of 0.3°C/sec.

Proteins tested in the assay were carbonic anhydrase; r*Pf*HRP-2; anti-r*Pf*HRP-2 IgY; r*Pf*LDH; anti-r*Pf*LDH IgY, r*Pf*LDH; r*Py*LDH; anti-r*Pf*LDH IgY raised against a common epitope (APGKSDKEWNRDDL) and r*Py*LDH.

2.2.11. Measuring antigen-antibody interactions

The standard conditions were used to measure protein-protein interactions. Varying concentration of proteins were used. r*Pf*HRP-2 (1 µg) and anti-r*Pf*HRP-2 IgY (4 µg) were pre incubated at 37°C for 2 h, r*Pf*LDH (1 µg) and anti-r*Pf*LDH IgY (1, 2, 3, 4 µg; against the whole protein) was incubated at 4°C or 37°C for 2 h, r*Pf*LDH (1 µg) and r*Py*LDH (1 µg) and anti-r*Pf*LDH IgY (1 or 4 µg; against the common peptide) were incubated for 2 h at 37°C. All incubations were done at pH values of 4, 7 and 9 in AMT buffer and then SYPRO Orange was added and DSF analysis was carried out.

2.2.12. DSF analysis of anti-malaria drugs with r*Pf*LDH and r*Pf*GAPDH

1 mM anti-malaria drugs (chloroquine, pyrimethamine, amodiaquine and quinine) were incubated with both r*Pf*LDH and r*Pf*GAPDH at 4°C for 30 min in AMT buffer (pH 6.0) followed by SYPRO Orange and DSF analysis was carried out under the standard assay.

2.2.13. Processing DSF data

Rotor-gene series 6000 software was used to capture fluorescence data from the thermodenaturation of proteins. The change in fluorescence/ change in temperature (dF/dT) was calculated and the dF/dT data was plotted against temperature and the highest dF/dT point on each peak was referred to as the T_m.

2.2.14. *In silico* methods showing chloroquine and quinine interacted with r*Pf*LDH and r*Pf*GAPDH

Molecular docking studies were carried out using the Schrodinger molecular docking suite (Schrodinger 2018-2). Chloroquine and quinine binding to r*Pf*LDH (PDB 1CET) and r*Pf*GAPDH (PDH 1WYG) were docked. The docking studies were followed as described by Kumar *et al*., (2015) where the default setting of the Schrodinger software was used. Protein was prepared by bringing the protein to its correct conformation, as sometimes when being crystallised, certain amino acid residues may be left out, bond lengths may be incorrect, and various other abnormalities are resolved. Thereafter, either chloroquine or quinine was drawn using the Maestro 2D work space to draw small molecules. The current bound ligand was removed, and the new drawn ligand was prepared. A grid was drawn around the site at which the previous ligand was bound. The grid determines the area analysed for binding sites, a grid of 15 $Å^2$ was used and a scan was performed to determine if binding had occurred. Validation by redocking was carried out. The validation was performed by removing the original ligand from either *Pf*LDH and *Pf*GAPDH. The receptor (binding site) was then prepared in the absence of the ligand, this was to bring the protein back to its native state. Then the ligand initially removed was docked once again to confirm the ligand bound in the same conformation as the x-ray crystallography structure depicts.

2.3. Results

2.3.1. Expression and purification of recombinant proteins from *E. coli* BL21 (DE3)

*Pf*HRP-2 was recombinantly expressed as a His-tag fusion protein from the gene cloned into a pET-15(b) plasmid in an *E. coli* Bl21 (DE3) bacterial host. The recombinant protein was affinity purified using a Ni^{2+} chelate chromatography matrix. An SDS-PAGE and a western blot illustrating the steps for purification of r*Pf*HRP-2 as shown in Figures 2.1A and B.

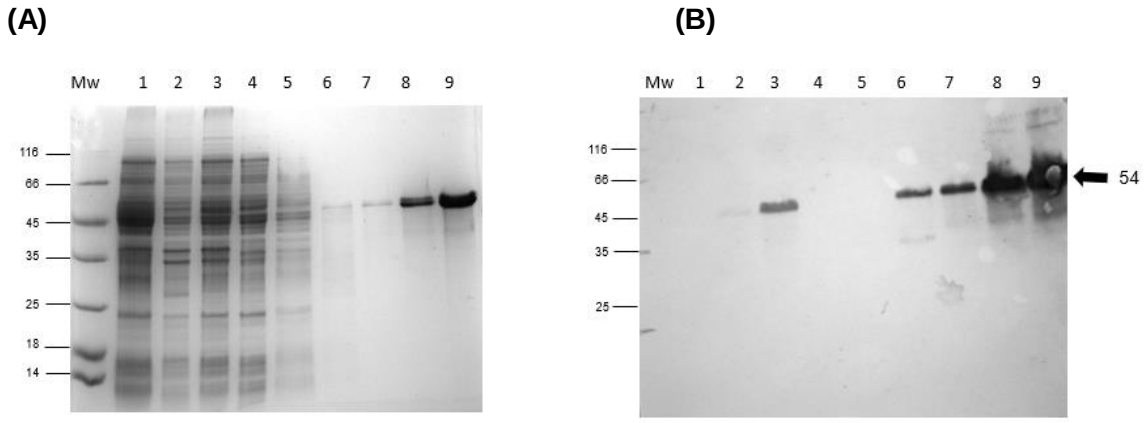

Figure 2.1: Recombinant expression and Ni^{2+}-chelate affinity purification of *Pf*HRP-2 analysed by SDS-PAGE and western blottting. *Pf*HRP-2 was expressed in *E. coli* BL21(DE3) cells as a His_6-tag fusion protein and was purified using Ni^{2+}-chelate affinity chromatography. Each step of the purification was analysed on a 12.5% reducing SDS-PAGE gel **(A)** and proteins on a duplicate gel were electrophoretically transferred to nitrocellulose and probed with anti-His tag mouse monoclonal antibody and a secondary goat anti-mouse-HRPC antibody **(B).** Molecular weight marker (Mw); *E. coli* BL21 (DE3) untransformed cell lysate (lane 1); cell culture pellet (lane 2); cell lysate supernatant (lane 3); r*Pf*HRP-2 unbound fraction (lane 4); 20 mM imidazole wash sample (lane 5); 250 mM imidazole wash sample (lane 6); eluents 1-3 with 500 mM imidazole (lanes 7 -9). The SDS-PAGE gel was stained with Coomassie brilliant blue R-250.

Untransformed *E*. *coli* BL21 (DE3) lysates showed that r*Pf*HRP-2 was not expressed by the host cells alone. r*Pf*HRP-2 was isolated as a 54 kDa protein band (Figure 2.1A lanes 7-9) and ran as a doublet. The fusion protein is 24 kDa larger than the expected size of PfHRP-2, which is 30 kDa (Ndonwi *et al*., 2011). An additional 250 mM wash step had to be included to remove contaminating proteins that were found to have a high binding affinity for the Ni^{2+}-NTA resin (Figure 2.1A lane 6).

To confirm the identity of the expressed His-tagged r*Pf*HRP-2, a western blot was performed (Figure 2.1B) and probed with mouse anti-His tag IgG antibody. No proteins were detected by the antibody in the *E.coli* BL21(DE3) untransformed cell lysate. Transformed *E. coli* cells had bands of 54 kDa detected (Figure 2.1B; lanes 2 and 3), which indicated that r*Pf*HRP-2 was present in the starting sample and lysate. r*Pf*HRP-2 was eluted over three fractions including proteins bands appearing above the 116 kDa protein marker were detected in (Figure 2.1B lanes 7 to 9), which could potentially be protein aggregates.

2.3.2. Detecting r*Pf*HRP-2 using anti-r*Pf*HRP-2 IgY

An observation was noticed in Figure 2.1A where several proteins in lane 6 had a high affinity for the Ni^{2+}-NTA resin. The 250 mM wash (Figure 2.1, lane 6) was diluted by the large volume of buffer therefore in a separate purification, individual fractions of each purification step were collected and run on an SDS-PAGE gel and western blot (Figure 2.2A and B).

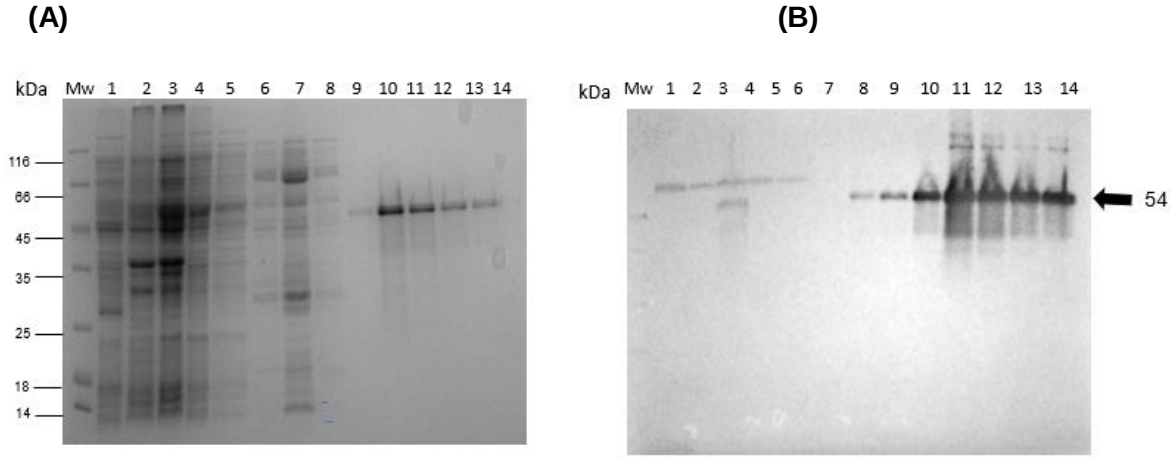

Figure 2.2: Recombinant expression and Ni^{2+}-chelate affinity purification of *Pf*HRP-2 analysed by SDS-PAGE and western blotting. *Pf*HRP-2 was expressed in *E.coli* BL21(DE3) cells as a His_6-tag fusion protein and was purified using Ni^{2+}-NTA chelate affinity chromatography. Each step of the purification was analysed on a 12.5% reducing SDS-PAGE gel **(A)** and proteins on a duplicate gel were electrophoretically transferred to a nitrocellulose and probed with polyclonal chicken anti-r*Pf*HRP-2 IgY and a secondary mouse anti-rabbit-HRPC IgG **(B).** Molecular weight marker (Mw); *E. coli* BL21(DE3) untransformed cell lysate (lane 1); cell culture pellet (lane 2); cell lysate supernatant (lane 3); r*Pf*HRP-2 unbound fraction (lane 4); 20 mM imidazole wash sample (lane 5); 250 mM imidazole wash samples (lane 6-8); eluents 1-6 with 500 mM imidazole (lanes 9 -14). The SDS-PAGE gel was stained with Coomassie brilliant blue R-250.

The pattern and samples for lanes 1 to 5 (Figure 2.2A) were the same as Figure 2.1A. The difference was in the running of the 3 250 mM imidazole wash steps (lanes 6 to 8). There are about 18 proteins (proteins) that were not eluted by the 20 mM imidazole wash (lane 5), indicating their high affinity for the Ni^{2+}-NTA resin.

All proteins were not detected by the mouse monoclonal anti-His-tag IgG (Figure 2.1B) or the chicken polyclonal anti-r*Pf*HRP-2 IgY (Figure 2.2B) except for r*Pf*HRP-2. Figure 2.2B also had a single band that was detected in lanes 1 to 5 which was larger than r*Pf*HRP-2, however, this protein was removed in the wash steps and there was no detection in lanes 9 to 14. Similarly, aggregated and degraded r*Pf*HRP-2 is detected both above and below the 54 kDa r*Pf*HRP-2 band as well as bands above 116 kDa (Figure 2.2B).

2.3.3. Expression and purification of recombinant *Pf*LDH

*Pf*LDH was recombinantly expressed as a His-tag fusion protein from the gene cloned into the pKK-233-3 plasmid in an *E. coli* BL21 (DE3) bacterial host.

The recombinant protein was affinity purified using a Ni^{2+}-chelate chromatography matrix. An SDS-PAGE gel and western blot were used to track the expression and purification of r*Pf*LDH (Figures 2.3A and B).

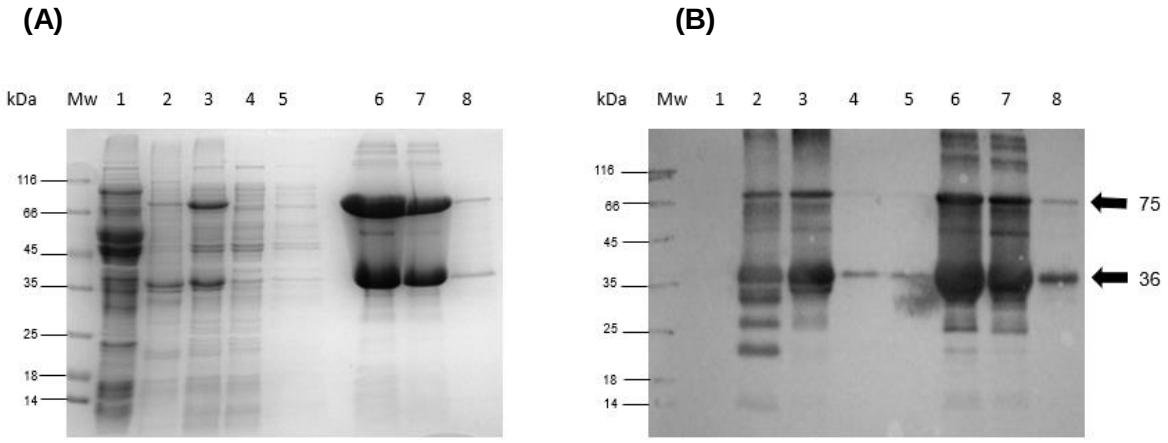

Figure 2.3: Recombinant expression and Ni^{2+}-chelate affinity purification of *Pf*LDH analysed by SDS-PAGE and western blotting. r*Pf*LDH was expressed in *E.coli* BL21(DE3) cells as a His_6-tag fusion protein and was purified using Ni^{2+}-chelate affinity chromatography. Each step of the purification was analysed on a 12.5% reducing SDS-PAGE gel **(A)** and protein on a duplicate gel were electrophoretically transferred to nitrocellulose and probed with anti-His tag mouse monoclonal IgG antibody and a secondary goat anti-mouse IgG-HRPC antibody **(B).** Molecular weight marker (Mw); *E. coli* BL21(DE3) untransformed cell lysate (lane 1); cell culture pellet (lane 2); cell lysate supernatant (lane 3); r*Pf*LDH unbound fraction (lane 4); 20 mM imidazole wash sample (lane 5); fractions eluted with 250 mM imidazole (lanes 6-8). The SDS-PAGE gel was stained with Coomassie brilliant blue R-250.

r*Pf*LDH was not expressed by the host cell alone (Figure 2.3A). Some r*Pf*LDH remained in the unbound fraction (lane 2 and 3). Two major bands at 75 and 36 kDa were eluted from the Ni^{2+}-NTA affinity matrix (lane 6 to 8).

The western blot of the same gel (Figure 2.3A) was probed with mouse anti-His tag IgG (Figure 2.3B). No protein was detected in the untransformed *E. coli* BL21 (DE3) (lane 1). Various bands were detected in lanes 2 and 3, below the 36 and 75 kDa marker. Some r*Pf*LDH at 36 kDa was detected in the unbound fractions (lane 4 and 5) and the eluted fractions picked up various bands, with the major band being 36 kDa (lane 6 to 8). The various bands detected in different lanes were suspected to be degraded and truncated r*Pf*LDH.

2.3.4. Expression and purification of recombinant *Pf*GAPDH

*Pf*GAPDH was recombinantly expressed as a His-tag fusion protein with the gene cloned within a pET-15(b) plasmid in an *E.coli* BL21 (DE3) bacterial host. The recombinant protein was affinity purified using a Ni^{2+}-chelate chromatography matrix. An SDS-PAGE gel and western blot were used to track the expression and purification of r*Pf*GAPDH (Figures 2.4A and B).

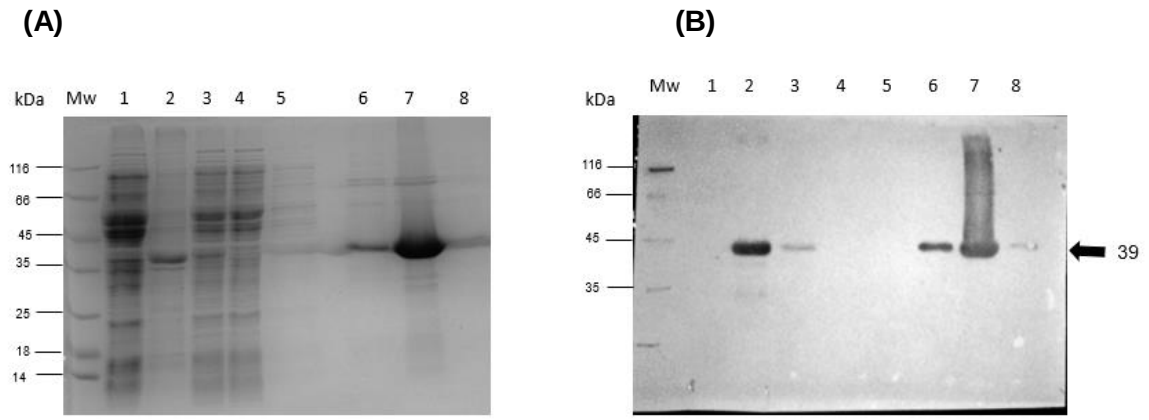

Figure 2.4: Recombinant expression and Ni^{2+}-chelate affinity purification of *Pf*GAPDH analysed by SDS-PAGE and western blotting. r*Pf*GAPDH was expressed in *E.coli* BL21(DE3) cells as a His_6-tag fusion protein and was purified using Ni^{2+}-chelate affinity chromatography. Each step of the purification was analysed on a 12.5% reducing SDS-PAGE gel **(A)** and proteins on a duplicate gel were electrophoretically transferred to nitrocellulose and probed with anti-His tag mouse monoclonal IgG antibody and a secondary goat anti-mouse IgG-HRPC antibody **(B).** Molecular weight marker (Mw); *E. coli* BL21(DE3) untransformed cell lysate (lane 1); cell culture pellet (lane 2); cell lysate supernatant (lane 3); r*Pf*GAPDH unbound fraction (lane 4); 20 mM imidazole wash sample (lane 5); eluents 1-3 with 250 mM imidazole (lanes 6-8). The SDS-PAGE gel was stained with Coomassie brilliant blue R-250.

r*Pf*GAPDH was not expressed by the *E. coli* BL21 (DE3) host cell alone (Figure 2.4A). The fractions eluted of the affinity matrix (lanes 6 to 8) had a major band at 39 kDa, and a few protein bands above and below the 39 kDa band.

The western blot (Figure 2.4B) from the gel (Figure 2.4A) was probed with mouse monoclonal anti-His tag IgG. No protein was detected in the untransformed lane, indicating no host *E. coli* BL21 (DE3) lysate. Only His-tag proteins were detected, indicating the bands in lane 7 could be aggregates or multimers of r*Pf*GAPDH.

2.3.5. Isolation of chicken polyclonal anti-r*Pf*HRP-2 IgY

Eggs from chickens that were previously immunised with r*Pf*HRP-2 were collected on a weekly basis and stored at 4°C. Using the method described by Polson *et al*., (1985). Isolated IgY was affinity purified for anti-r*Pf*HRP-2 IgY using anti-r*Pf*HRP-2 affinity matrix (Figure 2.5A and B).

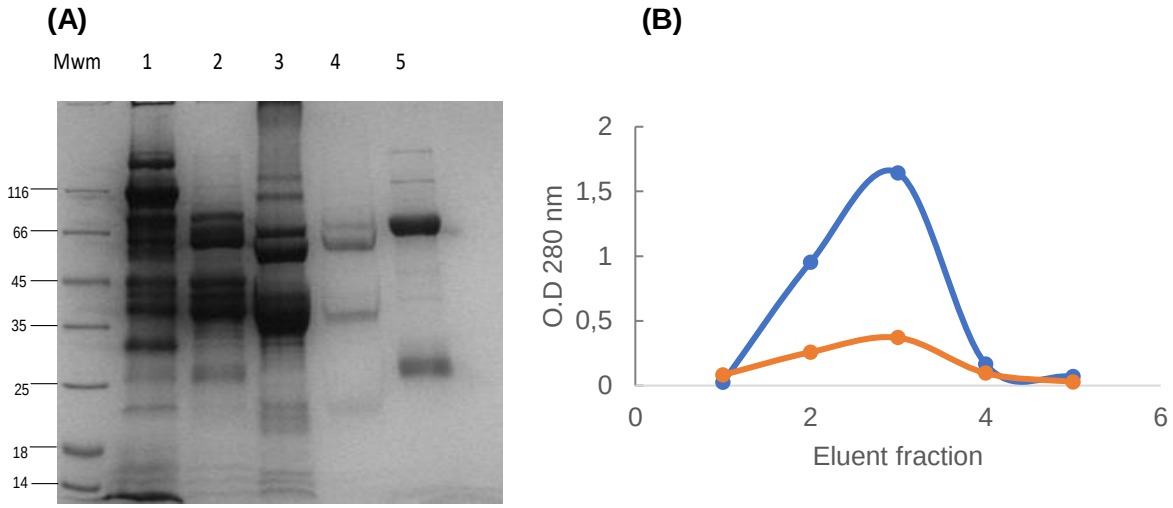

Figure 2.5: Purification of anti-r*Pf*HRP-2 IgY using PEG 6000 analysed by SDS-PAGE and affinity purified using an r*Pf*HRP-2 Aminolink® affinity matrix. A 12.5% reducing SDS-PAGE gels showing each step in IgY purification. The lanes were loaded as follows: molecular weight marker (Mw); whole egg yolk sample (lane 1); filtrate (lane 2); second supernatant (lane 3); third supernatant (lane 4); final pure isolated IgY (lane 5) **(A)**. Measure of affinity purification of anti-r*Pf*HRP-2 IgY. Crude IgY was pooled and affinity purified using a recombinant r*Pf*HRP-2 AminoLink® matrix (•) represents the initial eluents and (•) unbound fraction passed over the recombinant r*Pf*HRP-2 AminoLink® matrix for a second time **(B)**.

Each step in the purification shows proteins being removed (lane 1 to 5), two major bands remain- the heavy chain (HC; 65 kDa) and the light chain (LC; 25 kDa; Figure 2.5A). The bands above the HC are thought to be partially reduced IgY at 90 kDa (Heavy chain + light chain) and the highest band above the 116 kDa marker is unreduced IgY.

Following isolation of chicken IgY containing r*Pf*HRP-2 IgY from chicken egg yolk, the unbound fraction was passed over an r*Pf*HRP-2-Aminiolink® affinity resin. The anti-r*Pf*HRP-2 IgY was affinity purified and the eluents were tracked at an absorbance of 280 nm (Figure 2.5B).

2.3.6. Detection of r*Pf*HRP-2 using anti-r*Pf*HRP-2 IgY

The affinity purified antibody was used in an ELSIA to find the limit of detection of r*Pf*HRP-2 (Figure 2.6), which was 15 ng.

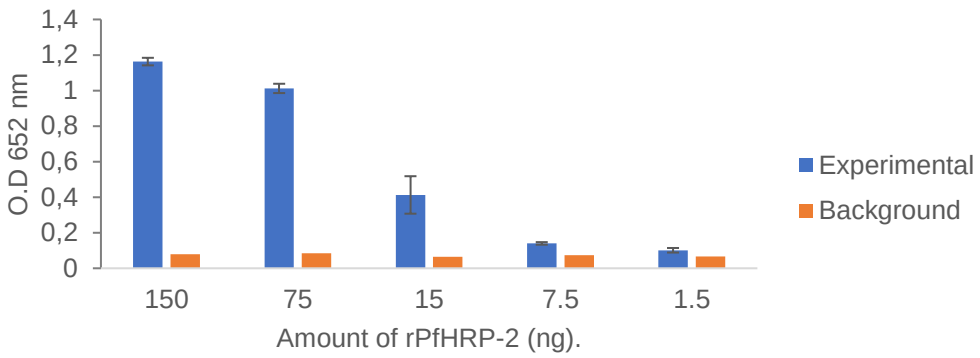

Figure 2.6: Measuring the limit of detection of r*Pf*HRP-2 using anti-r*Pf*HRP-2 IgY. Varying amounts of r*Pf*HRP-2 (150 to 1.5 ng) were coated onto Nunc® 96 well plates and incubated overnight at 4°C. 75 ng of anti-r*Pf*HRP-2 IgY served the primary antibody and rabbit anti chicken HRPC secondary antibody was used. Error bars indicate the S.D of triplicate results.

2.3.7. Differential scanning fluorometry: Optimising a DSF assay using carbonic anhydrase

Carbonic anhydrase was used as a control protein to optimise conditions for the DSF assay. The protein was shown by Wright *et al*., (2017) to be a suitable candidate for thermal melt curve analysis. Carbonic anhydrase shows very little initial fluorescence and fluorescence increases as the protein denatures. The fluorescence curves fitted with a sigmoidal curve are not shown as it is difficult to interpret the T_m from those curves. A first derivative (dF/dT) was employed as the peak of the curve corresponds to the predicted T_m (Niesen *et al*., 2007). AMT buffers ranging from pH 4 to 9 were tested with carbonic anhydrase (Figure 2.7).

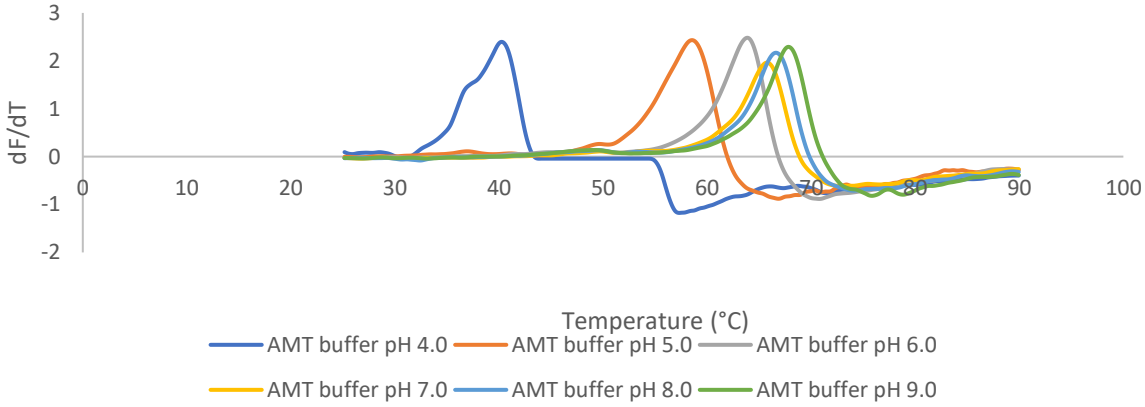

Figure 2.7: DSF first derivative of fluorescence data for carbonic anhydrase at different pH values. Carbonic anhydrase was added to AMT buffers ranging from pH 4 to 9. SYPRO Orange was added and the raw fluorescence data were measured from 25°C to 95°C and the first derivative was calculated and presented.

When carbonic anhydrase was in alkaline AMT buffers (Figure 2.7), the protein had a higher T_m. The highest T_m for carbonic anhydrase was at pH 9 (67.85°C) and the lowest at pH 4 (40.25°C). Calculation of the first derivative data from fluorescence raw data was done using Rotor-Gene-6000 software.

Each curve appeared ideal by starting off with a low dF/dT and there were no major changes in the thermal melt profile. This was significant as its implied AMT buffers were suitable with carbonic anhydrase at a pH of 4 to 9 while keeping the ionic strength constant.

2.3.8. Measurement of carbonic anhydrase T_m in the presence of Zn^{2+}

Carbonic anhydrase has been shown to bind Zn^{2+} at an allosteric site (Sanyal and Maren, 1981). Therefore, the T_m of carbonic anhydrase was determined in the presence of Zn^{2+} with an AMT buffer (pH 9.0) to test if there would be a shift in T_m (Figure 2.8).

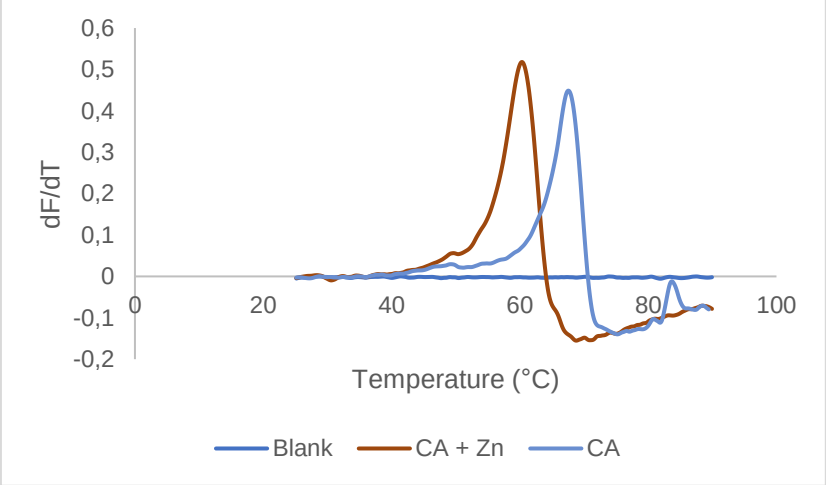

Figure 2.8: DSF first derivative of fluorescence data for carbonic anhydrase in the presence of Zn^{2+}. Carbonic anhydrase was added to AMT buffer at pH 9 and was incubated with Zn^{2+} (1 mM). SYPRO Orange was then added and raw fluorescence was measured from 25 to 95°C and the first derivative was calculated and presented.

A peak shift from 67.85°C (apo carbonic anhydrase) to 60.75°C (Zn^{2+}- carbonic anhydrase) was observed (Figure 2.8). This implies carbonic anhydrase was destabilised. Zn^{2+} did not interfere with SYPRO Orange in the control experiment.

2.3.9. Thermodenaturation of r*Pf*HRP-2

The stability of r*Pf*HRP-2, r*Pf*LDH and r*Pf*GAPDH and chicken IgY antibodies raised against r*Pf*HRP-2, r*Pf*LDH and antigen-antibody interactions were all analysed by looking at their thermodenaturation profiles using our optimised DSF assay. The first *P. falciparum* diagnostic protein analysed was r*Pf*HRP-2 (Figure 2.9).

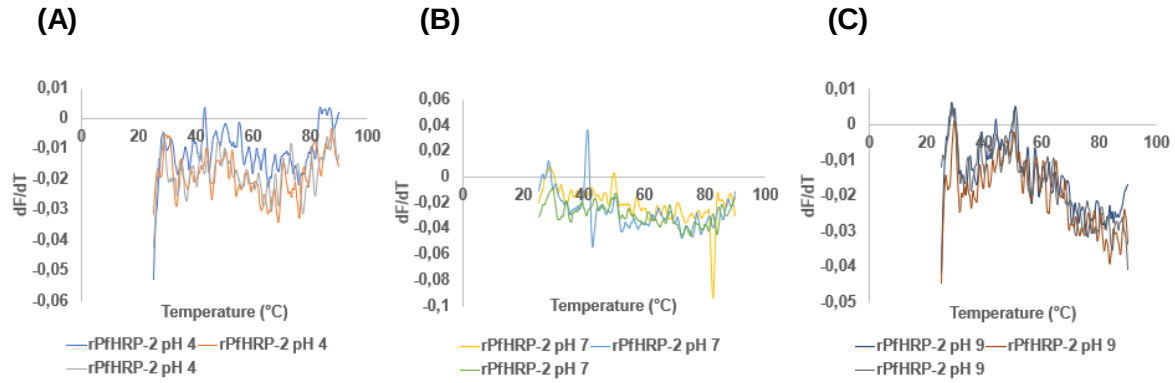

Figure 2.9: DSF First derivative of fluorescence data for r*Pf*HRP-2 at different pH values. r*Pf*HRP-2 in AMT buffer at pH 4 **(A)**, pH 7 **(B)** and pH 9 **(C)**. SYPRO Orange was added and the raw fluorescence data was measured from 25 to 95°C and the first derivative was calculated and presented. Each panel represents triplicate results.

The dF/dT curves (Figure 2.9A to C) could not be used to obtain a T_m value from, as there was no transition (peaks) observed at any of the 3 pH values (4,7 and 9) with SYPRO Orange.

2.3.10. DSF analysis of thermodenaturation of anti-r*Pf*HRP-2 IgY

The thermodenaturation analysis chicken anti-r*Pf*HRP-2 IgY at pH values of 4,7 and 9 and the DSF dF/dT curves of raw fluorescence data was plotted (Figure 2.10).

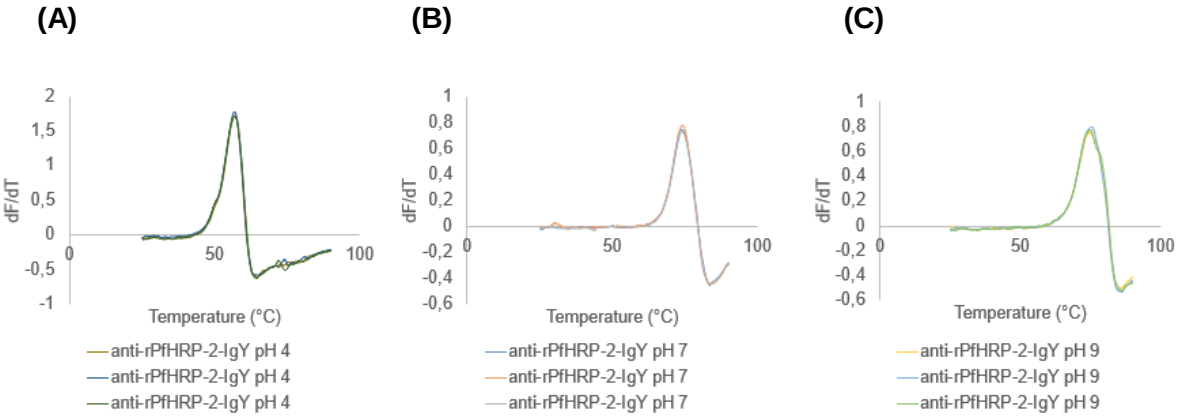

Figure 2.10:DSF first derivative of fluorescence data for anti-r*Pf*HRP-2 IgY at different pH values. Anti-r*Pf*HRP-2 IgY in AMT buffer at pH 4 **(A)**, pH 7 **(B)** and pH 9 **(C)**. SYPRO Orange was added and the raw fluorescence data was measured from 25 to 95°C and the first derivative was calculated and presented. Each panel represents triplicate results.

The analysis of anti r*Pf*HRP-2 IgY antibodies showed lower T_m observed at pH 4 (T_m 56.98°C) indicating it was least stable, while anti-r*Pf*HRP-2 IgY was most stable at pH 9 (T_m 75.08°C; Figure 2.10). A pH of 4 resulted in a 2-fold higher fluorescence peak amplitude compared to pH 7 and 9. The amplitude of the peak, however, is based on arbitrary relative fluorescence units (RFU) and does not play a role in determining T_m of a protein.

2.3.11. DSF analysis of thermodenaturation of r*Pf*HRP-2 interacting with anti-r*Pf*HRP-2 IgY

Since the T_m for r*Pf*HRP-2 could not be determined (Figure 2.9), r*Pf*HRP-2 binding to anti-r*Pf*HRP-2 IgY was evaluated with DSF (Figure 2.11).

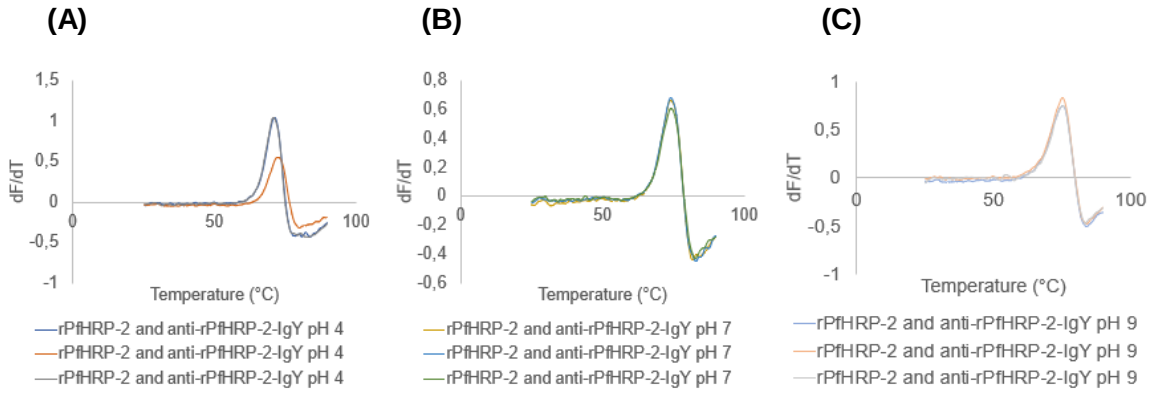

Figure 2.11: DSF first derivative of fluorescence data for anti-r*Pf*HRP-2 IgY interacting with r*Pf*HRP-2 at different pH values. Anti-r*Pf*HRP-2 IgY in AMT buffer at pH 4 **(A)**, pH 7 **(B)** and pH 9 **(C)** were incubated with r*Pf*HRP-2 in a 4:1 ratio. SYPRO Orange was added and the raw fluorescence data was measured from 25 to 95°C of which the first derivative was calculated and presented. Each panel represents triplicate results.

When r*Pf*HRP-2 is in the presence of anti-r*Pf*HRP-2 IgY, DSF dF/dT curves are obtained at all three pH values (4, 7 and 9). At pH 4, there is evidence of a more stable species being formed, as there is a T_m shift from 59.75°C (anti-r*Pf*HRP-2 IgY; Figure 10A) to 71.1°C (Figure 11A). The 11.35°C difference in T_m is an indication that anti-r*Pf*HRP-2 IgY bound to r*Pf*HRP-2 forming a more stable complex. At pH 7 and 9 (Figures 2.11B and C) there was no significant T_m shifts compared to anti-r*Pf*HRP-2 IgY alone (Figure 2.10B and 7). At pH 7, the complex had a Tm 0.07°C lower than anti- r*Pf*HRP-2 alone while at pH 9 the complex had a Tm of 0.47°C higher than the anti- r*Pf*HRP-2 IgY molecule.

2.3.12. DSF analysis of thermodenaturation of r*Pf*LDH and anti-r*Pf*LDH IgY

The second *P. falciparum* diagnostic protein analysed for its thermal stability was r*Pf*LDH using DSF dF/dT curves to obtain a T_m at different pH values (4 to 9; Figure 2.12).

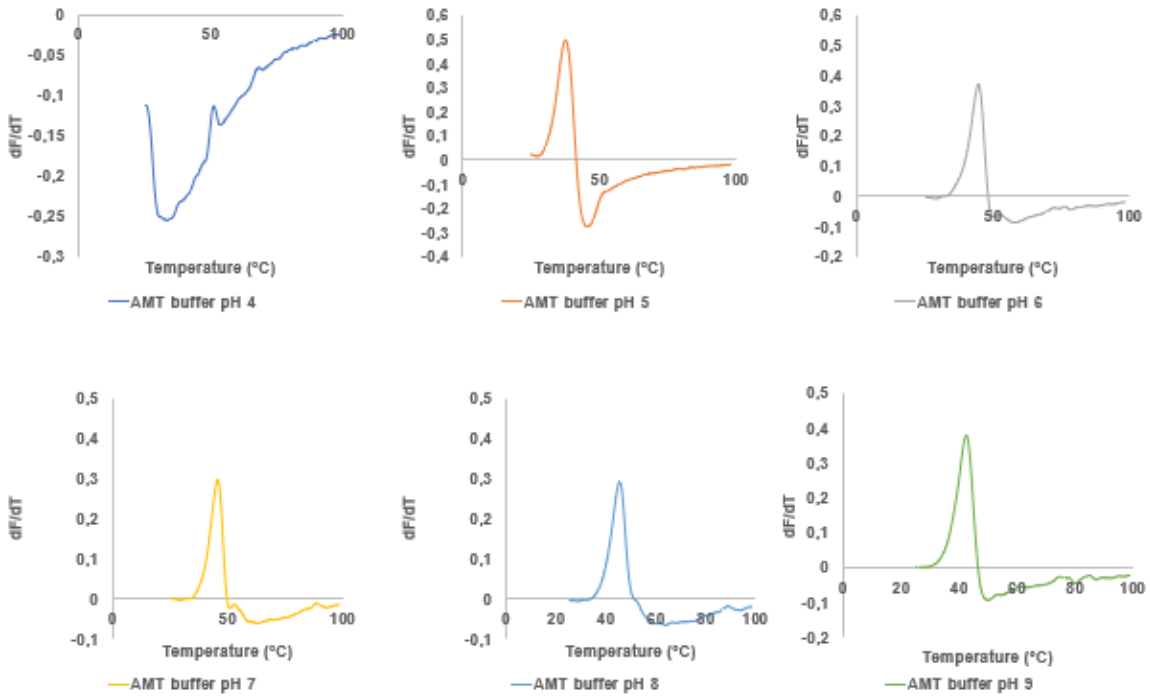

Figure 2.12: DSF first derivative of fluorescence data for r*Pf*LDH at different pH values. r*Pf*LDH in AMT buffer from pH 4 to 9. SYPRO Orange was added and the raw fluorescence data was measured from 25 to 95°C of which the first derivative was calculated and presented.

r*Pf*LDH at different pH values were shown to have different T_m's (Figure 2.12). A T_m for r*Pf*LDH at pH 4 could not be determined from the dF/dT profile. At pH 5, r*Pf*LDH was least stable with a T_m of 37.92, while at pH values of 6, 7 and 8 had similar T_m's at 44.58°C, 45.75°C and 45.59°C respectively and pH 9 had a T_m of 42.42°C. The T_m values indicate r*Pf*LDH is most stable at pH's 6 to 8. The amplitude of the peaks for r*Pf*LDH was in general higher when r*Pf*LDH was less stable (pH 5 and 9).

2.3.13. DSF thermodenaturation of anti-r*Pf*LDH IgY

Following the determination of T_m for r*Pf*LDH, DSF analysis for the thermodenaturation of anti-r*Pf*LDH IgY against the whole r*Pf*LDH protein was analysed (Figure 2.13).

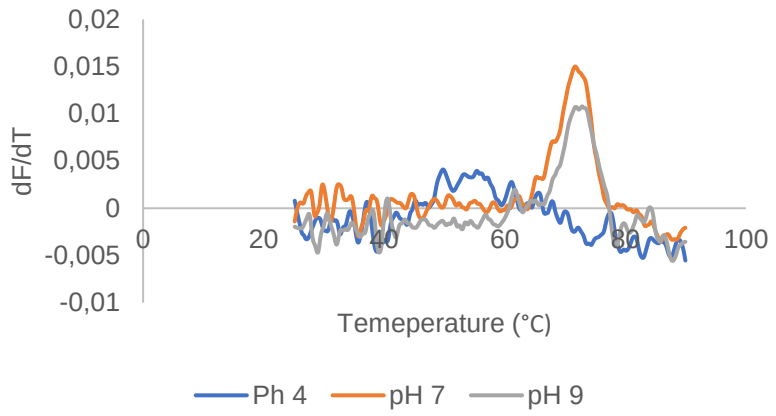

Figure 2.13: DSF first derivative of fluorescence data for anti-r*Pf*LDH IgY at different pH values. Anti-r*Pf*LDH IgY (against r*Pf*LDH) in AMT buffers at pH of 4 7 and pH 9. SYPRO Orange was added and the raw fluorescence data was measured from 25 to 95°C of which first derivative was calculated and presented.

Analysis of anti-r*Pf*LDH-IgY antibodies was found to have a high noise to signal ratio (Figure 2.13). At a pH of 4, a T_m for the anti-r*Pf*LDH IgY could not be determined by the dF/dT melt profile as there was an absence of a single transition, while the T_m at pH of 7 and 9 was 72.05°C and 73.45°C respectively. The peak at pH 9, seemed to have two minor peaks present, while the peak at pH 7 had a higher amplitude.

2.3.14. DSF analysis of the thermodenaturation of anti-r*Pf*LDH IgY + r*Pf*LDH

Next r*Pf*LDH and anti-r*Pf*LDH IgY were evaluated in the same sample using DSF (Figure 2.14).

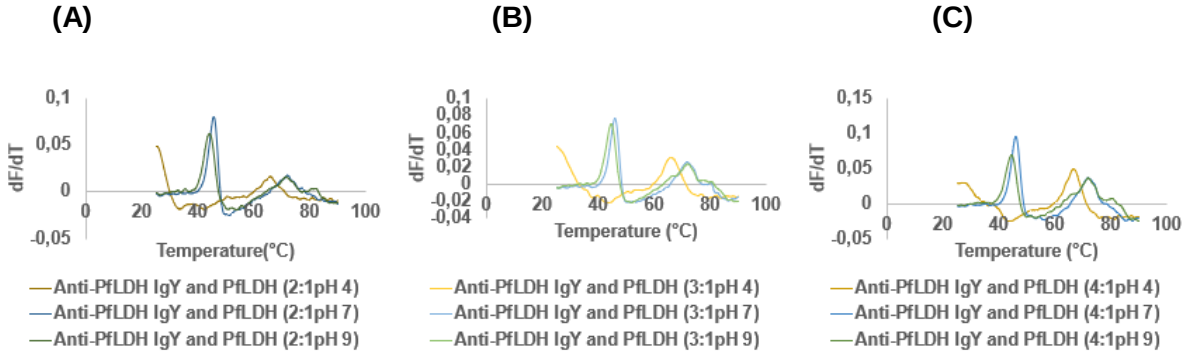

Figure 2.14: DSF first derivative of fluorescence data for anti-r*Pf*LDH IgY in the presence of r*Pf*LDH. Anti-r*Pf*LDH IgY in AMT buffer at pH 4, pH 7, pH 9 was incubated with r*Pf*LDH in a 2:1 ratio **(A)**; Anti-r*Pf*LDH IgY in AMT buffer at pH 4, pH 7, pH 9 was incubated with r*Pf*LDH in a 3:1 ratio (**B)**; Anti-r*Pf*LDH IgY in AMT buffer at pH 4, pH 7, pH 9 was incubated with r*Pf*LDH in a 4:1 ratio **(C)**. Each panel represents the interaction at 4°C. SYPRO Orange was added and the raw fluorescence data was measured from 25 to 90°C and the first derivative was calculated and presented.

A single peak (transition) was present at pH 4 with a T_m of 66.75°C (Figure 2.14A). This is an indication of a stabilised complex anti-r*Pf*LDH IgY due to r*Pf*LDH binding.

A similar result was observed for anti-r*Pf*HRP-2 IgY where it was stabilised by r*Pf*HRP-2 being bound at pH 4 (Figure 2.11A). For the sample with anti-r*Pf*LDH IgY and r*Pf*LDH Two peaks (transitions) were present with a T_m's of 45.45°C and 71.75°C for peaks 1 and 2 at pH 7 and 43.75°C and 71.75°C for peaks 1 and 2 at pH 9. At pH of 9 the r*Pf*LDH peak was 1.33°C higher T_m.

Similar trends in T_m were observed in Figure 2.14B and 2.14C, which was a single peak at a pH of 4 (the stabilised IgY), at pH 7 and 9 there were two peaks which was r*Pf*LDH with the lower T_m and anti-r*Pf*LDH IgY with the higher T_m. There was also the predicted increase in the amplitude of the second peak due to the presence of a higher anti-r*Pf*LDH IgY concentration. Due to the large volume of T_m data obtained, all values were summarised in Table 2.1. With the addition of r*Pf*LDH and anti-r*Pf*LDH IgY in a 1:1 ratio and the r*Pf*LDH and anti-r*Pf*LDH IgY been incubated together at 37°C.

2.3.15. DSF analysis of thermodenaturation of anti-r*Pf*LDH IgY

A third peak (Figure 14B and 14C) with a low amplitude was observed and is thought to be a stabilised anti-r*Pf*LDH IgY complex. To more clearly visualise the third peak and get the T_m, the DSF assay was repeated with the incubation of anti-r*Pf*LDH IgY with r*Pf*LDH done at 37°C (Figure 15A and B).

(A) **(B)**

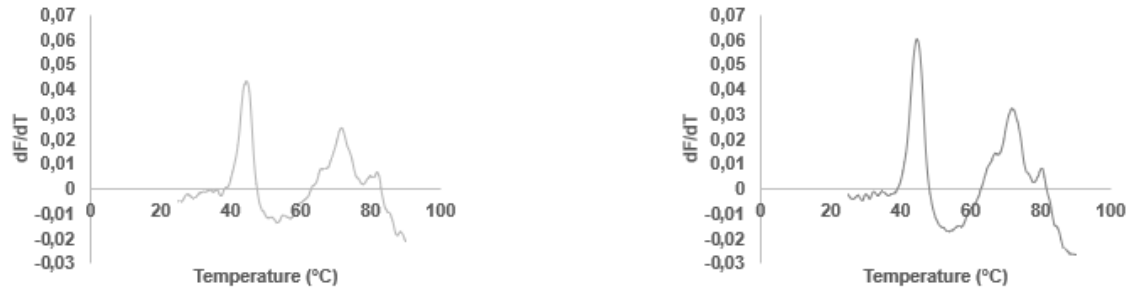

Figure 2.15: DSF first derivative of fluorescence data for anti-r*Pf*LDH IgY interacting with r*Pf*LDH at pH 9. Anti-r*Pf*LDH IgY in AMT buffer at pH 9 was incubated with r*Pf*LDH (3:1 ratio) **(A)**; Anti-r*Pf*LDH IgY in AMT buffer at pH 9 was incubated with r*Pf*LDH (in a 4:1 ratio) **(B)**. SYPRO Orange was added and the raw fluorescence data was measured from 25 to 95°C of which the first derivative was calculated and presented.

The T_m's of the three peaks (Figure 2.15A) were 44.65°C, 71.65°C and 81.85°C and 44.65°C, 71.75°C, and 80.35°C (Figure 2.15B). The third peak was more prominent when 4 µg of anti-r*Pf*LDH IgY was present, however the T_m was 1.5°C lower. Interestingly, the first peak (r*Pf*LDH) had a 2°C higher T_m compared to r*Pf*LDH at pH 9, signifying r*Pf*LDH in the presence of anti-r*Pf*LDH IgY was stabilised.

Table 2.1: Thermal melt temperature (T_m) results from DSF analysis of anti-r*Pf*LDH IgY interacting with r*Pf*LDH at different ratios.

The ratio of anti-r*Pf*LDH to r*Pf*LDH	Incubation temperature (°C)	pH	Melt temperature (°C)		
			Peak 1	Peak 2	Peak 3
1:1	4°C	4	-	65.75	-
		7	45.45	71.75	-
		9	43.75	71.75	-
2:1	4°C	4	-	65.75	-
		7	45.65	72.05	-
		9	43.95	71.65	80.75
3:1	4°C	4	-	65.85	-
		7	45.85	71.75	-
		9	44.45	71.95	80.35
4:1	4°C	4	-	66.65	-
		7	46.05	71.75	-
		9	44.45	71.85	80.35
1:1	37°C	4	-	66.05	-
		7	45.55	71.45	-
		9	43.95	71.65	-
2:1	37°C	4	-	65.85	-
		7	45.75	72.25	
		9	44.15	72.15	80.25
3:1	37°C	4	-	66.35	-
		7	45.85	71.75	-
		9	44.65	71.65	81.85
4:1	37°C	4	-	66.35	-
		7	45.95	71.95	-
		9	44.65	71.75	80.35

The first column refers to the ratios of protein used. The second column indicates the temperature at which anti-r*Pf*LDH IgY was incubated with r*Pf*LDH. The third column refers to the pH at which the experiment was performed. The last 3 columns are the T_m of each peak, with the dashes indicating a T_m could not be determined.

In summary, the results of Table 2.1 showed that when anti-r*Pf*LDH IgY was incubated with r*Pf*LDH at 4°C and 37°C, the change in temperature had no significant change in the species formed or significant change in the stabilising effect, since T_m were similar.

2.3.16. A comparison of common epitope anti-r*Pf*LDH IgY with r*Pf*LDH and r*Py*LDH

Following the thermodenaturation DSF dF/dT curves of r*Pf*LDH with anti-r*Pf*LDH IgY, DSF analysis was done on anti-r*Pf*LDH IgY that was raised against a common malaria LDH epitope (APGKSDKEWNRDDL). The aim was to compare two variables. Firstly, is a r*Pf*LDH complex with anti-r*Pf*LDH IgY raised against the whole protein is more stable than a r*Pf*LDH-anti-r*Pf*LDH IgY raised against the common epitope? The second experiment compared the T_m of the anti-r*Pf*LDH IgY (common epitope) and r*Pf*LDH to a complex of anti-r*Pf*LDH IgY (common epitope) and r*Py*LDH. The DSF thermodenaturation analysis of the common epitope ant-r*Pf*LDH IgY antibodies is shown in Figure 2.16.

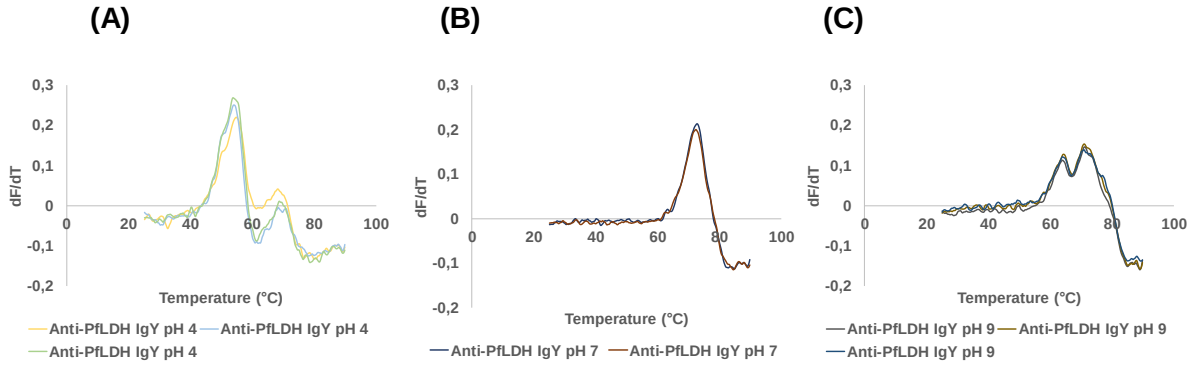

Figure 2.16: DSF first derivative of fluorescence data for anti-r*Pf*LDH IgY at different pH values. Anti-r*Pf*LDH IgY in AMT buffer at pH 4 **(A)**, pH 7 **(B)** and pH 9 **(C)**. SYPRO Orange was added and the raw fluorescence data was measured from 25 to 95°C and the first derivative was calculated and presented. Each panel represents triplicate results.

The T_m for anti-r*Pf*LDH IgY obtained from DSF analysis (Figure 2.16A to C), showed that the IgY was least stable at pH 4 as was the case for all IgY molecules analysed thus far. The T_m at pH 4 was 54.32°C, there was a presence of the formation of a second peak around 68°C, however, the peak was minor and not distinct (Figure 2.16A). At pH 7 the T_m was 72.65°C, the quality of the curve was good as there was little signal below the x-axis (Figure 2.16B). This indicates that the IgY molecules are likely in a stable conformation. At a pH value of 9 there is the presence of two peaks, the first and second with T_m of 64.15°C and 71.08°C (Figure 2.16C). Two peaks generally indicate the presence of different domains of the IgY molecule.

2.3.17. Comparison of both r*Pf*LDH molecules using DSF

Anti-r*Pf*LDH IgY raised against the entire protein (Figure 2.13) had a different dF/dT profile to that of anti-r*PfL*DH IgY raised against the common malaria LDH epitope (Figure 2.16).

At pH 4 (Figure 2.13A) the dF/dT curve for anti-r*Pf*LDH IgY (against the protein) had no transition therefore a T_m could not be interpreted from the dF/dT curve.

The second major difference between the both anti-r*Pf*LDH IgY molecules was observed at pH 9 where the anti-r*Pf*LDH IgY (against LDH) was most stable with a T_m of 73.45°C while in Figure 2.16C anti-r*Pf*LDH IgY (common epitope) dF/dT curve showed the presence of two peaks with T_m values of 64.15°C and 71.08°C. At pH 7 both molecules had similar T_m values 72.05°C (anti-r*Pf*LDH IgY whole protein) and 72.65°C (anti-r*Pf*LDH IgY common epitope).

2.3.18. Analysis of r*Py*LDH

DSF analysis of the thermodenaturation of r*Py*LDH (Figure 2.17).

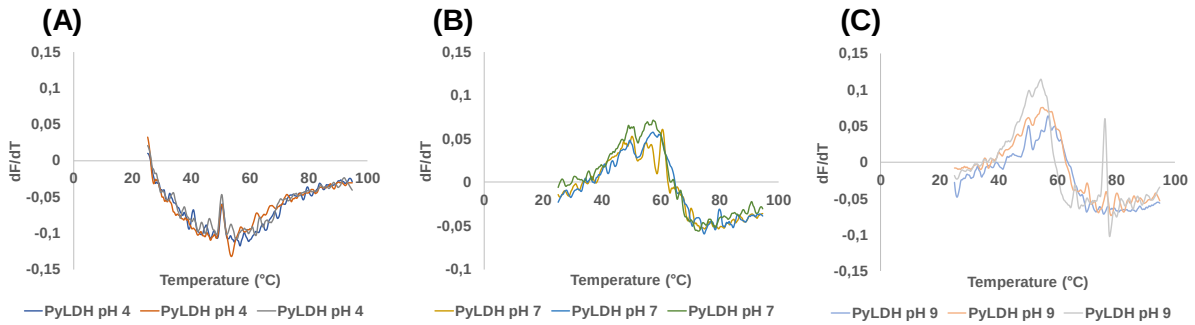

Figure 2.17: DSF First derivative of fluorescence data for r*Py*LDH at different pH values. r*Py*LDH in AMT buffer at pH 4 **(A)**, pH 7 B(B) and pH 9 **(C)**. SYPRO Orange was added and the raw fluorescence data was measured from 25 to 95°C and the first derivative was calculated and presented. Each panel represents triplicate results.

All thermodenaturation dF/dT curves for r*Py*LDH were not able to provide a clear T_m of the protein at different pH values 4, 7 and 9. At pH 4, r*Py*LDH was completely denatured as there is no transition observed, therefore a T_m could not be determined (Figure 2.17A). At pH values of 7 and 9 the curves had ambiguous transitions, which were not smooth or distinct. The peaks were broad with various kinks; however, an estimation was made using the highest dF/dT values. At pH 7 there were two peaks with T_m of 46.65°C and 57.12°C (Figure 2.17B). Following the same criteria at pH 9 which was used at pH 7, the T_m was 50.52°C and 55.68 for both peaks (Figure 2.17C).

The quality of dF/dT curves for r*Pf*LDH (Figure 2.12) was better than r*Py*LDH dF/dT curves, as single peaks were observed, at which distinct T_m could be obtained. Both proteins were most stable at pH 7 (Table 2.2). The state of the poor r*Py*LDH may be a result of the enzyme not being folded in its most stable conformation following IMAC purification of the protein from an *E. coli* cell lysate.

2.3.19. Interaction of anti-r*Pf*LDH IgY (common epitope) with r*Py*LDH

The interaction of r*Pf*LDH and r*Py*LDH with anti-r*Pf*LDH IgY (common epitope) was analysed using DSF. The analysis was conducted with r*Pf*LDH and r*Py*LDH in a 1:1 and a 1:4 ratio with anti-r*Pf*LDH IgY. The results for the antigen: antibody (1:4) ratio are presented (Figure 2.18).

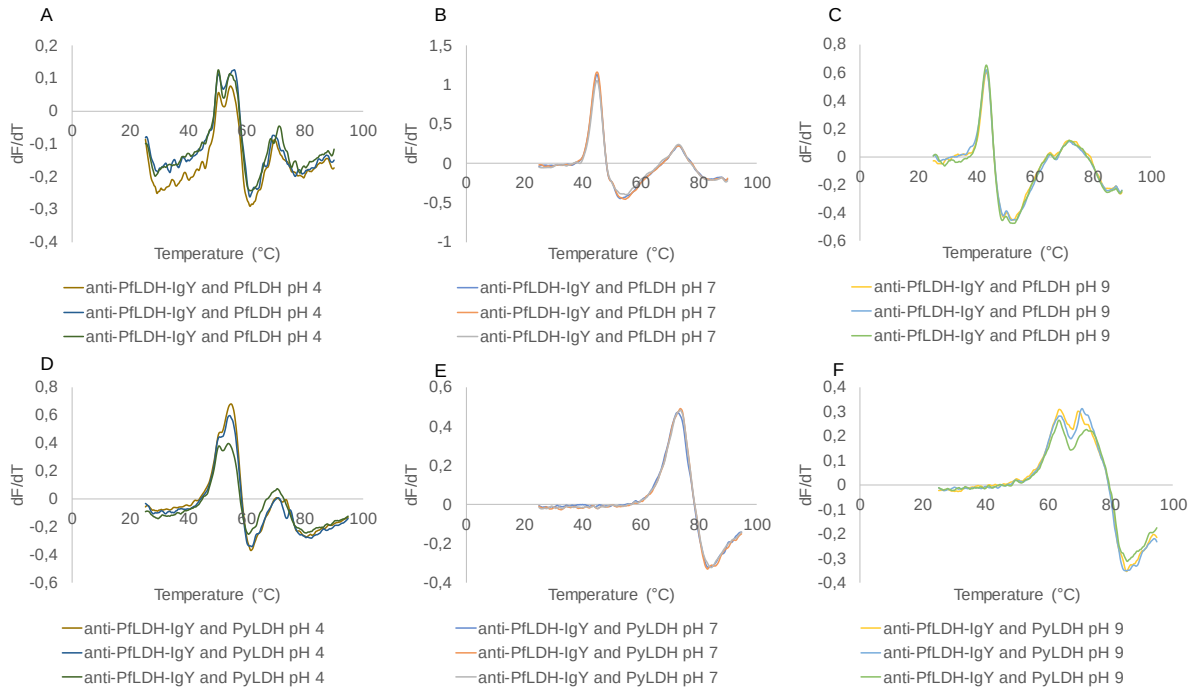

Figure 2.18: DSF first derivative of fluorescence data anti-r*Pf*LDH-IgY interacting with r*Pf*LDH and r*Py*LDH. r*Pf*LDH in AMT buffers at pH 4 **(A)**, at pH 7 **(B)**, at pH 9 **(C)** and r*Py*LDH in AMT buffers at pH 4 **(D)**, at pH 7 **(E)** and at pH 9 **(F)**, were incubated with anti-r*Pf*LDH-IgY in a (1:4 ratio) for two hours at 37°C. SYPRO Orange was added and the raw fluorescence data was measured from 25 to 95°C of which the first derivative was calculated and presented. Each panel represents triplicate results.

Incubation of r*Pf*LDH and r*Py*LDH with anti-r*Pf*LDH IgY (common epitope) dF/dT curves were analysed at pH values of 4,7 and 9 (Figure 2.18). r*Pf*LDH at pH 4 indicated two transitions (peaks) with similar T_m at 50°C and around 54.05°C (Figure 2.18A). The 50°C transition is thought to be a stabilised r*Pf*LDH-anti-r*Pf*LDH IgY (complex, with r*Pf*LDH in excess), while the 54.05°C T_m transition is the anti-r*Pf*LDH IgY and showed no increase in T_m compared to anti-r*Pf*LDH IgY alone in Figure 2.16. At pH 7 two transitions were observed, the first was r*Pf*LDH and the second r*Pf*LDH bound to anti-r*Pf*LDH IgY, both transitions T_m was 0.47°C higher than the original molecules (Figure 2.18B). At pH 9, two peaks were present, the first was r*Pf*LDH with a 0.96°C higher T_m than r*Pf*LDH alone and the second peak which had a T_m of 71.75°C, 0.67°C higher then anti-r*Pf*LDH IgY (common epitope; Figure 2.18C).

For r*Py*LDH with anti-r*Pf*LDH IgY (Figure 2.18D-F) different dF/dT profiles were compared to r*Pf*LDH interaction with anti-r*Pf*LDH IgY (Figure 2.18A-C).

At pH 4 (Figure 2.18D), a single main peak was present with a kink; the kink had a T_{m1} of 50.52°C and the main peak had a T_{m2} of 55.68°C. It is believed that T_m1 was a stabilised r*Py*LDH and T_{m2} was the anti-r*Pf*LDH IgY.

The second transition showed to have a T_m of 70.58 which is believed to be anti-r*Pf*LDH IgY-r*Py*LDH. The anti-r*Pf*LDH IgY (common epitope), showed only a single transition at pH 7 with a T_m 71.98°C which had a similar T_m to that of the anti-r*Pf*LDH IgY alone (T_m 72.65°C). At pH 9, there was no significant shifts in T_m for any of the transitions for anti-r*Pf*LDH IgY in the presence or absence of r*Py*LDH, both transitions T_m were similar (Table 2.2).

Table 2.2: Thermal melt temperature (T_m) results from DSF analysis of anti-r*Pf*LDH IgY (common epitope) interacting with r*Pf*LDH and r*Py*LDH at different ratios.

pH	Ratio (LDH: anti-rPfLDH IgY)	Tm (°C)							
		rPfLDH				rPyLDH			
		Peak 1	S.D	Peak 2	S.D	Peak 1	S.D	Peak 2	S.D
4	-	N.D		N.D	-	N.D	-	N.D	-
7	-	45.75		-	-	46.65	0.82	57.12	0.38
9	-	42.42		-	-	55.32	1.33	-	-
4	1:01	55.22	0.4	-	-	50.52	0.21	55.68	0.55
7	1:01	44.68	0.15	73.25	0.1	71.98	0.55	-	-
9	1:01	42.68	0.15	72.08	1	63.62	0.21	71.38	1.17
4	1:04	50.22	0.06	54.05	0.36	54.08	0.45	70.58	0.15
7	1:04	45.08	0.06	73.12	0.06	73.42	0.58	-	-
9	1:04	43.38	0.06	71.78	0.06	63.58	0.06	70.92	1.3

The first column refers to the pH of the AMT buffers used. The second column indicates the ratios of antibody and antigen used. The third column indicates the T_m of the protein. The dashes indicating a Tm could not be determined.

2.3.20. r*Pf*LDH incubated with anti-RSA IgY

To show the higher T_m seen when r*Pf*LDH incubated with anti-r*Pf*LDH IgY at pH 4 was due to the interaction of the antigen and antibody, r*Pf*LDH was incubated with anti-rabbit serum albumin (RSA) IgY at pH 4 (Figure 2.19).

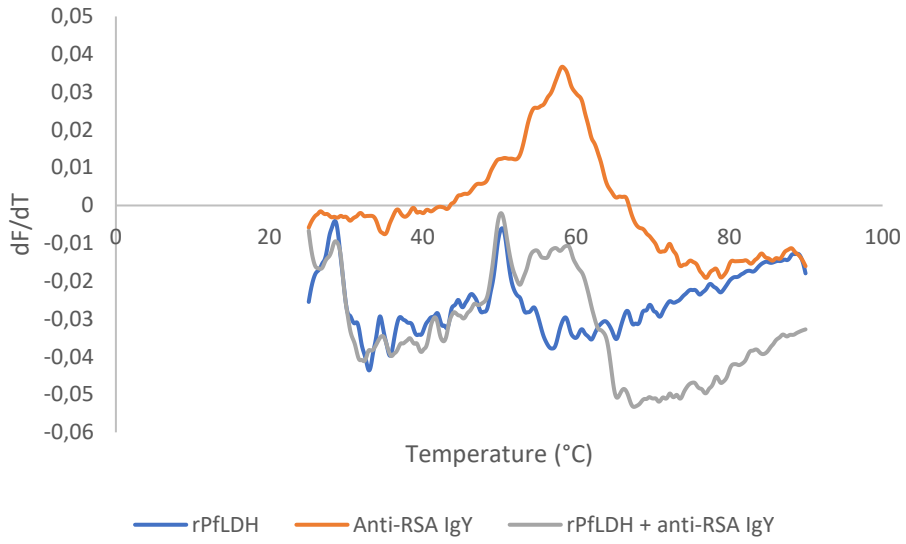

Figure 2.19: DSF first derivative of fluorescence data for r*Pf*LDH, anti-RSA IgY and a combination of both at different pH values. r*Pf*LDH, anti-RSA IgY and r*Pf*LDH + anti-RSA IgY were diluted into AMT buffer at pH 4. SYPRO Orange was added and the raw fluorescence data was measured from 25 to 90°C and the first derivative was calculated and presented. Each panel represents triplicate results.

Only anti-RSA IgY was shown to have a transition, which resulted in a T_m of 58.25°C. r*Pf*LDH showed no transitions as was seen in Figure 2.12 while the combination of r*Pf*LDH and anti-RSA did not have a transition peak. It is thought that this is due to the r*Pf*LDH's (in the mixture) high initial fluorescence preventing anti-RSA IgY transition being seen. Therefore, the results for r*Pf*LDH and r*Pf*HRP-2 shown to increase the T_m of their respective IgY antibodies at pH 4, is likely due to protein-protein interactions between both antigens' specific antibodies interacting with the respective antigens. The resulting antigen-antibody complex was more stable than the antibody alone (Figure 2.11, 2.14 and 2.18).

Table 2.3: Summary of T_m values for chicken IgY raised against different antigens analysed at pH values 4, 7 and 9.

	T_m (°C)		
pH	4	7	9
Naïve IgY	59.75	74.25	74.85
Anti-r*Pf*HRP-2 IgY	56.98	73.75	75.08
Anti-r*Pf*LDH IgY	N.D	72.05	73.45
Anti-r*Pf*LDH IgY	54.32	72.65	64.15
(raised a common malaria epitope)	68	-	71.08
Anti-RSA IgY	58.25	70.65	71.25

The T_m summarised in Table 2.3, show that each IgY antibody varies, indicating that the Fab portion plays an important role in determining the T_m of the entire molecule. The T_m showed that naïve IgY antibodies had the highest T_m values except for r*Pf*HRP-2 at pH 9.

2.3.21. Comparing the T_m of naïve chicken IgY to glycine-HCl buffer treated naïve chicken IgY

To show the affinity purified chicken IgY lower T_m is not a result of the affinity purification step requiring the use of a pH 2.8 glycine-HCl buffer and more is likely due to the variety of antibodies present in the naïve IgY pool. Naïve IgY was incubated in pH 2.8 glycine-HCl buffer for 10 minutes (Since chicken IgY is affinity purified with this buffer) and neutralised with 1 M Tris-HCl. This was compared to naïve IgY which was diluted into Tris-glycine buffer. The results are presented in Table 2.4.

Table 2.4: Comparing T_m of naïve IgY to glycine-HCl treated naïve IgY

			T_m (°C)	Average	S.D
Naïve IgY	74.42	74.58	74.58	74.53	0.092
Naïve IgY glycine-HCL buffer treated	74.41	74.25	74.25	74.3	0.092

The T_m values for both sets of naïve IgY were very close with little variance. This showed that chicken IgY can withstand elution with glycine-HCl at low pH without the conditions affecting the molecule, to any great extent.

2.3.22. DSF thermodenaturation of r*Pf*GAPDH

The third *P. falciparum* protein analysed by DSF was r*Pf*GAPDH. Analysis was conducted on the r*Pf*GAPDH at different pH values (Figure 2.20).

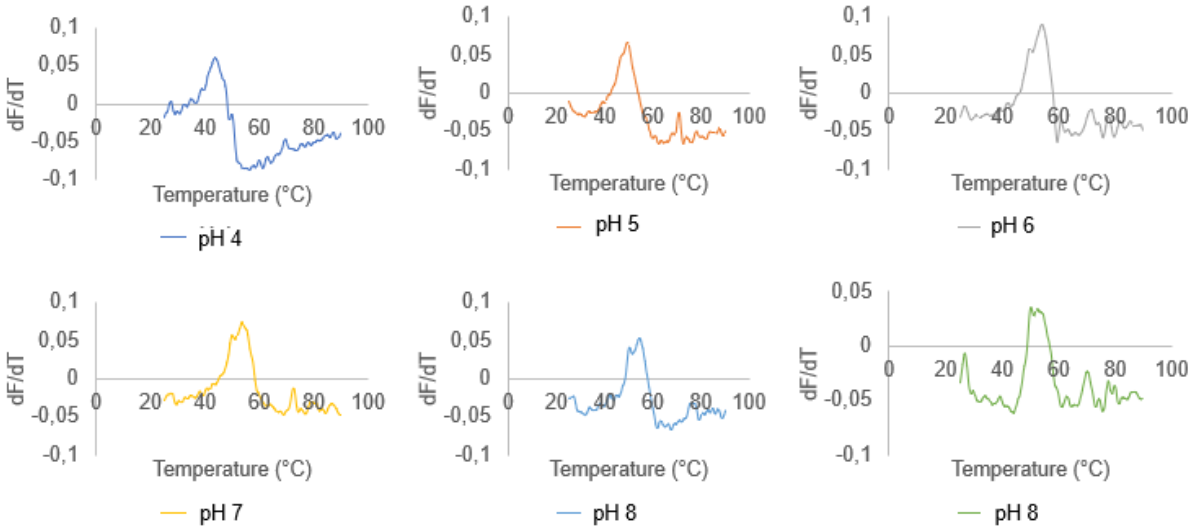

Figure 2.20: DSF first derivative of fluorescence data for r*Pf*GAPDH at different pH values. r*Pf*GAPDH in AMT buffers from pH 4 to 9. SYPRO Orange was added and the raw fluorescence data was measured from 25 to 95°C of which the first derivative was calculated and presented.

Evaluation of r*Pf*GAPDH in AMT buffers at different pH values had different T_m and different dF/dT profiles (Figure 2.20). At pH 4 and 5, a single peak for r*Pf*GAPDH was present with a T_m of 43.95°C and 49.55°C respectively. r*Pf*GAPDH at pH 6, 7 and 8 had two peaks present with T_m's at pH 6 of 49.75°C and 54.25°C; pH 7 was 50.05°C and 53.65°C; pH 8 was 50.25°C and 54.25°C.

2.3.23. Analysis of T_m of anti-malarial drug with r*Pf*GAPDH

Of the four anti-malarial drugs analysed with r*Pf*GAPDH, chloroquine and quinine were found to destabilise r*Pf*GAPDH shown by the decrease in the T_m (Figure 2.21A and D). Apo-r*Pf*GAPDH had a T_m of 54.75°C while r*Pf*GAPDH in the presence of chloroquine and quinine had T_m's of 47.75°C and 49.75°C respectively. Pyrimethamine interfered with the fluorescence signal and had a fluoresce curve with SYPRO Orange, while amodiaquine quenched all fluorescence (Figure 2.21B and C).

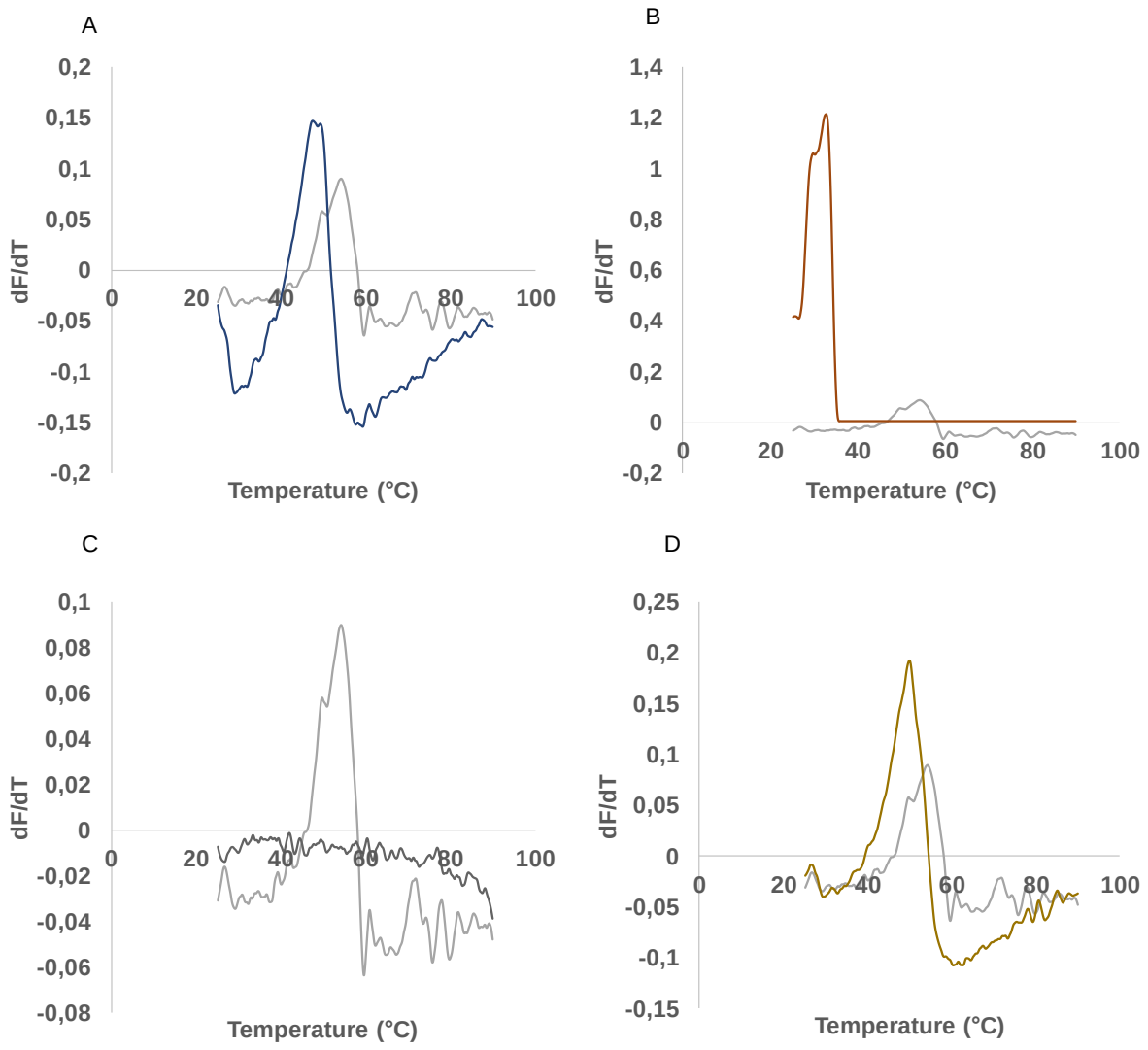

Figure 2.21: DSF first derivative of fluorescence data for r*Pf*GAPDH with anti-malaria drugs. r*Pf*GAPDH was incubated with chloroquine **(A)**, Pyrimethamine **(B)**, Amodiaquine **(C)**, Quinine **(D)**. At pH 6 in AMT buffer. SYPRO Orange was added and the raw fluorescence data was measured from 25 to 95°C of which the first derivative was calculated and presented.

Triplicate experiments were conducted on chloroquine and quinine to verify the results (Figure 2.20).

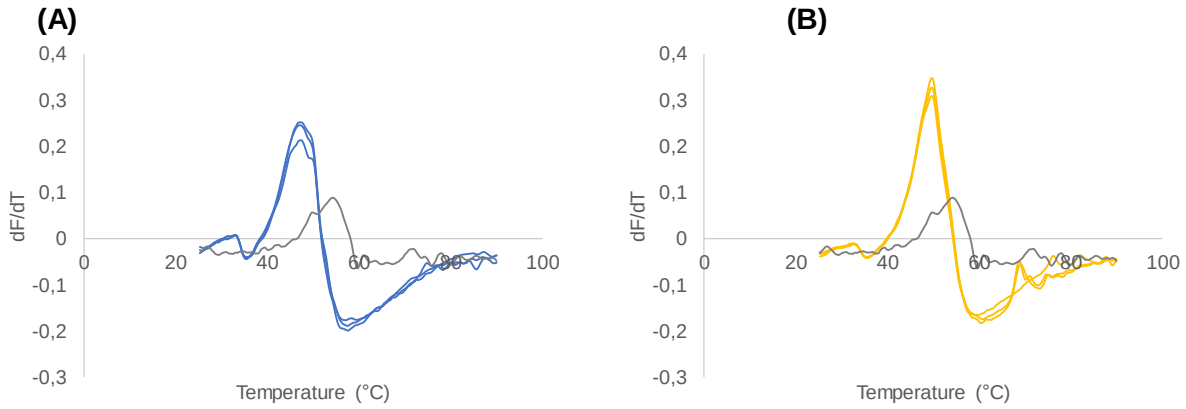

Figure 2.22: DSF first derivative of fluorescence data for r*Pf*GAPDH interacting with anti-malaria drugs. r*Pf*GAPDH was incubated with **(A)** chloroquine, **(B)** quinine. At pH 6 in AMT buffer. SYPRO Orange was added and the raw fluorescence data was measured from 25 to 95°C of which the first derivative was calculated and presented.

Chloroquine and quinine were repeated in triplicates and the data obtained matched the data before (Figure 2.21 A and D). An observation was made with increased amplitude in the samples containing the drug. The shift in T_m for chloroquine was 7.7°C and for quinine was 5.2°C (Figure 2.22). The result suggests that both drugs bound to and destabilised r*Pf*GAPDH.

2.3.24. Anti-malarial drug interaction with r*Pf*LDH

Following the changes in T_m of r*Pf*GAPDH with chloroquine and quinine both drugs were tested with r*Pf*LDH (Figure 2.23).

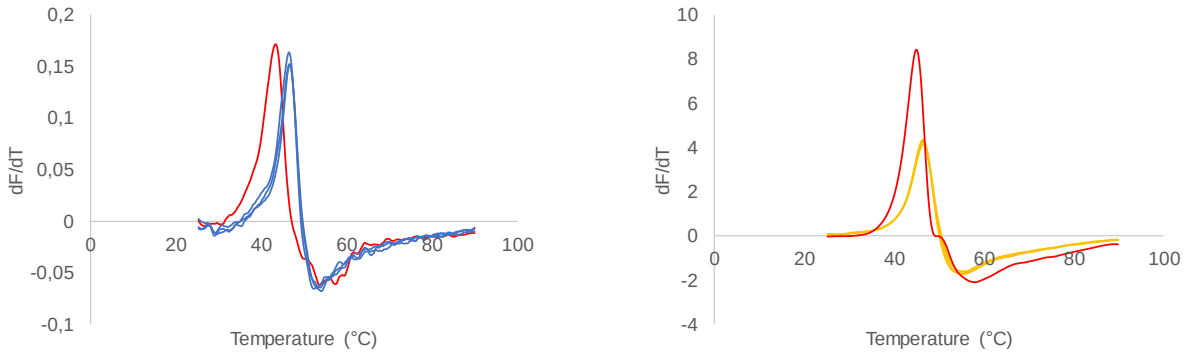

Figure 2.23: DSF first derivative of fluorescence data for r*Pf*LDH interacting with anti-malaria drugs. r*Pf*LDH was incubated with **(A)** chloroquine **(B)** quinine. At pH 6 in AMT buffer. SYPRO Orange was added and the raw fluorescence data was measured from 25 to 95°C of which the first derivative was calculated and presented.

Quine and chloroquine were shown to increase the T_m of r*Pf*LDH by 3.6°C and 3.43°C respectively. Chloroquine was shown to decrease the amplitude of the dF/dT signal (Figure 2.23).

To test if the anti-malarial drugs interfered with the assay, each of the drugs were analysed in the absence of protein (Figure 2.24). Only pyrimethamine was shown to have a signal indicating the drug fluoresces, as there was no protein to provide hydrophobic residues for SYPRO Orange to add fluorescence.

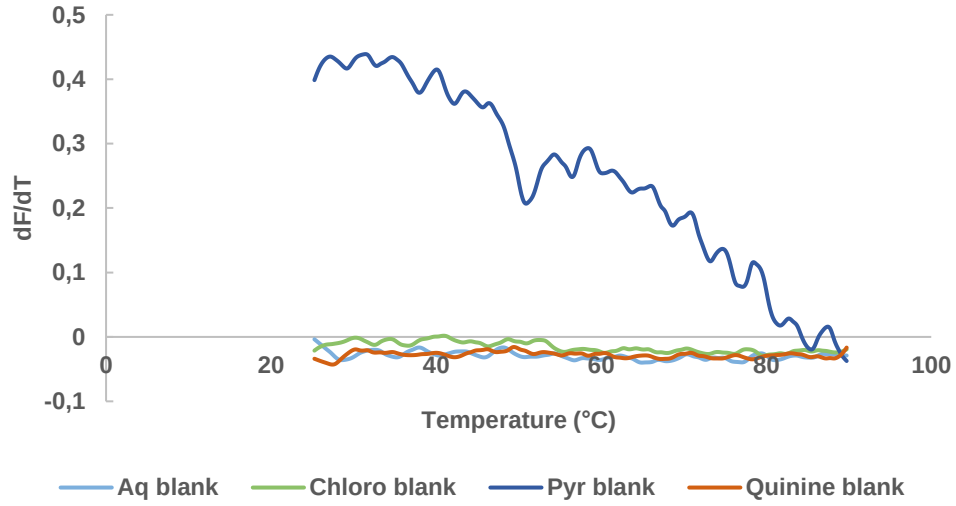

Figure 2.24: DSF first derivative of fluorescence data for anti-malaria drugs. Different Antimalarials were diluted in AMT buffer (pH 6). SYPRO Orange was added and the raw fluorescence data was measured from 25 to 95°C of which the first derivative was calculated and presented.

To show the T_m shifts caused by chloroquine and quinine interacting with r*Pf*LDH (Figure 2.23) were due to both drugs specifically interacting with r*Pf*LDH, quine was incubated with carbonic anhydrase as a control protein (Figure 2.25) and DSF analysis was carried out.

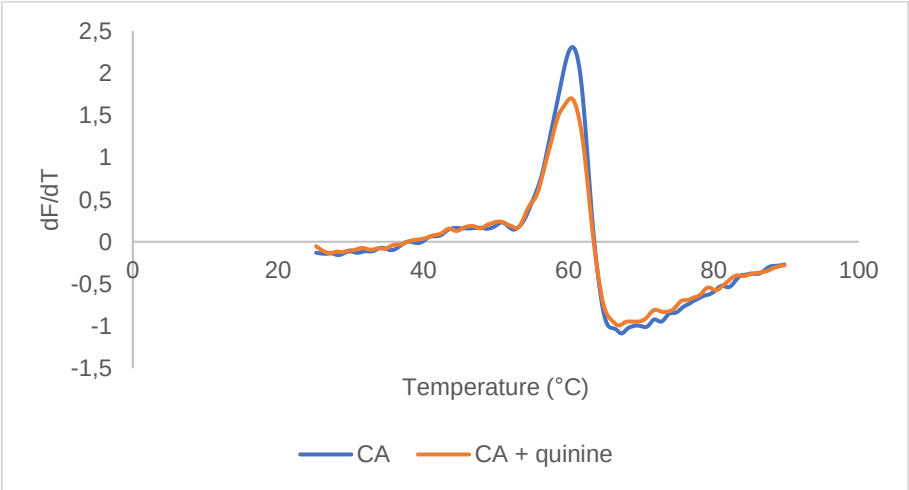

Figure 2.25: DSF first derivative of fluorescence data for carbonic anhydrase interacting with quinine. Carbonic anhydrase was incubated in the presence and absence of quinine at pH 6 in AMT buffer. SYPRO Orange was added and the raw fluorescence data was measured from 25 to 95°C of which the first derivative was calculated and presented.

1 mM quinine (Figure 2.25) did not interact with the carbonic anhydrase and the T_m shifts seen with r*Pf*GAPDH and r*Pf*LDH were due to quinine binding to the proteins.

2.3.25. Molecular docking chloroquine and quinine with *Pf*GAPDH and *Pf*LDH illustrating how the drugs bind to the protein

A monomer of *Pf*GAPDH in a ribbon conformation is illustrated (Figure 2.26A) with quinine represented as a space fill model (Figure 2.26A and B). Quinine is binding to the cofactor binding site of *Pf*GAPDH where NADPH would usually bind.

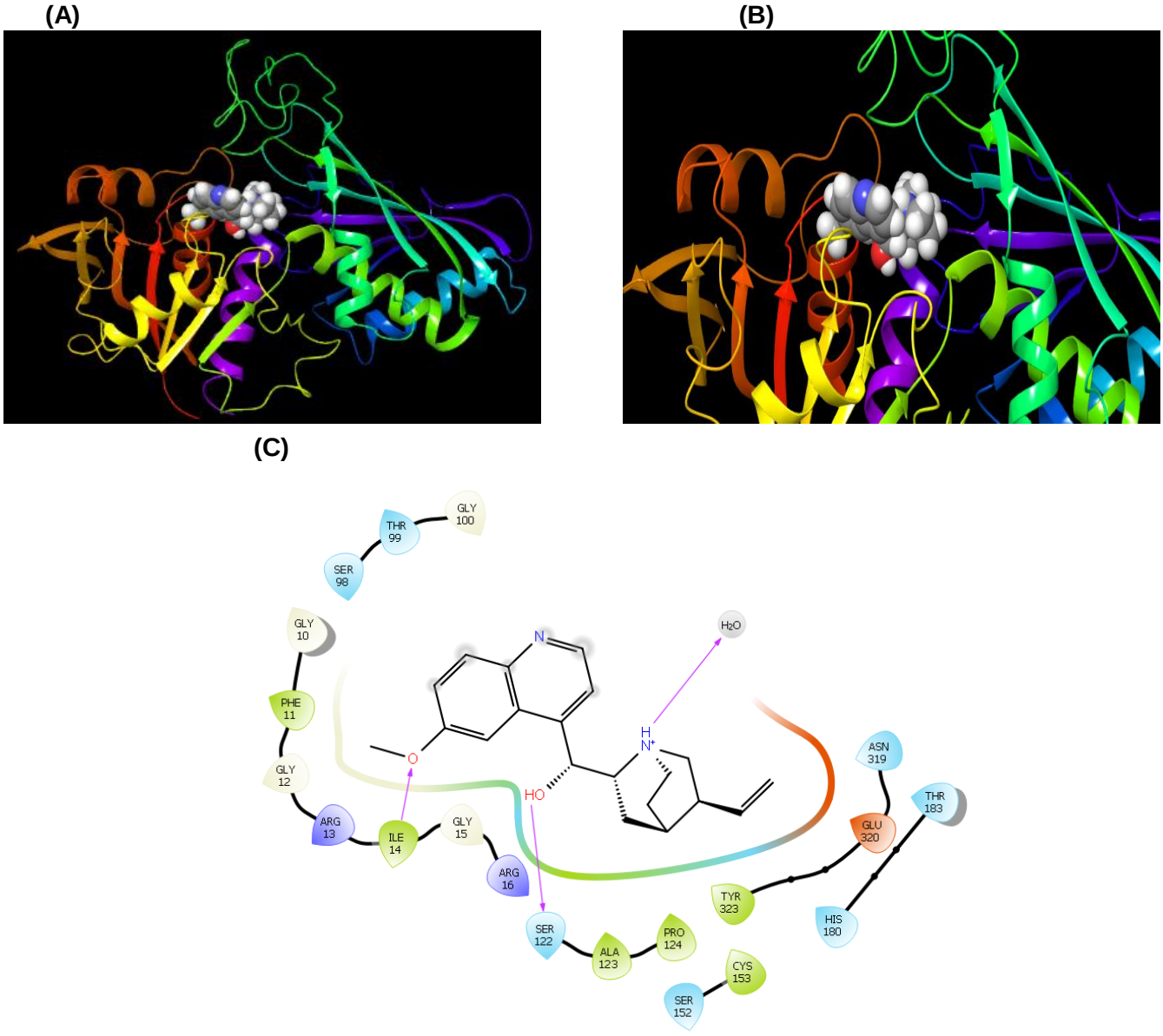

Figure 2.26: Docking of quinine to *Pf*GAPDH. *Pf*GAPDH (ribbon structure) with quinine (space fill structure) docked in the co-factor binding site **(A)**. A close view of quinine bound to the co-factor binding site of *Pf*GAPDH **(B)**. 2D view showing the amino acids in the co-factor binding site interacting with quinine **(C).**

The amino acids serine and isoleucine within the co-factor binding site interacting with quinine is shown in Figure 2.26C.

A monomer of *Pf*GAPDH in a ribbon conformation is illustrated (Figure 2.27A) with chloroquine represented as a space fill model. Chloroquine is binding to the cofactor binding site of *Pf*GAPDH where NADPH would usually bind (Figure 2.27A and B). The specific amino acids threonine, aspartate and phenylalanine within the co-factor binding site interacting with quinine is shown in Figure 2.27C.

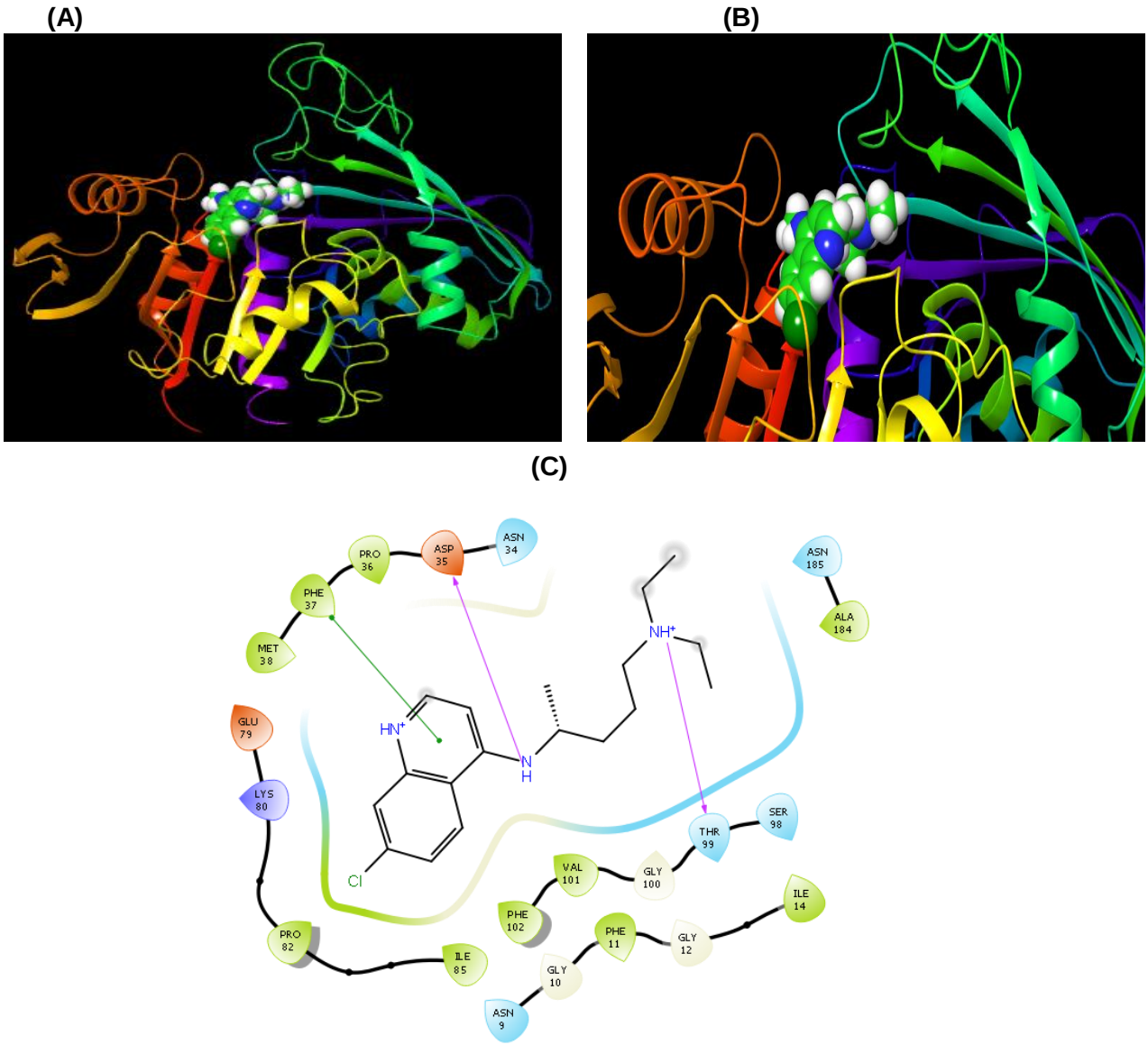

Figure 2.27: Docking of chloroquine to *Pf*GAPDH. *Pf*GAPDH (ribbon structure) with chloroquine (space fill model) docked in the co-factor binding site **(A)**. A close view of chloroquine bound to the co-factor binding site of *Pf*GAPDH **(B)**. 2D view showing the amino acids in the co-factor binding site interacting with chloroquine **(C).**

A monomer of *Pf*LDH in a ribbon conformation is illustrated (Figure 2.28A) with chloroquine represented as a space fill model. Chloroquine is binding to the cofactor binding site of *Pf*LDH where NADPH would usually bind (Figure 2.28A and B). The amino acids glutamate and the amino group in the ring of chloroquine interact with phenylalanine and two water molecules within the co-factor binding site interact with quinine (Figure 2.28C).

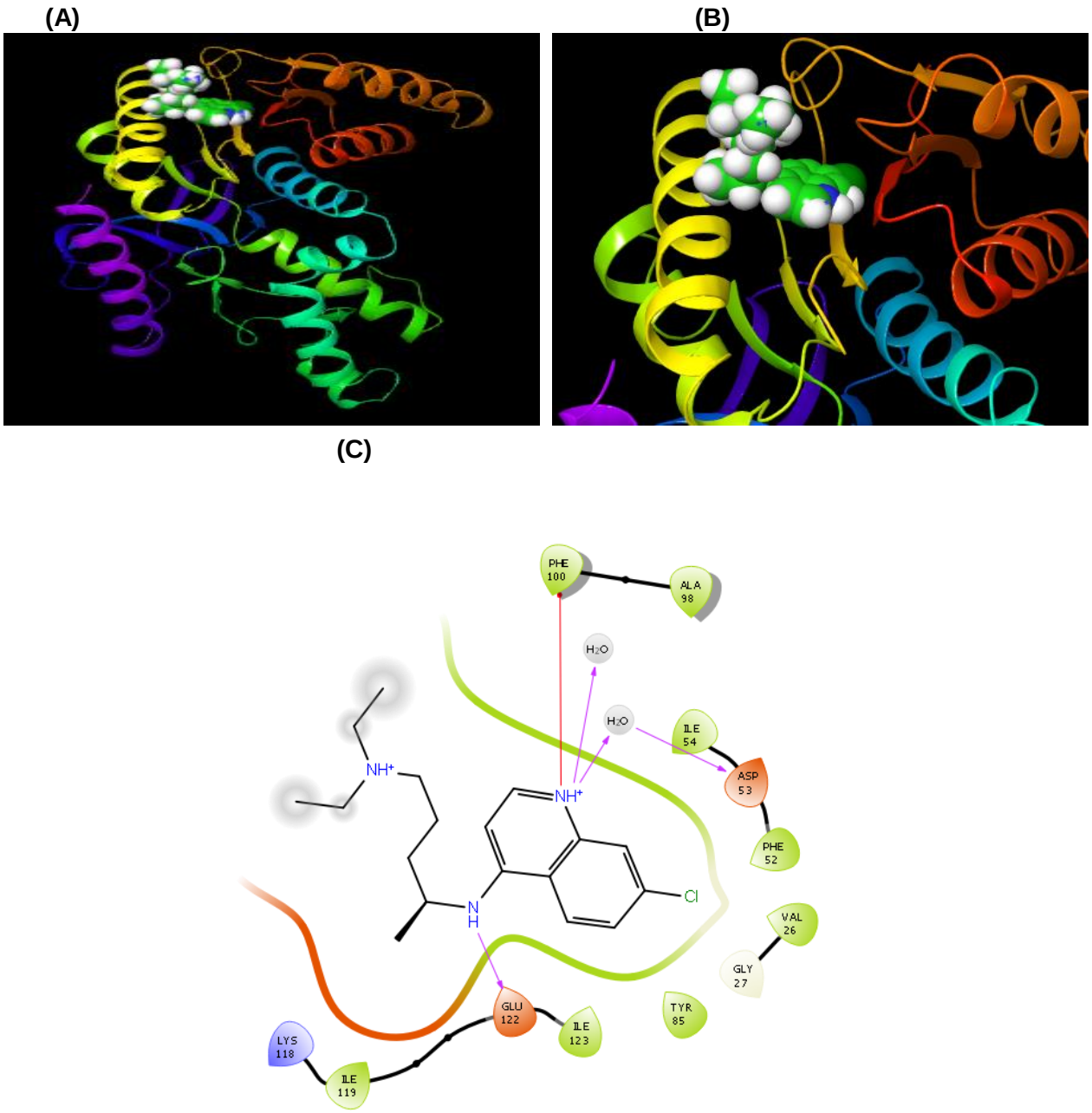

Figure 2.28: Docking of chloroquine to *Pf*LDH. *Pf*LDH (ribbon structure) with chloroquine (space fill model) docked in the co-factor binding site **(A)**. A close view of quinine binding to the co-factor binding site of r*Pf*LDH **(B)**. 2D view showing the amino acids in the co-factor binding site interact with chloroquine **(C).**

A monomer of *Pf*LDH in a ribbon conformation is illustrated (Figure 2.29A) with quinine represented as a space fill model. Quinine is binding to the cofactor binding site of *Pf*LDH where NADPH would usually bind (Figure 2.29A). The specific amino acids glutamate and lysine within the co-factor binding site interacting with quinine is shown in Figure 2.29B.

(A) **(B)**

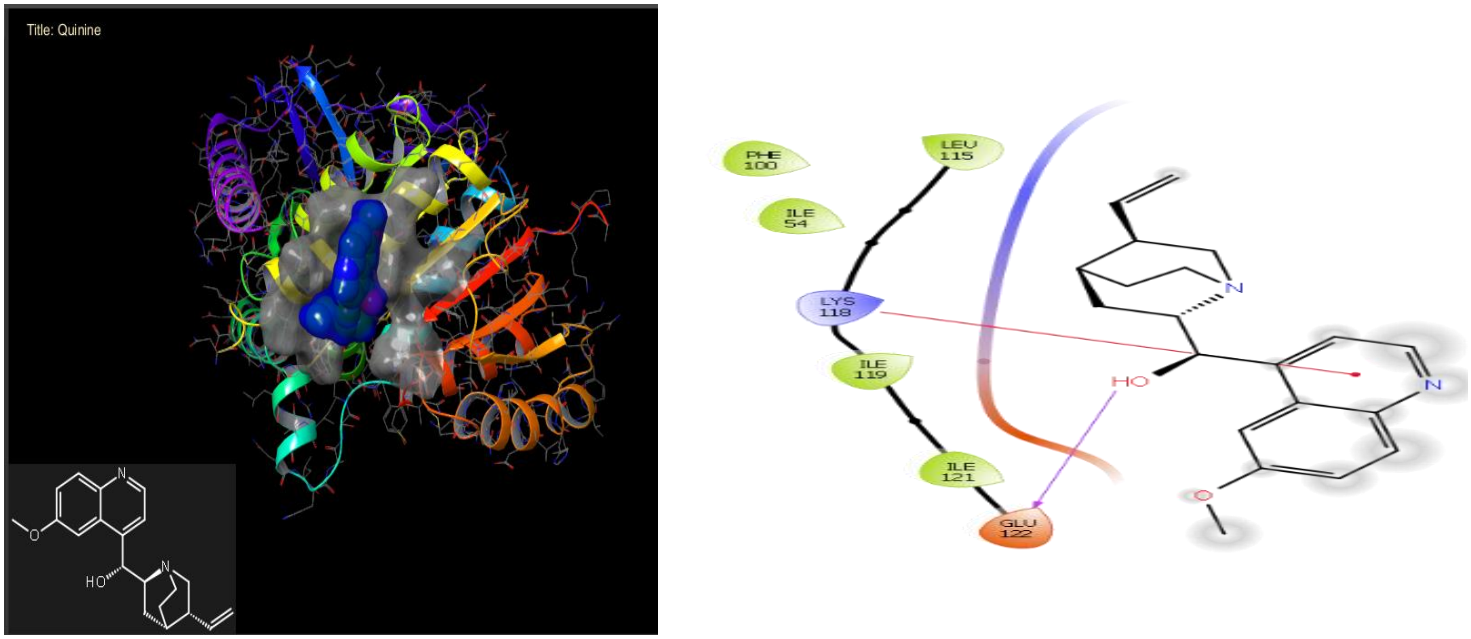

Figure 2.29: Docking of quinine to *Pf*LDH. *Pf*LDH (ribbon structure) with the quinine docked in the co-factor binding site**(A)**. 2D view showing the amino acids in the co-factor binding site interacting with quinine **(B)**.

Chloroquine and quinine were both shown to interact with r*Pf*LDH and r*Pf*GAPDH experimentally with DSF and *in silico* using docking studies. However, it is still unclear as to why r*Pf*GAPDH was destabilised while r*Pf*LDH was stabilised by both drugs. Glutamate (122) was found to be important for the binding of chloroquine and quinine.

2.4. Discussion

2.4.1. Recombinant expression and purification of *Pf*HRP-2

Conditions for the recombinant expression of *Pf*HRP-2 (Figure 2.1 and 2.2) were optimised previously. r*Pf*HRP-2 was purified using Ni^{2+}-chelate affinity chromatography and eluted using 500 mM imidazole (Figure 2.1A and Figure 2.2A), which were two-fold higher than the concentration used to elute r*Pf*LDH and r*Pf*GAPDH (Figure 2.3 and Figure 2.4).

The need for the higher concentration of imidazole is due to the r*Pf*HRP-2 consisting of 34% histidine which has a high affinity for the Ni^{2+}-NTA resin (Sulkowski, 1985; Bauer *et al*., 2017). r*Pf*HRP-2 was purified as a doublet at 54 kDa. The reported molecular weight of *Pf*HRP-2 is 30 kDa (Choi *et al.,* 1999; Ndonwi *et al.,* 2011).

The reason for the change in mobility of r*Pf*HRP-2 in the SDS-PAGE gel is unknown, however it could be due to its unique structure and high concentration of histidine residues, (Baker *et al*., 2010). Other histidine rich proteins have been reported to migrate at higher molecular weights in SDS-PAGE gels than the predicted size (Shelake *et al*., 2017), possibly, the proteins are in a more open conformation and therefore migrate slower through the acrylamide (Shelake *et al.,* 2017).

2.4.2. Stress on *E. coli* due to the expression of r*Pf*HRP-2

A plasmid induces stress on the *E. coli* host when the recombinant protein is overexpressed, resulting in a metabolic burden for the host cell (Hoffmann and Rinas, 2004). Understanding the full extent of the metabolic burden is complex and depends on the characteristics of each recombinant protein. r*Pf*HRP-2 is rich in His and Ala residues (Choi *et al*., 1999), therefore, the *E. coli* host will be depleted of both amino acids the most when expressing r*Pf*HRP-2. Depletion of His and Ser residues results in the deactivation of some pathways and the activation of alternate pathways for the cells to survive (Chang *et al*., 2002; Cashel and Kalbacher, 1970). Several proteins were expressed by the *E. coli* cells expressing r*Pf*HRP-2 (Figure 2.2, lane 6-8) that were not expressed by cells expressing r*Pf*LDH and r*Pf*GAPDH (Figure 2.3 and 2.4) that bound to the Ni^{2+}-NTA resin. The presence of these proteins is an indication of a stress response induced by the expression of r*Pf*HRP-2.

Chang *et al.,* (2002) looked at the stress response on *E. coli* when expressing a toxic recombinant protein (glucose-lactose diauxide) as well as the effect of oxidative stress from H_2O_2 on *E. coli*. The results showed that alternate pathways had to be upregulated for the bacterial cells to survive, including the His-operon, therefore proteins with high histidine content were expressed. The expression of proteins with higher than usual histidine contents was also reported by Robichon *et al.,* (2011). In their study, they reported 17 proteins with a high histidine content. Of the proteins15 bound strongly to IMAC resins and required above 55 mM imidazole to elute the proteins.

Similar results were observed for the recombinant expression of *Pf*HRP-2 (Figure 2.1A lane 6 and Figure 2.2A lanes 6-8). The proteins (Figure 2.3 and 2.4) were eluted of the Ni^{2+}-NTA matrix with 250 mM imidazole which is generally used to elute a His-tag recombinant protein. Interestingly in Figure2.2B lanes 6 to 8, 18 proteins eluted with 250 mM imidazole(Figure 2.2B lane 6-8). The contaminating proteins reduced the binding capacity of the Ni^{2+}-NTA resin therefore a 2ml resin was used.

2.4.3. r*Pf*LDH and r*Pf*GAPDH expression and purification

When r*Pf*LDH was expressed, protein of 36 kDa and 75 kDa (Figure 2.3A and B) were obtained. The size of native r*Pf*LDH is 34.7 kDa, while the predicated size of a His_6-tag r*Pf*LDH is around 35.7 kDa (1 kDa for the His_6-tag; Berwal *et al.,* (2008).

The 75 kDa band detected was a dimer of r*Pf*LDH. The purified r*Pf*GAPDH (Figure 2.4A and B) ran at an estimated size of 39 kDa on an SDS-PAGE gel which is similar to the 36.6 kDa found in studies by Satchell *et al.,* (2005) and Daubenberger *et al.,* (2003).

2.4.4. Expression conditions for all three proteins

E. coli BL21 (DE3) cells were used as the host strain for recombinant protein expression due to its advantages, such as the cell number doubling in 20 min which results in cell culture densities around 1 x 10^{10} cell per litre of cell culture in a short period of time. The hdsb mutation which prevents the plasmid being lost and it is lysogenised, which is a requirement for the pET-15(b) and pKK223-3 plasmid vectors (Chart *et al*., 2000; Rosano and Ceccarelli, 2014; Daegelen *et al*., 2009).

All three proteins were expressed in TB, which is a nutrient rich autoinduction broth containing lactose. The lactose is important to facilitate recombinant protein expression by binding to the LacI repressor on the lac (pET-15) or tac operator (pKK223-3). This allows T7 RNA polymerase to be transcribed and expressed as the recombinant protein. A disadvantage of using lactose was that it was used up by the cell unlike its structural analogue, IPTG, that is not degraded (Sørensen and Mortensen, 2005). One of the weaknesses of the expression was that ampicillin could not be supplemented into the culture every 3 hours as the cell culture was grown overnight. Therefore, in future, cultures grown overnight can be supplemented with carbenicillin in conjunction with ampicillin. Carbenicillin is not hydrolysed as ampicillin is and will maintain selective pressure throughout the 16-hour growth period (Busso *et al*., 2008).

2.4.5. Chicken IgY purification

Chicken IgY antibodies were chosen (Figure 2.5) because of their superior stability and the non-invasive methods used to isolate them from chicken eggs (Larsson *et al*., 1991; Schade *et al*., 1996). The anti-r*Pf*HP-2 IgY LOD for r*Pf*HRP-2 was 15 ng (Figure 2.6).

2.4.6. DSF analysis

Identifying the correct buffer is essential for DSF (Crowther *et al*., 2010). AMT buffers were used to determine thermal stability of proteins using DSF because of the pH range and having a constant ionic strength across pH 4 to 9 (Ellis and Morrison, 1982). The highest T_m for carbonic anhydrase obtained using AMT buffer was at pH 9 (Figure 2.7 and Figure 2.8) and corresponded to its optimal pH (Sanyal and Maren, 1981).

2.4.7. Using SYPRO Orange as the fluorophore

SYPRO Orange was the fluorophore used for DSF assays (Chapter 2 and 3) because it offers high fluorescence with a low dielectric constant when present in a hydrophobic environment.

The excitation wavelength is 490 nm (460 nm – 510 nm), where few small molecules interfere with SYPRO Orange (Hawe *et al*., 2008; Niesen *et al*., 2007; Steinberg *et al.,* 1996). 1-Anilino-8-naphthalene sulfonate is an alternative fluorophore that is twice as sensitive as SYPRO Orange, but the excitation wavelength is 350 nm, which may interfere in screening ligands (Niesen *et al*., 2007).

2.4.8. Why dF/dT was used to calculate T_m

The dF/dT curves were used to determine T_m of proteins (He *et al*., 2010; Menzen and Friess, 2013; Crowther *et al*., 2010; Uniewciz *et al*., 2010) because of its simplicity and good agreement with T_m obtained by other methods. However, T_m from dF/dT curves are sometimes higher than the actual T_m of the protein (He *et al*., 2010). Alternatively, T_m can be determined by finding the point of inflection on the Boltzmann function fluorescence curves (Nieasen *et al.,* 2007) or by finding the second derivative (Goldberg *et al*., 2011). If a user would prefer finding the point of inflection, Niesen *et al*., (2012) has created a Microsoft® spreadsheet to aid with the calculations.

2.4.9. DSF analysis of r*Pf*HRP-2 and anti-r*Pf*HRP-2 IgY interaction

A T_m for r*Pf*HRP-2 could not be determined, possibly due to the high concentration of Ala residues that may have bound SYPRO Orange, therefore, causing a high initial fluorescence and no transition to determine a T_m (Figure 2.9). Markwalter *et al*., (2018) suggested *Pf*HRP-2 is stable at 80°C. Thiol based fluorophores like BODIPY FL L-cystine (BFC) (Hofmann *et al*., 2016) and N-[4-(7-diethylamino-4-methyl-3-coumarinyl)phenyl] maleimide (CPM) (Alexandrov *et al*., 2008; Vedadi *et al*., 2010) can be used as an alternative to SYPRO Orange to determine the T_m of r*Pf*HRP-2 using DSF. Since CPM and BFC bind to cysteine residues, which are present on *Pf*HRP-2, cysteine residues are generally embedded within a protein and are exposed upon protein denaturation. Both thiol probes (BFC and CPM) have been used to determine the T_m of proteins when SYPRO Orange was not suitable and under the right conditions BFC is more sensitive. Thiol based probes are pH sensitive and need to be used with caution (Hofmann *et al*., 2016).

r*Pf*LDH and r*Py*LDH share 93% identity, but their dF/dT curves were different (Figure 2.12 and Figure 2.17), except at pH 4 where both proteins were denatured indicating LDH is sensitive to denaturation in an acidic pH environment. r*Pf*LDH produced ideal dF/dT curves while r*Py*LDH dF/dT curves had high background.

This could have been due to suboptimal purification conditions that resulted in r*Py*LDH being partially denatured, therefore hydrophobic patches could be exposed, resulting in the high background fluorescence (Reinhard *et al*., 2013).

r*Pf*GAPDH was less sensitive to acidic pH denaturation compared to the LDH molecules and had dF/dT peaks from pH 4 to 9 (Figure 2.20). The presence of a kink and a

major peak in the dF/dT curves is thought to be a tetramer and a monomer of r*Pf*GAPDH melting as the r*Pf*GAPDH expressed were shown to exist as both (Krause *et al*., 2017). DSF analysis on r*Pf*GAPDH had a T_m of 49.9°C, in an optimal HEPES buffer described by Crowther *et al*., (2010). Their T_m corresponds to the minor T_m (Figure 2.20) at pH 6-8, while the second T_m was ± 55°C. The HEPES buffer (Crowther *et al*., 2010) was tested with r*Pf*GAPDH and two T_m were obtained at 50 and 55°C respectively (Data not shown).

2.4.10. DSF analysis of the different IgY molecules

Different chicken IgY T_m varied slightly (Table 2.3) with naïve pool IgY having a ±2°C higher T_m than all affinity purified IgY (Figures 2.10; 2.13 and 2.16), except for anti-r*Pf*HRP-2 IgY at pH 9. Chicken IgY incubated in glycine-HCl buffer (Table 2.4) showed no change in T_m compared to the naïve chicken IgY i, indicating affinity purifying IgY with glycine-HCl buffer for 10 min does not affect the stability of the molecule. Based on the varying T_m values, majority of the dF/dT peak must depend on the Fab domain as it has the variable region and constant regions C_{H1-4} are identical across all chicken IgY (Zhao *et al*., 2000). Anti-r*Pf*LDH IgY (raised against a common epitope) was the only IgY molecule to show two transitions T_m's at 54.32°C and 68°C. It is suspected that the second T_m (68°C) corresponds to the Fab portion since the first T_m (54.32°C) is in a similar range as the other IgY molecules reported in Table 2.3 and only the T_m of the variable region should vary.

2.4.11. DSF analysis of protein-protein interactions

DSF was used to show protein-protein interactions of r*Pf*HRP-2 and r*Pf*LDH with their respective IgY antibodies (Figures 2.11 and 2.14). Both antigens at pH 4 did not show a transition, but when incubated with their respective IgY antibodies a significant increased T_m was seen only at pH 4. This indicated the antigens bound to and stabilised their respective antibodies. r*Pf*LDH incubated with anti-RSA IgY (Figure 2.19) served as a control and showed that this was not a non-specific interaction and antigen-antibody interactions can be visualised using DSF. At pH 7 and 9 there was no significant increase in T_m because at 72°C the antigen dissociates from the Fab domain the IgY molecule denatures (Markwalter *et al.,* 2018).

However, in Figure 2.14 r*Pf*LDH-anti-r*Pf*LDH IgY at pH 9 the third transition observed with a T_m above 80°C is thought to be r*Pf*LDH bound to the Fab domain of the anti-r*Pf*LDH IgY. This could be a thermally more stable polyclonal anti-r*Pf*LDH IgY isotype present.

2.4.12. DSF analysis of anti-r*Pf*LDH IgY common epitope interacting with r*Pf*LDH and r*Py*LDH

r*Pf*LDH interacting with anti-r*Pf*LDH IgY (Figure 2.14) was more stable than r*Pf*LDH interacting with anti-r*Pf*LDH IgY (against a common epitope; Figure 2.18A). This is likely due to the more peptides recognised and therefore will allow for more interactions with anti r*Pf*LDH

IgY (against whole protein) and better stability (Lipman *et al*., 2005). Anti-r*Pf*LDH IgY (against a common epitope) produced two peaks at pH 4, both are thought to be antigen-antibody complexes, with the first being the antigen in excess and the second peak the antibody is in excess. The T_m for r*Py*LDH was difficult to interpret due to its poor transition peak and the T_m was estimated from the highest point on the peak. Potentially, the purification conditions were not optimal for r*Py*LDH purification therefore poor transition peaks were present.

DSF analysis of anti-r*Pf*LDH IgY (common epitope) interacting with r*Pf*LDH was different compared r*Py*LDH and the T_m were different (Table 2.2). A common transition peak with a T_m of 54.08°C was present this was common with anti-r*Pf*LDH IgY alone and r*Pf*LDH with anti-r*Pf*LDH IgY indicating that must be C_{H2-4} and part of the Fab fragment as it is common.

2.4.13. Why the study could not predict the number of binding sites for the protein-protein interactions

Layton and Hellinga, (2011) used DSF to show the complexity for determining protein-protein interactions. A two-protein system with a lower melting partner (LMP) and a higher melting partner (HMP) and both having a single binding site results in 8 states. With polyclonal antibodies the number of binding sites is unknown and therefore it is impossible to predict the number of possible states. The minimum antibodies bound per protein would be 1, however an antibody raised against a single peptide will only recognise that peptide. This could possibly explain why the r*Pf*LDH-anti-r*Pf*LDH IgY (against the protein) complex was more stable than the r*Pf*LDH-anti-r*Pf*LDH IgY (against a common epitope).

2.4.14. Anti-malaria drug interaction with r*Pf*LDH and r*Pf*GAPDH

Binding of chloroquine and quinine to both r*Pf*GAPDH and r*Pf*LDH was shown experimentally using DSF and *in silico* using Maestro and bound to the co-factor binding site as reported by Read *et al.,* (1999). The *in silico* method may provide some insight into which amino acids play a role in binding, therefore those interactions can be used to develop new drugs against malaria (Figure 2.26 – 2.29).

Furthermore, by inhibiting both r*Pf*GAPDH and r*Pf*LDH, the glycolytic pathways are removed from the malaria parasite and it will not be able to survive as the glycolytic pathway is responsible for providing most of the energy for the parasite (Mehta *et al*., 2005).

2.4.15. Conclusion

r*Pf*HRP-2, r*Pf*LDH and r*Pf*GAPDH were all recombinantly expressed and affinity purified using Ni^{2+}-NTA affinity chromatography and tested using DSF. Interestingly r*Pf*GAPDH had a higher T_m compared to r*Pf*LDH, indicating it is more stable. DSF was confirmed to be a reliable technique for measuring protein-protein interactions. Furthermore, DSF confirmed chloroquine and quinine bound to r*Pf*LDH and r*Pf*GAPDH. The *in silico* data suggested a

potential mechanism as to how the drugs cure malaria by inhibition of the glycolytic pathway of the parasite.

3. CHAPTER 3: Comparing the thermodynamic stability of polyclonal chicken IgY, mammalian IgG and optimising a conjugation method for chicken IgY

3.1. Antibodies

Antibodies are glycoproteins expressed by B-lymphocytes when the B cells are stimulated by the binding of foreign antigens. Antibodies are expressed by all mammals, fish, amphibians, reptiles and birds (Marchalonis *et al*., 2006; Sun *et al*., 2008). Mammals have five classes of antibodies namely: IgA, IgM, IgE, IgD and IgG compared to IgA, IgM and IgY found in chickens (Sun *et al*., 2008) and IgH, IgM, IgD and IgM found in crocodiles (Han *et al*., 2016). Historically it was believed that IgY resembled IgG due to their similar function and concentrations in serum. However, due to large structural differences between the two meant this was not the case. Analysis of the DNA sequences of antibodies show that chicken IgY is closer to that of mammalian IgE than mammalian IgG (Warr *et al*., 1995).

A comparison of a chicken IgY and a rabbit IgG molecule is shown in Figure 3.1. Chicken IgY is a 167.250 KDa heterodimer, made up of two light chains (LC; variable region light chain (V_L) + constant region light chain (C_L); 18.660 kDa each) and two heavy chains (HC; C_{H1-4} + V_H; 65.105 KDa each; Sun *et al*., 2001). The light chains of both IgY and IgG have a single variable (V_L) and a constant (C_L) region, whilst the heavy chain of IgY has four constant (C_{H1} -C_{H4}) regions and one variable (V_H) region. The IgG molecule differs from that of IgY in the HC domain, in that there are only three constant regions (C_{H1-3}) and a single variable region (Schade *et al*., 2005). A hinge region is present in IgG but is less developed in IgY (Shimizu *et al.,* 1992). The general structure of IgY is depicted as a “Y” shape molecule. The arms consist of the antigen binding fragment (Fab; 45.359 kDa) regions which are responsible for recognition of an epitope on an antigen. The base of the “Y” is the Fc portion which is glycosylated by two carbohydrate side chains on C_{H2} and C_{H3} for IgY whereas IgG has a single glycosylated site on the C_{H2} domain (Schade *et al.,* 2005).

IgY and IgG antibodies are both used in immunochemistry with the latter being more popular. The advantages of IgY over IgG were recognised in 1996 by European center for the validation of alternate methods (ECVAM; Schalde *et al*., 1996). At the workshop they suggested the potential for using chicken IgY antibodies to replace mammalian IgG molecules for research purposes as IgY can be obtained using non-invasive techniques (Schade *et al*., 1996; Schade and Hilmak, 1996; Polson *et al*., 1985).

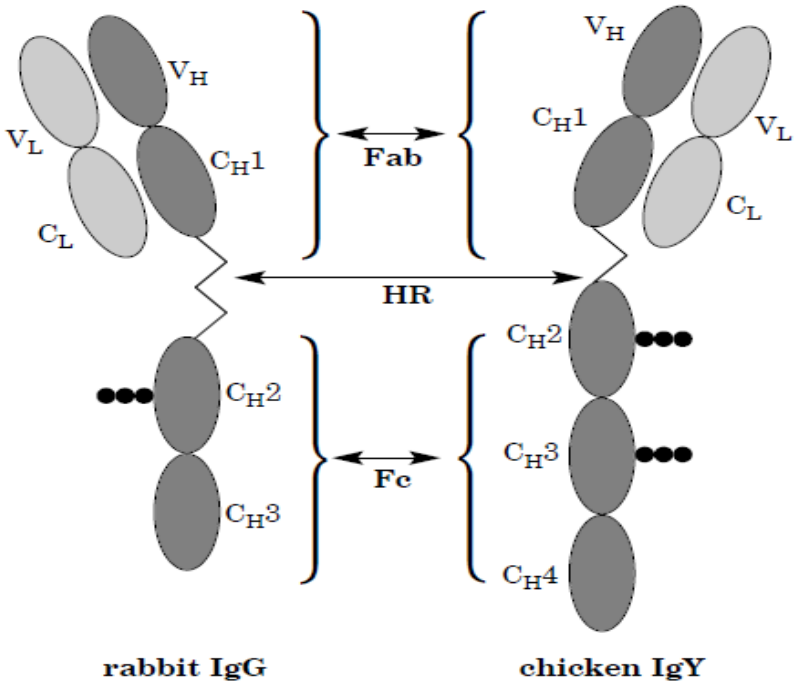

Figure 3.1: A cartoon comparison of a heavy and light chain fragment rabbit IgG been compared to chicken IgY heavy and light chain fragment. The C_H are the constant heavy chain domains, the V_H and the V_L are variable heavy chains and heavy light chains. (Figure adapted Shimizu *et al*., 1992).

Chicken IgY antibodies have been reported to have superior stability to IgG molecules because of its two glycosylation sites (Shimizu *et al*., 1992). To date there is no ΔμG DSF data comparing chicken IgY antibodies to mammalian polyclonal IgG molecules. Stability studies conducted by He *et al*., (2010); Li *et al*., (2011); and Menzen and Friess, (2013) found the melt temperature (T_m) of monoclonal IgG antibodies.

Typical methods to measure protein stability are the determination of Gibbs unfolding energy by DSC (Garbett and Chaires, 2012), isothermal calorimetry (ITC; Svilenov *et al.,* 2018), hydrogen-deuterium exchange mass spectroscopy (HDX-MS; Larsericsdotter *et al*., 2004), thermal denaturation and more recently DSF (Wright *et al*., 2017). The determination and the comparison of the Gibbs unfolding energy of different antibodies allows for the selection of the most stable class of antibody for use as immunochemical reagents.

Conjugating methods for antibodies to HRPC

Conjugated antibodies are used in immunochemical techniques, such as histochemistry and western blotting (Avrameas *et al*.,1978). A conjugated antibody is an enzyme which has been crosslinked and bound to the antibody. The most commonly used enzymes are horseradish peroxidase (HRPC) and alkaline phosphatase (AP).

Conjugation occurs at the Fc domain of the antibody and will not interfere with antigen binding.

Binding of a conjugated antibody to an antigen is visualised by the enzyme catalysed reaction with a suitable substrate. Recognition of the antigen by the antibody can be both quantitative or qualitative. Thus robust, sensitive and high affinity antibodies are required (Koivunen and Krogsrud*.,* 2005; Rosner *et al*., 1991).

The conjugating of enzymes to antibodies involves a small organic molecule, activating reactive groups on the enzyme. This allows the activated enzyme to couple to a second protein (antibody) by various mechanisms depending on the small organic molecule used (Avrameas *et al.,* 1978). These include cyanuric chloride (Avrameas *et al.,* 1978), p,p'-Difiuoro-rn,m'-dinitrophenyl sulfoite (FNPS) (Modesto and Pesce, 1973; Nakane and Pierce, 1966), N, N'-o-phenylenedimaleimide (Kato *et al*., 1976), Tetra-azofized o-diunisidine (Gregory and Williams, 1967), toluene diisocyanate (Modesto and Pesce, 1973) and m-maleimidobenzoyl-N-hydroxysuccinimide ester (MBS) (Peeters *et al*., 1989).

In the current study the stability and ΔμG of polyclonal chicken IgY, rabbit and mouse polyclonal IgG as well as crocodile IgY and IgM were determined using DSF. Glutaraldehyde (Avrameas 1969), sodium periodate (Nakane and Kawaoi, 1974) and (MBS) coupling reagents were tested for the conjugation of horseradish peroxidase to chicken IgY.

3.2. Materials and methods:

3.2.1. Materials and equipment

All common reagents, buffers, salts and SDS-PAGE reagents were purchased from Sigma and Merck. Protein molecular weight marker, containing: 116 kDa β-galactosidase; 66.2 kDa bovine serum albumin; 45 kDa ovalbumin; 35 kDa lactate dehydrogenase; 25 kDa REase Bsp981; 18.4 kDa β-lactoglobulin and 14.4 kDa lysozyme (Vilinius, Lithuania). Bovine serum albumin (BSA) was purchased from Roche (Mannheim, Germany). Maxi Sorp™ 96-well ELISA plates were from Nunc products (Roskilde, Denmark). PCR-X clear tubes (Star labs; Germany). SYPRO Orange (Sigma). HRPC (VI, 150 U/mg) were purchased from Sigma

AvantiTM J-26 XPI and AllegraTM X-22R centrifuges from Beckman Coulter (California, USA); UV-1800 Shimadzu spectrophotometer from Shimadzu corporation (Kyoto, Japan); pH meter from HANNA instruments; Corbett Research PCR Rotorgene 6000 and VersaMax™ ELISA plate reader was purchased from Molecular Devices Corporation (California, USA).

3.2.2. Thermal melt assay, sample preparation

Chicken IgY antibodies were isolated from chicken egg yolk by PEG precipitation (Polson *et al.*, 1985). Purified crocodile IgY and IgM were isolated, purified and available inhouse.

Mouse and rabbit IgG antibodies were kindly donated by Professor THT Coetzer.

All antibodies were diluted in dH_2O to a final concentration of 0.5 mg/ml. Antibodies at 2.5 µg, were added to 7.5 µl constant ionic strength AMT (Ellis and Morrison, 1982) buffer (200 mM MES, 200 mM Na-acetate, 400 mM Tris-HCl), at various pH values and the reaction volume made up to 20 µl with dH_2O. Before reading, SYPRO Orange (at a 10x final concentration) was added.

The DSF reactions were carried out in a Rotor Gene-6000 machine, at a temperature range of 25°C to 95°C. The Rotor-Gene-6000 software captured the data, plotted the Boltzan sigmoidal curve and was used to calculate the dF/dT data. All data was processed using Microsoft excel (365) Niesen *et al*., (2012).

3.2.3. Thermodynamic properties of proteins using DSF

The melt curves of chicken IgY, mouse IgG, rabbit IgG and crocodile IgY and IgM polyclonal antibodies were analysed (Section 3.2.1). The sigmoidal curve of fluorescence against temperature allows for the determination of the antibodies change in Gibbs unfolding energy (ΔµG; Eqn 1-5), entropy (ΔµS), melting temperature (T_m) and enthalpy (ΔµH) was calculated by the following equations:

Equation 1: $F_{max} = (F_{Tm} - F_{min}) + F_{Tm}$

F_{max} is maximum fluorescence; F_{Tm} is the melting temperature; F_{min} is the minimum fluorescence

Equation 2: $P_f = 1 – ((F – F_{min})/ (F_{max} – F_{min}))$

P_f is the ratio of folded protein; F is fluorescence at any time point

Equation 3: $P\mu = 1 - P_f$

$P\mu$ is the ratio of unfolded protein

Equation 4: $K\mu = (P\mu/P_f)$

$K\mu$ is the ratio of unfolded protein to folded protein

Equation 5: $\Delta\mu G = -RTln(K\mu)$

ΔµG is the unfolded Gibbs energy; R is the noble gas constant -8.314 $J.K^{-1}.mol^{-1}$; T is temperature in Kelvin; Ln is the natural log of the unfolded protein ratio.

Equations 1 to 5 were used and a linear plot of ΔµG against T(K) to obtain a linear fit line, allowed for the determination of ΔµG at any temperature. Using equations 6 and 7 unfolding entropy (ΔµS) and unfolding enthalpy (ΔµH) was calculated.

Equation 6: $\Delta\mu S = \Delta\mu G/(T_m - T)$

Equation 7: $\Delta\mu H = T_m\Delta\mu S$

3.2.4. Glutaraldehyde conjugation of chicken IgY to HRPC

Glutaraldehyde conjugation was performed as previously described (Boorsma and Kalsbeek, 1975). Briefly, 10 mg of HRPC was dissolved in 200 µl of phosphate buffer (100 mM, pH 6.8) containing 1.25% glutaraldehyde, resulting in a final concentration of 150 U/mg HRPC. After 18 h at RT the solution was filtered through a Sephadex G-25 column (bed volume (V_o) = 73 ml). Which had been equilibrated with phosphate buffer (100 mM NaH_2PO_4, pH 6.5), and the brown coloured fractions were collected, pooled and concentrated to 1 ml using Amicon filtration (MWCO 10 kDa). Chicken anti-rabbit albumin (RSA) IgY (5 mg) and 100 µl carbonate-bicarbonate buffer (1 M; pH 9.5) was added to HRPC fractions. After 24 h at 4°C, 100 µl of lysine (0.2 M) was added to deactivate any remaining glutaraldehyde for 2 h at 4°C.

The sample was dialysed twice for 2 h and once overnight in PBS (137 mM NaCl; 3 mM KCl; 7 mM Na_2HPO_4; 1.5 mM KH_2PO_4; pH 7.2) to remove lysine. Excess HRPC was removed by passing the dialysed solution over a rabbit albumin Aminolink™ affinity matrix. The chicken anti-rabbit albumin IgY conjugated to HRPC was eluted with 900 µl Glycine-HCl (100 mM, pH 2.8) and neutralised with 100 µl phosphate buffer (1 M, pH 8.5).

3.2.5. Periodate conjugation of chicken IgY to HRPC

Sodium periodate 200 µl (0.1 M) was added to 5 mg HRPC (150 U/mg) and dissolved. The solution turned from brown to greenish-brown and was mixed end over end for 20 min in the dark at RT. Sodium periodate was removed by dialysis against sodium acetate buffer (0.1 M sodium acetate; 0.22% (v/v) acetic acid; pH 4.4) twice for 2 hours and once overnight. To raise the pH to 9.5, 40 µl carbonate buffer (0.2 M; pH 9.5) was added. To this solution, 5 mg chicken anti-rabbit albumin IgY (5 mg) was added and the IgY-HRPC mixture was mixed over 2 hours at RT. All HRPC not coupled was reduced by the addition of 100 µl $NaBH_3$ (4 mg/ml) and the solution was left to stand for 2 hours at 4°C.

The solution was then dialysed against borate buffer (0.1 M; pH 7.4) twice for 2 hours and once overnight. Lastly, an equal volume borate buffer (0.1 M, 60% (v/v) glycerol) was added and the sample stored at 4°C.

3.2.6. MBS conjugation of chicken IgY to HRPC

Chicken anti-RSA IgY (3.2 mg) was dialysed overnight against reduction buffer (100 mM Tris-HCl, 1 mM EDTA; pH 8.0) at 4°C and reduced with 10 mM DTT for 90 min at 37°C. DTT was removed using a G-1 column (10 ml) equilibrated, washed and eluted with phosphate buffer (100 mM NaH_2PO_4 100 mM; pH 7.0). DTT was removed and the reduced samples were determined using Elman's reagent.

Four mg of HRPC (150 U/mg) was dissolved in 500 µl PBS was mixed with 500 µl of 1.2 mg of MBS (MBS dissolved in dimethyl formamide 200 µl + 300 µl PBS) incubated for 60 min at RT.

Unbound MBS was separated from HRPC using a G-25 gel filtration column (73 ml) equilibrated with phosphate buffer (100 mM NaH_2PO_4; pH 7.0). Eluted fractions with an absorbance at 280 nm A_{280} above 0.3 were pooled.

Reduced IgY and MBS-HRPC fractions were pooled and gently stirred for 3 h at RT, before been concentrated using centricon concentration (MWCO 10 kDA). Unbound HRPC was removed by passing the conjugated IgY-MBS-HRPC over a rabbit albumin Aminolink™ affinity matrix. Specific IgY antibodies were eluted with 900 µl Glycine-HCl buffer (100 mM; pH 2.8) and neutralised using 100 µl Phosphate buffer (1 M; pH 8.5).

3.2.7. The ELISA for detection of conjugated anti-RSA IgY

Varying concentrations of RSA were coated onto Nunc® 96 well plates overnight at 4°C. After washing with PBS (3 x 350 µl per well) and PBS-Tween 20 (0.1% v/v) (3 x 350 µl per well), wells were blocked with 200 µl 5% (w/v) milk-PBS for 2 h at 37 °C. Chicken anti-RSA IgY conjugated to HRPC (100 ng), was diluted in PBS (pH 7.0) was added and incubated for 2 hours at 37°C. The substrate tetramethylbenzidine (TMB) (284 µM TMB; 1.92 mM H_2O_2 in 0.15 M citrate-phosphate buffer pH 5.0), was added to each well, after 1 h at RT absorbance was measured at 652 nm using the Versamax™ microplate reader .

3.3. Results

The thermal stability of chicken IgY, mouse IgG, rabbit IgG, crocodile IgY and IgM was analysed at different pH values (4-9) in AMT buffers. The dF/dT curves of the Boltzmann non-linear fit function were analysed and plotted.

3.3.1. T_m of chicken IgY

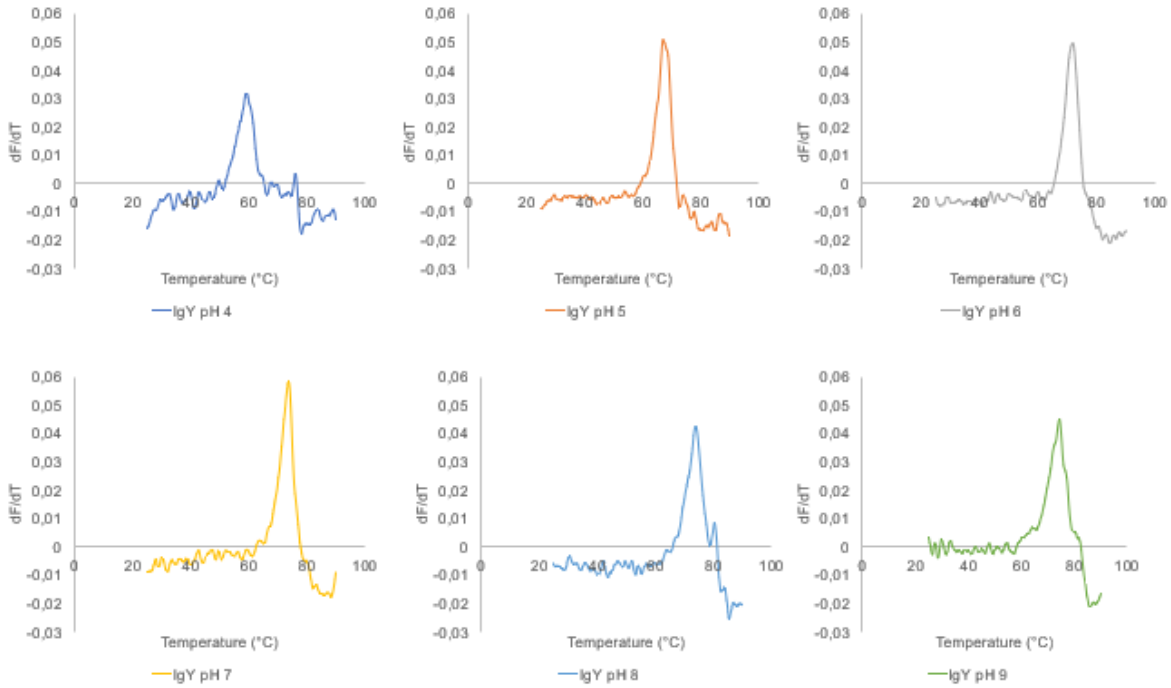

Figure 3.2: DSF first derivative data of fluorescence data for naïve polyclonal chicken IgY at different pH values. Chicken IgY thermodenaturation was analysed as a dF/dT function against temperature in AMT buffers at different pH values (4-9). SYPRO Orange was added and fluorescence data was measured from 25 to 90°C.

The thermodenaturation of naïve polyclonal chicken IgY was analysed at different pH values and produced a single dF/dT transition peak (Figure 3.2). From this peak the T_m could be determined at each pH value tested.

The T_m increased from pH 4 (59.45°C) to pH 9 (74.75°C), with a 1°C difference in T_m between pH 7 and 9.The antibody is most stable (higher T_m) in a pH 7 to 9 environment. A single transition peak suggests that all the domains comprising the chicken IgY molecule melted at the same T_m.

3.3.2. T_m of polyclonal mouse IgG

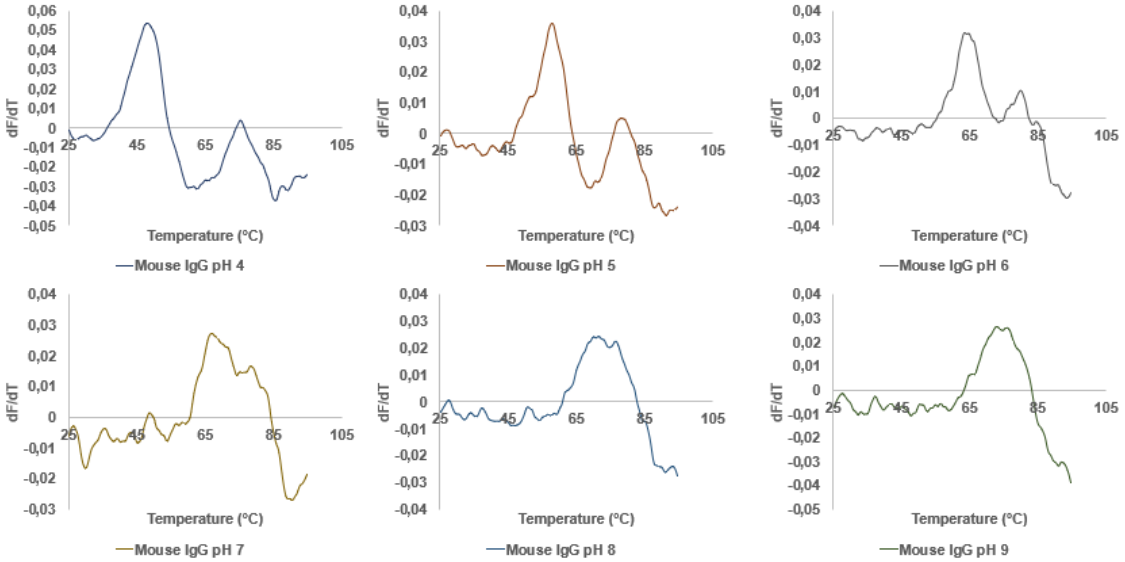

Figure 3.3: DSF first derivative of fluorescence data for polyclonal mouse IgG at different pH values. Mouse IgG thermodenaturation was analysed as a dF/dT function against temperature in AMT buffers at different pH values (4-9). SYPRO Orange was added and fluorescence data was measured from 25 to 90°C.

Mouse IgG was measured by DSF and the dF/dT curves had two transition peaks in acidic AMT buffers (Figure 3.3). At an alkaline pH a single transition peak was observed. The mouse IgG antibody was least stable at a pH value of 4, with the lowest T_m1 of 48.25°C and second peak T_m2 of 75.25°C. The T_m peaks increased with increasing pH up to pH 6. At pH 7, 8 and 9 the dF/dT curve was judged to have a single peak corresponding to a single transition with T_m values of 73.38, 76.68 and 76.08°C.

3.3.3. T_m analysis of polyclonal rabbit IgG

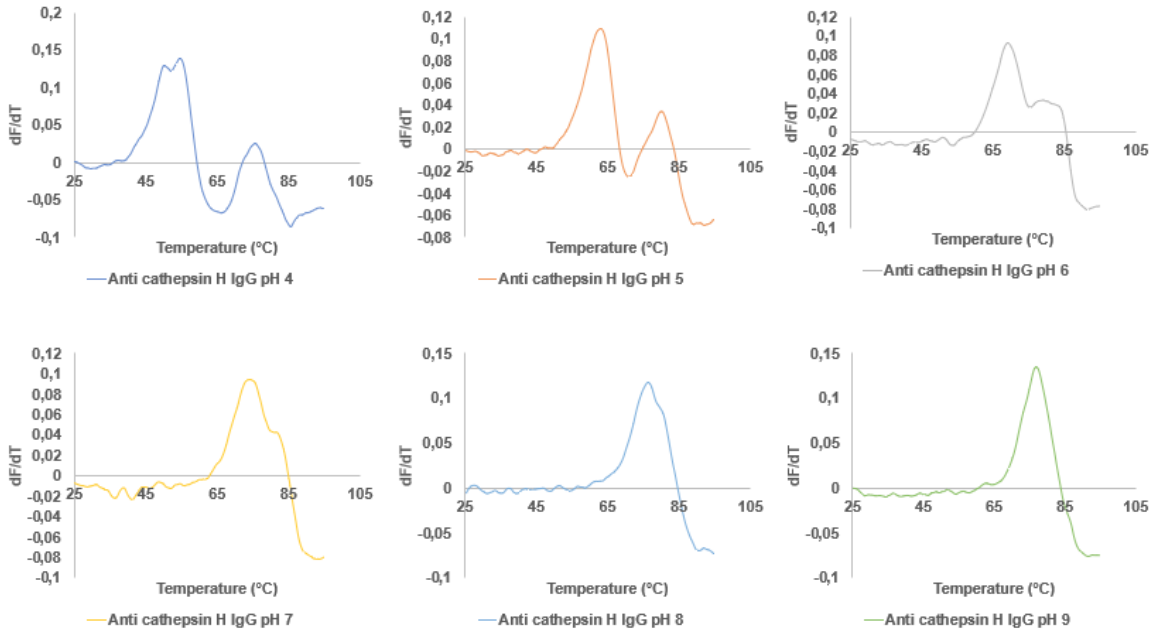

Figure 3.4: DSF first derivative of fluorescence data for pooled polyclonal rabbit IgG at different pH values. Rabbit IgG thermodenaturation was analysed as a dF/dT function against temperature in AMT buffers at different pH values (4-9). SYPRO Orange was added and fluorescence data was measured from 25 to 90°C.

The change in T_m with different pH values observed for chicken IgY (Figure 3.2) and mouse IgG (Figure 3.3) antibodies was similar for rabbit IgG (Figure 3.4) which had higher T_m values at neutral to alkaline pH values. Three transitions were observed with T_m values of 50.25, 54.58 and 75.75°C at pH 4, indicating three separate domains melted at different temperatures. At pH 5, two transition peaks were observed with T_m1 at 63.08°C and T_m2 at 80.08°C. At alkaline pH values rabbit IgG melted as a single transition and based on T_m values rabbit IgG was most stable at pH 9 with a T_m 76.92°C. A proteins stability using DSF is judged by the T_m of the domain with the lowest T_m. The DSF dF/dT results from the mouse IgG and rabbit IgG molecules unfolding in a similar fashion and different to that of naïve chicken IgY, which did not show multiple transitions at any pH tested.

3.3.4. T_m analysis of polyclonal crocodile IgM

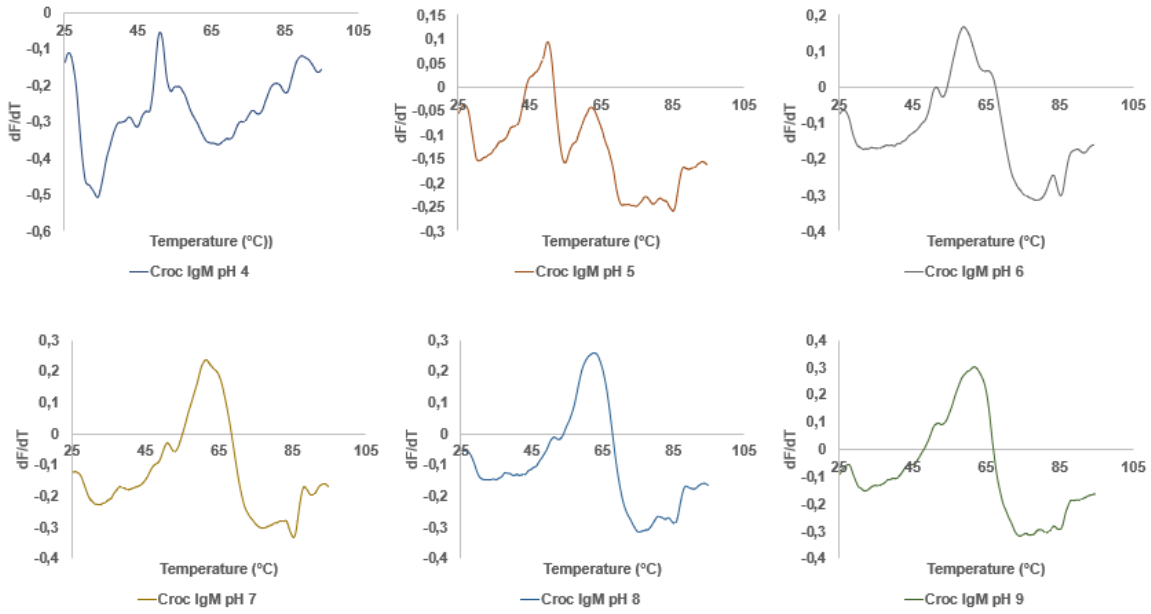

Figure 3.5: DSF first derivative of fluorescence data for crocodile IgM at different pH values. Crocodile IgM thermodenaturation was analysed as a dF/dT function against temperature in AMT buffers at different pH values (4-9). SYPRO Orange was added and fluorescence data was measured from 25 to 90°C.

The T_m of crocodile IgM increased with increasing pH and had the highest T_m at pH 8 (62.58°C), although the T_m at pH at 7 and 9 were very similar at 61.52 and 61.75°C respectively (Figure 3.5). At each pH value tested, a single transition was observed suggesting the entire molecule destabilised and unfolded at the same temperature.

3.3.5. T_m analysis of crocodile IgY

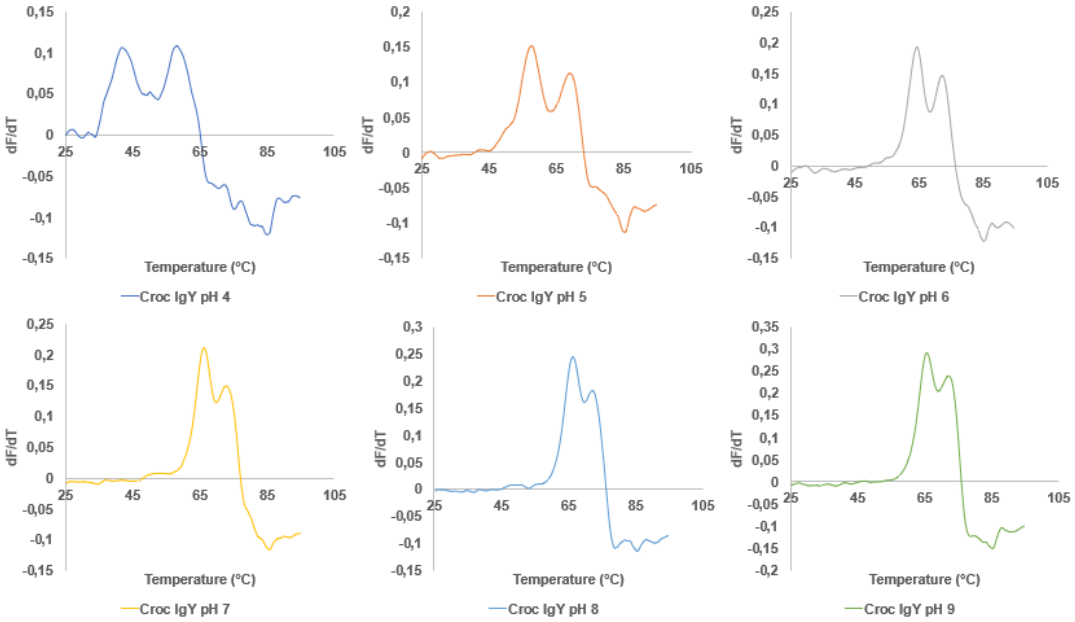

Figure 3.6: DSF first derivative of fluorescence data for crocodile IgY at different pH values. Crocodile IgY thermodenaturation was analysed as a dF/dT function against temperature in AMT buffers at different pH values (4-9). SYPRO orange was added and fluorescence data was measured from 25 to 95°C.

The dF/dT curves for crocodile IgY (Figure 3.6) differed from chicken IgY (Figure 3.2) as there were two transitions present at each pH value for crocodile IgY compared to the single transition with chicken IgY. Crocodile IgY was least stable at pH 4 with the first transition T_m1 41.92° and the second transition at T_m2 58.08°C. Increasing pH resulted in the molecule becoming more stable, which is seen by an increase in T_m. The two transitions are an indication that crocodile IgY has two domains that have different thermal stabilities or unfolding takes place in two phases. pH also effects the microenvironment around the IgY molecule as increasing pH results in both transition peaks moving closer together.

The two transition peaks for crocodile IgY were closest at pH 8, while the T_m at pH 7 was 12°C lower than that of pH 8 (54.08°C compared to 66.25°C). The increased amplitude of the dF/dT peaks at pH 6 to 9 is due the unfolding of the crocodile IgY molecule at a lower range of temperatures as compared to acidic conditions.

A T_m summary of all five antibodies is presented in Table 3.1.

Table 3.1: Summary of T_m of different polyclonal antibodies.

		T_m(°C)					
pH		4	5	6	7	8	9
Chicken IgY	T_m1	59.45	67.25	71.25	73.75	74.05	74.75
Mouse IgG	T_m1	48.25	57.92	64.75	73.38	76.58	76.08
	T_m2	75.25	78.25	80.08			
Rabbit IgG	T_m1	50.25	63.08	69.58	74.08	76.25	76.92
	T_m2	54.58	80.08				
	T_m3	72.75					
Crocodile IgM	T_m1	N.D	50.08	58.92	61.52	62.58	61.75
Crocodile IgY	T_m2	41.92	42.92	51.58	54.08	66.25	66.42
	T_m3	58.05	57.75	64.58	72.75	72.25	72.25

A summary of the T_m's determined by DSF at pH 4 to 9 of chicken IgY, mouse IgG, rabbit IgG, crocodile IgM and IgY is reported in Table 3.1.

3.3.6. Thermodynamic analysis of carbonic anhydrase

After dF/dT thermal melt analysis, the data was used to determine the Gibbs free unfolding energy (ΔμG), entropy of unfolding (ΔμS) and enthalpy of unfolding (ΔμH). As described by Wright *et al*., (2017). Carbonic anhydrase was used as a control and the data as it was used by Wright *et al*., (2017).

Table 3.2: Comparison of the thermodynamic parameters obtained for carbonic anhydrase to Wright *et al*., 2017.

	Wright *et al*., 2017	Current experiment	%Error
T_m	62.8	59.5	5
ΔμG $Kj.mol^{-1}$	60.4	56.7	6
ΔμH Kj/mol^{-1}	536	552	3
ΔμS $KJ.mol^{-1}.K^{-1}$	1.6	1.66	4

The results obtained in Table 3.2 are similar to that determined by Wright *et al*., (2017).

3.3.7. Fluorescence curves of different antibodies

A good transition is seen from a steady constant fluorescence to a visible sharp increase. Good transitions were observed for all antibodies except for crocodile IgM (Panel D). Using the Wright *et al*., (2017) method, the thermodenaturation DSF fluorescence curves were analysed (Figure 3.7). A sample calculation for chicken IgY is reported in Table 3.3 and the appendix.

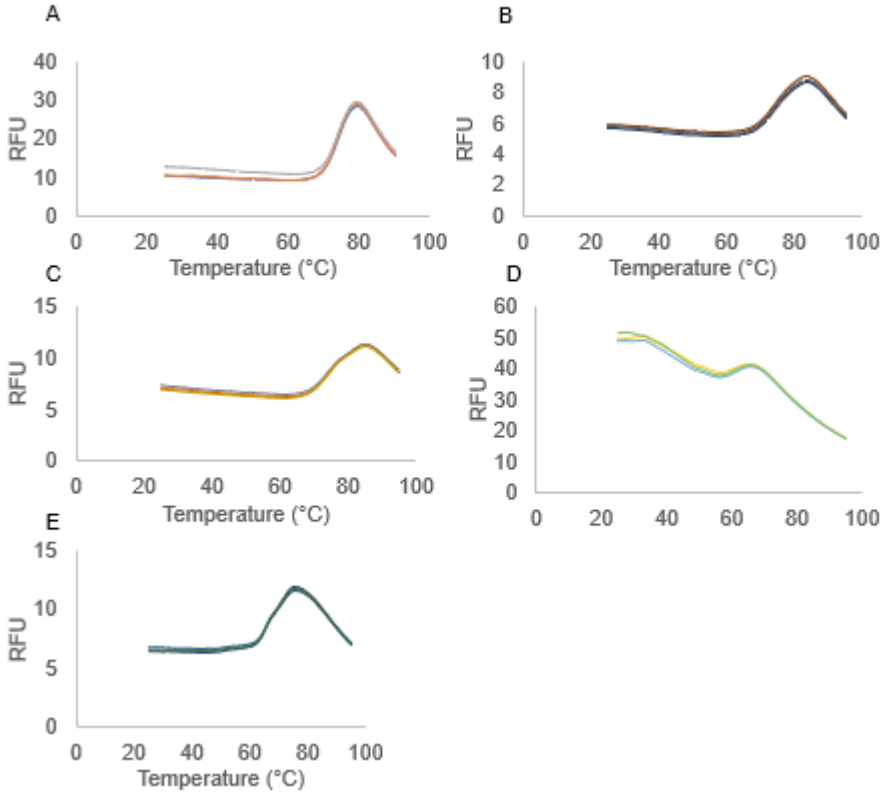

Figure 3.7: Thermodenaturation fluorescence curves of different naïve polyclonal antibodies. Thermodenaturation of polyclonal chicken IgY **(A)**; polyclonal mouse IgG **(B)**; polyclonal rabbit IgG **(C)** ;polyclonal crocodile IgM **(D)**; polyclonal crocodile IgY **(E)** was measured using DSF in AMT buffer pH 7.0. SYPRO Orange was used to monitor the transitions causing the RFU measured at different temperatures. Each panel shows triplicate results.

3.3.8. Thermodynamic calculations for the stability of antibodies

Using equation 2 (section 3.2.2) and applying it to the data from Figure 3.7, the partial folded (Pf) protein concentration was calculated. Thereafter, equation 3 was used to find the ratio of unfolded protein (Pμ). Together, the folded and unfolded protein concentration was used in equation 4 to calculate the unfolded protein equilibrium (Kμ). These results for chicken IgY are reported in the appendix. A sample calculation of chicken IgY is presented below in Table 3.3.

Table 3.3: Chicken IgY data calculated from equations 1-5.

Fmin	Chicken IgY Fluorescence data	F- F min	Fmax-Fmin	(F-Fmin)/Fmax-Fmin)	Pf = 1-(F-Fmin)/Fmax-Fmin) (F-Fmin)/Fmax-Fmin)	Pu	Pf	Ku= (pu/pf)	T in (K)	ΔGμ
9.37	9.401	0.031	19.5	0.002	0.998	0.002	0.998	0.002	335.2	17995.27
9.37	9.421	0.051	19.5	0.003	0.997	0.003	0.997	0.003	335.5	16595.49
9.37	9.438	0.068	19.5	0.003	0.997	0.003	0.997	0.003	335.8	15806.05
9.37	9.438	0.068	19.5	0.003	0.997	0.003	0.997	0.004	336.1	15800.2
9.37	9.447	0.077	19.5	0.004	0.996	0.004	0.996	0.004	336.4	15464.12
9.37	9.483	0.113	19.5	0.006	0.994	0.006	0.994	0.006	336.7	14407.64
9.37	9.54	0.17	19.5	0.009	0.991	0.009	0.991	0.009	337	13268.15
9.37	9.559	0.189	19.5	0.01	0.99	0.01	0.99	0.01	337.3	12983.31
9.37	9.588	0.218	19.5	0.011	0.989	0.011	0.989	0.011	337.6	12584.07
9.37	9.62	0.25	19.5	0.013	0.987	0.013	0.987	0.013	337.9	12205.67
9.37	9.69	0.32	19.5	0.016	0.984	0.016	0.984	0.017	338.2	11506.96
9.37	9.747	0.377	19.5	0.019	0.981	0.019	0.981	0.02	338.5	11048.33
9.37	9.815	0.445	19.5	0.023	0.977	0.023	0.977	0.023	338.8	10581.7
9.37	9.879	0.509	19.5	0.026	0.974	0.026	0.974	0.027	339.1	10205.95
9.37	9.956	0.586	19.5	0.03	0.97	0.03	0.97	0.031	339.4	9804.579
9.37	10.054	0.684	19.5	0.035	0.965	0.035	0.965	0.036	339.7	9362.345
9.37	10.165	0.795	19.5	0.041	0.959	0.041	0.959	0.042	340	8930.28
9.37	10.271	0.901	19.5	0.046	0.954	0.046	0.954	0.048	340.3	8564.89
9.37	10.389	1.019	19.5	0.052	0.948	0.052	0.948	0.055	340.6	8205.982
9.37	10.541	1.171	19.5	0.06	0.94	0.06	0.94	0.064	340.9	7795.888
9.37	10.721	1.351	19.5	0.069	0.931	0.069	0.931	0.074	341.2	7369.269
9.37	10.912	1.542	19.5	0.079	0.921	0.079	0.921	0.086	341.5	6970.612
9.37	11.133	1.763	19.5	0.09	0.91	0.09	0.91	0.099	341.8	6561.053
9.37	11.38	2.01	19.5	0.103	0.897	0.103	0.897	0.115	342.1	6154.677
9.37	11.629	2.259	19.5	0.116	0.884	0.116	0.884	0.131	342.4	5786.902
9.37	11.94	2.57	19.5	0.132	0.868	0.132	0.868	0.152	342.7	5371.514
9.37	12.276	2.906	19.5	0.149	0.851	0.149	0.851	0.175	343	4968.969
9.37	12.664	3.294	19.5	0.169	0.831	0.169	0.831	0.203	343.3	4547.671
9.37	13.056	3.686	19.5	0.189	0.811	0.189	0.811	0.233	343.6	4161.127
9.37	13.477	4.107	19.5	0.211	0.789	0.211	0.789	0.267	343.9	3778.317
9.37	13.975	4.605	19.5	0.236	0.764	0.236	0.764	0.309	344.2	3359.365
9.37	14.487	5.117	19.5	0.262	0.738	0.262	0.738	0.356	344.5	2960.62
9.37	15.074	5.704	19.5	0.293	0.707	0.293	0.707	0.413	344.8	2532.082
9.37	15.65	6.28	19.5	0.322	0.678	0.322	0.678	0.475	345.1	2136.039
9.37	16.286	6.916	19.5	0.355	0.645	0.355	0.645	0.55	345.4	1719.297
9.37	16.939	7.569	19.5	0.388	0.612	0.388	0.612	0.634	345.7	1308.417
9.37	17.647	8.277	19.5	0.424	0.576	0.424	0.576	0.738	346	875.788
9.37	18.361	8.991	19.5	0.461	0.539	0.461	0.539	0.856	346.3	449.35

These values (Table 3.3) were then substituted into equation 5 to calculate the Gibbs unfolding energy at different temperatures from the data for chicken IgY (Figure 3.8).

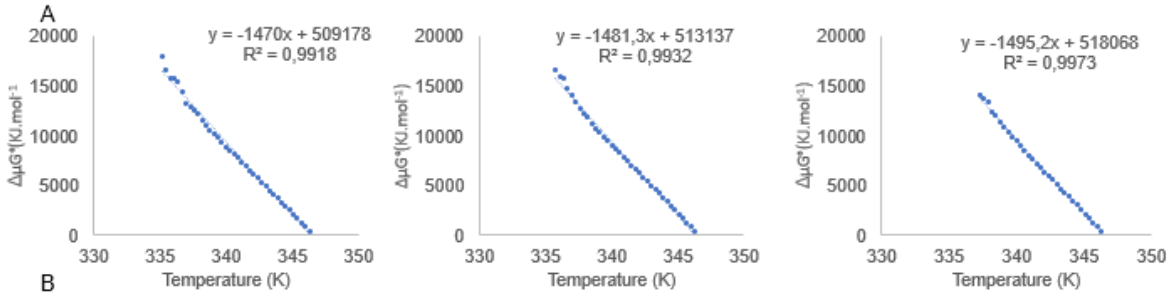

Figure 3.8: Fitting of DSF data to equation 5. DSF data (ΔμG) for polyclonal chicken IgY and R^2 values were calculated using excel.

Due to the large volume of data for each of the antibodies tested, equations of the remaining graphs for each antibody and the replicates whose R^2 is greater than 0.9 is reported (Table 3.4).

Table 3.4: Summary of linear equations for data fitted into equation 5 for the different antibodies.

	ΔμG equation in the form y = mx + c	R^2 - value
Chicken IgY	y= -1470x + 509178	0.992
	y = -1481x + 513137	0.993
	y = -1495,2x + 518068	0.997
Mouse IgG	y = -1103,2x + 381932	0.998
	y = -1208,3x + 417 474	0.995
	y = -1185,4x + 410205	0.996
Rabbit IgG	y = -1149x + 398391	0.998
	y = -1121,6x + 388814	0.998
	y = -1106,7x + 383708	0.994
Croc IgM	y = -2066,9x + 690612	0.994
	y = -2081,7x + 695631	0.996
	y = -2101x + 702903	0.995
Croc IgY	y = -2038,6x + 689227	0.999
	y = -2019,3x + 682899	0.999
	y = -2037,9x + 389104	0.999
Croc IgY	y = -1494,4x + 512846	0.994
	y = -1503,1x + 515663	0.984
	y = -1537,1x + 527452	0.992

The linear equations in Table 3.4 can be used to calculate the ΔμG energy for each antibody at any temperature. In this study, at 25°C (295K) the calculation of the ΔμG using linear equations was deemed accurate as all the R^2 values were above 0.99 except for a single replicate reading with crocodile IgY in the second transition. However, since the value was still above 0.9, it was included in the study. Using equation 6 and equation 7, the ΔμH and ΔμS were calculated and reported in Table 3.5.

Table 3.5: Thermal stability and thermodynamic data for antibodies.

		1	2	3	Average	S.D
Chicken IgY	ΔμG (KJ.mol^{-1})	71.12	71.71	71.60	71.48	0.32
	ΔμS (KJ.mol^{-1}.K^{-1}	1.46	1.47	1.47	1.47	0.01
	ΔμH (KJ.mol^{-1})	506.00	510.00	509.00	508.33	2,08
	T_m (°C)	73.75	73.55	73.95	73.75	0.2
Mouse IgG	ΔμG (KJ.mol^{-1})	53.13	52.40	56.96	54.16	2.45
	ΔμS (KJ.mol^{-1} K^{-1})	1.09	1.18	1.17	1.15	0.05
	ΔμH (KJ.mol^{-1})	378.30	391.11	405.00	391.47	13.35
	T_m (°C)	73.75	73.15	73.25	73.38	0.32
Rabbit IgG	ΔμG (KJ.mol^{-1})	55.99	54.58	53.91	54.83	1.06
	ΔμS (KJ.mol^{-1})	1.15	1.12	1.11	1.12	0.02
	ΔμH(KJ.mol^{-1})	398.10	388.00	383.20	389.77	7.61
	T_m (°C)	73.15	73.75	73.45	73.45	0.3
Croc IgM	ΔμG (KJ.mol^{-1})	74.68	75.28	75.96	75.31	0.64
	ΔμS (KJ.mol^{-1}K^{-1})	2.06	2.09	2.10	2.08	0.02
	ΔμH (KJ.mol^{-1})	688.60	698.60	701.00	696.07	6.58
	T_m (°C)	61.25	61.35	61.15	61.25	0.1
Crocodile IgY 1	ΔμG (KJ.mol^{-1})	81.72	81.15	81.81	81.56	0.36
	ΔμS (KJ.mol^{-1}K^{-1})	2.18	2.16	2.18	2.17	0.01
	ΔμH (KJ.mol^{-1}.K^{-1})	731.00	726.00	732.00	729.67	3.21
	T_m (°C)	65.25	65.15	65.45	62,30	0.15
Crocodile IgY 2	ΔμG (KJ.mol^{-1})	67.51	67.74	69.40	68.22	1.03
	ΔμS (KJ.mol^{-1}.K^{-1})	1.42	1.43	1.46	1.44	0.02
	ΔμH (KJ.mol^{-1})	491.00	492.00	504.00	495.67	7.23
	Tm (°C)	71.25	71.45	71.45	71.38	0.12

The fluorescence curves produced (Figure 3.7) were at pH 7. Only the crocodile IgY antibody had two transitions (Panel E) at pH 7.

Chicken IgY, mouse IgG and rabbit IgG had a similar T_m at pH 7 of 73.75, 73.38 and 73.45°C respectively (Table 3.5). Crocodile IgM had the lowest T_m of 61.25°C, whilst crocodile IgY second transition T_m (71.38°C) is similar to that of chicken IgY (Table 3.5). A higher ΔμG is an indication of a more stable antibody. Based on the results in Table 3.5 Crocodile IgY transition 1 had the highest ΔμG (81.56 KJ. Mol^{-1}) followed by crocodile IgM (75.31 $KJ.mol^{-1}$), chicken IgY (71.48 $KJ.mol^{-1}$), crocodile IgY transition 2 (68.27 $KJ.mMol^{-1}$) while mouse IgG and rabbit IgG had similar ΔμG (54.16 and 54.83 $KJ.mol^{-1}$). Alfano *et al*., (2017) stated that the two most common methods used to determine protein stability is T_m and ΔμG. Since only DSF was used, the proteins stability was judged based on the combined T_m and ΔμG. Therefore, the order of stability of the antibodies from most stable to least stable was chicken IgY, crocodile IgY, crocodile IgM, rabbit IgG and mouse IgG.

3.3.9. Stability of chicken IgY stored at 4°C from 1990

To investigate if chicken IgY is more stable than both the mouse and rabbit IgG, DSF analysis of chicken IgY which had been stored at 4°C since 1990 was performed (Figure 3.9).

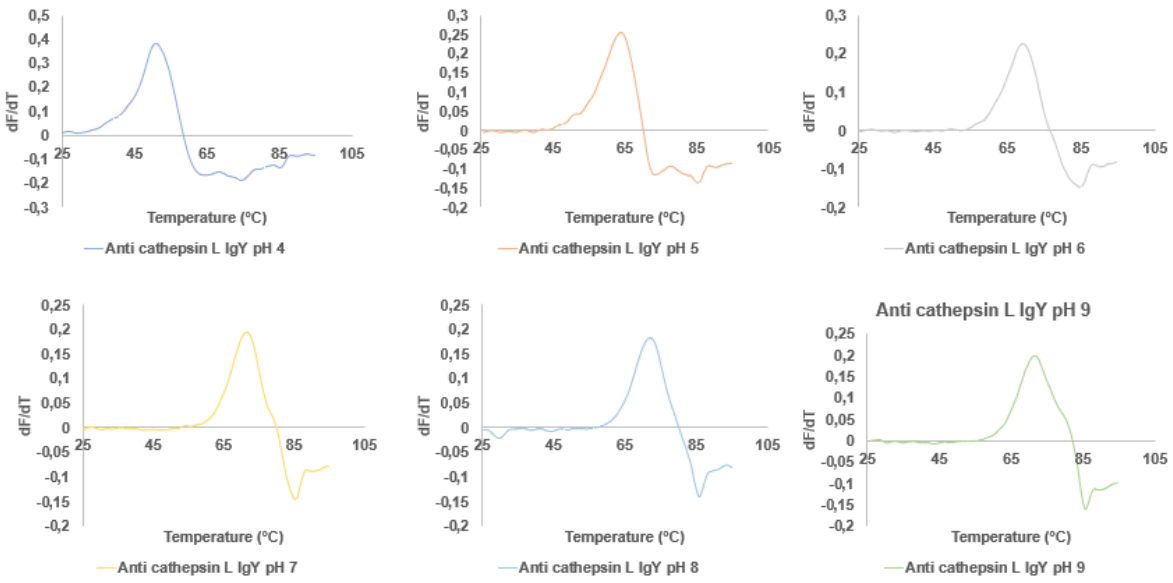

Figure 3.9: DSF first derivative of the fluorescence data for chicken IgY-1990 at different pH values. Chicken IgY-1990 in AMT buffer from pH 4 to 9. SYPRO Orange was added and the raw fluorescence data was measured from 25 to 95°C of which the first derivative was calculated.

Similar to the chicken IgY (Figure 3.2), chicken IgY-1990 had an increasing T_m with increasing pH and only a single transition. This indicates the chicken IgY is remarkably stable. The difference in both the chicken IgY molecules was the chicken IgY-1990 had a 2.17°C lower T_m (at pH 7) compared to the freshly isolated chicken IgY.

3.3.10. Comparing the conjugating efficiency of three cross linking reagents

The conjugating efficiency of HRPC to the chicken anti-RSA IgY using glutaraldehyde, sodium periodate and MBS was measured using a direct ELISA (Figure 3.10).

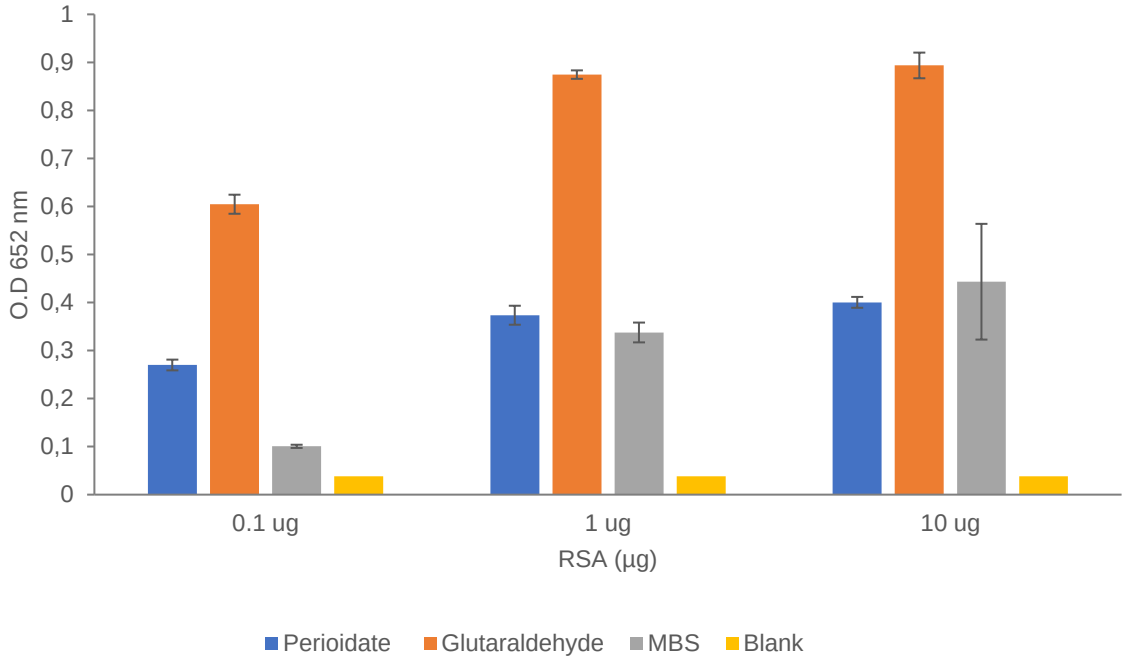

Figure 3.10: Comparison of glutaraldehyde, sodium periodate and MBS conjugation of HRPC to chicken anti-RSA IgY. Microplates were coated with RSA (0.1 – 10 µg) and detected with chicken anti-rabbit RSA IgY-HRPC conjugates, coupled with either glutaraldehyde, sodium periodate or MBS. TMB was used for detection and was measured at 652 nm. Error bars indicate S.D of triplicate results.

Detection of RSA by chicken anti-RSA IgY-HRPC conjugate confirmed that all three conjugating reagents resulted in successful conjugation of chicken anti-RSA IgY to HRPC. The conjugates detected RSA, detected between 0.1 to 10 µg (Figure 3.10).

RSA at 1 to 10 µg was detected by the Na-periodate IgY-HRPC, which was similar to the MBS conjugate. At 0.1 µg RSA, the Na-periodate detected it with a higher absorbance, while the glutaraldehyde IgY-HRPC conjugate had a higher absorbance for 0.1 – 10 µg RSA. All three conjugates had no non-specific binding and the results indicate the glutaraldehyde method was the most efficient method used to couple chicken IgY to HRPC.

3.3.11. Finding the LOD of glutaraldehyde coupled IgY

The LOD of the glutaraldehyde conjugate was determined (Figure 3.11).

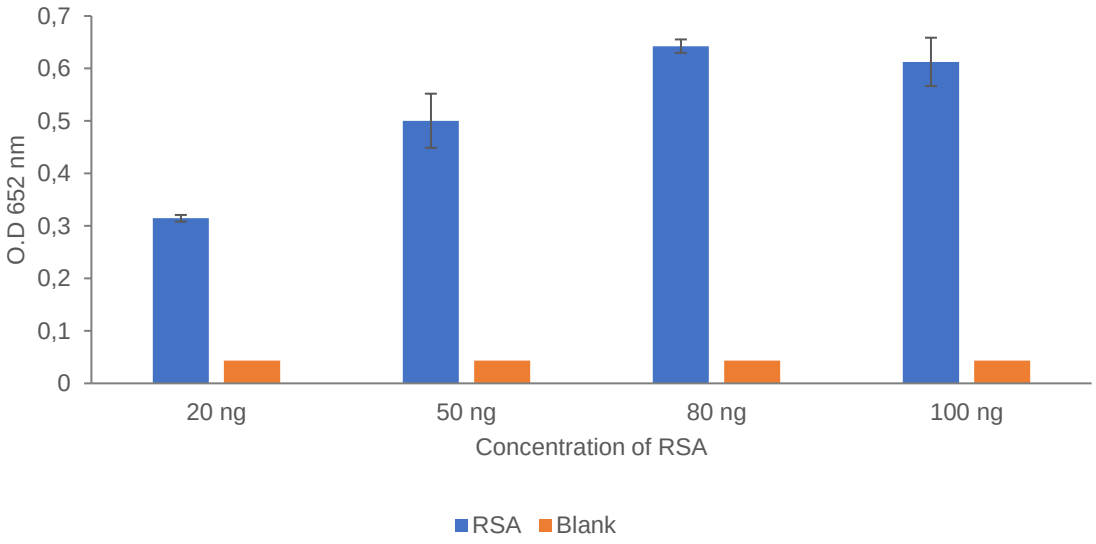

Figure 3.11: Glutaraldehyde coupled anti-RSA-IgY-HRPC detecting RSA in an ELISA. Microplates were coated with RSA (20 – 100 ng) and detected with glutaraldehyde coupled chicken anti-RSA IgY-HRPC conjugate (100 ng). TMB was as the substrate and was measured at 652 nm. Error bars indicate S.D of triplicate results.

When diagnosing a disease in the field using an ELISA, an O.D cut off is around 0.2 (Voller *et al*., 1980). Using the same cut off on our conjugates to define their LOD (Figure 3.10). Glutaraldehyde coupled IgY-HRPC detected 20 ng of RSA with an absorbance above 0.2 (Figure 3.11). This was 5 times less RSA, than the RSA concentration detected by anti-RSA IgY, coupled by the sodium periodate method and 50 times less RSA compared to the anti-RSA IgY coupled by the MBS method (comparing Figure 3.10 to Figure 3.11).

3.3.12. Analysis of MBS conjugation

MBS conjugation required the reduction of IgY with DTT to expose internal cysteines for their sulfhydryl groups, resulting in the reduction. This meant light and heavy chains were separated, which was confirmed by SDS-PAGE (Figure 3.12).

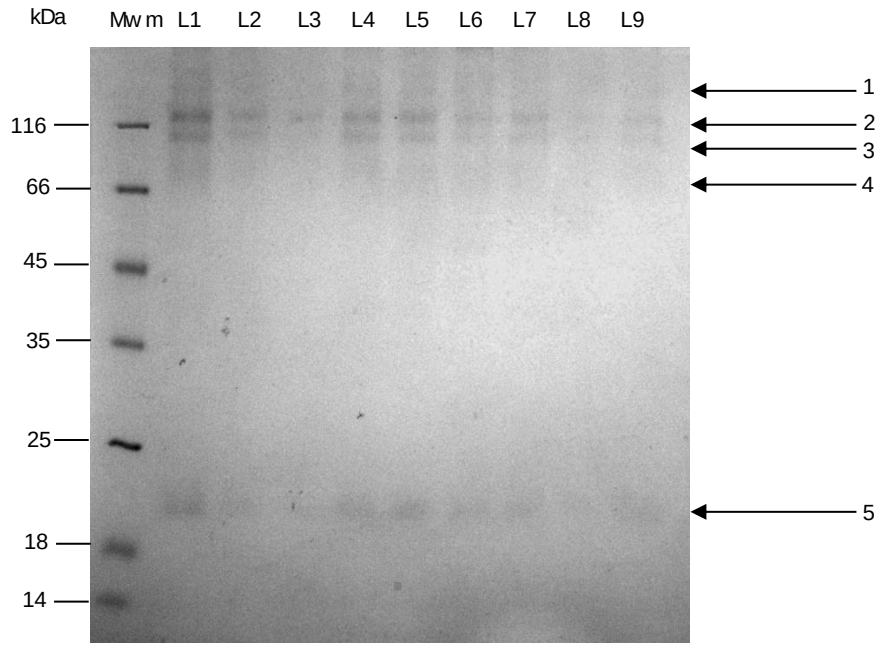

Figure 3.12: Analysis of anti-RSA IgY following DTT reduction and size exclusion chromatography on an SDS-PAGE. A 12.5% SDS-PAGE gel run in the absence of β-mercaptoetahnol showing chicken anti-rabbit RSA IgY fractions were run through a Sephadex G-25 matrix to remove DTT. Lanes 1 -9 are the 9 fractions that were the eluted collected fractions. Arrows 1-5 indicate the different species of IgY eluted from gel filtration chromatography after DTT reduction.

Two bands lie above the 116 kDa (arrow 1 and 2). The highest band (arrow 1) is thought to be non-reduced IgY, the second band (arrow 2) above 130 kDa could be two heavy chains (HC). The third band (arrow 3) below 116 kDa marker (90 kDa) may be the HC and Light chain (LC) joined. The remaining two bands could be the HC (65 kDa) and LC (25 kDa) (Figure 3.12).

3.3.13. MBS conjugation mechanism

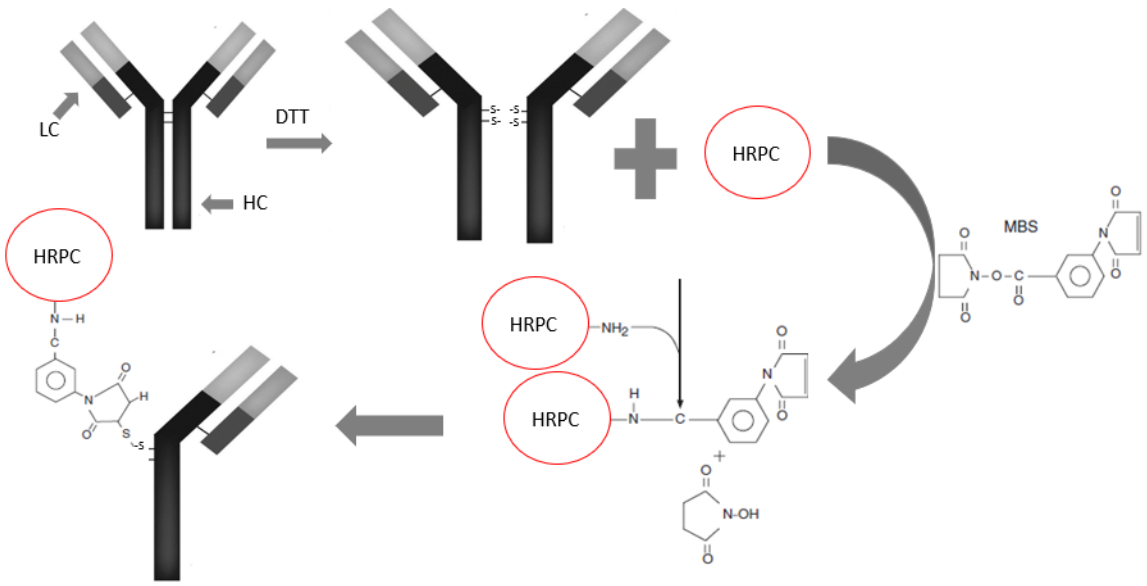

Figure 3.13: Proposed mechanism of HRPC conjugation to IgY the molecule using MBS. IgY is represented by "Y" shape molecule. LC and HC represent the heavy and light chains.

The image (Figure 3.13) shows the possible method for MBS conjugation of a chicken IgY molecule to HRPC. The IgY molecule is reduced with DTT into two HC and LC fragments with two exposed cysteine residues. The MBS molecule as a linker between the cysteine residues and the HRPC.

3.3.14. Conjugation of redox treated chicken anti-RSA IgY

Since glutaraldehyde conjugation was the most efficient at conjugating HRPC to IgY, it was used in conjunction with both oxidised and reduced IgY to couple a chicken IgY to HRPC. The efficiency of the co method was analysed using an ELISA (Figure 3.14).

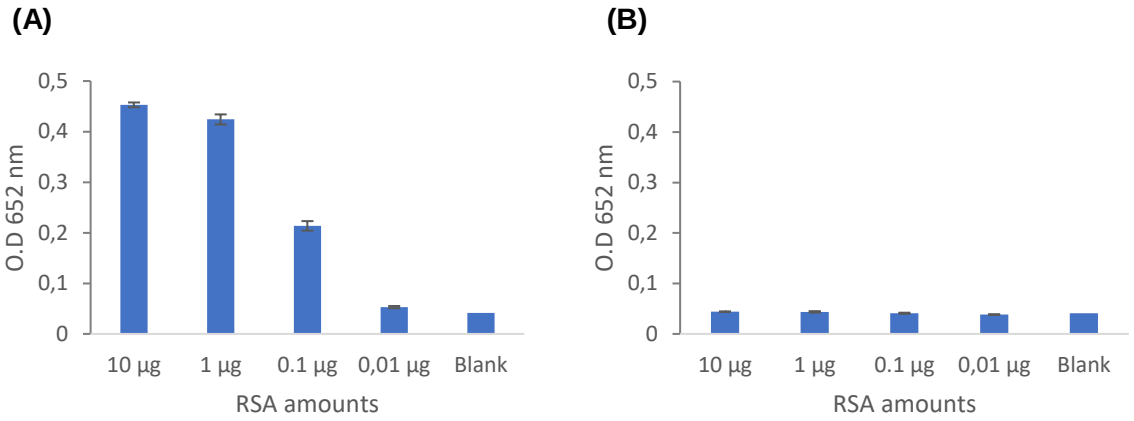

Figure 3.14: Redox-glutaraldehyde coupled anti-RSA IgY-HRPC detecting RSA in an ELISA. Microplates were coated with RSA (10 – 0.001 µg), detected with glutaraldehyde coupled to the reduced chicken anti-RSA IgY-HRPC conjugate **(A)** and the reduced chicken anti-RSA IgY that was oxidised **(B)**. Colorimetric substrate TMB was used for detection and measured at 652 nm. Error bars indicate S.D of triplicate results.

ELISA results on Figure 3.14A confirm that RSA could be detected with reduced anti-RSA IgY-HRPC conjugate, while Figure 3.14B showed no detection of RSA when anti-RSA-IgY was oxidised after reduction with H_2O_2. Reducing IgY did not increase the limit of detection of the glutaraldehyde conjugated anti-RSA IgY-HRPC.

3.3.15. Analysis of different HRPC samples with different limits of activity

The HRPC used in the assay was of low activity (150 U/mg). A 1000 U/mg HRPC and 150 U/mg HRPC were run on SDS-PAGE gel to evaluate the structure of the enzyme in the samples (Figure 3.15). The 150 U/mg HRPC, had additional proteins at different sizes compared to the 44 kDa HRPC molecule in the samples (Figure 3.15 lanes 1 and 2) which were not present in the 1000 U/mg activity HRPC (Figure 3.15 lanes 3 and 4). This meant the 150 U/mg HRPC present is in lower concentrations than anticipated.

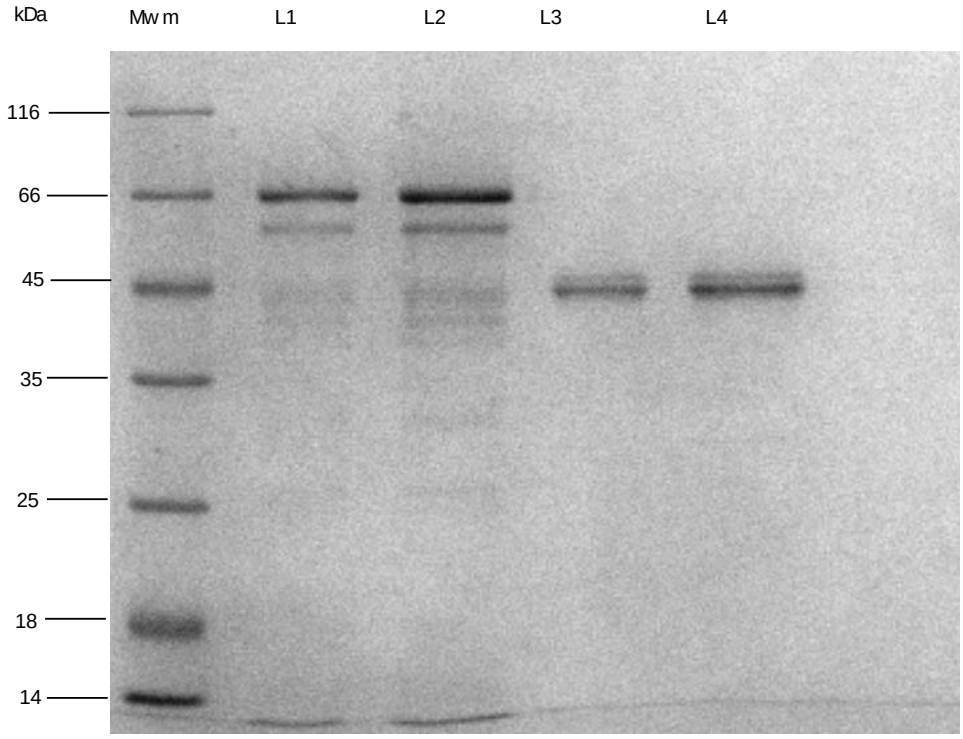

Figure 3.15: 150 U/mg and 1000 U/mg HRPC run on an SDS-PAGE gel. Two samples of HRPC (17 6U/mg and 1000 U/mg) were analysed on a 12.5% non-reducing SDS-PAGE gel. Lane 1 and 2 HRPC (150 U/mg). Lane 3 and 4 had HRPC (1000 U/mg). The gel was stained with Coomassie brilliant blue R-250.

3.4. Discussion

Using DSF a proteins stability is judged on its T_m value (Niesen *et al.,* 2007). By using the ΔμG the conformational stability of a protein was measured (Freire *et al*., 2013; Wright *et al.,* 2017). Based on the thermodynamically most stable antibody (polyclonal chicken IgY) different conjugation techniques were tested.

3.4.1. Using ΔμG as a measure of proteins stability

Wright *et al*., (2017) showed HRPC type I had a T_m of 64.1°C and a ΔμG of 24.6 KJ.mol^{-1} while carbonic anhydrase isozyme (II) from bovine erythrocytes has T_m 62.8°C and a ΔμG of 60.4 KJ.mol^{-1}. Both proteins had similar T_m but a ΔμG difference of 35.8 KJ.mol^{-1} indicating carbonic anhydrase was more stable than HRPC. The ΔμG of a protein represents the conformational stability, while T_m is based on when half the protein has unfolded (Freire *et al*., 2013; Niesen *et al*., 2007). Therefore, ΔμG may be a more accurate measure of protein stability.

3.4.2. Analysis of mouse and rabbit IgG molecules

DSF analysis of polyclonal IgG antibodies from mice and rabbits showed two peaks at acidic pH values while a single peak was observed at neutral and alkaline pH (Figures 3.3 and 3.4). The first peak is likely the C_{H2} domain while the second peak is the simultaneous thermodenaturation of the C_{H3} and Fab domains of the molecules melting, this was shown with mouse monoclonal IgG using DSC (Ionescu *et al*., 2008; Garber and Demarest, 2007) and DSF (He *et al*., 2010). The C_{H2} domain is glycosylated making it more sensitive to the acidity of the buffer compared to the C_{H3} and Fab fragment, therefore two peaks appear. At alkaline pH the entire molecule melts simultaneously (Wen *et al*., 2008; He *et al*., 2010). Similar results with mouse monoclonal IgG antibodies were observed in previous studies (Menzen and Friess, (2013); Svilenov *et al*., (2018); Garber and Demarest, (2007), Ionescu *et al*., (2008).

3.4.3. Comparison of polyclonal chicken IgY vs polyclonal mouse and rabbit IgG

Based only on the T_m (dF/dT curve), the chicken IgY antibodies were more stable than both IgG molecules in acidic AMT buffers (pH 4 to 6). A proteins stability is dependent on the stability of the weakest domain (He *et al*., 2010) .

Chicken IgY has two glycosylation sites and the additional glycosylation site has been reported to aid in the stabilisation of IgY (Spillner *et al*., 2012). Alsenaidy *et al*., (2014) showed that the absence of carbohydrates in mouse monoclonal IgG resulted in reduced thermal stability of the antibodies.

The absence of two transitions (peaks) for chicken IgY is probably due to the less developed hinge region. This was seen before when murine IgG1 which had a single transition while IgG2a had two, at pH 6.0 and was attributed to a less developed hinge region (Ionescu *et al*., 2008; Vermeer *et al*., 1998).

3.4.4. Analysis of crocodile IgM and IgY

Crocodile IgM (Figure 3.5) appeared to be more sensitive to pH denaturation compared to the other antibodies analysed as there was no transition at pH 4, indicating IgM was completely denatured. The IgM molecule is typically greater than 900 kDa and lacks a hinge region (Plomp *et al*., 2016), this could explain why a single transition was observed at all pH values. The results were surprising since IgM is made up of five 180 kDa monomers which are thought to be similar to IgY. It was expected that the T_m would be higher than 62°C or there would be multiple transitions.

Crocodile IgY (Figure 3.6) was different to that of chicken IgY as at each pH value there were two peaks. This could potentially be because the C_{H2} + C_{H3} domains and the C_{H4} + Fab domains melted at different temperatures. Since the C_{H2} + C_{H3} domains are glycosylated.

3.4.5. Comparing the ΔμG of the antibodies

ΔμG for all five antibodies (Wright *et al*., 2017) is shown in Table 3.5. ΔμG of chicken IgY was compared to rabbit IgG and mouse IgG, at pH 7 and all three molecules had a T_m of around 73°C. However, the ΔμG calculation showed that chicken IgY was 17 KJ.mol^{-1} more stable than both IgG molecules.

A higher ΔμH is expected for more stable molecules as it is based on the ΔμG and ΔμS of the system. Comparing the ΔμS, a value close to one is ideal, the ΔμG for both IgG molecules were lower than that of chicken IgY but the IgY ΔμS was marginally above 1 indicating 1 state.

Comparison of crocodile IgM and IgY were somewhat ambiguous and had to be considered. The T_m was for croc IgM was the lowest at 61.25°C, however the ΔμG was higher than chicken IgY and both IgG molecules which would be an indication that it was more stable but since the ΔμS was 2, it meant there were two states of disorder in the molecule.

An ΔμS 2 could be due to the pentameric structure of IgM. The crocodile IgY molecules was the only antibody that was shown to have two transitions. The transitions of the carbohydrate moiety of C_{H3} and C_{H4} and C_{H2} and Fab melting at different temperatures (Ionescu *et al*., 2008; Garber *et al*., 2007). Interestingly the ΔμS was above 2 for the first transition indicating it may not be the most stable. The second transition however was remarkably similar to the chicken IgY with all four thermodynamic parameters.

Based on the results polyclonal chicken IgY antibodies appeared to be the most stable. A 1990 sample IgY (28 years) stored at 4°C was analysed by DSF analysis showed the antibodies had a similar dF/dT profile and similar T_m (Figure 3.9) to freshly isolated chicken IgY indicating they were in their native conformation.

3.4.6. Using DSF to calculate ΔμG

DSF is not often used to compare the thermodynamic stability of proteins, while DSC remains the gold standard (Garbett and Chaires, 2012). To our knowledge this is the first-time polyclonal antibodies were compared with ΔμG rather than T_m alone. In previous studies when monoclonal antibodies were compared, acidic buffers were used due to monoclonal antibodies degrading in alkaline pH buffers (Manning *et al*., 2011). This was not observed for chicken IgY antibodies (stored at pH 7.4), as we show the molecule still had dF/dT peaks after 28 years (Figure 3.9).

He *et al*., (2010) showed that no transitions were missed with DSF compared to DSC with monoclonal antibodies and the SYPRO Orange fluorescence dye did not interfere with the assay.

Several studies have looked at the correlation between DSF and DSC for antibodies and shown that both methods have a linear correlation when estimating Tm. DSF usually overestimates Tm as compared to DSC (Menzen and Friess, 2013; He *et al*., 2010).

3.4.7. Comparison of the three cross linking reagents used to conjugate anti-RSA-IgY to HRPC

A two-step conjugation method coupled anti-RSA-IgY to HRPC using glutaraldehyde, Na-periodate and (Figure 3.10). Two-step conjugating methods show less non-specific binding, offer better conjugation quality and efficiency compared to single step conjugating (Beyzavi *et al*., 1987). Of the three methods the glutaraldehyde method was the most efficient followed by Na-periodate, reduced glutaraldehyde method and then MBS.

3.4.8. Na-periodate, Glutaraldehyde and MBS conjugating mechanism explained

Several previous studies have reported Na-periodate conjugation to be more efficient than glutaraldehyde (Tijssen and Kurstak, 1984; Beyzavi *et al*., 1987). However, those reports used IgG molecules. To explain why glutaraldehyde conjugation was fivefold better, than Na-periodate conjugation, the mechanisms of the methods were evaluated.

Na-periodate oxidises the carbohydrate glycans on HRPC to form reactive aldehydes. Once this mixture is added to the anti-RSA-IgY, Schiff bases form with the amino groups present on the antibody. A low concentration of Na-periodate results in poor conjugating efficiency of HRPC to IgY and too high concentration results in carboxyl groups forming rather than aldehyde groups (on IgY), which are less reactive in the covalent Schiff base formation. Further optimisation steps would need to be done to decide as to what led to the poor conjugating efficiency.

Migneault *et al*., (2004) indicated that up to 13 different forms of glutaraldehyde and about 8 different reactions could take place during conjugation. Depending on pH, temperature and ionic strength. The conditions used in this study seemed to favour HRPC conjugating to IgY.

The third conjugating reagent tested was MBS which is a bifunctional coupling reagent. MBS is popular in the conjugation of peptides to carrier proteins (Peeters *et el*., 1989) and is used for the conjugation of IgG to Urease. MBS coupling uses the benzoyl motif to benzoylate and the free amino acid groups on the antibody. N-hydroxysuccinimide ester acts as a linker between IgG and Urease. Urease sulfhydryl group undergoes thiolation with the malemide motif.

HRPC does not have surface cysteines to provide sulfhydryl groups. Since IgY was reduced, only fractions that have the Fab and an available sulfhydryl group would react with the MBS. Therefore, the IgY molecules was reduced with DTT to expose cysteine residues.

The HRPC was incubated with MBS to benzoylate the free amino groups, thereafter the fragments of reduced IgY would couple to HRPC by malemide motif. The proposed mechanism and conjugate are shown in Figure 3.13.

3.4.9. Glutaraldehyde redox coupled anti-RSA IgY

Results in Figure 3.14 compared glutaraldehyde conjugated to anti-RSA-IgY reduced with DTT. The rationale to test if using 90 kDA (HC + LC) fragment of the IgY molecule it may be more sensitive in detecting RSA due to less steric hinderance. The LOD of the conjugated fragment detected 100 ng and not a more sensitive conjugate.

This is likely due to a low concentration of 90 kDA (HC + LC) IgY coupled HRPC. Interestingly the coupling method was more efficient than MBS and less efficient compared to Na-periodate.

3.4.10. Strategy to the improve sensitivity of ELISA's

All three methods anti-RSA-IgY-HRPC conjugates were separated from unbound HRPC by passing the mixture over an RSA Aminolink® resin. The short fall is unconjugated anti-RSA-IgY would elute with the conjugated IgY. The two could be separated by size exclusion chromatography using a S-200 resin.

The HRPC used had 150 U/mg, many protocols suggest using the 1000 U/mg enzyme and above (Migneault *et al.,* 2004). Since lower activity and quality HRPC was used, the sensitivity was expected to be lower. The 150 U/mg HRPC sample (Figure 3.15) was impure, therefore, the HRPC concentration should be measured using the extinction coefficient E^{mM} = 100 at 403 nm, as this measures the heme of HRPC. A disadvantage of HRPC conjugates are they are less stable compared to urease and AP conjugates and some samples may have intrinsic peroxidase like activity which will result in false detection. The advantageous of HRPC are wide range of sensitive colorimetric and luminescence substrates, whereas urease does not have luminescence substrates, its relatively low cost as compared to urease and AP and if storage conditions are ideal it the conjugate will retain high activity.

3.4.11. Conclusion

DSF analysis of the different antibodies tested showed that polyclonal IgY was the most stable of all the antibodies analysed based on thermodynamic parameters. It would be interesting to measure the half-life of IgY. A second antibody that would be interesting to look at is mammalian IgE to compare to the chicken IgY. These two structures have been reported to be closer related than IgY to IgG (Warr *et al*., 1995). Na-periodate, MBS and glutaraldehyde were all used to couple HRPC to polyclonal chicken anti-RSA-chicken IgY. The glutaraldehyde method detected the lowest concentration of RSA (20 ng) in an ELISA indicating glutaraldehyde crosslinking was most efficient.

The result can be used as preliminary data for introducing IgY-HRPC conjugates into immunoassays by using higher activity HRPC. However, care should be taken if amino acids like lysine are on the site of IgY that recognises an epitope. This will not be involved in epitope recognition and potentially offer an alternative.

The study should also be broadened to compare the coupling procedure to IgG antibodies as well as testing the conjugation efficiency of different enzymes like AP or Urease.

4. CHAPTER 4: Detecting recombinant *P. falciparum* Histidine Rich Protein-2 a malaria diagnostic target with two copper-based assays

4.1. Introduction

CM has no diagnostic method

The most lethal form of malaria, in humans is caused by a *P. falciparum* infection. The disease can be cured if it is detected and treated early, therefore early detection is important. Current rapid diagnostic tests have several problems for example its sensitivity and specificity (Landier *et al*., 2016). An uncomplicated malaria infection can progress to cerebral malaria (CM), which is the most lethal form of malaria. To date there is no rapid diagnostic test for CM, though several studies have suggested high concentrations of *Pf*HRP-2 may play a role in an uncomplicated malaria infection progressing to a CM malaria infection. (Seyedel *et al.,* 2012; Rubach *et al.,* 2012; Park *et al.,* 2017; Fox *et al*., 2013). Therefore, detecting high concentrations of *Pf*HRP-2 may be a marker for diagnosing the potential for a *P. falciparum* malaria infection to progress to CM (Dvorin, 2017).

*Pf*HRP-2 binds metal ions

Plasmodium falciparum histidine rich protein-2 (*Pf*HRP-2) is a unique protein expressed and secreted by *P. falciparum* infections only. The *Pf*HRP-2 amino acid sequence is primarily made up of His, Ala and Asp (87%) amino acid residues hence the name (Howard *et al.,* 1986). *Pf*HRP-2 has been shown to have a high affinity for metal cations (Bauer *et al*., 2017). The metal cations bind to the imidazole motif of histidine residues via coordination bonds, where either the delta or epsilon nitrogen provides both electrons for the metal cation to bind (Park *et al*., 2014). The most stable conformation is a single metal cation binding between two imidazole residues. These residues are in abundance in *Pf*HRP-2, as the protein has 51 His-His-Ala repeats (Ndonwi *et al.,* 2011). The repeats have a high affinity for metal ions. Bauer *et al*., (2017) showed that *Pf*HRP-2 has the highest binding affinity for Cu ions compared to other metal ions.

HRPC-Cu^{+} as a detection assay

Xianyu *et al*., (2013) developed an ultrasensitive colorimetric assay to measure the concentration of Cu^{2+} in water samples. This was achieved by adding Na-ascorbate and horseradish peroxidase (HRPC) to water samples. If Cu^{2+} was present it would be reduced (by Na-ascorbate) to Cu^{+}, which is a potent inhibitor of HRPC activity. Therefore, HRPC would be inhibited to catalyse the oxidation of tetramethyl benzidine (TMB).

Shi *et al*., (2016) used this relationship to develop a Cu^{+}-HRPC system to detect alkaline phosphatase (ALP) and pyrophosphate based on the molecules binding affinity for Cu.

Fenton chemistry

Cu^{2+} and Fe^{3+} are two metal ions that have shown to possess peroxidase like activity via the Fenton chemistry mechanism (Xu *et al*., 2015; Wu *et al*., 2014). Shan *et al*., (2016) showed the peroxidase like activity of Cu^{2+} is significantly increased in the presence of chloride ions (Cl^{-}). The mechanism was termed chloride accelerated Fenton chemistry. The sensitivity of these mechanisms has allowed Fe^{3+} and Cu^{2+} to be used in detection assays, such as detection of free cysteine residues with Fe^{3+} in urine (Wu *et al*., 2014).

The Cu^{2+}-TMB-H_2O_2 system has been used for the detection of: Cu^{2+} in water samples (Shan *et al*., 2016); Uric acid (Lu *et al*., 2017); dopamine (Wang *et al*., 2017) and the specific detection of L-histidine in urine samples (Xu *et al.,* 2015). For the detection of L-histidine, uric acid and dopamine TMB oxidation was suppressed indicating the molecules were present. The advantage of using peroxidase like activity of metal ions to detect molecules are the assays are sensitive, cost effective and relatively simple to perform.

In this chapter, r*Pf*HRP-2 was used in two competition assays for the binding of Cu ions. The first assay was based on the presence of r*Pf*HRP-2 binding to Cu^{+} and preventing Cu^{+} inhibiting HRPC (Cu^{+}-HRPC-TMB assay). The second assay relied on Fenton chemistry and the presence of r*Pf*HRP-2 would bind Cu^{2+} and prevent oxidation of TMB.

4.2. Materials and Methods:

4.2.1. Materials and equipment

All common reagents, buffers, salts, metal ion salts, TMB, HRPC (VI, 150 U/mg and 1000 U/mg) were purchased from Sigma. H_2O_2 and Bovine serum albumin (BSA; fraction 4) was purchased from Roche (Mannheim, Germany). Maxi Sorp™ 96-well ELISA plates were from Nunc products (Roskilde, Denmark). Saliva used was that of the authors of this study.

UV-1800 Shimadzu spectrophotometer from Shimadzu corporation (Kyoto, Japan); pH meter from HANNA instruments. VersaMax™ ELISA plate reader was purchased from Molecular Devices Corporation (California, USA).

4.2.2. Optimising HRPC concentration for the Cu^{+}-HRPC-TMB assay

HRPC stocks (150 U/mg and 1000 U/mg both at 3 mg/ml) were prepared in Tris-HCl-MeOH buffer (Chapter 5; (50 mM Tris-HCl, pH 8.0; 20% MeOH; 50 mM $CaCl_2$)) and stored at 4°C in the dark. The HRPC stocks were diluted to different concentrations to determine the enzymes optimal concentration for the respective assays.

Stocks of TMB (7.1 mM) were prepared in DMSO and stored at -20°C. TMB stocks were thawed at RT and made up in 150 mM citrate-phosphate buffer with 1.96 mM H_2O_2.

A final concentration of 284 µM TMB and 0.784 µM H_2O_2 was used in the assays. TMB was added for 15 min before it was measured at O.D 652 nm using UV/Vis spectroscopy.

4.2.3. Testing Cu^+ and different metal ions inhibitory effect on HRPC activity

HRPC (150 U/mg; 1 ng), was incubated with 125 µM of both $CuCl_2 \bullet 2H_2O$ and Na-ascorbate. The Cu^+ was incubated with HRPC (30 min at RT). Thereafter TMB was added as described previously (Section 4.2.2). HRPC (1000 U/mg; 0.180 ng) was incubated with both 12.5 µM $CuCl_2 \cdot 2H_2O$ and Na-ascorbate. Cu^+ was incubated with HRPC (30 min at 37°C). Thereafter, TMB was added as described (Section 4.2.2). The inhibition of $CoCl_2 \cdot 7H_2O$, $NiCl_2 \cdot 6H_2O$, $FeCl_3 \cdot 6H_2O$, $CdCl_2 \cdot 2H_2O$, and $ZnCl_2 \cdot 7H_2O$ all at 12.5 µM were tested on HRPC in the same manner as Cu^+.

4.2.4. Enzyme assay to measure HRPC activity in the presence of Cu^+

HRPC 100 ng (150 U/mg) was incubated with Cu^+ (1 to 15 mM; 30 min at RT). TMB concentrations of 100, 500 and 1000 µM were added and the $O.D_{652}$ was taken every 60 seconds. Lineweaver-Burk plots were plotted as sugested by Keyhani *et al*., (2003., 2005). Extinction coefficient of $\varepsilon_{652\ nm}$ 3.9 x 10^4 M^{-1}. Cm^{-1} was used for TMB.

4.2.5. HRPC competition assay with imidazole

HRPC (concentrations described in section 4.2) was incubated with Cu^+ (125 µM or 12.5 µM) and imidazole concentrations ranging from 0 to 500 µM or 0 to 250 µM (30 min at 37°C). TMB was added as described (Section 4.2.2.).

4.2.6. Cu^+-HRPC-TMB for the detection of r*Pf*HRP-2 in aqueous solution

r*Pf*HRP-2 was dialysed extensively against HEPES buffer (20 mM pH 7.4; 2 x 2 h and 16 h) in 100-fold volume of 20 mM HEPES buffer (4°C). The dialysed r*Pf*HRP-2 (17 to 170 ng) was incubated with 12.5 µM Cu^+ for 10 min. HRPC (1000 U/mg, 180 pg) was added. The solution was incubated (30 min at 37°C) and TMB was added for detection as described (Section 4.2.2.).

4.2.7. Cu^+-HRPC-TMB assay for the detection of r*Pf*HRP-2 in saliva samples

A saliva sample from a healthy individual was taken and centrifuged (12 500 x g; 2 min). The clear supernatant was then removed and spiked with dialysed r*Pf*HRP-2 (50% v/v). The samples were then tested for the presence of r*Pf*HRP-2 as described (section 4.2.5).

4.2.8. Cu^+-HRPC-TMB assay for the detection of r*Pf*HRP-2 captured with anti-r*Pf*HRP-2 IgY

Polyclonal chicken anti-r*Pf*HRP-2 IgY antibodies (100 ng and 1 µg) were used to coat Nunc Maxi Sorp™ 96-well ELISA plates overnight at 4°C.

BSA (0.05%) solution was used to block the plate for an hour (37°C). r*Pf*HRP-2 was added at varying concentrations (4.2 ng to 4.2 µg). The r*Pf*HRP-2 was allowed to bind to the antibodies on the plate (2 h; 37°C). After each step, plates were washed with PBS.

Thereafter, a 12.5 µM Cu^{+} solution was added and incubated (30 min; 37°C), after which HRPC (180 pg) was added and incubated (30 min). Finally, TMB was added as described (Section 4.2.2).

4.2.9. Cu^{+}-HRPC-TMB assay with captured r*Pf*HRP-2

r*Pf*HRP-2 (5 ng to 5 µg) was coated onto Nunc Maxi Sorp™ 96-well ELISA plates overnight (4°C). Wells were blocked with 0.05% (w/v) BSA (1 h; 37 °C). A 12.5 µM Cu^{+} solution was added and incubated (30 min; 37°C). HRPC (180 pg) was added to incubate with the solution for a further 30 minutes. Finally, TMB was added (4.2.2). The other proteins tested in the assay were rabbit serum albumin (RSA), bovine serum albumin (BSA) and polyclonal chicken anti-r*Pf*HRP-2 IgY as described previously.

4.2.10. The oxidation of TMB with RCl^{-} generated from NaCl and H_2O_2

Reactive chloride species (RCl^{-}) were used to oxidise TMB via Fenton chemistry. RCl^{-} were generated using NaCl (100 mM) and H_2O_2 (750 mM). The chromogen was TMB (0.5 mM). The reaction was catalysed using various concentrations of Cu^{2+} and Fe^{3+} in MES buffer (2 mM). To determine the peroxidase-like activity of different transition metals, the method was performed in a similar manner as before where, Co^{2+}, Ni^{2+} and Zn^{2+} (5 µM) were used instead of either Cu^{2+} or Fe^{3+}.

4.2.11. Inhibition of Cu^{2+} oxidation of TMB by chelation of Cu^{2+} with imidazole

To test if imidazole inhibited the reaction, 1 µM Cu^{+} or 5 µM Fe^{3+} ions was incubated (10 min; RT) with increasing concentrations of imidazole. A range of 0 – 500 µM imidazole for Cu^{2+} and 0 - 50 µM for Fe^{3+} in MES buffer (2 mM) was used. After 10 min a solution of H_2O_2 (750 mM) and NaCl (100 mM) was added, allowing for the creation of RCl^{-}. Finally, TMB (0.5 M; DMSO) was added and the absorbance was measured at 652 nm.

4.2.12. Detection of r*Pf*HRP-2 using the Cu^{2+}-RCl^{-}-TMB assay

Polyclonal chicken anti-r*Pf*HRP-2 IgY antibodies (100 ng and 1 µg) were used to coat Nunc Maxi Sorp™ 96-well ELISA plates overnight at 4°C. BSA (0.05% (w/v)) solution was used to block the plate for an hour (37°C). r*Pf*HRP-2 was added at varying concentrations (4.2 ng to 4.2 µg). The r*Pf*HRP-2 was allowed to bind to the antibodies on the plate (2 h; 37°C). A solution of 1 µM Cu^{2+} was incubated with the plate (30 min; 37°C). Afterwards a RCl^{-}-TMB solution (100 mM NaCl, 750 mM MES pH 6.0 buffer and TMB (0.5 M) in DMSO) was added and the oxidation of TMB was measured at 652 nm.

4.3. Results

4.3.1. Optimising 150 U/mg HRPC concentrations

In order to develop a basic assay for the detection of copper (Cu), optimal concentrations of HRPC, Cu and Na-ascorbate were established. The concentration of H_2O_2 and TMB were kept constant. HRPC catalyses the oxidation of TMB in the presence of H_2O_2 and the oxidised TMB (TMB-diamine) absorbance can be measured at 652 nm. The absorbance values will be referred to as HRPC activity. The optimal concentration of HRPC (150 U/mg) was determined (Figure 4.1).

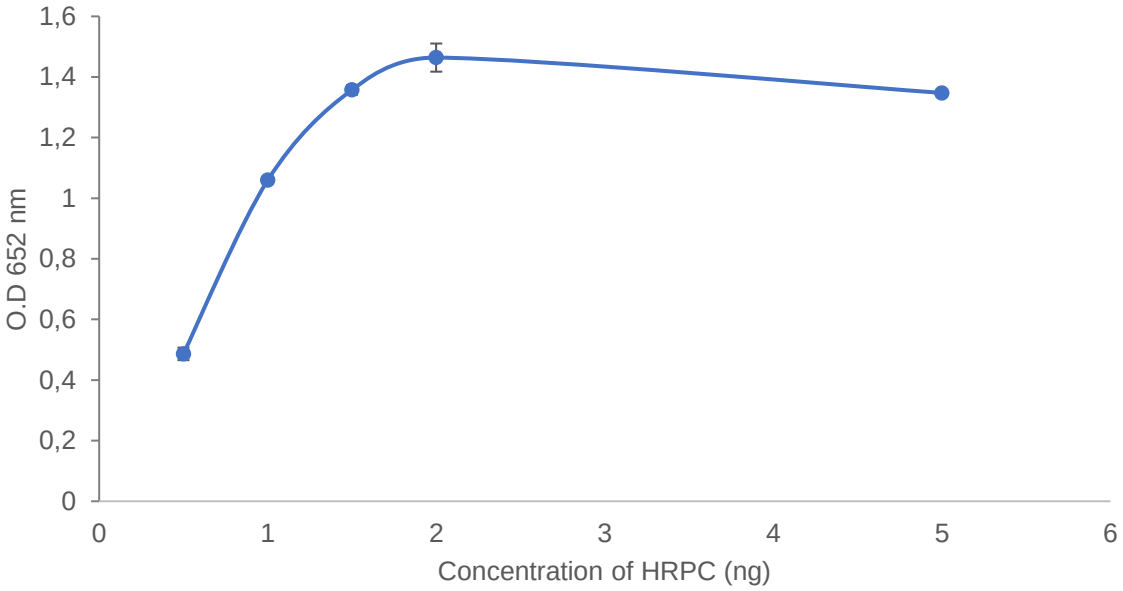

Figure 4.1: HRPC activity was measured at different concentrations. Concentrations of HRPC (0.5 to 5 ng) was used to oxidize TMB in the presence of H_2O_2 over a 15-minute time period Error bars indicate S.D of triplicate results.

Increasing concentrations of HRPC resulted in higher absorbance values due to the oxidation of TMB (Figure 4.1). Up to 2 ng of HRPC there was a two-fold increase in absorbance values with a two-fold increase in enzyme concentration. HRPC concentrations above 2 ng resulted in complete oxidation of TMB. 5 ng of HRPC oxidised TMB more rapidly, resulting in the TMB- diamine to precipitate, therefore the absorbance of the oxidised TMB with 5 ng HRPC was lower than 2ng of HRPC. HRPC at a concentration of 1 ng was the optimal concentration.

4.3.2. Inhibition of HRPC with Cu^{+}

Cu^{2+} was reduced to Cu^{+} in the presence of Na-ascorbate and the Cu^{+} was used to inhibit HRPC activity. The HRPC activity was measured with the addition and oxidation of TMB (Figure 4.2).

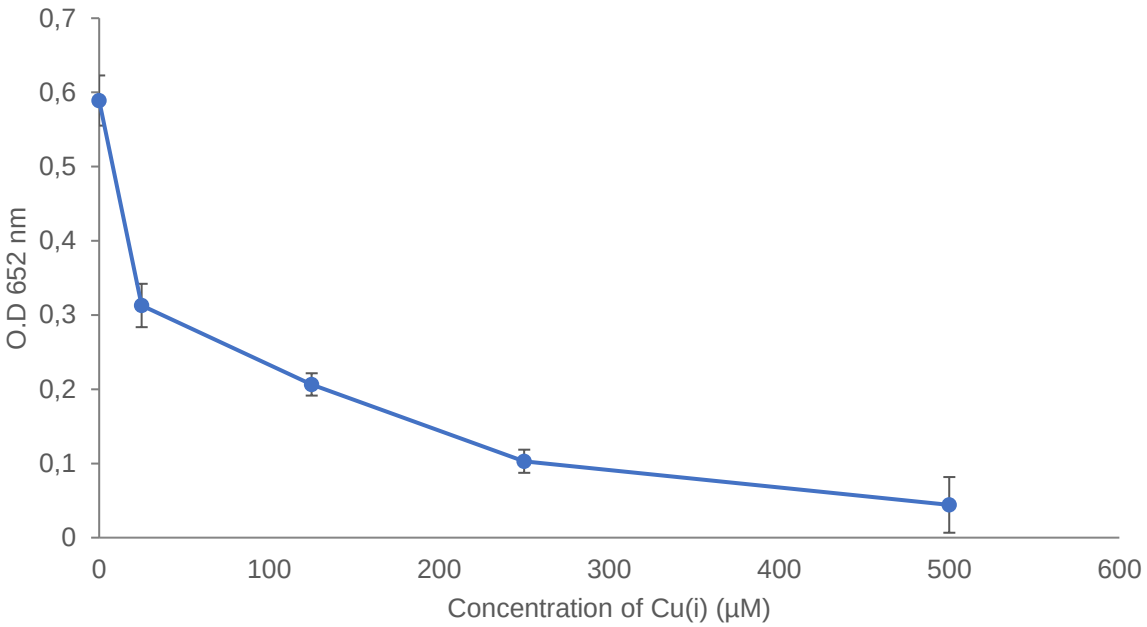

Figure 4.2: HRPC activity in the presence of increasing concentrations of Cu^{+}. Varying (0-500 µM) concentrations of Cu^{2+} were reduced to Cu^{+} in the presence of (0-500 µM) sodium ascorbate in 1:1 ratio. The Cu^{+} was incubated with HRPC at 37°C after which TMB was added and $O.D_{652}$ was measured (15 min). Error bars indicate S.D of triplicate results.

HRPC activity was inhibited with Cu^{+} in a dose dependent manner (Figure 4.2). HRPC activity was almost completely inhibited with 500 µM Cu^{+}. The optimal inhibitory concentration of Cu^{+} chosen was 125 µM because any additives changing the activation or inhibition could be evaluated by a change in absorbance.

4.3.3. Evaluating incubation times and incubation temperatures for optimal HRPC activity

The time period for which Cu^{+} was incubated with HRPC (Figure 4.2) was adapted from the study by Xianyu *et al*., (2013). Therefore, the optimal incubation time for Cu^{+} with HRPC for this study had to be optimised (Figure 4.3A) as well as the optimal incubation temperatures at which HRPC is most active at (Figure 4.3B).

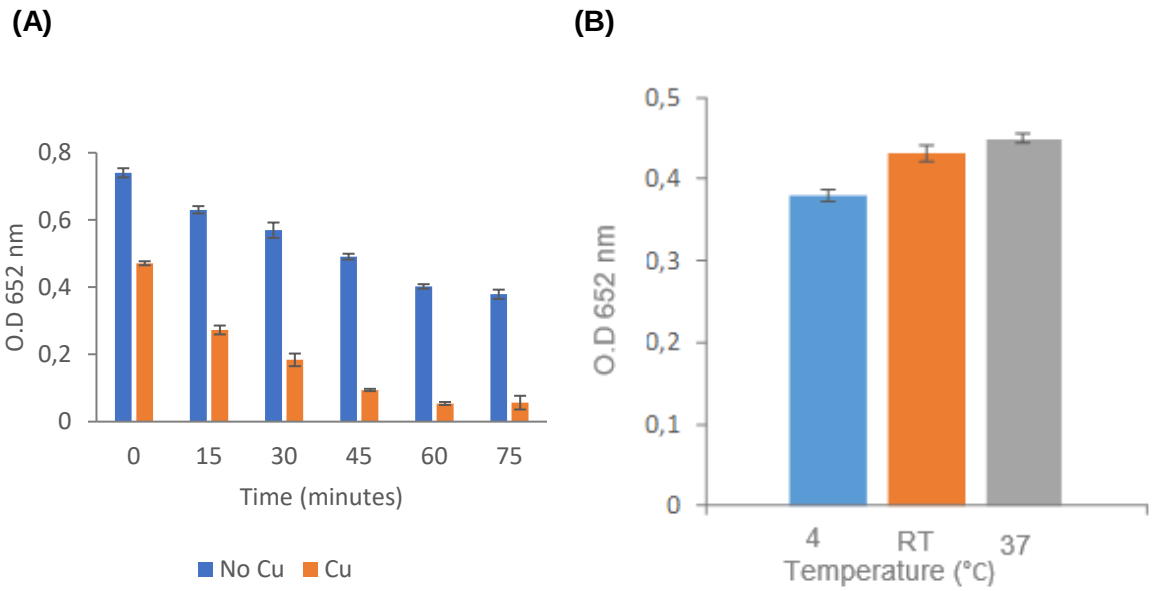

Figure 4.3: HRPC activity at different times and temperatures in the presence and absence of Cu^+. HRPC activity in the presence and absence of Cu^+ measured every 15 min **(A)**. The effect 4°C (•), RT (•) and 37°C (•) on HRPC activity **(B)**. Error bars on both figures represent S.D of triplicate results of two experiments.

Over the 75 min incubation period, HRPC activity decreased in both the absence and presence of Cu^+ (Figure 4.3A). The optimal incubation time was 30 min as 23% HRPC activity was lost in the absence of Cu^+, while 76% HRPC activity was lost when Cu^+ was present. HRPC had similar activity at all three temperatures but was highest at 37°C therefore, 37°C was used (Figure 4.3B).

4.3.4. Enzyme Kinetics

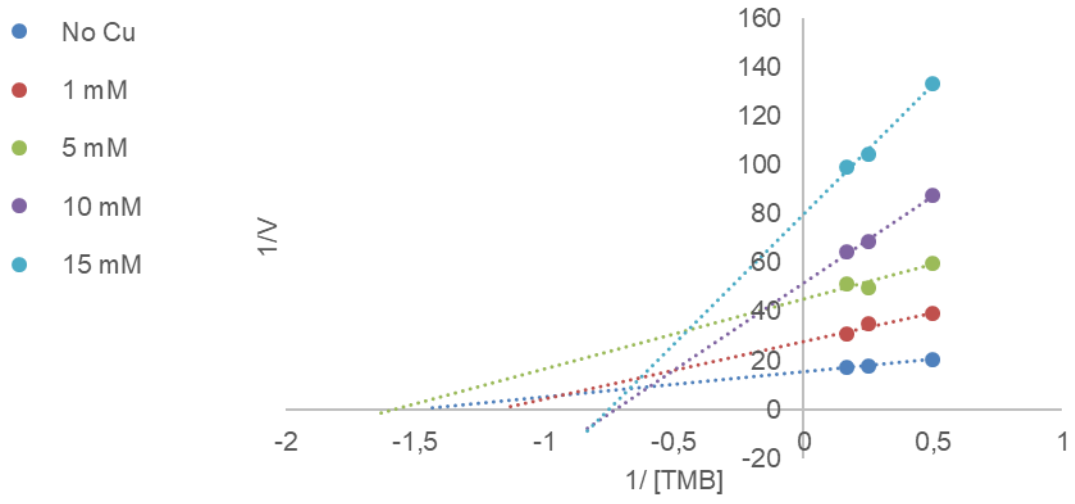

Figure 4.4: Lineweaver-Burk plot of HRPC showing mixed inhibition in the presence of Cu^+. 1 to 15 mM Cu^+ was used to inhibit HRPC activity in the presence of H_2O_2 and TMB.

The Lineweaver-Burk plot (Figure 4.4) illustrates a mixed inhibition when Cu^+ binds to HRPC. Cu^+ concentrations of 1 and 5 mM resulted in non-competitive inhibition, while 10 and 15 mM Cu^+ showed uncompetitive inhibition.

The result suggests Cu^+ ions bind to allosteric sites and not the active site. Therefore, the HRPC Cu^+ interaction could be reversed. (The assay was done in triplicates with similar trend, only one set of data is shown).

4.3.5. Optimising 1000 U/mg HRPC activity and inhibition of HRPC with Cu^+

The assay was defined as the Cu^+-HRPC-TMB assay. Thus far low activity HRPC (150 U/mg) was used, to economically ensure Cu^+ significantly inhibited HRPC. To have a good chance at detecting low concentrations of *Pf*HRP-2, minimal Cu^+ would need to be used. Therefore, the Cu^+-HRPC-TMB assay was optimised once again using a higher activity HRPC (1000 U/m; Figure 4.5) rather than the 150 U/mg HRPC used in Figures 4.1 – 4.4.

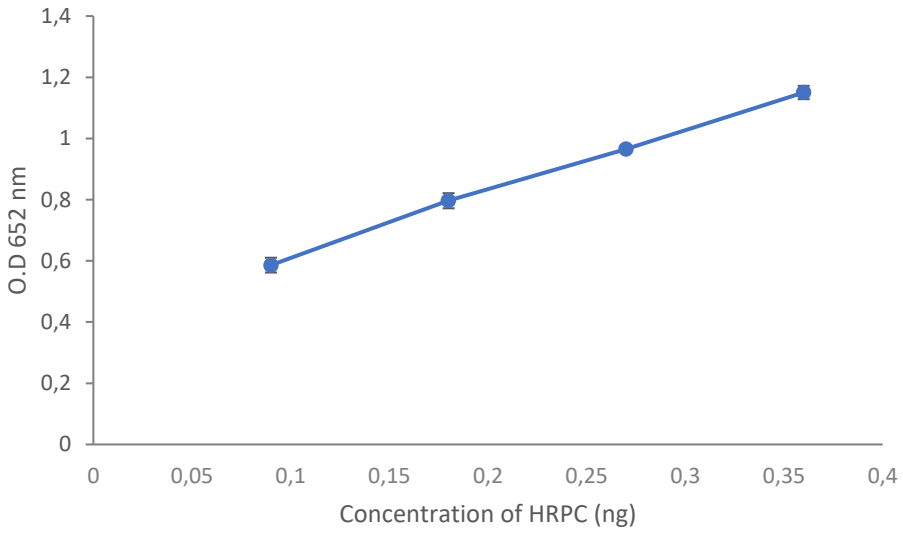

Figure 4.5: HRPC activity was determined by measuring the oxidation of TMB. Amount of HRPC (1000 U/mg) (0.09 ng– 0.36 ng) was used to oxidize TMB in the presence of H_2O_2 for 15 min. Error bars indicate S.D of triplicate results of the experiment done 3 times.

Increasing amounts of HRPC (0.09 ng to 0.36 ng; Figure 4.5) resulted in an increased rate of TMB oxidation. The concentration of HRPC chosen was 0.18 ng, which was fivefold less than the chosen concentration HRPC (150 U/mg).

4.3.6. Inhibition of HRPC (1000 U/mg) using Cu^{+}

The minimum concentration of Cu^{+} required to inhibit HRPC (1000 U/mg) was determined (Figure 4A and 4B).

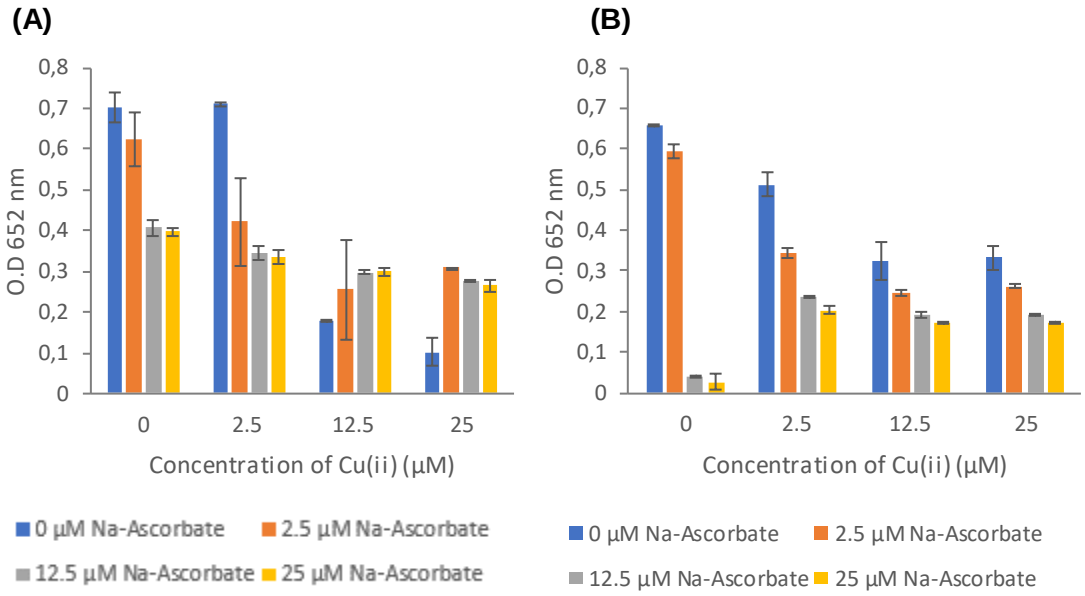

Figure 4.6: HRPC activity in the presence of increasing concentrations of Cu^{+} at RT and 37°C. 0-25 µM Cu^{2+} was reduced to Cu^{+} in the presence of 0-25 µM sodium ascorbate in 1:1 ratio. Cu^{+} was incubated with HRPC at RT **(A)** and 37°C **(B)** and TMB was added. O.D readings was measured (15 min) at 652 nm. Error bars indicate S.D of triplicate results of the two experiments.

Increasing Cu^{+} concentrations (Figure 4.6) inhibited HRPC activity in a dose dependent manner. HRPC activity inhibited by Cu^{+} at RT (Figure 4.6A) had more variance compared to HRPC-Cu^{+} at 37°C (Figure 4.6B). A Cu^{+} concentration of 12.5 µM at 37°C resulted in a 71% inhibition of HRPC activity and was therefore chosen as the inhibitory concentration to be used in the assay. At RT 12.5 and 25 µM Cu^{2+} (Figure 4.6A) was a more potent inhibitor of HRPC compared to Cu^{+} at 12.5 and 25 µM. At 37°C 12.5 and 25 µM Na-ascorbate completely prevented TMB oxidation (Figure 4.6B). The conclusion for the different inhibitory effects at RT and 37°C is thought to be due to the different conformation changes HRPC undergoes at different temperatures (Azevedo *et al*., 2001). In Figure 4.6B, Na-ascorbate may have reduced the TMB- back to TMB at a faster rate than observed in Figure 4.6A.

4.3.7. The effect of metal ions on HRPC activity

Different transition metal ions have been reported to inhibit HRPC activity. These transition metal ions inhibitory effect on HRPC activity was tested to determine if Cu^{+} was the most potent inhibitor. The metal ions were incubated with HRPC and the enzymes activity was measured using TMB (Figure 4.7).

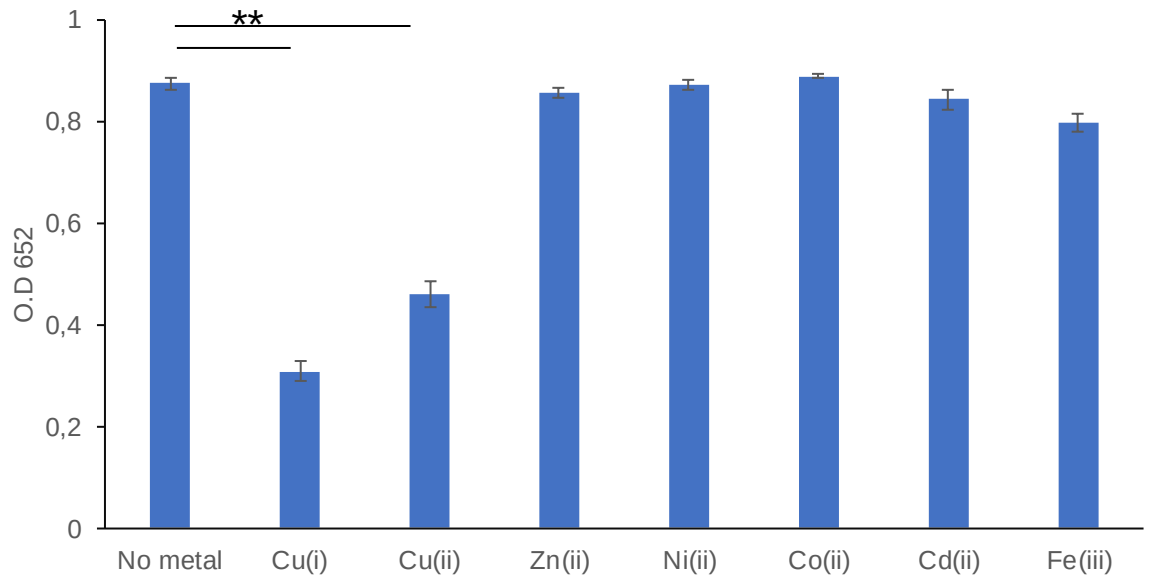

Figure 4.7: The effect of various metals on the activity of HRPC. The effect of copper (Cu^{+} and Cu^{2+}), zinc (Zn^{2+}), nickel (Ni^{2+}) cobalt (Co^{2+}), cadmium (Cd^{2+}) and iron (Fe^{3+}) on HRPC activity. All metal ions were used at 12.5 µM. TMB was added and $O.D_{652}$ was measured (15 min). Error bars indicate S.D of triplicate results of three experiments. $P<0.05$.

Both Cu^{2+} and Cu^{+} showed significant inhibition (47% and 64%), with Cu^{+} being the most potent metal ion inhibitor. All other metal ions tested, had a minimal influence on HRPC activity (0 and 3%) except for Fe^{3+} which inhibited enzyme activity by 8.93%. Co^{2+} marginally increased enzyme activity (1.7%).

4.3.8. Effectiveness of imidazole binding Cu^{+}

The aim of the Cu^{+}-HRPC-TMB assay was to be used as a malaria biosensor based on the detection of r*Pf*HRP-2. The imidazole motif on the histidine residue binds Cu^{+} and removes the Cu^{+} from solution allowing HRPC to maintain activity. A preliminary experiment was performed, using imidazole, to test if it would bind Cu^{+} and to test if imidazole interferes with HRPC activity (Figure 4.8A and 4.8B).

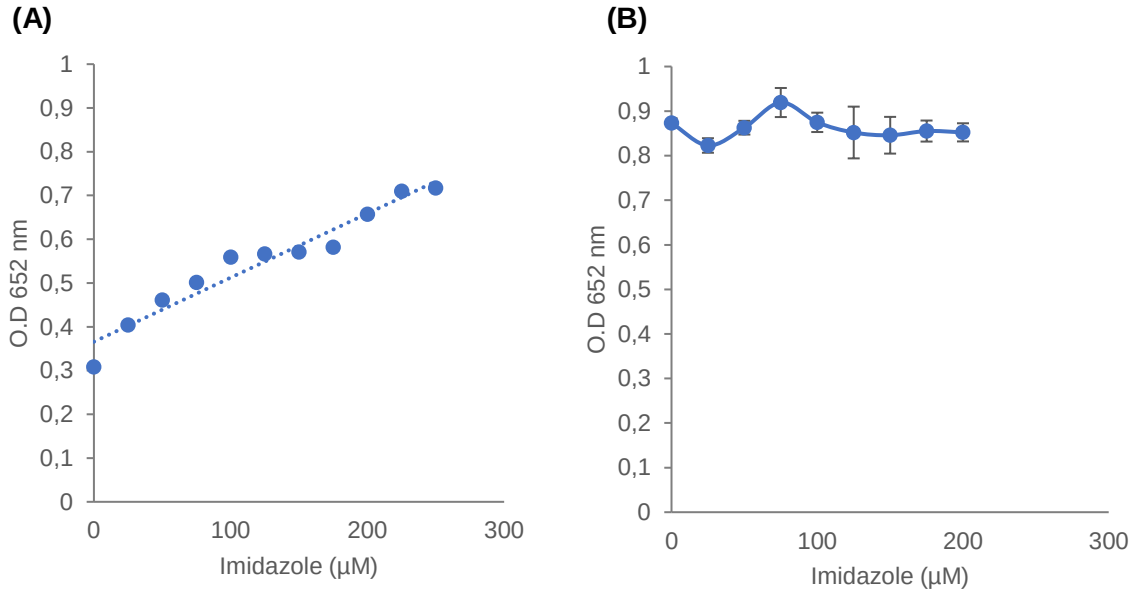

Figure 4.8: The effect of imidazole and Cu^+ on HRPC activity in the presence of imidazole. A range (0 µM – 250 µM imidazole was incubated with HRPC and 12.5 µM Cu^+ **(A).** HRPC was incubated with imidazole (0 – 200 µM) in the absence of Cu^+ **(B)**. After incubation, TMB was added and $O.D_{652}$ was measured (15 min). Error bars indicate S.D of triplicate results.

Increasing concentration of imidazole bound and removed Cu^+ from solution, allowing HRPC to retain activity (Figure 4.8A). The linear increase in absorbance at 652 nm showed HRPC retained more activity in the presence of higher concentrations of imidazole because more Cu^+ was bound and removed. The result also indicates imidazole has a higher binding affinity for Cu^+ compared to HRPC. The enzyme was incubated with imidazole in the absence of Cu^+ (Figure 4.8B) and imidazole does not influence enzyme activity. The result (Figure 4.8A) was due to the removal of Cu^+.

4.3.9. Testing if the Cu^+-HRPC-TMB biosensor assay could detect r*Pf*HRP-2 in aqueous solution

Imidazole was shown to prevent HRPC inhibition by Cu^+ (Figure 4.8A). r*Pf*HRP-2 (recombinantly expressed and purified in Chapter 2) was tested in the Cu^+-HRPC-TMB assay (Figure 4.9).

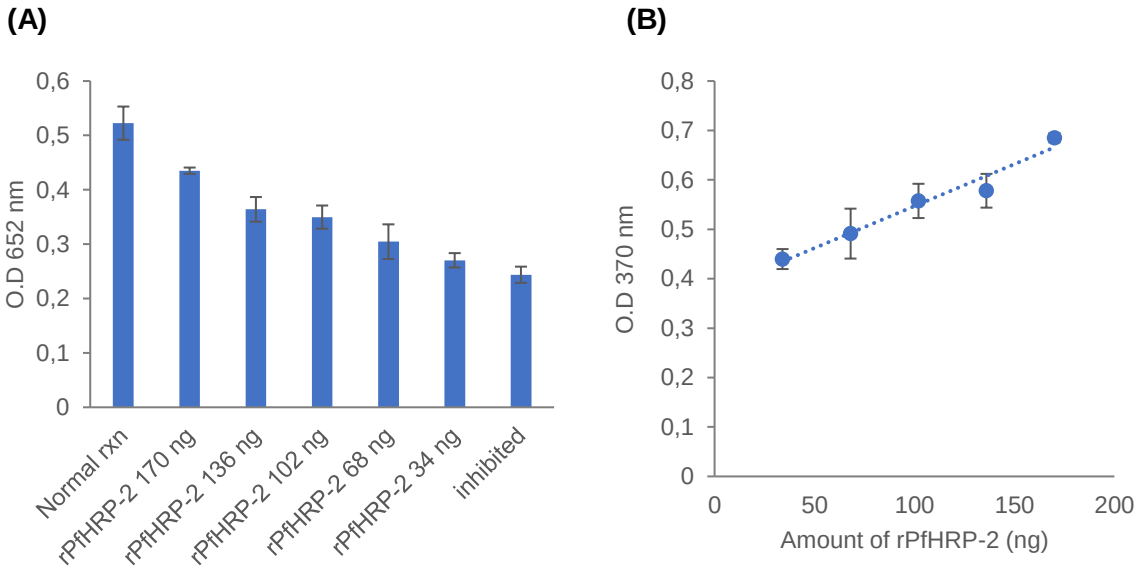

Figure 4.9: Detection of r*Pf*HRP-2 in aqueous solution using the Cu^{+}-HRPC-TMB assay. Varying amounts of r*Pf*HRP-2 (34 – 170 ng) were added to bind the Cu^{+} (12.5 µM) **(A)**. Thereafter, 180 pg of HRPC was added. TMB was added and $O.D_{652}$ was measured (15 min). Linear range of r*Pf*HRP-2 detected from **(B)**. Error bars indicate S.D of triplicate results.

The samples containing r*Pf*HRP-2 (dialysed in HEPES buffer) allowed for HRPC to have higher activity compared to the Cu^{+} inhibited HRPC (Figure 4.9A). An increasing absorbance was found with increasing concentrations of r*Pf*HRP-2. This indicated that high concentrations of r*Pf*HRP-2 bound to and removed Cu^{+} ions. However, r*Pf*HRP-2 concentrations of 102 ng and above were significant. To determine which r*Pf*HRP-2 amounts detected were significant, the absorbance of HRPC inhibited by Cu^{+} was compared to the absorbance of the samples containing r*Pf*HRP-2. The O.D of Cu^{+}- HRPC activity in the presence of r*Pf*HRP-2 was shown to have a linear relationship (Figure 4.9B). The linear result meant an unknown r*Pf*HRP-2 concentration can be calculated. The absorbance in Figure 4.9B was measured at 370 nm, whic is a less commonly used wavelength at which oxidised TMB can be read spectrophotometrically. A wavelength of 370 nm was used since the absorbance readings at 370 nm are higher than absorbance readings at 652 nm.

4.3.10. Detecting r*Pf*HRP-2 in saliva

r*Pf*HRP-2 is found in several body fluids including saliva. This is an attractive material to base a diagnostic on, as it in non-invasive. The Cu^{+}-HRPC-TMB assay was used to test for r*Pf*HRP-2 in saliva samples spiked with the protein (Figure 4.10).

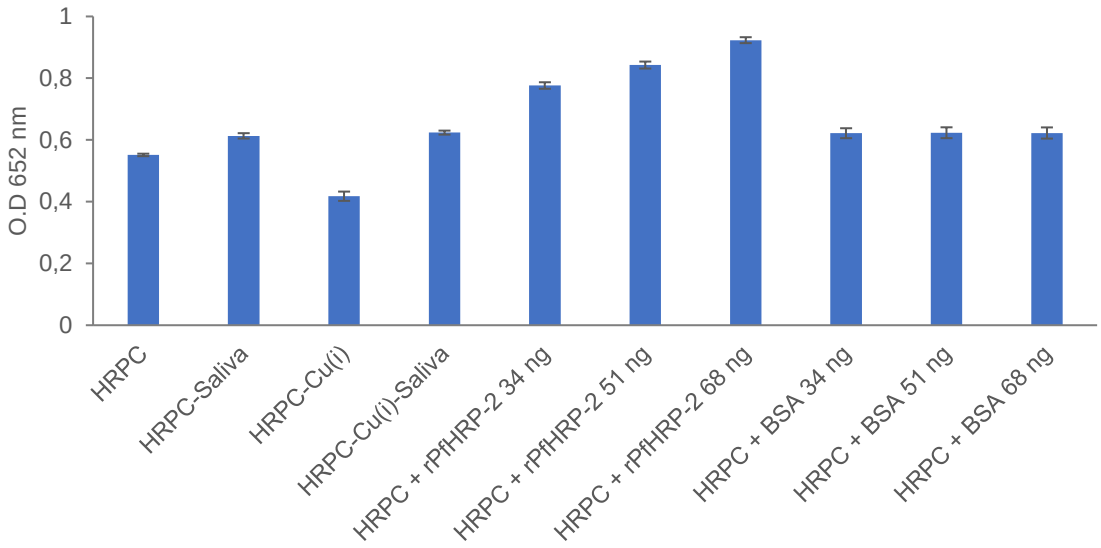

Figure 4.10: Using the Cu^{+}-HRPC-TMB assay for the detection of r*Pf*HRP-2 and BSA spiked into a saliva. Varying concentrations of r*Pf*HRP-2 (34 to 68 ng) were spiked into uninfected saliva samples for detection. HRPC, HRPC-saliva, HRPC-Cu(i) and HRPC-BSA served as controls. TMB was added and $O.D_{652}$ was measured (15 min). Error bars indicate S.D of triplicate results.

HRPC-Saliva had a 10.9% higher activity than HRPC alone. HRPC-Cu(i) was the control (Figure 4.10). The BSA spiked saliva samples were included to show a change in absorbance was due to r*Pf*HRP-2 and not a protein added to a saliva sample. The presence of saliva prevented the inhibition seen with Cu^{+}. r*Pf*HRP-2 activated HRPC in a dose dependent manner, resulting in higher concentrations of r*Pf*HRP-2 having higher absorbance readings. The mechanism involved is not understood. With the several proteins already present in saliva it is likely the increased activity of TMB oxidation is related to r*Pf*HRP-2.

4.3.11. Detection of rPfHRP-2 in an ELISA based format

Before a blood sample was tested for *Pf*HRP-2, a general ELISA based format was developed (Figure 4.11). The assay entailed using anti-r*Pf*HRP-2 IgY to capture r*Pf*HRP-2 and the Cu^{+}-HRPC-TMB assay could be used for detection of r*Pf*HRP-2.

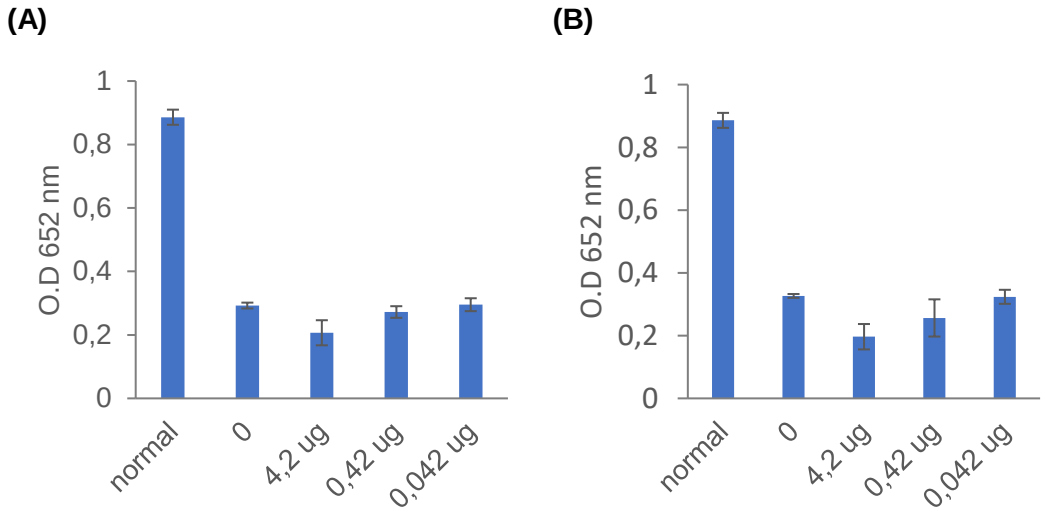

Figure 4.11: Using the Cu^{+}-HRPC-TMB assay to detect r*Pf*HRP-2 in an ELISA. Anti-r*Pf*HRP-2 IgY **(A)** 1 µg/ml **(B)** 10 µg/ml was used to capture r*Pf*HRP-2. The Cu^{+}-HRPC-TMB assay was added for detection and TMB was added and $O.D_{652}$ was measured (15 min). Error bars indicate S.D of triplicate results.

When the Cu^{+}-HRPC-TMB assay was applied to an ELISA based format, r*Pf*HRP-2 was not detected (Figure 4.11A and 4.11B). Cu^{+} inhibited HRPC, however, when r*Pf*HRP-2 was present (4.2 µg to 0.042 µg) it did not remove the Cu^{+}.

4.3.12. Detection of r*Pf*HRP-2 coated directly onto microplates

After r*Pf*HRP-2 was not detected in the antibody capture ELISA (Figure 4.11) . r*Pf*HRP-2, anti-r*Pf*HRP-2 IgY, BSA and RSA were coated onto a microplate (Figure 4.12A - D). r*Pf*HRP-2 (5 µg) was able to reduce the inhibition of HRPC activity by Cu^{+} by 48% (Figure 4.12A). However, HRPC-Cu^{+} in the presence of r*Pf*HRP-2 of 500 ng to 5 ng had the same activity (Figure 4.12A). It was suspected that BSA which was used as a block agent, may have interfered with the assay (Figure 12A- 12D). Similarly, for RSA, BSA and anti-r*Pf*HRP-2 IgY (Figure 12B, 12C and 12D) the Cu^{+} inhibition was reduced at all protein concentrations (5 µg to 5 ng) but none gave the same effect as 5 µg r*Pf*HRP-2.

It is uncertain why r*Pf*HRP-2 was only detected in aqueous solution (Figure 4.9 and 4.10) and not detected in a capture ELISA (Figure 4.11) or when coated directly onto a microplate (Figure 4.12).

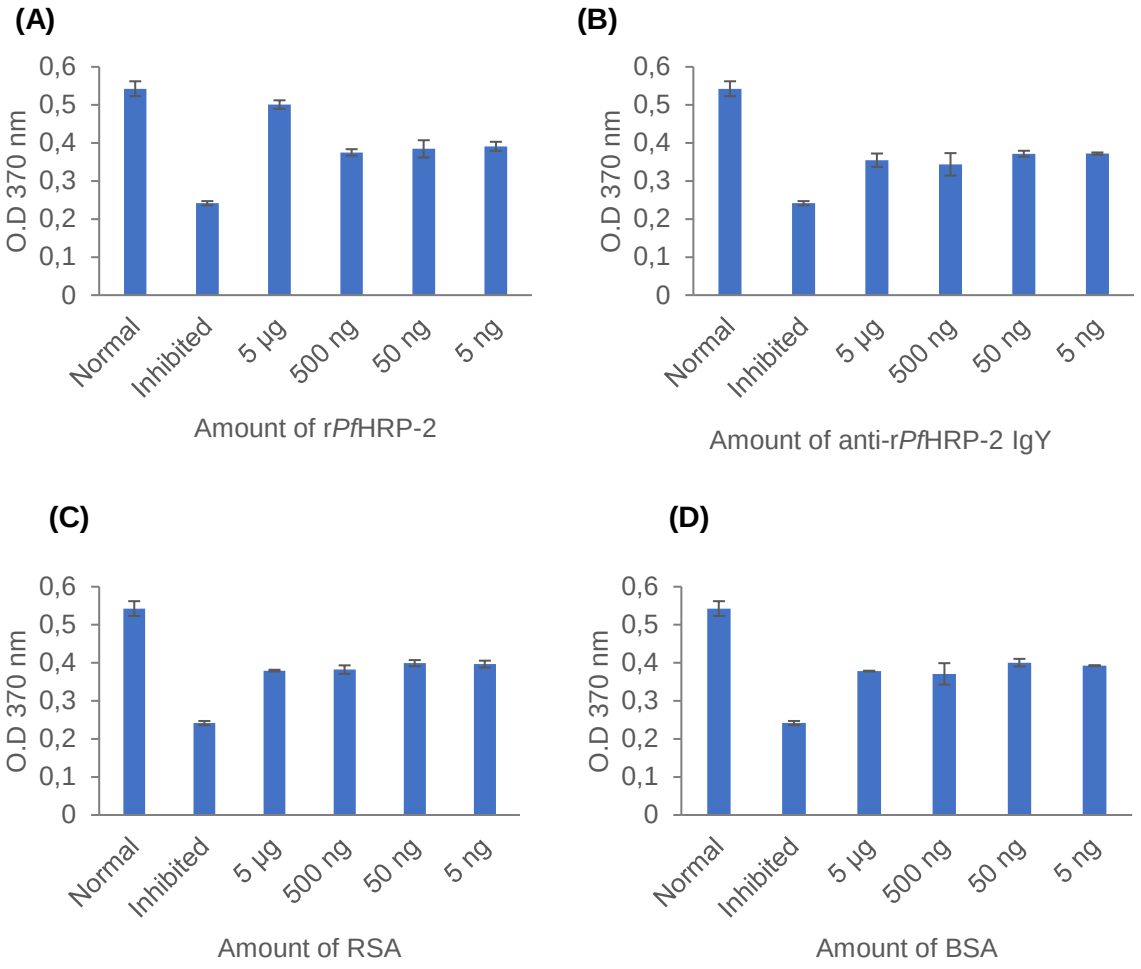

Figure 4.12: Using the Cu^{+}-HRPC-TMB assay for the detection of r*Pf*HRP-2 coated directly onto ELISA plates. 5 µg to 5 ng of r*Pf*HRP-2 **(A)**; anti-r*Pf*HRP-2 IgY **(B)**; RSA **(C)** and BSA **(D)** were coated onto Nunc® 96 well plates and incubated overnight (4°C). The Cu^{+}-HRPC-TMB assay was used for detection and TMB was added and $O.D_{370}$ was measured (15 min). Error bars indicate S.D of triplicates results.

4.3.13. Chemiluminescence

A Chemiluminescent assay was evaluated to determine if it would be more sensitive than the colorimetric Cu^{+}-HRPC-TMB assays described so far. However, when using the same concentration of HRPC for chemiluminescence that was used for the Cu^{+}-HRPC-TMB assays there was no signal. Therefore, no further testing was carried out.

4.3.14. Fenton catalysed reactions (Fe^{3+})

Since the Cu^{+}-HRPC-TMB assay did not detect r*Pf*HR-2 in an ELISA a second assay was optimised based on the peroxidase like activity of Fe^{3+} and Cu^{2+} ions. For the assay to be suitable as a biosensor for *Pf*HRP-2, low concentrations of metal ions are required. Wu *et al*., (2014) reported the peroxidase like activity of Fe^{3+} ions, however, to enhance the oxidation of TMB, Fe^{3+} was a catalyst used to generate reactive chloride species (RCl^{-}) from H_2O_2 and NaCl.

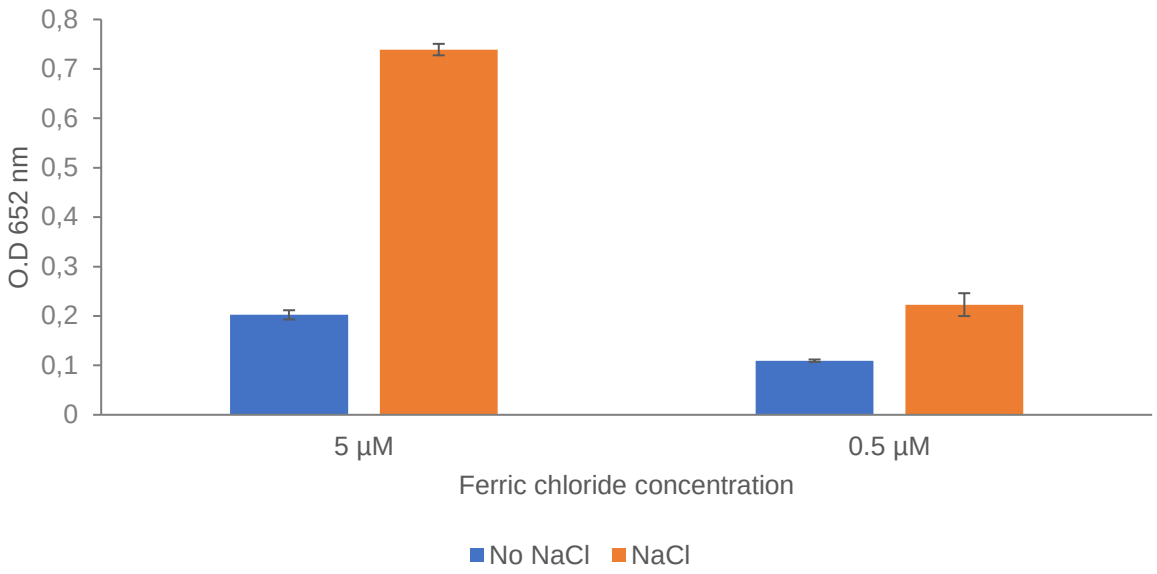

Figure 4.13: Colorimetric assay of Fe^{3+} based on Fe^{3+}-Fenton chemistry used to catalyse TMB oxidation. Fe^{3+} was used in the form of $FeCl_3$ at 5 µM and 0.5 µM respectively in the presence of H_2O_2 alone (•) H_2O_2 with NaCl (•). TMB was added and $O.D_{652}$ was measured (15 min). Error bars represent S.D of triplicate results.

RCl^- species (generated by Fe^{3+}, H_2O_2 and NaCl) was a significantly more potent oxidant of TMB compared to reactive oxygen species (ROS; generated by Fe^{3+} and H_2O_2) at 5 µM and 0.5 µM of Fe^{3+} (Figure 4.13).

4.3.15. Optimizing conditions for the generation of RCl^-

For the generation of RCl^- species and to attempt to improve the sensitivity of Fe^{3+} catalysed oxidation of TMB, H_2O_2 and NaCl concentrations were optimised. Both were evaluated at concentrations from 0.1 M to 1 M while Fe^{3+} was used at a fixed concentration of 5 µM (Figure 4.14).

Increasing H_2O_2 concentrations lead to an increased rate of TMB oxidation (Figure 4.14A), saturation was reached at 500 mM H_2O_2. However, 750 mM was selected as the optimal concentration, as it was present in the centre of the linear saturation curve and was suggested by Shan *et al*., (2016).

In Figure 4.14B increasing concentrations of Cl^- ions resulted in increased catalysed oxidation of TMB up to 500 mM NaCl after which the absorbance decreased. This was due to aggregation of TMB within the 15-minute incubation period. Shortly after the incubation, both 250 mM and 500 mM samples also began aggregating, therefore, 100 mM NaCl was chosen.

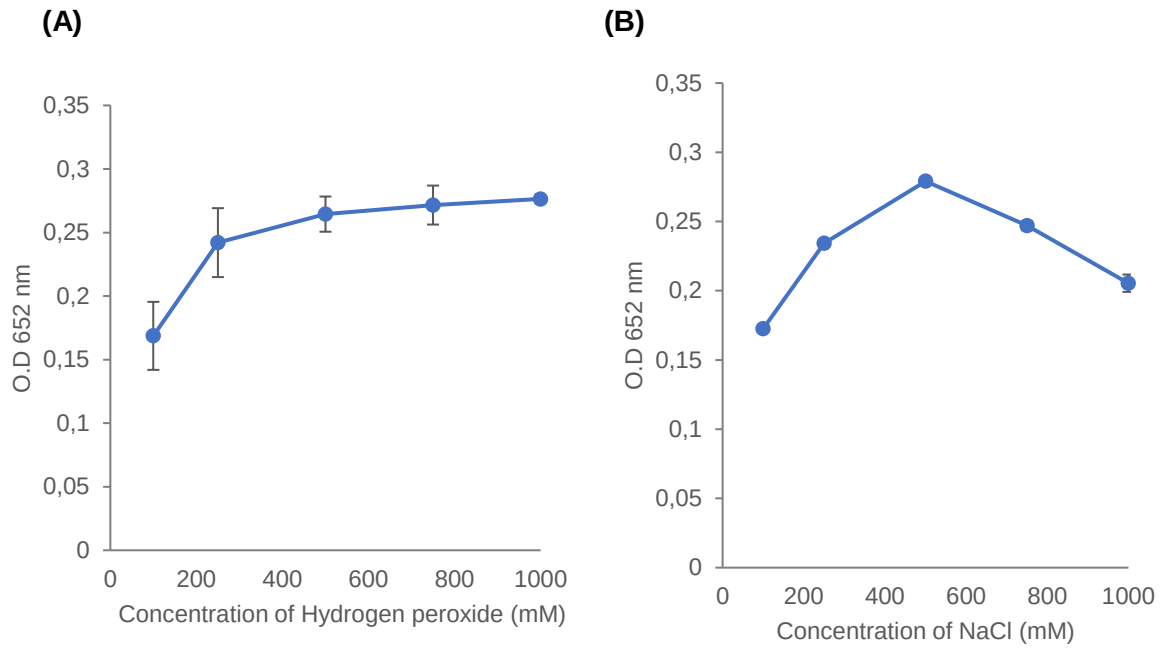

Figure 4.14: TMB oxidation catalysed by Fe^{3+}-Fenton chemical reactions by either H_2O_2 or NaCl to find their optimal concentrations. Varying concentrations of H_2O_2 (0.1 M to 1 M) were looked at in the absence of NaCl to catalyse the oxidation of TMB **(A)**. Varying concentrations of NaCl (0.1 M to 1 M) were looked at in the absence of H_2O_2 **(B)**. TMB was added and $O.D_{652}$ was measured (15 min) Error bars represent S.D of triplicate results.

4.3.16. Assessing peroxidase like activity of different metal cations

The peroxidase like activity of different metal ions on TMB (Figure 4.15).

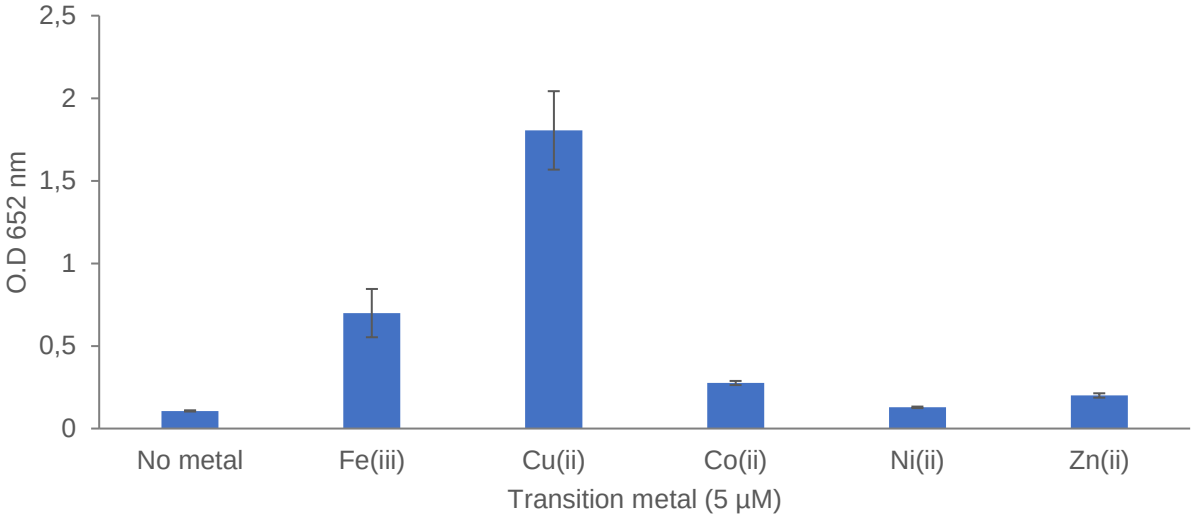

Figure 4.15: Peroxidase like activity of metal cations measured by the oxidation of TMB. No metal (control), 5 µM of Fe^{3+}, Cu^{2+}, Co^{2+}, Ni^{2+} and Zn^{2+} were all incubated with H_2O_2 (0.75 M) and NaCl (0.1 M). TMB was added and its oxidation was measured at 652 nm. Error bars indicate S.D of triplicate results.

It was important to show that the catalysis of TMB oxidation was not due to the presence of a transition metal and was rather due to Cu^{2+} and Fe^{3+} forming ROS and RCl^{-}, that caused oxidation of TMB. Cu^{2+} was the most potent catalyst for the oxidation of TMB followed by Fe^{3+} (Figure 4.15). The Co^{2+}, Ni^{2+} and Zn^{2+} had very little peroxidase like activity. To our knowledge none of the metal ions used above have been reported to have peroxidase like activity or known to catalyse Fenton reactions.

4.3.17. Imidazole binding Fe^{3+}

Fe^{3+} oxidation of TMB was referred to as the Fe^{3+}-RCl^{-}-TMB assay. *Pf*HRP-2 has been shown to play a role in heme detoxification (Choi *et al*., 1999). His residues on *Pf*HRP-2 bind to heme via its Fe^{3+} centre as well as pi-pi interactions. Imidazole was used to see if it would bind Fe^{3+}, which may suppress Fe^{3+}-RCl^{-} formation and inhibit TMB oxidation (Figure 4.16).

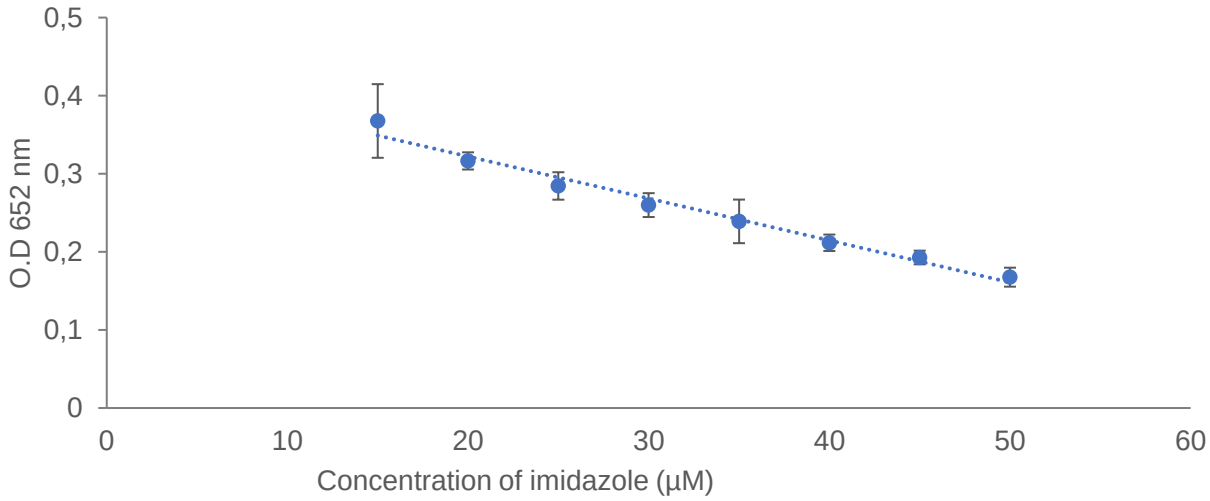

Figure 4.16: The Fe^{3+}-RCl^{-}- TMB assay in the presence of imidazole. Varying imidazole (15 to 50 µM) concentrations were incubated with Fe^{3+} for 10 minutes before the addition of H_2O_2, NaCl, TMB was added and $O.D_{652}$ was measured (15 min). Error bars indicate S.D of triplicate results.

Increasing concentrations of imidazole bound and removed Fe^{3+} ions form solution (Figure 4.16). Therefore, less Fe^{3+} ions remained to catalyse the formation of RCl^{-} and TMB oxidation was decreased.

Cu^{2+} like Fe^{3+} is also involved in Fenton chemistry (Figure 4.15) and Cu^{2+} was shown to be the most potent catalyst of TMB oxidation. Similarly, Shan *et al*., (2016) had reported Cu^{2+} catalyses the generation of RCl^{-} that oxidise TMB. For the detection of r*Pf*HRP-2, Cu^{2+} concentrations had to be optimised (Figure 4.17).

4.3.18. Cu^{2+} catalysed oxidation of TMB

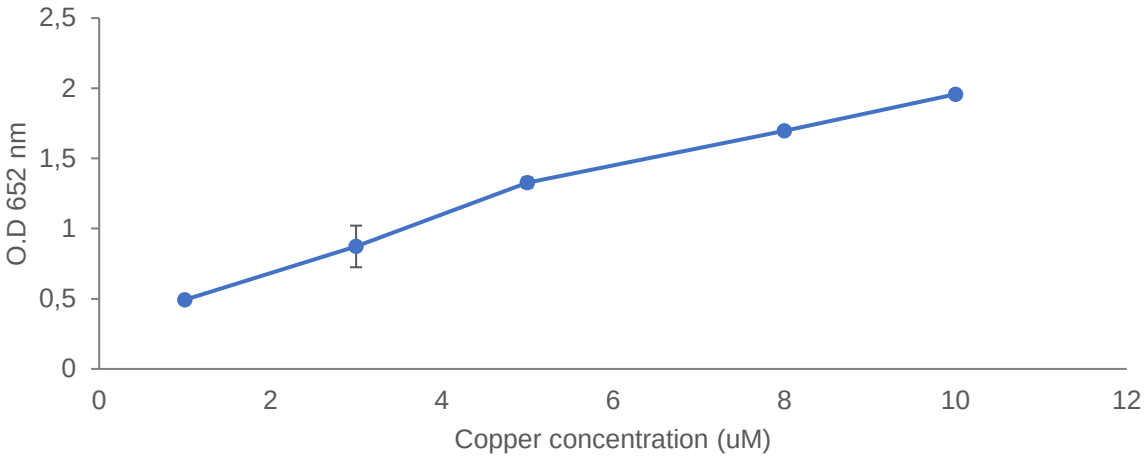

Figure 4.17: O.D of TMB oxidation catalysed by different concentrations of Cu^{2+}. Various Cu^{2+} (1 to 10 µM) concentrations were used in the presence of 100 mM NaCl and 750 mM H_2O_2. TMB was added and $O.D_{652}$ was measured (15 min). Error bars indicate S.D of triplicate results of three experiments.

The absorbance at 652 nm increased with increasing concentrations of Cu^{2+} (Figure 4.17). The concentration of Cu^{2+} chosen was 1 µM, which was 5-fold less than that of Fe^{3+} (5 µM) suggesting that Cu^{2+} was a better catalyst is oxidising TMB. The Cu^{2+} oxidation of TMB was defined as Cu^{2+}-RCl^-- TMB assay.

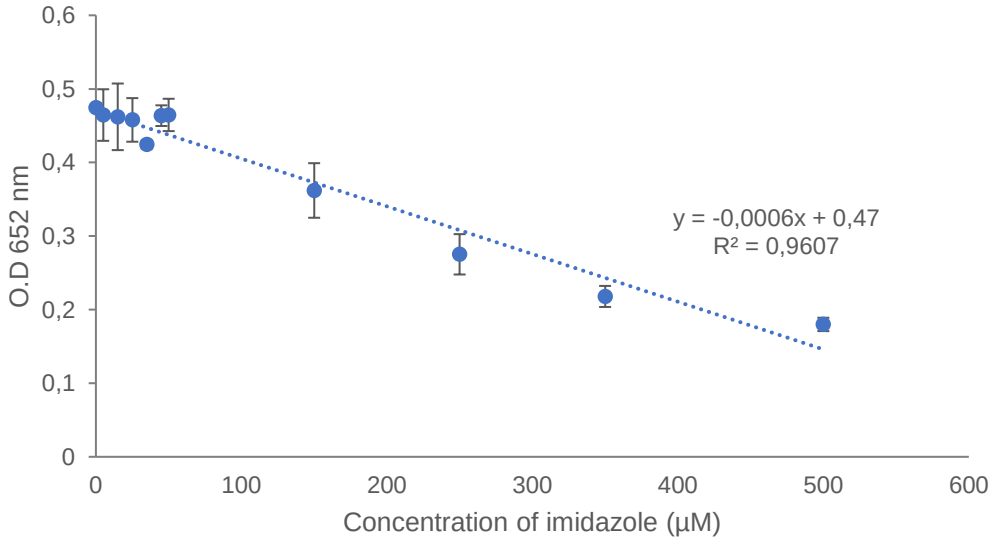

Figure 4.18: The Cu^{2+} -RCl^--TMB assay in the presence of imidazole. Varying imidazole (0 to 500 µM) concentrations were incubated with Cu^{2+} for 10 minutes before a reaction mixture containing H_2O_2, NaCl, TMB was added and $O.D_{652}$ was measured (15 min) was added. An optimal decline was followed at 652 nm. Error bars indicate S.D of triplicate results.

A decrease in absorbance was observed as imidazole concentration increased (0 to 500 µM) due to Cu^{2+} being bound by (Figure 4.18). The imidazole range detected was 10-fold greater than that for Fe^{3+} in the presence of imidazole (Figure 4.16). The result is an indication that Cu^{2+} more efficiently complexes with imidazole compared to Fe^{3+}.

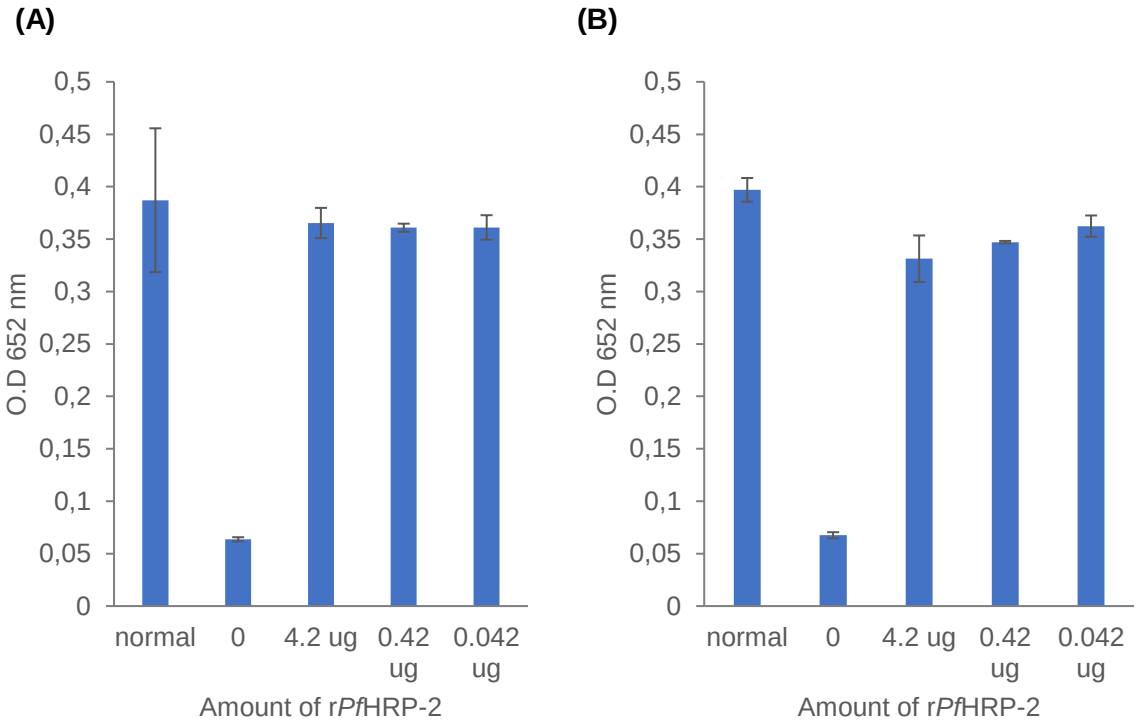

Figure 4.19: Using the Cu^{2+}-RCl^{-}-TMB assay for the detection of r*Pf*HRP-2 in an ELISA based format. Specific chicken polyclonal anti-r*Pf*HRP-2 IgY at 100 ng **(A)** and1 µg **(B)** was used to capture r*Pf*HRP-2. Thereafter the Cu-RCl^{-}-TMB assay was added for detection. Error bars indicate S.D of triplicate results.

The next step was to see if r*Pf*HRP-2 could be detected using an ELISA based format. r*Pf*HRP-2 was captured with anti-r*Pf*HRP-2 IgY (Figure 4.19). With all the concentrations of r*Pf*HRP-2 (4.2µg to 0.042 µg) none suppressed the oxidation of TMB. The results were similar to that of the Cu^{+}-HRPC-TMB assay (Figure 4.11).

4.4. Discussion

A graphical representation of both Cu assays developed for the detection of r*Pf*HRP-2 is illustrated in Figure 2.20.

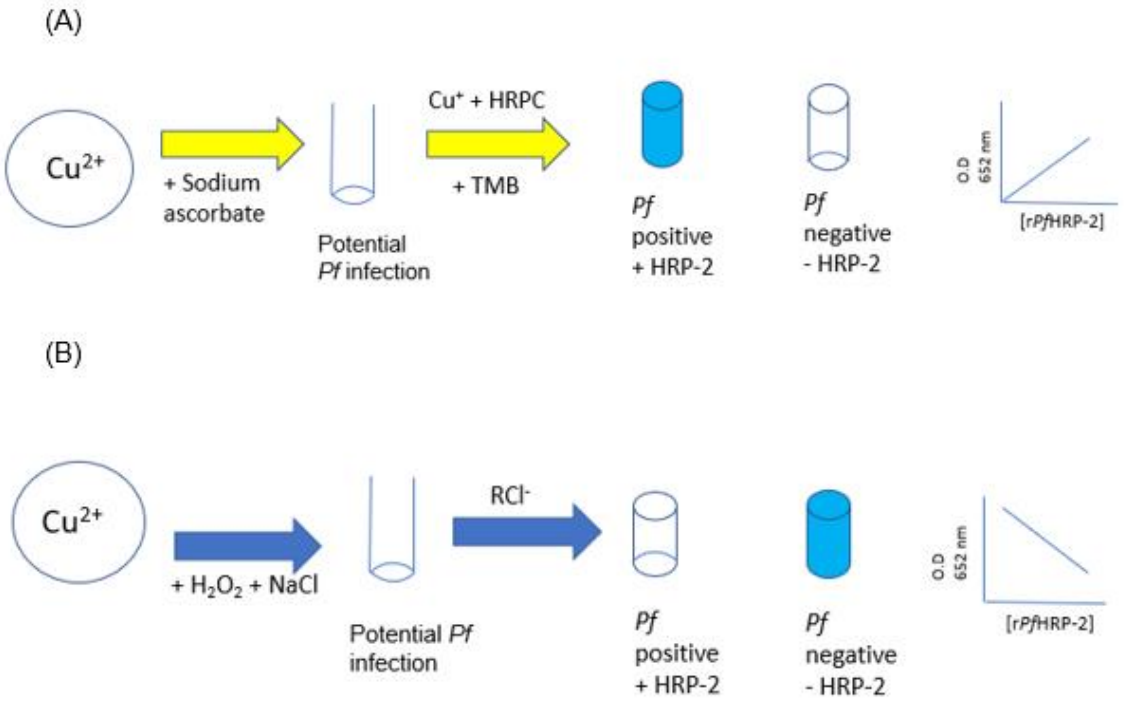

Figure 4.20: A graphical representation of two copper assays for the detection of r*Pf*HRP-2. The first assay illustrates the presence of *Pf*HRP-2 in a sample allows for HRPC to oxidise TMB **(A)**. The second assay illustrates the presence of *Pf*HRP-2 in a sample allows RCl^- to oxidise TMB **(B)**.

The first assay (Figure 2.20A) shows Na-ascorbate reduces Cu^{2+} to Cu^+ which inhibits HRPC activity. The presence of *Pf*HRP-2 binds and removes Cu^+, therefore allowing HRPC to remain active and oxidise TMB. The second assay (Figure 2.20B) shows Cu^{2+} catalyses the formation of RCl^- from H_2O_2 and NaCl, the presence of *Pf*HRP-2 in a sample binds and removes Cu^{2+}, therefore preventing the oxidation of TMB. The absorbance value is dependent on the concentration of *Pf*HRP-2 present in the sample.

4.4.1. Optimal HRPC concentration

Two HRPC molecules with 150 U/mg and 1000 U/mg of enzyme activity were evaluated. Initially the 150 U/mg HRPC was used to save cost (Figure 4.1-4.4). The optimal pH for HRPC activity is at a pH of 6-6.5 (Critchlow and Dunford, 1972) but pH 7.0 was used to allow deprotonation of the imidazole motif on r*Pf*HRP-2 which has a pka of 7 (Perrin *et al*., 1981). A HRPC concentration 180 pg (Figure 4.5) was in the range used in a Cu^+-HRPC-TMB assay for the detection of ALP (500 pg HRPC used) and pyrophosphate (Shi *et al.,* 2016).

4.4.2. Optimising $CuCl_2$ and sodium ascorbate concentration

The 1000 U/mg HRPC required 10 times less Cu^+ (12.5 µM; Figure 4.6) to inhibit enzyme activity compared the 150 U/mg HRPC (125 µM; Figure 4.2).

$CuCl_2$ and Na-ascorbate were used in a 1:1 stoichiometric ratio. Excess Na-ascorbate would reduce the TMB-diamaine (blue) back to TMB (colourless) which will be perceived as false HRPC inhibition (Arnao *et al.*, 1996; Figure 4.6). If Cu^{2+} were in excess, it could bind to amino acid residues that Cu^{+} would bind to, such as Phe, Try and Tyr (Xianyu *et al*., 2013; Burdett and Sevov, 1995). This is predicted to decrease the inhibition of HRPC activity. To prevent Cu^{+} been oxidised to Cu^{2+} by environmental O_2, Na-Ascorbate was added immediately before the assay began.

4.4.3. Incubation time and temperature effect of Cu^{+} binding to HRPC

Temperatures 4°C, RT and 37° had little effect on HRPC activity (Figure 4.3A). HRPC losing activity over 15 minutes when incubated at 37°C (Figure 4.3B) is probably due to the enzyme unfolding, therefore having a reduced activity. The T_m of HRPC is 64.1°C and the unfolding $\Delta_u G$ is 24.6 $KJ.mol^{-1}$ (Wright *et al*., 2017). The ΔμG of HRPC suggest the enzyme unfolds rapidly.

4.4.4. Mixed inhibition of HRPC by Cu^{+} on HRPC

Xianyu *et al*., (2013) reported Cu^{+} binds to amino acids residues on HRPC and not the active site. This was supported in Figure 4.4 where Cu^{+} was shown to be a mixed inhibitor of HRPC. There are currently no studies stating the number of Cu^{+} ions that bind to HRPC. Keyhani *et al*., 2003 and 2005 reported Cd^{2+} and Ni^{2+} had similar inhibitory effects on HRPC activity. Cu^{+}, Ni^{2+} and Cd^{2+} inhibit HRPC by causing a conformational change in the structure of the enzyme, therefore making the active site less accessible to substrates by blocking the hydrophobic access channel (Zaton and Ochoa De Aspuru, 1995; Veitch and Smith, 2000).

4.4.5. Effect of transitions metal ions on HRPC activity

Co^{2+} (Mahmoudi *et al*., 2003; Han *et al*., 2008), Ni^{2+} (Keyhani *et al.*, 2005), Zn^{2+} (Moyo, 2014), Cd^{2+} (Keyhani *et al*., 2003) Fe^{3+}, Cu^{2+} and Cu^{+} (Mahmoudi *et al*., 2003; Xianyu *et al.*, 2013) have all been reported to inhibit HRPC activity, where Cu^{+} is the most potent inhibitor (Figure 4.7). Xianyu *et al*., (2013) showed this using UV-spectroscopy, Density functional theory (DFT) calculations and inductively coupled plasma optical emission spectrometry (ICP-OES).

4.4.6. Imidazole binds and removes Cu^{+} allowing HRPC to maintain activity

Imidazole has been shown to bind Cu^{+} atoms by Rannulu and Rodgers, (2005). They suggested 4 possible ligands resulting between 1 to 4 imidazole molecules binding to a single Cu^{+} atom. The Gibbs energy for each $Cu(imidazole)_x$ complex (where x is 1-4) was determined, 0.0 $KJ.mol^{-1}$, 18.6 $KJ.mol^{-1}$ and 48.3 $KJ.mol^{-1}$ respectively. The stable ligand formed is $Cu^{+}(imidazole)_2$ and is likely the ligand in highest concentration in Figure 4.8A.

When Cu^{+} is chelated by imidazole, a lower concentration is free to inhibit HRPC therefore, HRPC will be more active. Experiments found Cu^{+} needed 30 minutes to bind to imidazole (Figure 4.8).

4.4.7. Fenton reactions, Cu^{2+} and Fe^{3+} oxidation of TMB

RCl^{-} species have been described to be more potent catalyst of TMB compared to ROS (Shan *et al*., 2016). Cu is a catalyst for ROS formation and works by breaking down H_2O_2 into OH• and O_2^{-} (ROS), however if Cl^{-} ions are present they scavenge OH• and form RCl^{-} species (Bokare and Choi, 2014). Results from Figure 4.13 show RCl^{-} species are more potent oxidants than ROS.

RCl^{-} species oxidises TMB either directly or the RCl^{-} species dissociate into Cl^{-} anions which can bind to Cu^{2+} forming a reactive intermediate $[CuCl^{-}]^{+}$. The reactive intermediate is reduced by H_2O_2 (H_2O_2 -> $^{-}OOH + H^{+}$) into a more stable CuCl intermediate which is more stable and allows for the decomposition of H_2O_2 into OH• radicals that also oxidise TMB. The cycle continues, and the CuCl intermediate provides the ions for RCl^{-} formation. (Shan *et al*., 2016; De Laat and Le, 2006). The absorbance was proportional to the increase in Cu^{2+} concentration (Figure 4.17). Shan *et al.,* (2016) observed that if TMB is oxidised by OH•, the rate of the of oxidation is consistent.

The first reported assay using Fe^{3+} ions peroxidase like activity was in 2014, when Wu *et al*., showed that Fe^{3+} can be used for the detection of cysteine residues. Th mechanism of Fe^{3+} RCl^{-} to oxidised TMB (Figure 4.13) is Fe^{3+} complexes with Cl^{-} to form a reactive intermediate $[FeCl^{-}]^{2+}$. The reactive intermediate would allow for the accelerated decomposition of H_2O_2 into OH• radicals. The OH• radicals then react with Cl^{-} to from RCl^{-}, which attacks and oxidises TMB more effectively than that OH• alone.

4.4.8. Optimising H_2O_2 and NaCl concentrations for Fenton reactions

Metal ions catalyse break down H_2O_2 is to produce ROS, which oxidise TMB. The optimal concentration of H_2O_2 chosen was 750 mM (Figure 4.14A) which was used by Shan *et al*., (2016). TMB was oxidised in the absence of H_2O_2 (Figure 4.14B). This meant the Cl^{-} ions formed a reactive complex with Fe^{3+} and it is hypothesized to be $[FeCl^{-}]^{2+}$. A concentration of 500 mM NaCl allowed for the highest oxidation of TMB, however 100 mM was selected as concentrations above 100 mM caused TMB to precipitate. Shan *et al*., 2016 used 250 mM, but their assay was for Cu^{2+} limit of detection instead of detecting molecules. Aggregation was noticed for their assay at concentrations of NaCl above 250 mM.

4.4.9. Assessing the peroxidase like activity of different metal ions

Cu^{2+} showed the highest oxidation of TMB followed by Fe^{3+}. Zn^{2+}, Co^{2+} and Ni^{2+} had little significant peroxidase like activity (Figure 4.15).

Other reported metal ions reported with peroxidase like activity are Cr^{3+}, Au^{3+} and Ag^{+} (Shan *et al*., 2016), but those metal ions work with direct TMB oxidation where as Cu^{2+} and Fe^{3+}allow for oxidation of TMB via Fenton chemistry. Cu^{2+} works best because Cu^{2+} can easily be reduced and has a relatively low electron potential (0.16V).

4.4.10. Imidazole binding Fe^{3+} and Cu^{2+}

Imidazole was used for two reasons. Firstly, imidazole is the moiety on histidine residues that is most likely to bind to and remove Fe^{3+} and Cu^{2+} thus preventing the oxidation of TMB. Alternatively, the experiment was to test if Cu^{2+} and Fe^{3+} bind imidazole rings and act as probes to increase the oxidation of substrates, as was observed when Cu^{2+} was combined with alizarin for the detection of BSA (Wu *et al*., 2014). The oxidation of TMB by both metal ions was inhibited by imidazole (Figure 4.16 and 4.18), indicating Cu^{2+} and Fe^{3+} were not able to catalyse H_2O_2 decomposition, hence the mechanism was inhibited. The interaction of transition metals with the imidazole ring is very well characterized and reviewed by Sundberg and Martin, (1974). The results from Figures 4.16 and 4.18 were consistent to studies that detected free Cys and His residues (Wu *et al*., 2014; Xu *et al*., 2015; Zhou *et al*., 2014).

4.4.11. Detection of r*Pf*HRP-2: using the Cu^{+}-HRPC-TMB

For r*Pf*HRP-2 the limit of detection was 102 ng in aqueous solution (HEPES buffer; Figure 4.8; 4.20), Mash and Chin, (2003) reported that a non-sulfonated HEPES molecule in HEPES buffer bound Cu. Controls (Figure 4.9 and Figure 4.10) show the HEPES buffer did not interfere with the assay in this study.

The stoichiometric ratio of the potential binding sites on r*Pf*HRP-2 and Cu^{+} were calculated, using a Mw of 30 kDa for r*Pf*HRP-2 and 27 binding sites, 51 His-His-Ala repeats and His_6-tag and if 1 Cu^{+} binds 2 histidine's. If a maximum of 27 Cu^{+} atoms bound per molecule of r*Pf*HRP-2, 5.53 x 10^{13} Cu^{+} can bind. If Cu^{+} bound in the same binding sites as hemozoin binds there would only be 21 sites (18 of the protein + 3 from His_6-tag), therefore 4.3 x 10^{13} Cu^{+} could bind. The optimal Cu^{+} concentration has 1.51 x 10^{15} (12.5 µM) atoms of Cu^{+} (Figure 4.6). Therefore, if the maximum amount of theoretical Cu^{+} is removed (by binding to r*Pf*HRP-2), HRPC would not reach full activity as there would still be Cu^{+} in excess (2.44 nM) that remains to inhibit HRPC.

Since *Pf*HRP-2 is found in saliva (Nantavisa, 2014; Fung *et al*., 2012), r*Pf*HRP-2 was added to saliva samples and detected using the Cu^{+}-HRPC-TMB assay (Figure 4.10). Samples with HRPC in the presence of r*Pf*HRP-2 had higher activity compared to samples with BSA. BSA was selected as a control because it has been shown to bind Cu at the Asp-Thr-His N-terminus end (Orlovskaia and Belitser, 1964 and Peters and Blumenstock, 1967).

The mechanism behind the increased HRPC activity in the presence of r*Pf*HRP-2 in saliva is not understood.

A potential explanation could be that the saliva favoured Cu^{+} atoms binding to the epsilon nitrogen rather than the delta nitrogen of the imidazole ring, resulting in Cu^{+} facilitating the decomposition of H_2O_2 (substrate for HRPC) producing OH• radicals which can oxidise TMB directly. Therefore, both OH• and HRPC would catalyse the oxidation of TMB and may explain the increased absorbance as the concentration of r*Pf*HRP-2 increases (Figure 4.10).

The concentrations of r*Pf*HRP-2 (4.2 µg to 420 ng) captured by the ELISA was not able to remove enough Cu^{+} to allow HRPC to regain activity (Figures 4.11). The result was unexpected based on the stoichiometry 4.215 x 10^{16} to 4215 x 10^{17} (420 ng to 4.2 µg) binding sites were available to bind 1.51 x 10^{15} Cu^{+} atoms. The Cu^{2+}-RCl^{-}- TMB assay, the Cu^{2+} concentration was 1 µM which means 1.204 x 10^{14} atoms were present (Figure 4.19).

4.4.12. Potential reasons as to why both copper binding assays did not work

Both the Cu^{+}-HRPC-TMB and Cu^{2+}-RCl^{-} - TMB assay were not able to detect r*Pf*HRP-2 that was captured using anti-r*Pf*HRP-2 IgY. The reason why r*Pf*HRP-2 was not detected could not be explained in the study. A reason could be that the polyclonal anti-r*Pf*HRP-2 IgY used could have prevented Cu atoms binding to the His residues on r*Pf*HRP-2 by causing steric hinderance, therefore the Cu^{+} remained in solution and inhibited HRPC. Alternatively, the hydrophobic interactions on the microtiter plate may have interfered and prevented Cu atoms binding to r*Pf*HRP-2, Figure 4.12 showed that when r*Pf*HRP-2 was coated directly to the microtiter plate the Cu^{+}-HRPC-TMB assay was less sensitive compared to when r*Pf*HRP-2 was in aqueous solution.

4.4.13. Choice of buffers for both copper assays

For the Cu^{+}-HRPC-TMB assay PBS was used, since the buffer was used successfully by Xianyu *et al*., (2013) with no interferences. Buffers for the Cu^{2+}-RCl^{-}-TMB assay were a more complicated as the pH must be acidic or additives like acetonitrile need to be supplemented (Xu *et al*., 2015). Therefore, MES buffer was used as recommended by Shan *et al.,* (2016). Na-acetate buffer is an alternative to consider, it was used to detect dopamine and uric acid (Wang *et al*., 2017 and Lu *et al*., 2017).

4.4.14. Conclusion

Two copper binding assays were developed for the detection of r*Pf*HRP-2 namely the Cu^{+}-HRPC-TMB assay and the Cu^{2+}-RCl^{-}-TMB assay. The Cu^{+}-HRPC-TMB assay was shown when Cu^{+} is present, HRPC is inhibited, but when a molecule is present that binds Cu^{+} the inhibition on HRPC is reduced. r*Pf*HRP-2 was detected in aqueous solution and when coated directly onto a microplate.

The Cu^{2+}-RCl^{-}TMB assay was shown when imidazole was present, which binds Cu^{2+} the oxidation of TMB is reduced signifying the detection of a copper binding molecule. Both assays were not sensitive enough for the detection of r*Pf*HRP-2 when captured using specific polyclonal anti-r*Pf*HRP-2 IgY antibodies, therefore both assays cannot be used as a malaria diagnostic. Currently from the data does not suggest an exact reason for r*Pf*HRP-2 not been detected in the ELISA assay.

5. CHAPTER 5: An aqueous-organic buffer to increase storage stability of horseradish peroxidase

5.1. Introduction

Enzymes are used as biocatalysts in many industries, such as the chemical, pharmaceutical, wastewater, biomedical industries, and is becoming more popular. Enzymes offer high catalytic efficiency while being regarded as biofriendly. Therefore, enzymes are the "green" solution (Li *et al*., 2017, Xianyu *et al.,* 2013). Industrial processes often result in heat being generated as a by-product, which creates an unfavourable microenvironment around the enzyme catalyst, resulting in enzymes being degraded. Poor storage conditions for enzymes also result in a loss of enzyme activity (Schmidt *et al*., 2002; Sato *et al*., 1995). Therefore, techniques to stabilise enzymes are vital for use in the field of biotechnology and industry (Schmidt *et al*., 2002).

Enzymes can be stabilised for storage with organic solvents, which has become a popular stabilising component in some enzyme buffers. Unlike water in aqueous environments, organic solvents reduce the enzyme's flexibility, preventing the unfolding of the tertiary structure. The result is the catalytic efficiency of enzymes are often lost, and concentrations of organic solvents of 60-70% completely inactive enzymes (Stepenkova *et al*., 2013).

Various strategies have been used to preserve enzyme structure and activity such as adsorption to mesoporous particles, covalent binding, cross-linking, entrapment (by adsorption), reversed micelle, chemical modification, protein engineering, propanol rinsed preparation, ionic liquid coating and additives. Unfortunately, each technique has different levels of success, depending on variables such as the morphology of the enzyme, and the process for which an enzyme must be stabilised (Stepenkova *et al*., 2013).

HRPC is commonly conjugated to secondary antibodies for use in molecular biology and biotechnology. The enzyme is small (44 kDa), has high catalytic oxidation of chromogenic substrates and is relatively stable in high concentrations. However, when the enzymes are used, they are diluted several folds. The diluted enzyme solution has low storage stability (Mozhaez, 1993; Eremin *et al*., 2002). To combat loss of stability, new dilutions must be prepared frequently to ensure reproducible results. The loss of activity is believed to be primarily due to HRPC unfolding when stored in dilute solutions.

Several different approaches have been made to stabilize HRPC and HRPC-conjugated antibodies for extended periods of time in solution:

(i) Immobilization: Silica beads are used as a support structure to covalently bind to HRPC. The HRPC was used in an aqueous-organic solvent medium containing 20% DMSO, which increased stability by 300% (Azevedo *et al*., 2001).

(ii) Eremin *et al*., (2002) compared an aqueous-organic solvent mixture and a protein-based stability mixture. The result showed the organic solvent worked better.

(iii) Schutz *et al.,* (1997) explored using the substrates luminol and TMB to stabilise HRPC in a 50 mM PBS buffer was explored.

(iv) Chemical additives are some of the simplest and most cost-effective reagents added to organic solvents to stabilise HRPC. Ca^{2+} improved HRPC stability (Haschke and Friedhoff, 1978).

The numerous patented reagents sold to stabilise enzymes signifies the importance of preserving enzyme stability. A buffer cocktail that could preserve the storage stability of HRPC would be advantageous to biochemical reactions using HRPC. This study reports a chemical buffer containing Tris-HCl, methanol and Ca^{2+} improved the storage stability of HRPC.

5.2. Materials and Methods:

5.2.1. Materials and equipment

All buffers and salts were purchased from Sigma and Merck with no further purification required. HRPC (type VI 150 U/mg and 1000 U/mg; Sigma). Maxi Sorp™ 96-well ELISA plates were from Nunc products (Roskilde, Denmark), UV-1800 Shimadzu spectrophotometer from Shimadzu corporation (Kyoto, Japan); pH meter from HANNA instruments. VersaMax™ ELISA plate reader was purchased from Molecular Devices Corporation (California, USA).

5.2.2. Preparation of buffers

HRPC activity was evaluated at different pH values. Citrate phosphate buffer (150 mM) was used for pH values 5.0 and pH 6.0. phosphate buffered saline (PBS; 137 mM NaCl; 3 mM KCl; 7 mM Na2HPO4; 1.5 mM KH2PO4) at pH 7.4, PBS (50 mM; 150 mM NaCl) at pH 7.6. Tris-HCl (50 mM) at pH 8.0, carbonate buffer (100 mM) at pH 9.0 and Glycine buffer-Na (100 mM) at pH 10.4. HRPC (150 Units) lyophilized powder was resuspended in dH_2O at a concentration of 3 mg/ml).

5.2.3. Measuring HRPC enzyme activity

The optimal pH of HRPC was determined by using 0.5 ng HRPC to oxidise the chromogenic substrate tetramethyl benzidine (TMB) in the presence of H_2O_2. The assay was carried out in a 96 well microplate format, at room temperature (22-24°C). HRPC activity was determined by the oxidation of TMB (284 µM) to the TMB-diamine in the presence of H_2O_2 (1.92 mM) and the absorbance at 652 nm was measured after 15 minutes.

5.2.4. Preparation of different concentration Tris-HCl buffers and Tris-HCl- organic solvent buffers

Tris-HCl at pH 8.0 was prepared at concentrations of 10 mM, 50 mM, and 100 mM. 50 mM Tris-HCl buffer was prepared with methanol or ethanol (10, 20, 30 and 40% (v/v)).

5.2.5. Optimising Ca^{2+} concentrations with Tris-HCl-MeOH buffer

As described in Section 5.2.3, an aqueous-solvent buffer was prepared with 10 and 20% (v/v) methanol. Each preparation/buffer was supplemented with $CaCl_2 \cdot 2H_2O$ at a final concentration of either 10, 20, 50, 100, or 200 mM.

The stabilising effects of the buffer on HRPC were measured after 0, 3 and 7 days, using the TMB substrate (described in Section 5.2.2.). The optimised buffer conditions were then used to stabilise HRPC over a longer period, and this was assessed weekly.

5.2.6. Comparing HRPC activity in Tris-HCl to HRPC in Tris-HCl-MeOH buffer

HRPC (1000 U/mg) was diluted to a final concentration of 0.5 ng in Tris-HCl (50 mM; pH 8.0) or Tris-HCl-MeOH (50 mM; 20% MeOH(v/v) with 50 mM Ca^{2+}). HRPC was stored at 37°C and the activity of the enzyme was measured (described in section 5.2.4) at 1, 3, 5 and 20 hours.

5.3. Results:

5.3.1. Comparing the stability of low concentration HRPC stored for a week

HRPC activity was tested by measuring the absorbance (O.D) at 652 nm of oxidised TMB (Figure 5.1).

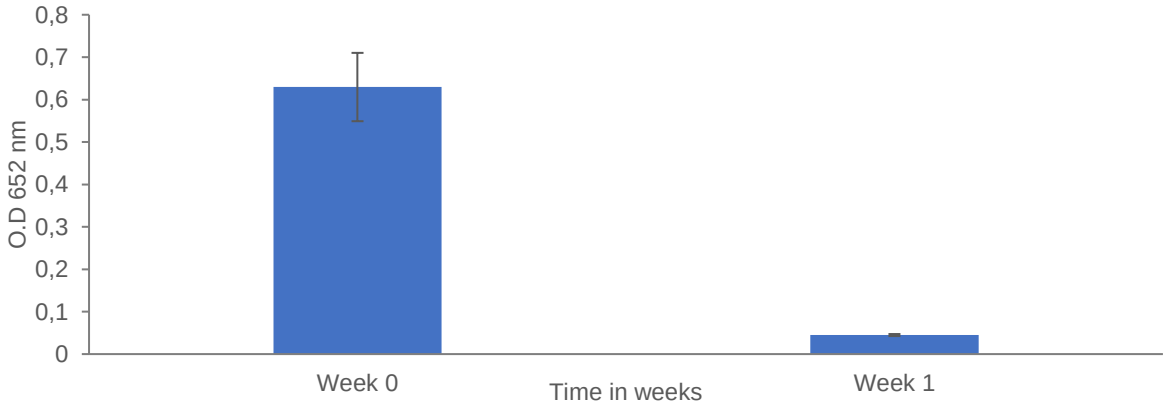

Figure 5.1: Comparison of HPRC activity in Tris-HCl after one week. HRPC in 50 mM Tris-HCl activity was measured (week 0), and after been stored for a week at 4°C . TMB was added and $O.D_{652}$ was measured (15 min). Error bars S.D of triplicate results of an experiment repeated 3 times.

Tris-HCl is a commonly used biological buffer (Mohan, 2003), however the buffer was unsuitable for storage of dilute concentrations of HRPC, as the enzyme lost 93% of its activity in a week (Figure 5.1).

5.3.2. Comparing HRPC activity in different buffers

HRPC was incubated in different buffers and the enzyme activity was measured at different times (Figure 5.2). All the buffers tested have either been used in other HRPC stability studies or are common buffers.

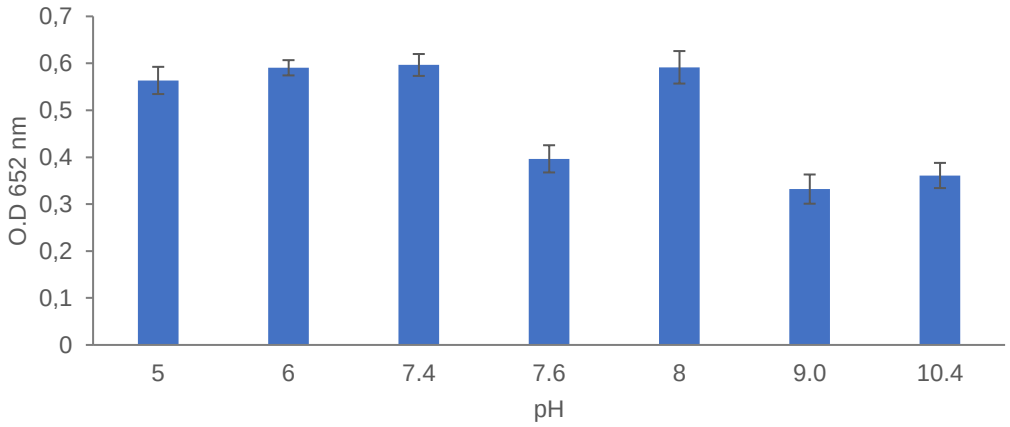

Figure 5.2: HRPC activity in different biological buffers at different pH values. HRPC was prepared in 150 mM citrate-phosphate buffer pH 5.0 and 6.0, 7 mM PBS pH 7.4, 50 mM PBS pH 7.6, 50 mM Tris-HCl pH 8.0, 100 mM carbonate buffer pH 9.0, and 100 mM Glycine-NaOH pH 10.4. The activity of HRPC was determined by oxidation of TMB as determined from the measurement of absorbance after 15 min, at 652 nm. Error bars indicate S.D of triplicate results of the experiment done twice.

Citrate-phosphate buffer (pH 5.0, pH 6.0) showed the activity of HRPC was similar to that of PBS (7 mM; pH 7.4) and Tris-HCl. The activity of HRPC in PBS (50 mM; pH 7.6) was 33.5% lower than PBS (7 mM, pH 7.4). HRPC prepared in carbonate (pH 9.0) and Glycine-NaOH buffers (pH 10.4), had the lowest activity.

Downstream experiments showed that PBS and citrate-phosphate buffer were not compatible with Ca^{2+} because both phosphate and citrate chelated the Ca^{2+} leading to precipitation Tris-HCl was selected as the buffer for HRPC storage.

5.3.3. Analysis of different concentration Tris-HCl buffer on HRPC activity

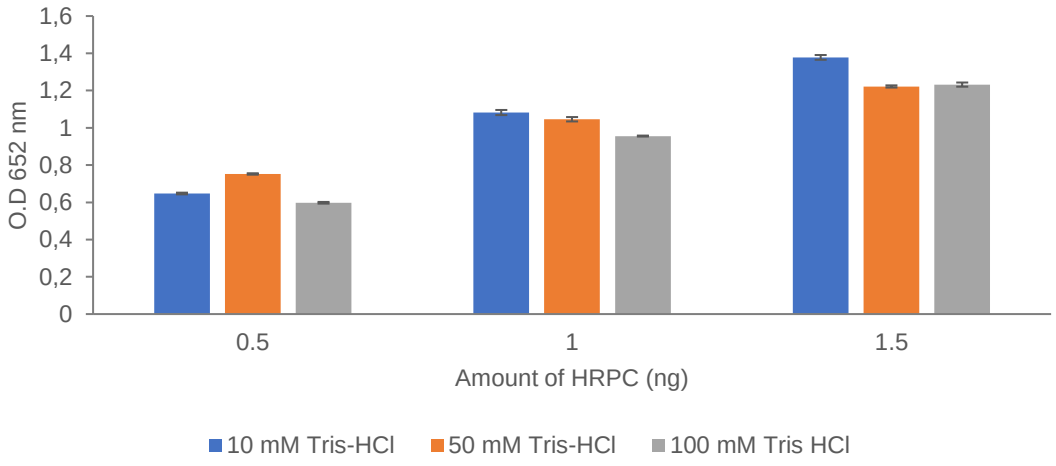

Figure 5.3: HRPC activity at different concentrations of Tris-HCl. HRPC at 0.5, 1 and 1.5 ng were diluted in 10 mM, 50 mM and 100 mM Tris-HCl. The activity of HRPC was determined by oxidation of TMB measured after 15 min at 652 nm. Error bars indicate S.D of triplicate results.

HRPC in different concentrations of Tris-HCl buffers had comparable activity (Figure 5.3). As the concentration of HRPC increased, so did the enzyme activity. At each concentration, HRPC had the least activity in 100 mM Tris-HCl. Tris-HCl at 50 mM was selected for further assays.

The buffer selected in Figure 5.3 was the same Tris-HCl buffer in which HRPC was stored in and lost most activity after a week (Figure 5.1). However, to improve the storage stability of low concentration solutions of HRPC over longer periods of time, two aqueous-organic solvents buffer systems were analysed.

5.3.4. Effect of ethanol and methanol of HRPC activity

Various solvents have been tested to stabilize HRPC, such as tetrahydrofuran, dimethylformamide, dimethyl sulfoxide, acetonitrile and ethanol (Azevedo *et al*., 2001; Eremin *et al*., 2002). All solvents had different influence on HRPC activity. Ethanol was shown to have promise to stabilise HRPC (Eremin *et al*., 2002). There has been no reported use of MeOH in long-term storage buffers for HRPC. Therefore, the two organic solvents ethanol and methanol at different concentrations were tested (Figure 5.4).

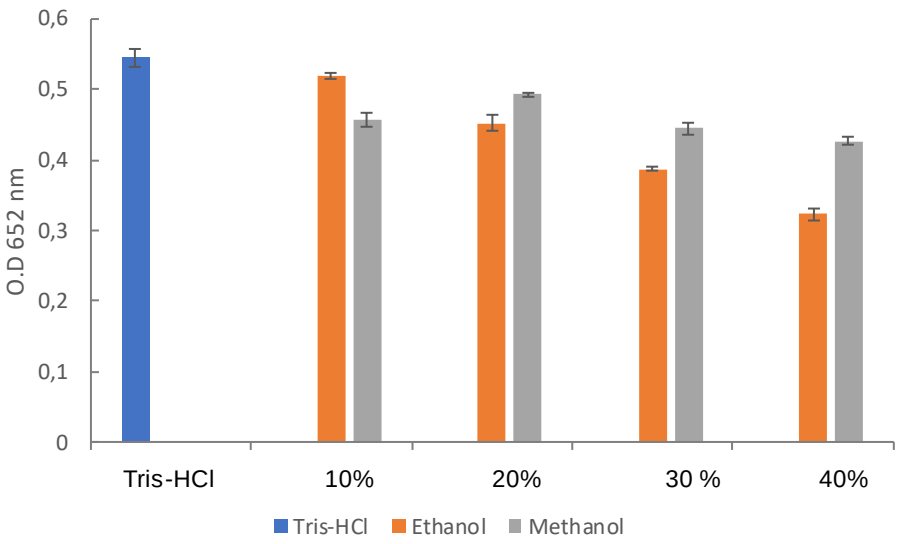

Figure 5.4: Effect of different concentrations of aqueous-organic solvent buffers on HRPC activity. HRPC was dissolved 10 to 40% (v/v) of either ethanol or methanol ranging from 10 to 40% in 50 mM Tris-HCl pH 8.0. Oxidation of TMB was measured after 15 minutes at 652 nm. Error bars indicate S.D of triplicate results.

HRPC in Tris-HCl alone had the highest activity (Figure 5.4) indicating both EtOH and MeOH inhibited HRPC activity. When HRPC was tested with Tris-HCl-EtOH buffer, HRPC activity decreased with increasing concentrations of EtOH.

EtOH at 10% (v/v) had the least inhibition (4%) and EtOH 40% (v/v) the highest inhibitory effect (41%). HRPC in Tris-HCl-MeOH buffer showed MeOH 10 – 40% (v/v) inhibited HRPC activity by 17 and 22% respectively.

5.3.5. HRPC activity in Tris-HCl-EtOH and Tris-HCl-MeOH supplemented with Ca^{2+}

To attempt to improve the stability of HRPC, Ca^{2+} was added to the buffer because Ca^{2+} ions are sometimes lost and are important to maintain the active site of HRPC (Gajhede *et al*., 1997).

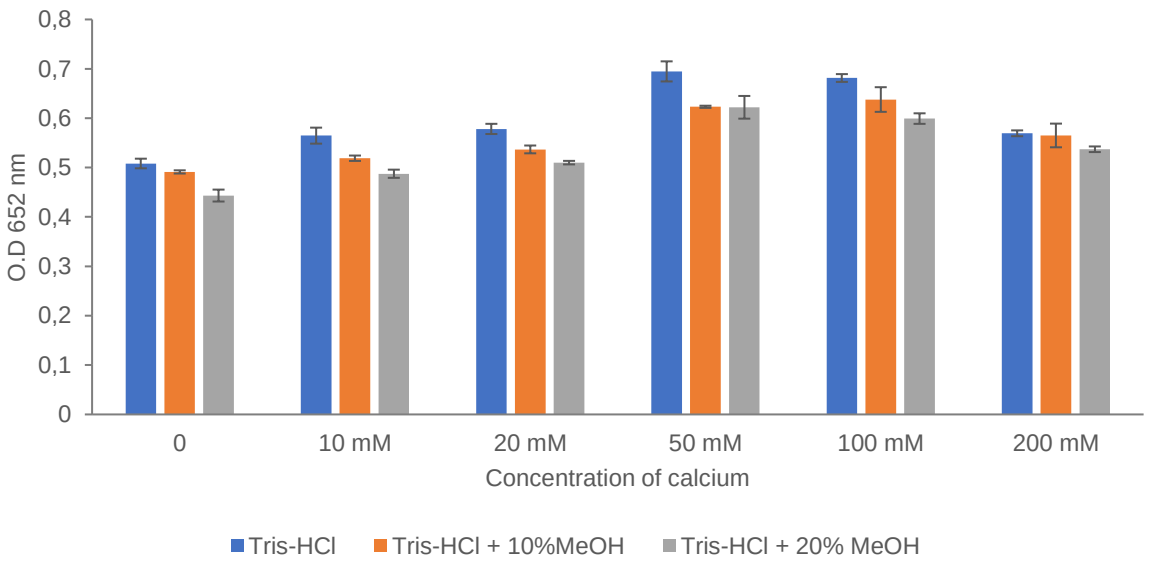

Figure 5.5: The effect of Ca^{2+} in Tris-HCl and Tris-HCl-MeOH on the activity of HRPC. Ca^{2+} (0 – 200 mM) was added to different buffers to test their stabilising effect on dilute HRPC and HRPC activity was measured by the oxidation of TMB measured after 15 min at 652 nm. Error bars indicate S.D of triplicate results.

The addition of Ca^{2+} increased the activity of HRPC at concentrations from 10 mM to 50 mM in both Tris-HCl and Tris-HCl-MeOH buffers (Figure 5.5). HRPC in Tris-HCl alone (with Ca^{2+}) had the highest activity and had the highest activity in the presence of 50 and 100 mM Ca^{2+}.

5.3.6. Comparing HRPC activity Tris-HCl with 10 or 20% MeOH supplemented with Ca^{2+} over a week

It was unclear which MeOH concentration was better for stabilising HRPC. Therefore, both buffers were tested over a week (Figure 5.6).

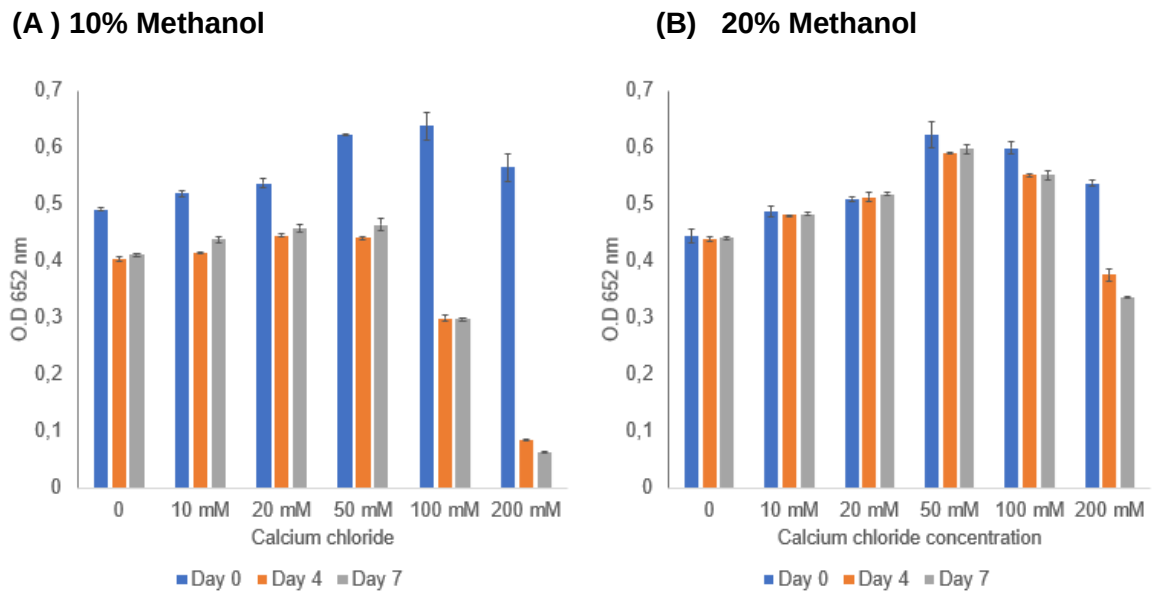

Figure 5.6: Stabilising effects of Tris-HCl-MeOH supplemented with Ca^{2+} on HRPC activity over a week. HRPC was diluted and stored in (Tris HCl-(10% (v/v)) MeOH **(A)** and 20% Tris HCl-(20% (v/v)) MeOH **(B).** Both storage buffers were supplemented with $CaCl_2$ ranging from 0 – 200 mM and stored at 4°C. Samples were evaluated for HRPC activity by the oxidation of TMB at 0, 4 and 7 days at 652 nm. Error bars indicate S.D of triplicate results.

Day 0 (Figure 5.6A and 5.6B) represents the initial HRPC activity. HRPC had the highest activity in the presence of 50 mM Ca^{2+}. HRPC in Tris-HCl (10% (v/v)) MeOH buffer (Figure 5.6A) and 200 mM Ca^{2+} lead to a decrease in HRPC activity (86%). Interestingly after 4 days of storage HRPC activity was marginally higher with10 – 50 mM Ca^{2+} compared to no Ca^{2+}. HRPC stored in Tris-HCl-(20% (v/v)) MeOH buffer (Figure 5.6B) lost no activity over the 7-day storage period, except when 200 mM Ca^{2+} was added. Therefore, the buffer chosen was a 50 mM Tris-HCl buffer supplemented with 20% MeOH and 50 mM Ca^{2+} as the stability buffer.

5.3.7. Long-term stability of a dilute concentration of HRPC under different conditions

HRPC (10 ng/ml) solutions were prepared in the Tris-HCl-MeOH buffer (50 mM Tris-HCl; 20% MeOH and 50 mM Ca^{2+}) buffer and stored at 4°C, 4°C in the dark, RT (22°C- 25°C) and at 37°C and enzyme activity was measured weekly (Figure 5.7).

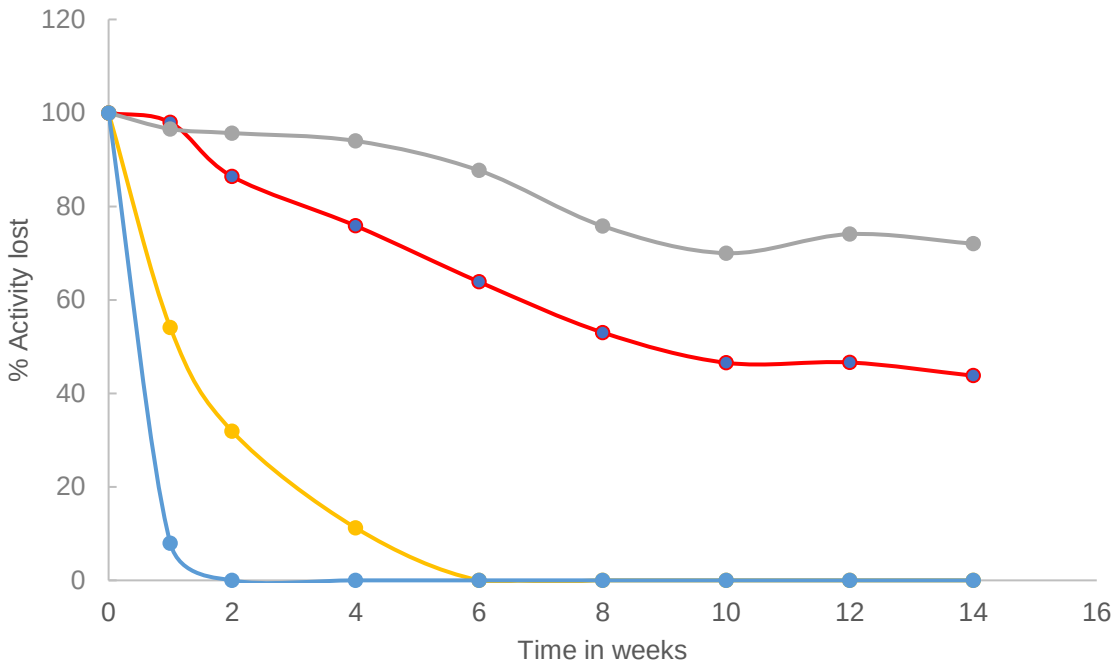

Figure 5.7: A 14-week study of HRPC activity under different storage conditions. HRPC was stored at 4°C (•), 4°C in the dark (•), RT (•) and 37°C (•). The % Activity was the activity of HRPC at each week compared to the initial activity.

The storage temperature was an important for HRPC stability as HRPC only had 8% activity after one week when stored at 37°C and at RT 11% activity after 4 weeks. HRPC at 4°C had 43% and 72% when stored in the dark activity after the 14-weeks (Figure 5.7). This is a significant improvement in HRPC activity.

HRPC in Tris-HCl-MeOH buffer (50 mM Tris-HCl; 20% MeOH and 50 mM Ca^{2+}) had retained 44% activity after 6 months (Figure 5.8B).

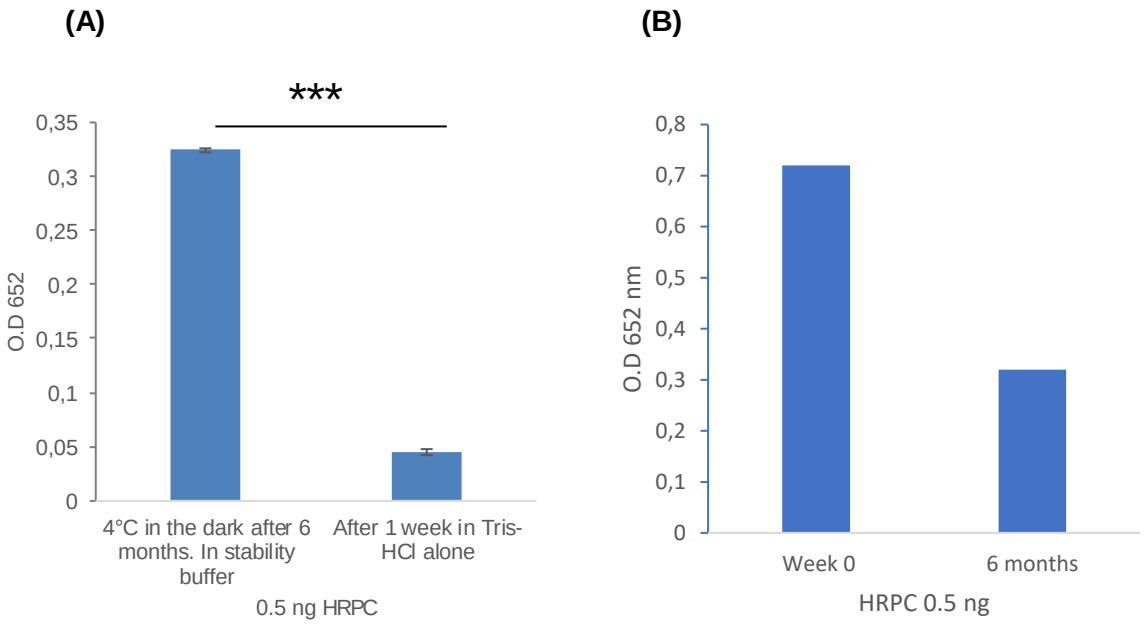

Figure 5.8: Comparison of HRPC in stability buffer after 6 months. 0.5 ng HRPC in stability buffer after 6 months is compared to HRPC in Tris-HCl **(A)**. 0.5 ng HRPC in stability buffer storage was compared at week 0 to 6 months **(B)**. P<0.001.

5.3.8. Thermal stability of HRPC

In industrial applications, the thermal stability of enzymes is of great importance, since elevated temperatures result in denaturation of enzymes resulting in lower activities. The Tris-HCl-MeOH stability buffer was compared to Tris-HCl (50 mM) to see if there was any thermal stability allowed for (Figure 5.9).

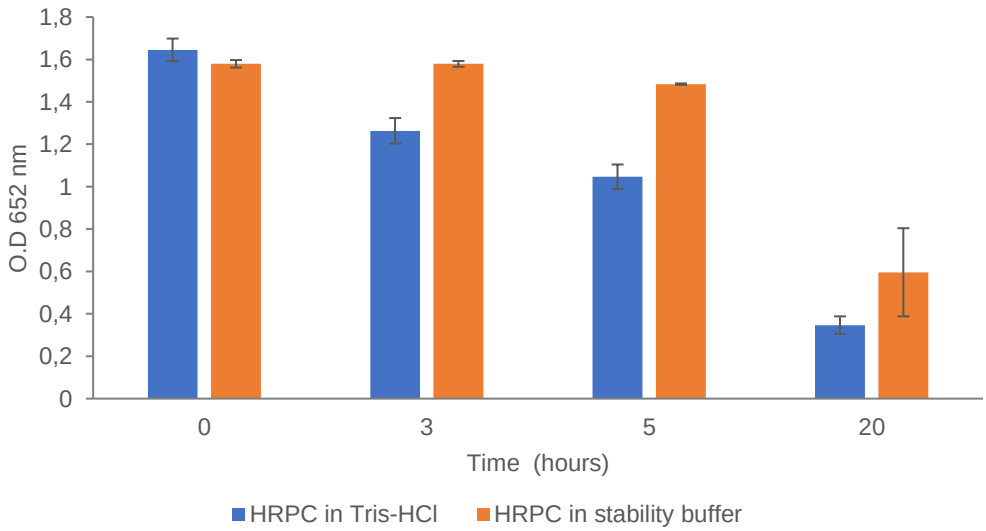

Figure 5.9: Comparison of HRPC activity in Tris-HCl and Tris-HCl-MeOH at 37°C. HRPC (0.5 ng) was stored at 37°C and the activity was compared in each buffer at 0, 3, 5 and 20 hours. Error bars indicate S.D of triplicate results of the experiment done twice.

Initially, the activity of HRPC in Tris-HCl was marginally higher than HRPC in the Tris-HCl (20% MeOH; 50 mM Ca^{2+}) buffer. After 3 and 5 hours HRPC in the Tris-HCl-MeOH buffer retained 100 and 94% activity, while in Tris-HCl HRPC had 76 and 64% activity. At 20 hours enzyme activity was much lower in both buffers.

5.4. Discussion

5.4.1. Selecting a buffer for storage of HRPC

Several studies have reported using buffers for optimal storage of HRPC and HRPC conjugates (Mogharrab *et al*., 2007; Farzamfar *et al*., 2010; Lopes *et al*., 2015; Azvedo *et al*., 2001; Schuetz *et al*., 1997). Some of the buffers used in Figure 5.2 are based on previous studies.

The citrate ions from citrate phosphate buffer improve the conformation and enhance molecular interactions of HRPC therefore stabilising the enzyme (Eremin *et al*., 2002). PBS is one of the most commonly used biological buffers (Mohan, 2003) therefore, PBS (7 mM; pH 7.4) was tested, and 50 mM PBS was used as a buffer by Schuetz *et al.,* (1997) to store HRPC conjugates. High concentrations of phosphate ions reduce HRPC stability, possibly explaining how HRPC in 50 mM PBS had 44% lower activity than in 7 mM PBS (Haifeng *et al.,* 2008, Asad *et al.,* 2011). Tris-HCl (50 mM) was tested because it was used in a stability study of HRPC conjugates by Eremin *et al*., (2002). HRPC had the lowest activity at pH 9 and 10.4, which is likely due to the alkalinity of the buffers causing the Ca^{2+} ions to leach (Stepenkova *et al*., 2013).

HRPC was most active in citrate phosphate buffer (pH 6.0), PBS (7 mM; pH 7.4) and Tris-HCl (50 mM; pH 8.0). Tris-HCl was chosen as to our knowledge, there are no reports of reduced HRPC stability or the chelation of Ca^{2+} ions when in Tris-HCl buffer, while the citrate in citrate phosphate buffer and phosphate in PBS bind Ca^{2+} which was used to supplement the buffer causing a precipitate to form.

5.4.2. The effect of organic solvents on HRPC activity and stability

Organic solvents have been used to stabilise HRPC-conjugates (Farzamfar *et al*., 2010; Lee *et al*., 2006; Eremin *et al*., 2002) because organic solvents reduce the flexibility and mobility of an enzyme by replacing the aqueous medium around it. Therefore, slowing down the unfolding and denaturation of the enzyme. Organic solvents often cause a conformational change of an enzyme's 3D structure, which possibly explains the reduced HRPC activity in Figure 5.4. Organic solvent concentrations of above 60% (v/v) can denature HRPC (Stepenkova *et al*., 2013). Therefore, 40% (v/v) MeOH was the maximum concentration used in this study.

Eremin *et* al., (2002) compared a Tris-HCl-EtOH buffer to a Tris-HCl-BSA buffer to stabilise HRPC. And found the organic solvent buffer was superior for storing HRPC. In the current study, buffers with protein additives were not analysed.

MeOH has not been used to improve the storage stability of HRPC but has been shown to reduce enzyme activity by 2.3% (Sato *et al*., 1995). Streefkerk and Van der Ploeg, (1974) showed that MeOH had no effect on HRPC activity, when the enzyme was on polyacrylamide films. Contrary to their finding HRPC had approximately 22% reduced activity at 40% (v/v) MeOH in this study (Figure 5.4). This could be due to MeOH altering the conformation of HRPC resulting in the active site becoming accessible to substrates, while HRPC attached to a polyacrylamide film may have prevented the conformation change of the enzyme.

5.4.3. Supplementing the Tris-HCl-MeOH buffer with Ca^{2+} ions

Ca^{2+} ions are important for the stability of HRPC and if the Ca^{2+} ions are depleted both the specific enzyme activity and thermal stability of HRPC decrease (Haschke and Friedhoff, 1978). Howes *et al*. (2001) showed that the proximal Ca^{2+} atom is vital to stabilising HRPC because of its role in maintaining the structure of the heme pocket but is often lost which results in HRPC binding of substrates becoming less efficient (Howes *et al*., 2001).

The increased HRPC activity observed when Ca^{2+} was added in Figure 5.5 and 5.6 could be due to the Ca^{2+} ions replacing the Ca^{2+} ions lost at the proximal region of HRPC, therefore, making the heme pocket more accessible to substrates like H_2O_2. H_2O_2 can enter and oxidise Fe^{3+} in the protoporphyrin heme to Fe^{4+}=O, more efficiently since the active site is maintained in the correct conformation by the Ca^{2+} ion. Even in the presence of 20% methanol which reduced HRPC activity (Figure 5.5), 10 mM to 100 mM Ca^{2+} allowed HRPC to have higher activity than HRPC in Tris-HCl alone.

5.4.4. Long-term stability of HRPC

HRPC had highest activity when stored in the Tris-HCl-MeOH buffer stored at 4°C in the dark (Figure 5.7). However, the HRPC activity progressively decreased each week. Haifeng *et al*., (2008) showed the unfolding of HRPC follows the first order Lumry-Eyering model, indicating the reversible unfolding steps are followed by irreversible denaturation. Suggesting, once HRPC is denatured its activity cannot be regained.

5.4.5. Conclusion

The Tris-HCl (50 mM; 20% (v/v) MeOH; 50 mM Ca^{2+}) buffer was shown to significantly increase the storage stability of dilute HRPC (Figure 5.7 and 5.8). The dilute solutions of HRPC should not be stored for longer than 3 months in the buffer, where HRPC retained 72% of its activity. The thermal stability of 1000 U/mg HRPC was improved at 37°C for 20 h (Figure 5.9). A weakness of the study was Ca^{2+} ions were not tested independent of MeOH, therefore, there

is a degree of uncertainty as to whether Ca^{2+} activated HRPC only or aided in the storage stability of the enzyme.

The (1000 U/mg) HRPC used in Chapter 4, was prepared in the Tris-HCl-MeOH stability buffer and was used over the course of a year for the various experiments, with little deviation in HRPC enzyme activity.

6. CHAPTER 6: General discussion

6.1. Brief review

Around half the world's population is at risk of contracting a malaria infection. At the beginning of the 21st century (the year 2000) malaria related deaths were estimated to be around 839 000. The number of deaths has since then dropped to 435 000 in 2017 (WHO, 2018; fact sheet November), However, in 2017 there were 219 million reported malaria infections. *P. falciparum* malaria infections are the most common and account for 99.7% malaria cases in the WHO Africa region, 62.8% in South-East Asia, 69% in the Mediterranean and 71.9% in the Western Pacific. In South America, *P. vivax* is the most common malaria infection (WHO, malaria fact sheet November 19.2018).

Mortality due to a malaria infection has decreased by around 50% since the year 2000. This is largely due to the increased use of insecticide-treated bed nets and more frequent diagnosis of suspected malaria infected patients (Sepúlveda *et al.,* 2017). Early diagnosis of a malaria infection allows a patient to receive appropriate treatment and could save lives (Sepúlveda *et al.,* 2017). The increased use of malaria rapid diagnostic tests (RDT's) is due to the Test and Treat policy by the WHO and his has increased sales of RDT's from under 200 000 (2005) (WHO, http:// www. WHO.int/malaria/test_treat_track/en/index.html) to 270 million in 2015. RDT's have become household diagnostic reagents in malaria endemic regions, however, due to RDT's weaknesses the WHO recommends using an RDT in conjunction with a second diagnostic method such as light microscopy.

Weakness of RDT's are they detect parasitaemia of 100 -200 parasites per µl of blood which is at least 5 times less sensitive than light microscopy of a Giemsa stained thick blood film, therefore some infections can be missed (Murray *et al*., 2008). A second issue is the high temperatures in some malaria endemic areas and the lack of cold chain storage facilities resulting in RDT's losing performance. Gillet *et al*., (2011) reported 80% of RDT's they had tested can withstand a maximum temperature of 30°C, whereas temperatures in storage facilities for RDT's may exceed 40°C. A third problem is most RDT's detect the *Pf*HRP-2 protein (Cheng *et al*., 2014). *Pf*HRP-2 gene deletions have been reported in 10 countries, mainly in South America but more recently in Africa (Sepúlveda *et al.,* 2017).

A meta-analysis study by Sepúlveda *et al.,* (2017) estimated *Pf*HRP-2 gene deletion to be ~17%, with most being in the Peruvian Amazon basin. An uncomplicated *P. falciparum* malaria infection can progress into a CM infection Pal *et al*., (2016 and 2017) showed via *in vitro* and mouse *in vivo* models *Pf*HRP-2 may participate in the development of CM. Since HRP-2 is not found in *P. berghi* malaria, r*Pf*HRP-2 was injected into mice for *in vivo* analysis.

Studies have also shown high concentrations of *Pf*HRP-2 could be an indicator for the development of CM (Park *et al.,* 2017; Fox *et al.,* 2013; Rubach *et al*., 2012; Seydel *et al.,* 2012). Currently there is no diagnostic test for a CM infection (Seydel *et al*., 2012).

Even though the *Pf*HRP-2 gene is deleted in some *P. falciparum* isolates (Gamboa *et al*., 2010; Sepúlveda *et al.,* 2017), a rapid quantification method for *Pf*HRP-2 after a patient has been diagnosed with a *P. falciparum* infection may aid in determining if the patient's illness would become CM. This will allow correct treatment to be administrated to the patients (Seydel *et al*., 2012; Dvorin, 2017; Sinha *et al*., 2015).

The administration of the correct anti-malaria treatment for infected patients will reduce the unnecessary use of drugs. This is important as it would reduce malaria parasite drug resistance which is thought to be due to the misuse of the these anti-malarials.

6.1.1. Determining the thermal stability of three malaria antigens, protein-protein interactions of antigens and antibodies; anti-malaria drugs interacting with r*Pf*LDH and r*Pf*GAPDH. (Chapter 2)

Krause *et al.,* (2017) showed that *Pf*GAPDH has potential as a diagnostic marker for a *P. falciparum* malaria infection. A new *P. falciparum* malaria diagnostic marker is needed as the gene for *Pf*HRP-2 is no longer present in some isolates. Therefore, the aim in Chapter 2 was to compare the thermal stability of r*Pf*GAPDH, r*Pf*LDH and r*Pf*HRP-2. All three proteins were recombinantly expressed as His_6-tag fusion proteins and purified using Ni^{2+}-chelate affinity chromatography.

The thermal stability of the three recombinant proteins were tested using DSF. r*Pf*GAPDH was found to be more stable than r*Pf*LDH. r*Pf*HRP-2 T_m could not be evaluated as the denaturation profile of r*Pf*HRP-2 did not produce a transition peak. The stability of r*Pf*GAPDH was fortunate as stable antigens are better diagnostic targets and antigens should be heat stable for RDT quality controls (Lon *et al*., 2005).

Using DSF, r*Pf*LDH and r*Pf*HRP-2 interactions with their respective antibodies were analysed for two reasons: (i) Firstly to see if a protein-protein interaction can be followed using DSF (ii) and secondly to see if the antigen-antibody complex is more stable than either of the individual species. The largest T_m shifts were observed at pH 4 where both anti-r*Pf*LDH IgY and r*Pf*HRP-2 IgY were stabilised in the presence of the respective antigens and showed that DSF can be used to monitor protein-protein interactions.

Initially DSF was developed by Pantoliano *et al*., (2001) to screen small ligands for drug discovery. Therefore, using DSF different anti-malaria drugs were tested with r*Pf*LDH and r*Pf*GAPDH. Chloroquine and quinine did not interfere with fluorescence signal in the assay and resulted in a positive T_m shift for r*Pf*LDH indicating it bound to and stabilised it, while r*Pf*GAPDH had a negative shift in T_m indicating it was destabilised.

Following experimental work, molecular docking studies were carried out. The Schrodinger molecular docking suite (2018-2), showed both quinine and chloroquine bound to *Pf*LDH and *Pf*GAPDH in the co-factor binding sites. The *in silico* docking studies showed the bonds in the co-factor binding site bind to motifs on the drugs. This information may be useful for new drug development as it indicates which amino acids are involved in drug binding. Chloroquine and quinine are important to look for the design of new drugs (Wells *et al*., 2015).

6.1.2. Comparing the thermal stability of polyclonal antibodies and the optimal conjugation method for chicken IgY (Chapter 3).

Since most RDT's are not stable above 30°C (Gillet *et al*., 2011), there is a need to find stable antibodies to use in malaria diagnostics tests. Thermodynamic (ΔμG, ΔμH, ΔμS) unfolding energy of Chicken IgY was analysed and compared to rabbit IgG, mouse IgG, crocodile IgY and IgM using DSF (Wright *et al*., 2017). Chicken IgY was found to be the most stable from the thermodynamic parameters. DSF analysis of a 28-year-old chicken IgY sample, showed that the sample had similar T_m to a sample of freshly isolated chicken IgY indicating chicken IgY can be stored for long periods of time with minimal degradation.

The data supports the workshop held by the European centre for the validation of alternate method (ECVAM) which suggested testing if chicken IgY can be used to replace monoclonal antibodies (Schade *et al*., 1996). Polyclonal antibodies offer higher sensitivity in detecting antigens compared to monoclonal antibodies but have lower specificity (Lipman *et al.,* 2005).

Different conjugating methods were analysed for the coupling of chicken IgY to HRPC. Glutaraldehyde conjugation was shown to work best for chicken IgY. This was useful since it provides a method for effective coupling of HRPC to chicken IgY to be used as immunological reagents.

6.1.3. Detection of *Pf*HRP-2 using two copper-based assays

Two assays were developed based on *Pf*HRP-2 high binding to Cu ions to detect and quantify *Pf*HRP-2. The first assay was based on reducing Cu^{2+} to Cu^{+}. The Cu^{+} is a potent inhibitor of HRPC and *Pf*HRP-2 present binds Cu^{+} allowing HRPC to remain active. The assay was termed the Cu^{+}-HRPC-TMB assay. The assay detected r*Pf*HRP-2 in an aqueous solution, in a saliva spoked sample (by a mechanism not understood) and r*Pf*HRP-2 coated directly into the wells of a microtiter plate. The second assay was Cu^{2+} catalysing the oxidation of TMB by generating RCl^{-}. The presence of *Pf*HRP-2 binds and removes Cu^{2+}, therefore preventing the oxidation of TMB. The assay was termed the Cu^{2+}-RCl^{-} -TMB assay. The Cu^{+}-HRPC-TMB assay detected r*Pf*HRP-2 in an aqueous solution, in a saliva spiked sample (by a mechanism not understood) and r*Pf*HRP-2 coated directly into wells of a microtiter plate. Both assays did not work in an ELISA based format, for reasons we were not able to explain.

The theory was if *Pf*HRP-2 could be quantified using either of the Cu based assays, it could be further developed into a field test for quantifying *Pf*HRP-2 therefore, prevents detecting the potential for an uncomplicated malaria infection progressing to a CM infection.

Since both Cu based assays did not work, chemiluminescence using HRPC was also tested, unfortunately the assay was less sensitive then the colorimetric assay. It should be noted that high concentrations of *Pf*HRP-2 is not a definitive indication of a *P. falciparum* malaria infected patient's conditioning worsening to CM but rather a precautionary marker (Seydel *et al*., 2012).

6.1.4. A stability buffer for storing dilute solutions of HRPC

During optimisation of the Cu^{+}-HRPC-TMB assay, low concentrations of HRPC lost activity in short periods of time. Therefore, a stability buffer was developed which was a Tris-HCl buffer (50 mM; pH 8.0; 20% (v/v) MeOH; 50 mM Ca^{2+}). The buffer allowed 0.5 ng HRPC to maintain 70% activity over 3 months and even allowed HRPC to remain significantly more stable at 37°C after 20 hours compared to HRPC in Tris-HCl (50 mM; pH 8).

6.2.1. Further work for the DSF assay

To determine the Tm of proteins that did not produce transitions in the DSF assay, alternative dyes can be considered such as CFC and BFC which are thiol probes. Protein stability should be obtained using DSC and this data can be compared to the current DSF data to measure the suitability of DSF.

The DSF assay showed it could follow the interaction between two proteins. Protein-protein interactions can be further investigated with other proteins and compared to more commonly used biophysical techniques such as surface plasma resonance, dynamic light scattering or isothermal titration calorimetry. This will confirm if DSF is accurate at determining protein-protein interactions and expand the DSF assay.

6.2.2. Further work on thermodynamic data

Chicken IgY and Rabbit IgG polyclonal antibodies could be raised against the same antigen. Thermodynamic parameters of both antibodies should be calculated following. Both antibodies can be stored at different temperatures (4°C, 25°C, 37°C and 50°C) and the stability of the antibodies should be compared.

The thermodynamic stability of different species polyclonal antibodies can be calculated using DSF and compared to chicken IgY. Commonly used IgG molecules that could be tested are sheep IgG, horse IgG, bovine IgG and goat IgG.

6.2.3. Further work for the conjugation of chicken IgY to HRPC

The glutaraldehyde method to conjugate chicken IgY to HRPC can be improved by separating non-coupled IgY from IgY-HRPC. This can be done using gel filtration chromatography. Higher activity HRPC can be coupled to chicken IgY, to allow for the conjugate to have higher sensitivity.

6.2.4. Further work for the HRPC-Cu^{+}-TMB assay

Na-ascorbate absorbs at 255 nm, when Na-ascorbate is oxidised by Cu^{2+} the absorbance at 255 nm decreases. If *Pf*HRP-2 is present it could potentially bind Cu^{2+}, therefore preventing Na-ascorbate oxidation. The decrease in absorbance at 255 nm indicates the presence of *Pf*HRP-2.

6.2.5. Further work for the HRPC stability buffer

Different activity HRPC storage stability can be measured in the Tris-HCl buffer (50 mM; pH 8.0; 20% (v/v) MeOH; 50 mM Ca2+), as well as testing the stability of a HRPC conjugate in the buffer.

6.3. Conclusion

This study initially aimed to develop a diagnostic test for *Pf*HRP-2 based on its high affinity for Cu ions. Unfortunately, both developed assays were unable to detect r*Pf*HRP-2 in the ELISA based format. However, the study identified r*Pf*GAPDH as thermally more stable than r*Pf*LDH and showed that DSF has more potential than just drug screening. Interestingly, chicken IgY is a very stable molecule and is best coupled with HRPC using glutaraldehyde. The study provided some data for diagnostic reagents for malaria RDT's

7. REFERENCES

Alemzadeh, I. and Nejati, S., 2009. Removal of phenols with encapsulated horseradish peroxidase in calcium alginate. *Iranian Journal of Chemistry and Chemical Engineering*, *28*(2), pp.43-49.

Alexandrov, A.I., Mileni, M., Chien, E.Y., Hanson, M.A. and Stevens, R.C., 2008. Microscale fluorescent thermal stability assay for membrane proteins. *Structure*, *16*(3), pp.351-359.

Alfano, C., Sanfelice, D., Martin, S.R., Pastore, A. and Temussi, P.A., 2017. An optimized strategy to measure protein stability highlights differences between cold and hot unfolded states. *Nature Communications*, *8*, pp.15428.

Alsenaidy, M.A., Okbazghi, S.Z., Kim, J.H., Joshi, S.B., Middaugh, C.R., Tolbert, T.J. and Volkin, D.B., 2014. Physical stability comparisons of IgG1-Fc variants: effects of N-glycosylation site occupancy and Asp/Gln residues at site Asn 297. *Journal of Pharmaceutical Sciences*, *103*(6), pp.1613-1627.

Arnao, M.B., Cano, A., Hernandez-Ruiz, J., Garcıa-Cánovas, F. and Acosta, M., 1996. Inhibition byl-ascorbic acid and other antioxidants of the 2, 2′-azino-bis (3-ethylbenzthiazoline-6-sulfonic Acid) oxidation catalyzed by peroxidase: A new approach for determining total antioxidant status of foods. *Analytical Biochemistry*, *236*(2), pp.255-261.

Asad, S., Torabi, S.F., Fathi-Roudsari, M., Ghaemi, N. and Khajeh, K., 2011. Phosphate buffer effects on thermal stability and H_2O_2-resistance of horseradish peroxidase. *International Journal of Biological Macromolecules*, *48*(4), pp.566-570.

Avrameas, S., 1969. Coupling of enzymes to proteins with glutaraldehyde: use of the conjugates for the detection of antigens and antibodies. *Immunochemistry*, *6*(1), pp.43-52.

Avrameas, S., Ternynck, T. and Guesdon, J.L., 1978. Coupling of enzymes to antibodies and antigens. *Scandinavian Journal of Immunology*, *8*, pp.7-23.

Azevedo, A.M., Duarte M.F.P., Joaquim M.S.C. and Luís P. F., 2001. Stability of free and immobilised peroxidase in aqueous–organic solvents mixtures. *Journal of Molecular Catalysis B: Enzymatic*, 15(4-6), pp.147-153.

Azevedo, A.M., Martins, V.C., Prazeres, D.M., Vojinovic, V., Cabral, J.M. and Fonseca, L.P., 2003. Horseradish peroxidase: a valuable tool in biotechnology. *Biotechnology Annual Review*, *9*(3), pp.1387-2656.

Baker, J., Ho, M.F., Pelecanos, A., Gatton, M., Chen, N., Abdullah, S., Albertini, A., Ariey, F., Barnwell, J., Bell, D. and Cunningham, J., 2010. Global sequence variation in the histidine-rich proteins 2 and 3 of Plasmodium falciparum: implications for the performance of malaria rapid diagnostic tests. *Malaria Journal*, *9*(1), pp.129-140.

Bauer, W.S., Richardson, K.A., Adams, N.M., Ricks, K.M., Gasperino, D.J., Ghionea, S.J., Rosen, M., Nichols, K.P., Weigl, B.H., Haselton, F.R. and Wright, D.W., 2017. Rapid concentration and elution of malarial antigen histidine-rich protein II using solid phase Zn (II) resin in a simple flow-through pipette tip format. *Biomicrofluidics*, *11*(3), pp.034115.

Beare, N.A., Taylor, T.E., Harding, S.P., Lewallen, S. and Molyneux, M.E., 2006. Malarial retinopathy: a newly established diagnostic sign in severe malaria. *The American Journal of Tropical Medicine and Hygiene*, *75*(5), pp.790-797.

Benedetti, C.E., Kobarg, J., Pertinhez, T.A., Gatti, R.M., de Souza, O.N., Spisni, A. and Meneghini, R., 2003. Plasmodium falciparum histidine-rich protein II binds to actin, phosphatidylinositol 4, 5-bisphosphate and erythrocyte ghosts in a pH-dependent manner and undergoes coil-to-helix transitions in anionic micelles. *Molecular and Biochemical Parasitology*, *128*(2), pp.157-166.

Berwal, R., Gopalan, N., Chandel, K., Prasad, G.B.K.S. and Prakash, S., 2008. Plasmodium falciparum: enhanced soluble expression, purification and biochemical characterization of lactate dehydrogenase. *Experimental Parasitology*, *120*(2), pp.135-141.

Beshir, K.B., Sepúlveda, N., Bharmal, J., Robinson, A., Mwanguzi, J., Busula, A.O., Boer, J.G., Sutherland, C., Cunningham, J. and Hopkins, H., 2017. Plasmodium falciparum parasites with histidine-rich protein 2 (pfhrp2) and pfhrp3 gene deletions in two endemic regions of Kenya. *Scientific Reports*, *7*(1), pp.14718.

Beyzavi, K., Hampton, S., Kwasowski, P., Fickling, S., Marks, V. and Clift, R., 1987. Comparison of horseradish peroxidase and alkaline phosphatase-labelled antibodies in enzyme immunoassays. *Annals of Clinical Biochemistry*, *24*(2), pp.145-152.

Bokare, A.D. and Choi, W., 2014. Review of iron-free Fenton-like systems for activating H2O2 in advanced oxidation processes. *Journal of Hazardous Materials*, *275*, pp.121-135.

Boorsma, D.M. and Kalsbeek, G.L., 1975. A comparative study of horseradish peroxidase conjugates prepared with a one-step and a two-step method. *Journal of Histochemistry and Cytochemistry*, *23*(3), pp.200-207.

Bos, E.S., Van der Doelen, A.A., Rooy, N.V. and Schuurs, A.H., 1981. 3, 3′, 5, 5′-Tetramethylbenzidine as an Ames test negative chromogen for horseradish peroxidase in enzyme-immunoassay. *Journal of Immunoassay and Immunochemistry*, *2*(3-4), pp.187-204.

Bradford, M.M., 1976. A rapid and sensitive method for the quantitation of microgram quantities of protein utilizing the principle of protein-dye binding. *Analytical Biochemistry*, *72*(1-2), pp.248-254.

Brooke, B.D., Robertson, L., Kaiser, M.L., Raswiswi, E., Munhenga, G., Venter, N., Wood, O.R. and Koekemoer, L.L., 2015. Insecticide resistance in the malaria vector Anopheles arabiensis in Mamfene, KwaZulu-Natal. *South African Journal of Science*, *111*(11-12), pp.1-3.

Bruylants, G., Wouters, J. and Michaux, C., 2005. Differential scanning calorimetry in life science: thermodynamics, stability, molecular recognition and application in drug design. *Current Medicinal Chemistry*, *12*(17), pp.2011-2020.

Buppan, P., Putaporntip, C., Pattanawong, U., Seethamchai, S. and Jongwutiwes, S., 2010. Comparative detection of Plasmodium vivax and Plasmodium falciparum DNA in saliva and urine samples from symptomatic malaria patients in a low endemic area. *Malaria Journal*, *9*(1), pp.72.

Burdett, J.K. and Sevov, S., 1995. Stability of the oxidation states of copper. *Journal of the American Chemical Society*, *117*(51), pp.12788-12792.

Busso, D., Stierlé, M., Thierry, J.C. and Moras, D., 2008. A comparison of inoculation methods to simplify recombinant protein expression screening in Escherichia coli. *Biotechniques*, *44*(1), pp.101-106.

Cashel, M. and Kalbacher, B., 1970. The control of ribonucleic acid synthesis in Escherichia coli V. Characterization of a nucleotide associated with the stringent response. *Journal of Biological Chemistry*, *245*(9), pp.2309-2318.

Chakravorty, S.J. and Craig, A., 2005. The role of ICAM-1 in Plasmodium falciparum cytoadherence. *European Journal of Cell Biology*, *84*(1), pp.15-27.

Chang, D.E., Smalley, D.J. and Conway, T., 2002. Gene expression profiling of Escherichia coli growth transitions: an expanded stringent response model. *Molecular Microbiology*, *45*(2), pp.289-306.

Chart, H., Smith, H.R., La Ragione, R.M. and Woodward, M.J., 2000. An investigation into the pathogenic properties of Escherichia coli strains BLR, BL21, DH5α and EQ1. *Journal of Applied Microbiology*, *89*(6), pp.1048-1058.

Cheng, Q., Gatton, M.L., Barnwell, J., Chiodini, P., McCarthy, J., Bell, D. and Cunningham, J., 2014. Plasmodium falciparum parasites lacking histidine-rich protein 2 and 3: a review and recommendations for accurate reporting. *Malaria Journal*, *13*(1), pp.283.

Cheung, Y.W., Kwok, J., Law, A.W., Watt, R.M., Kotaka, M. and Tanner, J.A., 2013. Structural basis for discriminatory recognition of Plasmodium lactate dehydrogenase by a DNA aptamer. *Proceedings of the National Academy of Sciences*, *110*(40), pp.15967-15972.

Choi, C.Y., Cerda, J.F., Chu, H.A., Babcock, G.T. and Marletta, M.A., 1999. Spectroscopic characterization of the heme-binding sites in Plasmodium falciparum histidine-rich protein 2. *Biochemistry*, *38*(51), pp.16916-16924.

Christensen, S.S. and Eslick, G.D., 2015. Cerebral malaria as a risk factor for the development of epilepsy and other long-term neurological conditions: a meta-analysis. *Transactions of the Royal Society of Tropical Medicine and Hygiene*, *109*(4), pp.233-238.

Cimmperman, P., Baranauskienė, L., Jachimovičiūtė, S., Jachno, J., Torresan, J., Michailovienė, V., Matulienė, J., Sereikaitė, J., Bumelis, V. and Matulis, D., 2008. A quantitative model of thermal stabilization and destabilization of proteins by ligands. *Biophysical Journal*, *95*(7), pp.3222-3231.

Cowman, A.F. and Crabb, B.S., 2006. Invasion of red blood cells by malaria parasites. *Cell*, *124*(4), pp.755-766.

Craig, A. and Scherf, A., 2001. Molecules on the surface of the Plasmodium falciparum infected erythrocyte and their role in malaria pathogenesis and immune evasion. *Molecular and Biochemical Parasitology*, *115*(2), pp.129-143.

Critchlow, J.E. and Dunford, H.B., 1972. Studies on horseradish peroxidase IX. Kinetics of the oxidation of p-cresol by compound II. *Journal of Biological Chemistry*, *247*(12), pp.3703-3713.

Crowther, G.J., He, P., Rodenbough, P.P., Thomas, A.P., Kovzun, K.V., Leibly, D.J., Bhandari, J., Castaneda, L.J., Hol, W.G., Gelb, M.H. and Napuli, A.J., 2010. Use of thermal melt curves to assess the quality of enzyme preparations. *Analytical biochemistry*, *399*(2), pp.268-275.

Daegelen, P., Studier, F.W., Lenski, R.E., Cure, S. and Kim, J.F., 2009. Tracing ancestors and relatives of Escherichia coli B, and the derivation of B strains REL606 and BL21 (DE3). *Journal of Molecular Biology*, *394*(4), pp.634-643.

Das, P., Grewal, J.S. and Chauhan, V.S., 2006. Interaction of Plasmodium falciparum histidine-rich protein II with human lymphocytes leads to suppression of proliferation, IFN-γ release, and CD69 expression. *Parasitology Research*, *100*(1), pp.39-50.

Daubenberger, C.A., Tisdale, E.J., Curcic, M., Diaz, D., Silvie, O., Mazier, D., Eling, W., Bohrmann, B., Matile, H. and Pluschke, G., 2003. The N'-terminal domain of glyceraldehyde-3-phosphate dehydrogenase of the apicomplexan Plasmodium falciparum mediates GTPase Rab2-dependent recruitment to membranes. *Biological Chemistry*, *384*(8), pp.1227-1237.

Davidson, A.E., Balciunas, D., Mohn, D., Shaffer, J., Hermanson, S., Sivasubbu, S., Cliff, M.P., Hackett, P.B. and Ekker, S.C., 2003. Efficient gene delivery and gene expression in zebrafish using the Sleeping Beauty transposon. *Developmental Biology*, *263*(2), pp.191-202.

De Laat, J. and Le, T.G., 2006. Effects of chloride ions on the iron (III)-catalyzed decomposition of hydrogen peroxide and on the efficiency of the Fenton-like oxidation process. *Applied Catalysis B: Environmental*, *66*(1-2), pp.137-146.

Demain, A.L. and Vaishnav, P., 2009. Production of recombinant proteins by microbes and higher organisms. *Biotechnology Advances*, *27*(3), pp.297-306.

Desakorn, V., Silamut, K., Angus, B., Sahassananda, D., Chotivanich, K., Suntharasamai, P., Simpson, J. and White, N.J., 1997. Semi-quantitative measurement of Plasmodium falciparum antigen PfHRP2 in blood and plasma. *Transactions of the Royal Society of Tropical Medicine and Hygiene*, *91*(4), pp.479-483.

Dondorp, A.M., Desakorn, V., Pongtavornpinyo, W., Sahassananda, D., Silamut, K., Chotivanich, K., Newton, P.N., Pitisuttithum, P., Smithyman, A.M., White, N.J. and Day, N.P., 2005. Estimation of the total parasite biomass in acute falciparum malaria from plasma PfHRP2. *PLoS Medicine*, *2*(8), pp.e204.

Douse, C.H., Vrielink, N., Wenlin, Z., Cota, E. and Tate, E.W., 2015. Targeting a dynamic protein–protein interaction: fragment screening against the malaria myosin A motor complex. *ChemMedChem*, *10*(1), pp.134-143.

Dvorin, J.D., 2017. Getting your head around cerebral malaria. *Cell Host and Microbe*, *22*(5), pp.586-588.

Ellis, K.J. and Morrison, J.F., 1982. Buffers of constant ionic strength for studying pH-dependent processes. *Methods in Enzymology*, 8, pp. 405-426.

Eremin, A.N., Budnikova, L.P., Sviridov, O.V. and Metelitsa, D.I., 2002. Stabilization of diluted aqueous solutions of horseradish peroxidase. *Applied Biochemistry and Microbiology*, *38*(2), pp.151-158.

Ericsson, U.B., Hallberg, B.M., DeTitta, G.T., Dekker, N. and Nordlund, P., 2006. Thermofluor-based high-throughput stability optimization of proteins for structural studies. *Analytical Biochemistry*, *357*(2), pp.289-298.

Farzamfar, B., Bayanolhagh, S., Mahboudi, F. and Zahrai, M., 2010. The effect of different stabilizers on stability of horseradish peroxidase-bovine serum albumin-aflatoxin B1, a conjugated tracer for detection of aflatoxin B1 in immunoassay-based methods. *Iranian Journal of Pharmaceutical Research*, pp.179-184.

Fox, L.L., Taylor, T.E., Pensulo, P., Liomba, A., Mpakiza, A., Varela, A., Glover, S.J., Reeves, M.J. and Seydel, K.B., 2013. Histidine-rich protein 2 plasma levels predict progression to cerebral malaria in Malawian children with Plasmodium falciparum infection. *The Journal of Infectious Diseases*, *208*(3), pp.500-503.

Freire, E., Schön, A., Hutchins, B.M. and Brown, R.K., 2013. Chemical denaturation as a tool in the formulation optimization of biologics. *Drug Discovery Today*, *18*(19-20), pp.1007-1013.

Frith, K.A., Fogel, R., Goldring, J.D., Krause, R.G., Khati, M., Hoppe, H., Cromhout, M.E., Jiwaji, M. and Limson, J.L., 2018. Towards development of aptamers that specifically bind to lactate dehydrogenase of Plasmodium falciparum through epitopic targeting. *Malaria Journal*, *17*(1), pp.191.

Fu, G., Sanjay, S.T., Zhou, W., Brekken, R.A., Kirken, R.A. and Li, X., 2018. Exploration of nanoparticle-mediated photothermal effect of TMB-H_2O_2 colorimetric system and its application in a visual quantitative photothermal immunoassay. *Analytical Chemistry*, *90*(9), pp.5930-5937.

Fung, A.O., Damoiseaux, R., Grundeen, S., Panes, J.L., Horton, D.H., Judy, J.W. and Moore, T.B., 2012. Quantitative detection of Pf HRP2 in saliva of malaria patients in the Philippines. *Malaria Journal*, *11*(1), pp.175.

Gajhede, M., Schuller, D.J., Henriksen, A., Smith, A.T. and Poulos, T.L., 1997. Crystal structure of horseradish peroxidase C at 2.15 Å resolution. *Nature Structural and Molecular Biology*, *4*(12), pp.1032.

Gamboa, D., Ho, M.F., Bendezu, J., Torres, K., Chiodini, P.L., Barnwell, J.W., Incardona, S., Perkins, M., Bell, D., McCarthy, J. and Cheng, Q., 2010. A large proportion of P. falciparum isolates in the Amazon region of Peru lack pfhrp2 and pfhrp3: implications for malaria rapid diagnostic tests. *PloS One*, *5*(1), pp.e8091.

Gao, L., Zhuang, J., Nie, L., Zhang, J., Zhang, Y., Gu, N., Wang, T., Feng, J., Yang, D., Perrett, S. and Yan, X., 2007. Intrinsic peroxidase-like activity of ferromagnetic nanoparticles. *Nature Nanotechnology*, *2*(9), pp.577.

Garber, E. and Demarest, S.J., 2007. A broad range of Fab stabilities within a host of therapeutic IgGs. *Biochemical and Biophysical Research Communications*, *355*(3), pp.751-757.

Garbett, N.C. and Chaires, J.B., 2012. Thermodynamic studies for drug design and screening. *Expert Opinion on Drug Discovery*, *7*(4), pp.299-314.

Garcia, L.S. and Isenberg, H.D., 2007. Clinical microbiology procedures handbook, 2nd ed. ASM Press, Washington, DC.

Geleta, G. and Ketema, T., 2016. Severe malaria associated with Plasmodium falciparum and P. vivax among children in Pawe Hospital, Northwest Ethiopia. *Malaria Research and Treatment*, *2016*.

Ghazanfari, N., Mueller, S.N. and Heath, W.R., 2018. Cerebral Malaria in Mouse and Man. *Frontiers in Immunology*, *9*.

Gillet, P., Maltha, J., Hermans, V., Ravinetto, R., Bruggeman, C. and Jacobs, J., 2011. Malaria rapid diagnostic kits: quality of packaging, design and labelling of boxes and components and readability and accuracy of information inserts. *Malaria Journal*, *10*(1), pp.39.

Goldberg, D.S., Bishop, S.M., Shah, A.U. and Sathish, H.A., 2011. Formulation development of therapeutic monoclonal antibodies using high-throughput fluorescence and static light scattering techniques: Role of conformational and colloidal stability. *Journal of pharmaceutical sciences*, *100*(4), pp.1306-1315.

Gottesman, S., 1996. Proteases and their targets in Escherichia coli. *Annual Review of Genetics*, *30*(1), pp.465-506.

Gregory, D.W. and Williams, M.A., 1967. The preparation of ferritin-labelled antibodies and other protein-protein conjugates with bis-diazotized benzidine. *Biochimica et Biophysica Acta-Protein Structure*, *133*(2), pp.319-332.

Grodberg, J. and Dunn, J.J., 1988. ompT encodes the Escherichia coli outer membrane protease that cleaves T7 RNA polymerase during purification. *Journal of Bacteriology*, *170*(3), pp.1245-1253.

Haifeng, L., Yuwen, L., Xiaomin, C., Zhiyong, W. and Cunxin, W., 2008. Effects of sodium phosphate buffer on horseradish peroxidase thermal stability. *Journal of Thermal Analysis and Calorimetry*, *93*(2), pp.569-574.

Han, H.Y., Xu, W.A., Lü, Z.R., Zou, F. and Li, S., 2008. Activation and inactivation of horseradish peroxidase by cobalt ions. *Journal of Biomolecular Structure and Dynamics*, *26*(1), pp.83-91.

Han, B., Yuan, H., Wang, T., Li, B., Ma, L., Yu, S., Huang, T., Li, Y., Fang, D., Chen, X. and Wang, Y., 2016. Multiple IgH isotypes including IgD, subclasses of IgM, and IgY are expressed in the common ancestors of modern birds. *The Journal of Immunology*, pp.1600307.

Haschke, R.H. and Friedhoff, J.M., 1978. Calcium-related properties of horseradish peroxidase. *Biochemical and Biophysical Research Communications*, *80*(4), pp.1039-1042.

Hawe, A., Sutter, M. and Jiskoot, W., 2008. Extrinsic fluorescent dyes as tools for protein characterization. *Pharmaceutical Research*, *25*(7), pp.1487-1499.

Hayward, R.E., Sullivan, D.J. and Day, K.P., 2000. Plasmodium falciparum: histidine-rich protein II is expressed during gametocyte development. *Experimental Parasitology*, *96*(3), pp.139-146.

He, F., Hogan, S., Latypov, R.F., Narhi, L.O. and Razinkov, V.I., 2010. High throughput thermostability screening of monoclonal antibody formulations. *Journal of Pharmaceutical Sciences*, *99*(4), pp.1707-1720.

Hoffmann, F. and Rinas, U., 2004. Stress induced by recombinant protein production in Escherichia coli. *In Physiological Stress Responses in Bioprocesses*, Springer, Berlin, Heidelberg,1, pp.73-92.

Hofmann, L., Gulati, S., Sears, A., Stewart, P.L. and Palczewski, K., 2016. An effective thiol-reactive probe for differential scanning fluorimetry with a standard real-time polymerase chain reaction device. *Analytical Biochemistry*, *499*, pp.63-65.

Howard, R.J., Uni, S., Aikawa, M., Aley, S.B., Leech, J.H., Lew, A.M., Wellems, T.E., Rener, J. and Taylor, D.W., 1986. Secretion of a malarial histidine-rich protein (Pf HRP II) from Plasmodium falciparum-infected erythrocytes. *The Journal of Cell Biology*, *103*(4), pp.1269-1277.

Howes, B.D., Feis, A., Raimondi, L., Indiani, C. and Smulevich, G., 2001. The critical role of the proximal calcium ion in the structural properties of horseradish peroxidase. *Journal of Biological Chemistry*, *276*(44), pp.40704-40711.

Hoyle, M.C., 1977. High resolution of peroxidase-indoleacetic acid oxidase isoenzymes from horseradish by isoelectric focusing. *Plant Physiology*, *60*(5), pp.787-793.

https://www.uniprot.org/uniprot/P90582 (05.01.2019)

Hudson, S.A., McLean, K.J., Surade, S., Yang, Y.Q., Leys, D., Ciulli, A., Munro, A.W. and Abell, C., 2012. Application of fragment screening and merging to the discovery of inhibitors of the Mycobacterium tuberculosis cytochrome P450 CYP121. *Angewandte Chemie International Edition*, *51*(37), pp.9311-9316.

Huynh, K. and Partch, C.L., 2015. Analysis of protein stability and ligand interactions by thermal shift assay. *Current Protocols in Protein Science*, *79*(1), pp.28-29.

Ionescu, R.M., Vlasak, J., Price, C. and Kirchmeier, M., 2008. Contribution of variable domains to the stability of humanized IgG1 monoclonal antibodies. *Journal of Pharmaceutical Sciences*, *97*(4), pp.1414-1426.

Iqbal, J., Sher, A. and Rab, A., 2000. Plasmodium falciparum histidine-rich protein 2-based immunocapture diagnostic assay for malaria: cross-reactivity with rheumatoid factors. *Journal of Clinical Microbiology*, *38*(3), pp.1184-1186.

Jafari, R., Almqvist, H., Axelsson, H., Ignatushchenko, M., Lundbäck, T., Nordlund, P. and Molina, D.M., 2014. The cellular thermal shift assay for evaluating drug target interactions in cells. *Nature Protocols*, *9*(9), pp.2100.

Jain, P., Chakma, B., Singh, N.K., Patra, S. and Goswami, P., 2016. Aromatic surfactant as aggregating agent for aptamer-gold nanoparticle-based detection of Plasmodium lactate dehydrogenase. *Molecular Biotechnology*, *58*(7), pp.497-508.

Jaradat, Z.W. and Marquardt, R.R., 2000. Studies on the stability of chicken IgY in different sugars, complex carbohydrates and food materials. *Food and Agricultural Immunology*, *12*(4), pp.263-272.

Jimenez, A., Rees-Channer, R.R., Perera, R., Gamboa, D., Chiodini, P.L., González, I.J., Mayor, A. and Ding, X.C., 2017. Analytical sensitivity of current best-in-class malaria rapid diagnostic tests. *Malaria Journal*, *16*(1), pp.128.

Josephy, P.D., Eling, T. and Mason, R.P., 1982. The horseradish peroxidase-catalyzed oxidation of 3, 5, 3', 5'-tetramethylbenzidine. Free radical and charge-transfer complex intermediates. *Journal of Biological Chemistry*, *257*(7), pp.3669-3675.

Kato, K., Hamaguchi, Y., Fukui, H. and Ishikawa, E., 1976. Enzyme-Linked Immunoassay: conjugation of rabbit anti-(Human Immunoglobulin G) antibody with β-d-galactosidase from Escherichia coli and Its use for human immunoglobulin G assay. *European Journal of Biochemistry*, *62*(2), pp.285-292.

Kebaier, C., Voza, T. and Vanderberg, J., 2009. Kinetics of mosquito-injected Plasmodium sporozoites in mice: fewer sporozoites are injected into sporozoite-immunized mice. *PLoS Pathogens*, *5*(4), pp.e1000399.

Keeley, A. and Soldati, D., 2004. The glideosome: a molecular machine powering motility and host-cell invasion by Apicomplexa. *Trends in Cell Biology*, *14*(10), pp.528-532.

Keyhani, J., Keyhani, E., Einollahi, N., Minai-Tehrani, D. and Zarchipour, S., 2003. Heterogeneous inhibition of horseradish peroxidase activity by cadmium. *Biochimica et Biophysica Acta-General Subjects*, *1621*(2), pp.140-148.

Keyhani, J., Keyhani, E., Zarchipour, S., Tayefi-Nasrabadi, H. and Einollahi, N., 2005. Stepwise binding of nickel to horseradish peroxidase and inhibition of the enzymatic activity. *Biochimica et Biophysica Acta-General Subjects*, *1722*(3), pp.312-323.

Kim, J., Jang, J.W., Kim, J.Y., Oh, D.J. and Lim, C.S., 2016. Combined use of malaria antigen and antibody enzyme-linked immunosorbent assay for blood screening of Plasmodium vivax in the Republic of Korea. *Medical Principles and Practice*, *25*(3), pp.212-218.

King, A.C., Woods, M., Liu, W., Lu, Z., Gill, D. and Krebs, M.R., 2011. High-throughput measurement, correlation analysis, and machine-learning predictions for pH and thermal stabilities of Pfizer-generated antibodies. *Protein Science*, *20*(9), pp.1546-1557.

Koita, O.A., Doumbo, O.K., Ouattara, A., Tall, L.K., Konaré, A., Diakité, M., Diallo, M., Sagara, I., Masinde, G.L., Doumbo, S.N. and Dolo, A., 2012. False-negative rapid diagnostic tests for malaria and deletion of the histidine-rich repeat region of the hrp2 gene. *The American Journal of Tropical Medicine and Hygiene*, *86*(2), pp.194-198.

Koivunen, M.E., Gee, S.J., Park, E.K., Lee, K., Schenker, M.B. and Hammock, B.D., 2005. Application of an enzyme-linked immunosorbent assay for the analysis of paraquat in human-exposure samples. *Archives of Environmental Contamination and Toxicology*, *48*(2), pp.184-190.

Kraemer, S.M. and Smith, J.D., 2006. A family affair: var genes, PfEMP1 binding, and malaria disease. *Current Opinion in Microbiology*, *9*(4), pp.374-380.

Krainer, F.W. and Glieder, A., 2015. An updated view on horseradish peroxidases: recombinant production and biotechnological applications. *Applied Microbiology and Biotechnology*, *99*(4), pp.1611-1625.

Krause, R.G., Hurdayal, R., Choveaux, D., Przyborski, J.M., Coetzer, T.H. and Goldring, J.D., 2017. Plasmodium glyceraldehyde-3-phosphate dehydrogenase: A potential malaria diagnostic target. *Experimental Parasitology*, *179*, pp.7-19.

Krieg, R. and Halbhuber, K.J., 2003. Recent advances in catalytic peroxidase histochemistry. *Cellular and Molecular Biology (Noisy-le-Grand, France)*, *49*(4), pp.547-563.

Kumar, N., Pande, V., Bhatt, R.M., Shah, N.K., Mishra, N., Srivastava, B., Valecha, N. and Anvikar, A.R., 2013. Genetic deletion of HRP2 and HRP3 in Indian Plasmodium falciparum population and false negative malaria rapid diagnostic test. *Acta Tropica*, *125*(1), pp.119-121.

Kumar, A., Roy, S., Tripathi, S. and Sharma, A., 2016. Molecular docking based virtual screening of natural compounds as potential BACE1 inhibitors: 3D QSAR pharmacophore mapping and molecular dynamics analysis. *Journal of Biomolecular Structure and Dynamics*, *34*(2), pp.239-249.

Laemmli, U.K., 1970. Cleavage of structural proteins during the assembly of the head of bacteriophage T4. *Nature*, *227*(5259), pp.680.

Landier, J., Parker, D.M., Thu, A.M., Carrara, V.I., Lwin, K.M., Bonnington, C.A., Pukrittayakamee, S., Delmas, G. and Nosten, F.H., 2016. The role of early detection and treatment in malaria elimination. *Malaria Journal*, *15*(1), pp.363.

Larsericsdotter, H., Oscarsson, S. and Buijs, J., 2004. Thermodynamic analysis of lysozyme adsorbed to silica. *Journal of Colloid and Interface Science*, *276*(2), pp.261-268.

Larsson, A., Karlsson-Parra, A. and Sjöquist, J., 1991. Use of chicken antibodies in enzyme immunoassays to avoid interference by rheumatoid factors. *Clinical Chemistry*, *37*(3), pp.411-414.

Lavinder, J.J., Hari, S.B., Sullivan, B.J. and Magliery, T.J., 2009. High-throughput thermal scanning: a general, rapid dye-binding thermal shift screen for protein engineering. *Journal of the American Chemical Society*, *131*(11), pp.3794-3795.

Layton, C.J. and Hellinga, H.W., 2011. Quantitation of protein–protein interactions by thermal stability shift analysis. *Protein Science*, *20*(8), pp.1439-1450.

Lee, N., Baker, J., Andrews, K.T., Gatton, M.L., Bell, D., Cheng, Q. and McCarthy, J., 2006. Effect of sequence variation in Plasmodium falciparum histidine-rich protein 2 on binding of specific monoclonal antibodies: implications for rapid diagnostic tests for malaria. *Journal of Clinical Microbiology*, *44*(8), pp.2773-2778.

Lee, S., Song, K.M., Jeon, W., Jo, H., Shim, Y.B. and Ban, C., 2012. A highly sensitive aptasensor towards Plasmodium lactate dehydrogenase for the diagnosis of malaria. *Biosensors and Bioelectronics*, *35*(1), pp.291-296.

Li, Y., Mach, H. and Blue, J.T., 2011. High throughput formulation screening for global aggregation behaviors of three monoclonal antibodies. *Journal of Pharmaceutical Sciences*, *100*(6), pp.2120-2135.

Lipman, N.S., Jackson, L.R., Trudel, L.J. and Weis-Garcia, F., 2005. Monoclonal versus polyclonal antibodies: distinguishing characteristics, applications, and information resources. *ILAR Journal*, *46*(3), pp.258-268.

Lo, M.C., Aulabaugh, A., Jin, G., Cowling, R., Bard, J., Malamas, M. and Ellestad, G., 2004. Evaluation of fluorescence-based thermal shift assays for hit identification in drug discovery. *Analytical Biochemistry*, *332*(1), pp.153-159.

Lon, C.T., Alcantara, S., Luchavez, J., Tsuyuoka, R. and Bell, D., 2005. Positive control wells: a potential answer to remote-area quality assurance of malaria rapid diagnostic tests. *Transactions of the Royal Society of Tropical Medicine and Hygiene*, *99*(7), pp.493-498.

Lopes, L.C., Barreto, M.T., Goncalves, K.M., Alvarez, H.M., Heredia, M.F., de Souza, R.O.M., Cordeiro, Y., Dariva, C. and Fricks, A.T., 2015. Stability and structural changes of horseradish peroxidase: Microwave versus conventional heating treatment. *Enzyme and Microbial Technology*, *69*, pp.10-18.

Lu, H.F., Li, J.Y., Zhang, M.M., Wu, D. and Zhang, Q.L., 2017. A highly selective and sensitive colorimetric uric acid biosensor based on Cu (II)-catalyzed oxidation of 3, 3′, 5, 5′-tetramethylbenzidine. *Sensors and Actuators B: Chemical*, *244*, pp.77-83.

Mahmoudi, A., Nazari, K., Mohammadian, N. and Moosavi-Movahedi, A.A., 2003. Effect of Mn^{2+}, Co^{2+}, Ni^{2+}, and Cu^{2+} on horseradish peroxidase. *Applied Biochemistry and Biotechnology*, *104*(1), pp.81-94.

Major, L.L. and Smith, T.K., 2011. Screening the MayBridge rule of 3 fragment library for compounds that interact with the Trypanosoma brucei myo-inositol-3-phosphate synthase and/or show trypanocidal activity. *Molecular Biology International*, *2011*.

Malaria in South Africa 2017: An Update. *Communicable Diseases Communiqué,* 16(5), pp.1. http://www.nicd.ac.za/wp-content/uploads/2017/05/Malaria-update.pdf

Manana, P.N., Kuonza, L., Musekiwa, A., Mpangane, H.D. and Koekemoer, L.L., 2018. Knowledge, attitudes and practices on malaria transmission in Mamfene, KwaZulu-Natal Province, South Africa 2015. *BMC Public Health*, *18*(1), pp.41.

Manning, L., Laman, M., Stanisic, D., Rosanas-Urgell, A., Bona, C., Teine, D., Siba, P., Mueller, I. and Davis, T.M., 2011. Plasma Plasmodium falciparum histidine-rich protein-2 concentrations do not reflect severity of malaria in Papua new guinean children. *Clinical Infectious Diseases*, *52*(4), pp.440-446.

Marchalonis, J.J., Adelman, M.K., Schluter, S.F. and Ramsland, P.A., 2006. The antibody repertoire in evolution: chance, selection, and continuity. *Developmental and Comparative Immunology*, *30*(1-2), pp.223-247.

Markwalter, C.F., Mudenda, L., Leelawong, M., Kimmel, D.W., Nourani, A., Mbambara, S., Thuma, P.E. and Wright, D.W., 2018. Evidence for histidine-rich protein 2 immune complex formation in symptomatic patients in Southern Zambia. *Malaria Journal*, *17*(1), pp.256.

Mash, H.E., Chin, Y.P., Sigg, L., Hari, R. and Xue, H., 2003. Complexation of copper by zwitterionic aminosulfonic (good) buffers. *Analytical Chemistry*, *75*(3), pp.671-677.

Mathison, B.A. and Pritt, B.S., 2017. Update on malaria diagnostics and test utilization. *Journal of Clinical Microbiology*, pp.02562.

Matulis, D., Kranz, J.K., Salemme, F.R. and Todd, M.J., 2005. Thermodynamic stability of carbonic anhydrase: measurements of binding affinity and stoichiometry using ThermoFluor. *Biochemistry*, *44*(13), pp.5258-5266.

McMahon, R.M., Scanlon, M.J. and Martin, J.L., 2014. Interrogating fragments using a protein thermal shift assay. *Australian Journal of Chemistry*, *66*(12), pp.1502-1506.

Mehta, M., Sonawat, H.M. and Sharma, S., 2005. Malaria parasite-infected erythrocytes inhibit glucose utilization in uninfected red cells. *FEBS Letters*, *579*(27), pp.6151-6158.

Menzen, T. and Friess, W., 2013. High-throughput melting-temperature analysis of a monoclonal antibody by differential scanning fluorimetry in the presence of surfactants. *Journal of Pharmaceutical Sciences*, *102*(2), pp.415-428.

Migneault, I., Dartiguenave, C., Bertrand, M.J. and Waldron, K.C., 2004. Glutaraldehyde: behavior in aqueous solution, reaction with proteins, and application to enzyme crosslinking. *Biotechniques*, *37*(5), pp.790-802.

Modesto, R.R. and Pesce, A.J., 1973. Use of tolylene diisocyanate for the preparation of a peroxidase-labelled antibody conjugate: quantitation of the amount of diisocyanate bound. *Biochimica et Biophysica Acta-Protein Structure*, *295*(1), pp.283-295.

Mogharrab, N., Ghourchian, H. and Amininasab, M., 2007. Structural stabilization and functional improvement of horseradish peroxidase upon modification of accessible lysines: experiments and simulation. *Biophysical Journal*, *92*(4), pp.1192-1203.

Mohan, C., 2003. Buffers a guide for the preparation and use of buffers in biological systems. (Accessed 02.01.2019)

Moody, A., 2002. Rapid diagnostic tests for malaria parasites. *Clinical Microbiology Reviews*, *15*(1), pp.66-78.

Moyo, M., 2014. Horseradish peroxidase biosensor to detect zinc ions in aqueous solutions. *Open Journal of Applied Biosensor*, *3*(01), pp.1.

Mozhaev, V.V., 1993. Mechanism-based strategies for protein thermostabilization. *Trends in Biotechnology*, *11*(3), pp.88-95.

Munhenga, G., Brooke, B.D., Chirwa, T.F., Hunt, R.H., Coetzee, M., Govender, D. and Koekemoer, L.L., 2011. Evaluating the potential of the sterile insect technique for malaria control: relative fitness and mating compatibility between laboratory colonized and a wild population of Anopheles arabiensis from the Kruger National Park, South Africa. *Parasites and Vectors*, *4*(1), pp.208.

Murray, C.K., Gasser, R.A., Magill, A.J. and Miller, R.S., 2008. Update on rapid diagnostic testing for malaria. *Clinical Microbiology Reviews*, *21*(1), pp.97-110.

Nakane, P.K. and Pierce JR, G.B., 1966. Enzyme-labeled antibodies: preparation and application for the localization of antigens. *Journal of Histochemistry and Cytochemistry*, *14*(12), pp.929-931.

Nakane, P.K. and Kawaoi, A., 1974. Peroxidase-labeled antibody a new method of conjugation. *Journal of Histochemistry and Cytochemistry*, *22*(12), pp.1084-1091.

Nakatani, K., Ishikawa, H., Aono, S. and Mizutani, Y., 2014. Identification of essential histidine residues involved in heme binding and Hemozoin formation in heme detoxification protein from Plasmodium falciparum. *Scientific Reports*, *4*, p.6137.

Nantavisai, K., 2014. Malaria detection using non-blood samples. *Songklanakarin Journal of Science and Technology*, *36*(6).

Ndonwi, M., Burlingame, O.O., Miller, A.S., Tollefsen, D.M., Broze, G.J. and Goldberg, D.E., 2011. Inhibition of antithrombin by Plasmodium falciparum histidine-rich protein II. *Blood*, pp.2010.

Newbold, C., Warn, P., Black, G., Berendt, A., Craig, A., Snow, B., Msobo, M., Peshu, N. and Marsh, K., 1997. Receptor-specific adhesion and clinical disease in Plasmodium falciparum. *The American Journal of Tropical Medicine and Hygiene*, *57*(4), pp.389-398.

Niesen, F.H., Berglund, H. and Vedadi, M., 2007. The use of differential scanning fluorimetry to detect ligand interactions that promote protein stability. *Nature protocols*, *2*(9), pp.2212.

Niesen F. 2012. DSF Analysis v3.0.2. Accessed October 29, 2018, at: http://www.beta-sheet.org/resources/T24-DSF-Analysis-Manual-v3.0.pdf

Ochola, L.B., Vounatsou, P., Smith, T., Mabaso, M.L.H. and Newton, C.R.J.C., 2006. The reliability of diagnostic techniques in the diagnosis and management of malaria in the absence of a gold standard. *The Lancet Infectious Diseases*, *6*(9), pp.582-588.

Orlovskaia, N. and Belitser, V., 1964. Studies of the N-terminal amino acid sequence in the serum albumins of different animals. *Biokhimiia*, *29*, pp.741-748.

Ortiz de Montellano, P.R., David, S.K., Ator, M.A. and Tew, D., 1988. Mechanism-based inactivation of horseradish peroxidase by sodium azide. Formation of meso-azidoprotoporphyrin IX. *Biochemistry*, *27*(15), pp.5470-5476.

Pal, P., Daniels, B.P., Oskman, A., Diamond, M.S., Klein, R.S. and Goldberg, D.E., 2016. Plasmodium falciparum histidine-rich protein II compromises brain endothelial barriers and may promote cerebral malaria pathogenesis. *MBio*, *7*(3), pp.e00617-16.

Pal, P., Balaban, A.E., Diamond, M.S., Sinnis, P., Klein, R.S. and Goldberg, D.E., 2017. Plasmodium falciparum histidine-rich protein II causes vascular leakage and exacerbates experimental cerebral malaria in mice. *PloS One*, *12*(5), pp.e0177142.

Pantoliano, M.W., Petrella, E.C., Kwasnoski, J.D., Lobanov, V.S., Myslik, J., Graf, E., Carver, T., Asel, E., Springer, B.A., Lane, P. and Salemme, F.R., 2001. High-density miniaturized thermal shift assays as a general strategy for drug discovery. *Journal of Biomolecular Screening*, *6*(6), pp.429-440.

Panton, L.J., McPhie, P., Maloy, W.L., Wellems, T.E., Taylor, D.W. and Howard, R.J., 1989. Purification and partial characterization of an unusual protein of Plasmodium falciparum: histidine-rich protein II. *Molecular and Biochemical Parasitology*, *35*(2), pp.149-160.

Park, G.Y., Lee, J.Y., Himes, R.A., Thomas, G.S., Blackburn, N.J. and Karlin, K.D., 2014. Copper–peptide complex structure and reactivity when found in conserved His-Xaa-His sequences. *Journal of the American Chemical Society*, *136*(36), pp.12532-12535.

Park, G.S., Opoka, R.O., Shabani, E., Wypyszynski, A., Hanisch, B. and John, C.C., 2017, July. Plasmodium falciparum histidine-rich protein-2 plasma concentrations are higher in retinopathy-negative cerebral malaria than in severe malarial anemia. *In Open Forum Infectious Diseases, US: Oxford University Press*, 4(3), pp. ofx151.

Peeters, J.M., Hazendonk, T.G., Beuvery, E.C. and Tesser, G.I., 1989. Comparison of four bifunctional reagents for coupling peptides to proteins and the effect of the three moieties on the immunogenicity of the conjugates. *Journal of Immunological Methods*, *120*(1), pp.133-143.

Perrin, D.D., Dempsey, B. and Serjeant, E.P., 1981. pKa prediction for organic acids and bases. *Springer*. Springer Netherlands, Chapman and Hall, 1, pp 67

Peters, T. and Blumenstock, F.A., 1967. Copper-binding properties of bovine serum albumin and its amino-terminal peptide fragment. *Journal of Biological Chemistry*, *242*(7), pp.1574-1578.

Plomp, R., Bondt, A., de Haan, N., Rombouts, Y. and Wuhrer, M., 2016. Recent advances in clinical glycoproteomics of immunoglobulins. *Molecular and Cellular Proteomics*, pp.mcp-O116.

Polson, A., Coetzer, T., Kruger, J., Von Maltzahn, E. and Van der Merwe, K.J., 1985. Improvements in the isolation of IgY from the yolks of eggs laid by immunized hens. *Immunological Investigations*, 14(4), pp.323-327.

Ponsford, M.J., Medana, I.M., Prapansilp, P., Hien, T.T., Lee, S.J., Dondorp, A.M., Esiri, M.M., Day, N.P., White, N.J. and Turner, G.D., 2011. Sequestration and microvascular congestion are associated with coma in human cerebral malaria. *Journal of Infectious Diseases*, *205*(4), pp.663-671.

Pope, B. and Kent, H.M., 1996. High efficiency 5 min transformation of Escherichia coli. *Nucleic Acids Research*, *24*(3), pp.536-537.

Qoronfleh, M.W., Ren, L., Emery, D., Perr, M. and Kaboord, B., 2003. Use of immunomatrix methods to improve protein-protein interaction detection. *BioMed Research International*, *2003*(5), pp.291-298.

Ragavan, K.V., Kumar, S., Swaraj, S. and Neethirajan, S., 2018. Advances in biosensors and optical assays for diagnosis and detection of malaria. Biosensors and Bioelectronics, 105, pp.188-210.

Rannulu, N.S. and Rodgers, M.T., 2005. Solvation of copper ions by imidazole: structures and sequential binding energies of Cu+(imidazole) x, x= 1–4. Competition between ion solvation and hydrogen bonding. *Physical Chemistry Chemical Physics*, *7*(5), pp.1014-1025.

Read, J.A., Wilkinson, K.W., Tranter, R., Sessions, R.B. and Brady, R.L., 1999. Chloroquine Binds in the Cofactor Binding Site ofPlasmodium falciparum Lactate Dehydrogenase. *Journal of Biological Chemistry*, *274*(15), pp.10213-10218.

Redhead, M., Satchell, R., Morkūnaitė, V., Swift, D., Petrauskas, V., Golding, E., Onions, S., Matulis, D. and Unitt, J., 2015. A combinatorial biophysical approach; FTSA and SPR for identifying small molecule ligands and PAINs. *Analytical Biochemistry*, *479*, pp.63-73.

Redhead, M., Satchell, R., McCarthy, C., Pollack, S. and Unitt, J., 2017. Thermal shift as an entropy-driven effect. *Biochemistry*, *56*(47), pp.6187-6199.

Reinhard, L., Mayerhofer, H., Geerlof, A., Mueller-Dieckmann, J. and Weiss, M.S., 2013. Optimization of protein buffer cocktails using Thermofluor. *Acta Crystallographica Section F: Structural Biology and Crystallization Communications*, *69*(2), pp.209-214.

Reyburn, H., 2010. New WHO guidelines for the treatment of malaria. *BMJ (Clinical Research ed)*, *340*, pp.c2637.

Robichon, C., Luo, J., Causey, T.B., Benner, J.S. and Samuelson, J.C., 2011. Engineering BL21 (DE3) derivative strains to minimize Escherichia coli protein contamination after IMAC purification. *Applied and Environmental Microbiology*, pp.00119.

Rosano, G.L. and Ceccarelli, E.A., 2014. Recombinant protein expression in Escherichia coli: advances and challenges. *Frontiers in Microbiology*, *5*, pp.172.

Rosner, M.H., Grassman, J.A. and Haas, R.A., 1991. Immunochemical techniques in biological monitoring. *Environmental Health Perspectives*, *94*, pp.131.

Rubach, M.P., Mukemba, J., Florence, S., John, B., Crookston, B., Lopansri, B.K., Yeo, T.W., Piera, K.A., Alder, S.C., Weinberg, J.B. and Anstey, N.M., 2012. Plasma Plasmodium falciparum histidine-rich protein-2 concentrations are associated with malaria severity and mortality in Tanzanian children. *PloS One*, *7*(5), pp.e35985.

Sanyal, G. and Maren, T.H., 1981. Thermodynamics of carbonic anhydrase catalysis. A comparison between human isoenzymes B and C. *Journal of Biological Chemistry*, *256*(2), pp.608-612.

Sariri, R., Sajedi, R.H. and Jafarian, V., 2006. Inhibition of horseradish peroxidase activity by thiol type inhibitors. *Journal of Molecular Liquids*, *123*(1), pp.20-23.

Satchell, J.F., Malby, R.L., Luo, C.S., Adisa, A., Alpyurek, A.E., Klonis, N., Smith, B.J., Tilley, L. and Colman, P.M., 2005. Structure of glyceraldehyde-3-phosphate dehydrogenase from Plasmodium falciparum. *Acta Crystallographica Section D: Biological Crystallography*, *61*(9), pp.1213-1221.

Sato, K., Hasumi, H., Tsukidate, A., Sakurada, J., Nakamura, S. and Hosoya, T., 1995. Effects of mixed solvents on three elementary steps in the reactions of horseradish peroxidase and lactoperoxidase. *Biochimica et Biophysica Acta-Protein Structure and Molecular Enzymology*, *1253*(1), pp.94-102.

Schade, R. and Hlinak, A., 1996. Egg yolk antibodies, state of the art and future prospects. *Altex*, *13*(5), pp.5-9.

Schade, R., Staak, C., Hendriksen, C., Erhard, M., Hugl, H., Koch, G., Larsson, A., Pollmann, W., Van Regenmortel, M., Rijke, E. and Spielmann, H., 1996. The production of avian (egg yolk) antibodies: IgY. *Atla*, *24*, pp.925-934.

Schade, R., Calzado, E.G., Sarmiento, R., Chacana, P.A., Porankiewicz-Asplund, J. and Terzolo, H.R., 2005. Chicken egg yolk antibodies (IgY-technology): a review of progress in production and use in research and human and veterinary medicine. *Altern Lab Anim*, *33*(2), pp.129-54.

Schmidt, A., Schumacher, J.T., Reichelt, J., Hecht, H.J. and Bilitewski, U., 2002. Mechanistic and molecular investigations on stabilization of horseradish peroxidase C. *Analytical Chemistry*, *74*(13), pp.3037-3045.

Schuetz, A.J., Winklmair, M., Weller, M.G. and Niessner, R., 1997, May. Stabilization of horseradish peroxidase (HRP) for use in immunochemical sensors. In *Chemical, Biochemical and Environmental Fiber Sensors IX*, 3105, pp. 332-341.

Sepúlveda, N., Manjurano, A., Campino, S.G., Lemnge, M., Lusingu, J., Olomi, R., Rockett, K.A., Hubbart, C., Jeffreys, A., Rowlands, K. and Clark, T.G., 2017. Malaria host candidate genes validated by association with current, recent, and historical measures of transmission intensity. *The Journal of Infectious Diseases*, *216*(1), pp.45-54.

Seydel, K.B., Fox, L.L., Glover, S.J., Reeves, M.J., Pensulo, P., Muiruri, A., Mpakiza, A., Molyneux, M.E. and Taylor, T.E., 2012. Plasma concentrations of parasite histidine-rich protein 2 distinguish between retinopathy-positive and retinopathy-negative cerebral malaria in Malawian children. *The Journal of Infectious Diseases*, *206*(3), pp.309-318.

Sezonov, G., Joseleau-Petit, D. and D'Ari, R., 2007. Escherichia coli physiology in Luria-Bertani broth. *Journal of bacteriology*, *189*(23), pp.8746-8749.

Shan, Z., Lu, M., Wang, L., MacDonald, B., MacInnis, J., Mkandawire, M., Zhang, X. and Oakes, K.D., 2016. Chloride accelerated Fenton chemistry for the ultrasensitive and selective colorimetric detection of copper. *Chemical Communications*, *52*(10), pp.2087-2090.

Shelake, R.M., Ito, Y., Masumoto, J., Morita, E.H. and Hayashi, H., 2017. A novel mechanism of “metal gel-shift” by histidine-rich Ni^{2+}-binding Hpn protein from Helicobacter pylori strain SS1. *PloS One*, *12*(2), pp.e0172182.

Shi, D., Sun, Y., Lin, L., Shi, C., Wang, G. and Zhang, X., 2016. Naked-eye sensitive detection of alkaline phosphatase (ALP) and pyrophosphate (PPi) based on a horseradish peroxidase catalytic colorimetric system with Cu (ii). *Analyst*, *141*(19), pp.5549-5554.

Shimizu, M., Nagashima, H., Sano, K., Hashimoto, K., Ozeki, M., Tsuda, K. and Hatta, H., 1992. Molecular stability of chicken and rabbit immunoglobulin G. *Bioscience, Biotechnology, and Biochemistry*, *56*(2), pp.270-274.

Silamut, K., Phu, N.H., Whitty, C., Turner, G.D., Louwrier, K., Mai, N.T., Simpson, J.A., Hien, T.T. and White, N.J., 1999. A quantitative analysis of the microvascular sequestration of malaria parasites in the human brain. *The American Journal of Pathology*, *155*(2), pp.395-410.

Sinha, I., Ekapirat, N., Dondorp, A.M. and Woodrow, C.J., 2015. Use of a rapid test to assess plasma Plasmodium falciparum HRP2 and guide management of severe febrile illness. *Malaria Journal*, *14*(1), pp.362.

Singh, B. and Daneshvar, C., 2013. Human infections and detection of Plasmodium knowlesi. *Clinical Microbiology Reviews*, *26*(2), pp.165-184.

Smith, A.T., Santama, N., Dacey, S., Edwards, M., Bray, R.C., Thorneley, R.N. and Burke, J.F., 1990. Expression of a synthetic gene for horseradish peroxidase C in Escherichia coli and folding and activation of the recombinant enzyme with Ca^{2+} and heme. *Journal of Biological Chemistry*, *265*(22), pp.13335-13343.

Snow, R.W., Guerra, C.A., Noor, A.M., Myint, H.Y. and Hay, S.I., 2005. The global distribution of clinical episodes of Plasmodium falciparum malaria. *Nature*, *434*(7030), pp.214.

Sørensen, H.P. and Mortensen, K.K., 2005. Advanced genetic strategies for recombinant protein expression in Escherichia coli. *Journal of Biotechnology*, *115*(2), pp.113-128.

Spillner, E., Braren, I., Greunke, K., Seismann, H., Blank, S. and du Plessis, D., 2012. Avian IgY antibodies and their recombinant equivalents in research, diagnostics and therapy. *Biologicals*, *40*(5), pp.313-322.

Steinberg, T.H., Jones, L.J., Haugland, R.P. and Singer, V.L., 1996. SYPRO orange and SYPRO red protein gel stains: one-step fluorescent staining of denaturing gels for detection of nanogram levels of protein. *Analytical Biochemistry*, *239*(2), pp.223-237.

Stepankova, V., Bidmanova, S., Koudelakova, T., Prokop, Z., Chaloupkova, R. and Damborsky, J., 2013. Strategies for stabilization of enzymes in organic solvents. *American Chemical Society Catalysis*, *3*(12), pp.2823-2836.

Streefkerk, J.G. and Van Der Ploeg, M., 1974. The effect of methanol on granulocyte and horseradish peroxidase quantitatively studied in a film model system. *Histochemistry*, *40*(2), pp.105-111.

Sulkowski, E., 1985. Purification of proteins by IMAC. *Trends in Biotechnology*, *3*(1), pp.1-7.

Sullivan, D.J., Gluzman, I.Y. and Goldberg, D.E., 1996. Plasmodium hemozoin formation mediated by histidine-rich proteins. *Science*, *271*(5246), pp.219-222.

Sun, S., Mo, W., Ji, Y. and Liu, S., 2001. Preparation and mass spectrometric study of egg yolk antibody (IgY) against rabies virus. *Rapid Communications in Mass Spectrometry*, *15*(9), pp.708-712.

Sun, J.H., Jiang, Z.Q. and Hu, S.H., 2008. Effect of four adjuvants on immune response to F4 fimbriae in chickens. *Veterinary Immunology and Immunopathology*, *121*(1-2), pp.107-112.

Sundberg, R.J. and Martin, R.B., 1974. Interactions of histidine and other imidazole derivatives with transition metal ions in chemical and biological systems. *Chemical Reviews*, *74*(4), pp.471-517.

Svilenov, H., Markoja, U. and Winter, G., 2018. Isothermal chemical denaturation as a complementary tool to overcome limitations of thermal differential scanning fluorimetry in predicting physical stability of protein formulations. *European Journal of Pharmaceutics and Biopharmaceutics*, *125*, pp.106-113.

Taylor, T.E., Fu, W.J., Carr, R.A., Whitten, R.O., Mueller, J.G., Fosiko, N.G., Lewallen, S., Liomba, N.G. and Molyneux, M.E., 2004. Differentiating the pathologies of cerebral malaria by post mortem parasite counts. *Nature Medicine*, *10*(2), pp.143.

Terzolo, H., Chacana, P., Vivas, A., Greco, C., Goya, R. and Schade, R., 2003. IgY technology in Argentina. *ALTEX*, *20*, pp.202-203.

Tijssen, P. and Kurstak, E., 1984. Highly efficient and simple methods for the preparation of peroxidase and active peroxidase-antibody conjugates for enzyme immunoassays. *Analytical Biochemistry*, *136*(2), pp.451-457.

Towbin, H., Staehelin, T. and Gordon, J., 1979. Electrophoretic transfer of proteins from polyacrylamide gels to nitrocellulose sheets: procedure and some applications. *Proceedings of the National Academy of Sciences*, *76*(9), pp.4350-4354.

Uniewicz, K.A., Ori, A., Xu, R., Ahmed, Y., Wilkinson, M.C., Fernig, D.G. and Yates, E.A., 2010. Differential scanning fluorimetry measurement of protein stability changes upon binding to glycosaminoglycans: a screening test for binding specificity. *Analytical Chemistry*, *82*(9), pp.3796-3802.

Vasoo, S. and Pritt, B.S., 2013. Molecular diagnostics and parasitic disease. *Clinics in Laboratory Medicine*, *33*(3), pp.461-503.

Vedadi, M., Niesen, F.H., Allali-Hassani, A., Fedorov, O.Y., Finerty, P.J., Wasney, G.A., Yeung, R., Arrowsmith, C., Ball, L.J., Berglund, H. and Hui, R., 2006. Chemical screening methods to identify ligands that promote protein stability, protein crystallization, and structure determination. *Proceedings of the National Academy of Sciences*, *103*(43), pp.15835-15840.

Vedadi, M., Arrowsmith, C.H., Allali-Hassani, A., Senisterra, G. and Wasney, G.A., 2010. Biophysical characterization of recombinant proteins: a key to higher structural genomics success. *Journal of Structural Biology*, *172*(1), pp.107-119.

Veitch, N.C. and Smith, A.T., 2000. Horseradish peroxidase. *Advances in Inorganic Chemistry*, 51, pp.107-162

Veitch, N.C., 2004. Horseradish peroxidase: a modern view of a classic enzyme. *Phytochemistry*, *65*(3), pp.249-259.

Vermeer, A.W., Bremer, M.G. and Norde, W., 1998. Structural changes of IgG induced by heat treatment and by adsorption onto a hydrophobic Teflon surface studied by circular dichroism spectroscopy. *Biochimica et Biophysica Acta-General Subjects*, *1425*(1), pp.1-12.

Viana, G.M.R., Okoth, S.A., Silva-Flannery, L., Barbosa, D.R.L., de Oliveira, A.M., Goldman, I.F., Morton, L.C., Huber, C., Anez, A., Machado, R.L.D. and Camargo, L.M.A., 2017. Histidine-rich protein 2 (pfhrp2) and pfhrp3 gene deletions in Plasmodium falciparum isolates from select sites in Brazil and Bolivia. *PloS One*, *12*(3), pp.e0171150.

Vivoli, M., Novak, H.R., Littlechild, J.A. and Harmer, N.J., 2014. Determination of protein-ligand interactions using differential scanning fluorimetry. *Journal of Visualized Experiments*, 1(91), pp.1-13.

Voller, A., Cornille-Brögger, R., Storey, J. and Molineaux, L., 1980. A longitudinal study of Plasmodium falciparum malaria in the West African savanna using the ELISA technique. *Bulletin of the World Health Organization*, *58*(3), p.429.

Wang, S., Cazelles, R., Liao, W.C., Vázquez-González, M., Zoabi, A., Abu-Reziq, R. and Willner, I., 2017. Mimicking horseradish peroxidase and NADH peroxidase by heterogeneous Cu^{2+}-modified graphene oxide nanoparticles. *Nano Letters*, *17*(3), pp.2043-2048.

Wang, H.B., Li, Y., Dong, G.L., Gan, T. and Liu, Y.M., 2017. A convenient and label-free colorimetric assay for dopamine detection based on the inhibition of the Cu (ii)-catalyzed oxidation of a 3, 3′, 5, 5′-tetramethylbenzidine–H_2O_2 system. *New Journal of Chemistry*, *41*(23), pp.14364-14369.

Wardman, P. and Candeias, L.P., 1996. Fenton chemistry: an introduction. *Radiation Research*, *145*(5), pp.523-531.

Wardman, P., 2002. Indole-3-acetic acids and horseradish peroxidase: a new prodrug/enzyme combination for targeted cancer therapy. *Current Pharmaceutical Design*, *8*(15), pp.1363.

Warr, G.W., Magor, K.E. and Higgins, D.A., 1995. IgY: clues to the origins of modern antibodies. *Immunology Today*, *16*(8), pp.392-398.

Welinder, K.G., 1979. Amino acid sequence studies of horseradish peroxidase: amino and carboxyl termini, cyanogen bromide and tryptic fragments, the complete sequence, and some structural characteristics of horseradish peroxidase C. *European Journal of Biochemistry*, *96*(3), pp.483-502.

Wellems, T.E. and Howard, R.J., 1986. Homologous genes encode two distinct histidine-rich proteins in a cloned isolate of Plasmodium falciparum. *Proceedings of the National Academy of Sciences*, *83*(16), pp.6065-6069.

Wells, T.N., Van Huijsduijnen, R.H. and Van Voorhis, W.C., 2015. Malaria medicines: a glass half full?. *Nature Reviews Drug Discovery*, *14*(6), pp.424.

Wen, J., Jiang, Y. and Nahri, L., 2008. Effect of carbohydrate on thermal stability of antibodies. *Am Pharm Rev*, *11*(6), pp.98-104.

WHO., (2015b). World malaria Report 2015. *WHO Press*. Available at: http://apps.who.int/iris/bitstream/10665/200018/1/9789241565158_eng.pdf

WHO, http:// www. WHO.int/malaria/test_treat_track/en/index.html

WHO, https://www.who.int/malaria/media/factsheets_qa/en/ (19.11.2018)

Wright, T.A., Stewart, J.M., Page, R.C. and Konkolewicz, D., 2017. Extraction of Thermodynamic parameters of protein unfolding using parallelized differential scanning fluorimetry. *The Journal of Physical Chemistry Letters*, *8*(3), pp.553-558.

Wu, H., Fan, S., Chen, H., Shen, J., Geng, Y., Peng, L. and Du, H., 2014. Effects of Cu^{2+} and pH on the binding of alizarin red S to bovine serum albumin based on the analysis of protein conformation. *Analytical Methods*, *6*(13), pp.4729-4733.

Wu, X.Q., Xu, Y., Chen, Y.L., Zhao, H., Cui, H.J., Shen, J.S. and Zhang, H.W., 2014. Peroxidase-like activity of ferric ions and their application to cysteine detection. *RSC Advances*, *4*(110), pp.64438-64442.

Wurtz, N., Fall, B., Bui, K., Pascual, A., Fall, M., Camara, C., Diatta, B., Fall, K.B., Mbaye, P.S., Diémé, Y. and Bercion, R., 2013. Pfhrp2 and pfhrp3 polymorphisms in Plasmodium falciparum isolates from Dakar, Senegal: impact on rapid malaria diagnostic tests. *Malaria Journal*, *12*(1), pp.34.

Xianyu, Y., Zhu, K., Chen, W., Wang, X., Zhao, H., Sun, J., Wang, Z. and Jiang, X., 2013. Enzymatic assay for Cu (II) with horseradish peroxidase and its application in colorimetric logic gate. *Analytical Chemistry*, *85*(15), pp.7029-7032.

Xu, Y., Wu, X.Q., Shen, J.S. and Zhang, H.W., 2015. Highly selective and sensitive recognition of histidine based on the oxidase-like activity of Cu^{2+} ions. *RSC Advances*, *5*(112), pp.92114-92120.

Zatón, A.M.L. and Ochoa de Aspuru, E., 1995. Horseradish peroxidase inhibition by thiouracils. *FEBS Letters*, *374*(2), pp.192-194.

Zhao, Y., Rabbani, H., Shimizu, A. and Hammarström, L., 2000. Mapping of the chicken immunoglobulin heavy-chain constant region gene locus reveals an inverted α gene upstream of a condensed υ gene. *Immunology*, *101*(3), pp.348-353.

Zhao, H. and Waite, J.H., 2006. Proteins in load-bearing junctions: the histidine-rich metal-binding protein of mussel byssus. *Biochemistry*, *45*(47), pp.14223-14231.

Zhao, J., Lu, C. and Franzen, S., 2015. Distinct enzyme–substrate interactions revealed by two dimensional kinetic comparison between dehaloperoxidase-hemoglobin and horseradish peroxidase. *The Journal of Physical Chemistry B*, *119*(40), pp.12828-12837.

Zhou, Y., Zhou, T., Zhang, M. and Shi, G., 2014. A DNA–scaffolded silver nanocluster/Cu^{2+} ensemble as a turn-on fluorescent probe for histidine. *Analyst*, *139*(12), pp.3122-3126.

8. APPENDIX A: INFORMATION ON APPENDICES

The following Tables (Table 1-18) show the data and calculations used to obtain the ΔμG, used to make the equations in Table 3.4. The Tables represent all five antibodies tested. Equations for the data are present in the materials and methods at the beginning of Chapter 3 and has also been reported by Wright *et al*., (2017).

Table A.1: Crocodile IgM data calculated from equations 1 – 5 (Chapter 3). First replicate.

Fmin	Crocodile IgM	F- F min	Fmax-Fmin	(F-Fmin)/Fmax-Fmin)	1-(F-Fmin)/Fmax-Fmin) (F-Fmin)/Fmax-Fmin)	Therefore Pu is:	Pf	Ku	T		T in kelvin	ΔμG
38.82	38.831	0.011	2.98	0.004	0.996	0.004	0.996	0.0036	57.1	273	330.1	15456.01
38.82	38.887	0.067	2.98	0.022	0.978	0.022	0.978	0.0229	57.4	273	330.4	10370.63
38.82	38.941	0.121	2.98	0.041	0.959	0.041	0.959	0.0424	57.7	273	330.7	8693.39
38.82	38.983	0.163	2.98	0.055	0.945	0.055	0.945	0.0579	58	273	331	7839.14
38.82	39.040	0.220	2.98	0.074	0.926	0.074	0.926	0.0797	58.3	273	331.3	6967.17
38.82	39.135	0.315	2.98	0.106	0.894	0.106	0.894	0.1184	58.6	273	331.6	5883.59
38.82	39.262	0.442	2.98	0.148	0.852	0.148	0.852	0.1742	58.9	273	331.9	4822.05
38.82	39.404	0.584	2.98	0.196	0.804	0.196	0.804	0.2435	59.2	273	332.2	3901.53
38.82	39.511	0.691	2.98	0.232	0.768	0.232	0.768	0.3018	59.5	273	332.5	3311.80
38.82	39.642	0.822	2.98	0.276	0.724	0.276	0.724	0.3807	59.8	273	332.8	2672.44
38.82	39.784	0.964	2.98	0.323	0.677	0.323	0.677	0.4782	60.1	273	333.1	2043.54
38.82	39.935	1.115	2.98	0.374	0.626	0.374	0.626	0.5981	60.4	273	333.4	1425.01
38.82	40.071	1.251	2.98	0.420	0.580	0.420	0.580	0.7234	60.7	273	333.7	898.50
38.82	40.196	1.376	2.98	0.462	0.538	0.462	0.538	0.8582	61	273	334	424.70

Table A.2: Crocodile IgM data calculated from equations 1 – 5 (Chapter 3). Second replicate.

Fmin	PfLDH IgY Fluoro data	F- F min	Fmax-Fmin	(F-Fmin)/Fmax-Fmin)	1-(F-Fmin)/Fmax-Fmin) (F-Fmin)/Fmax-Fmin)	Therefore Pu is:	Pf	Ku	T	273	T in kelvin	ΔμG
37.42	37.473	0.053	3.6	0.0147	0.985	0.0147	0.985	0.0149	57.1	273	330.1	11543.46
37.42	37.525	0.105	3.6	0.0292	0.971	0.0292	0.971	0.0301	57.4	273	330.4	9623.79
37.42	37.597	0.177	3.6	0.0492	0.951	0.0492	0.951	0.0517	57.7	273	330.7	8144.40
37.42	37.666	0.246	3.6	0.0683	0.932	0.0683	0.932	0.0733	58	273	331	7190.81
37.42	37.766	0.346	3.6	0.0962	0.904	0.0962	0.904	0.1064	58.3	273	331.3	6171.21
37.42	37.870	0.45	3.6	0.1250	0.875	0.1250	0.875	0.1429	58.6	273	331.6	5365.13
37.42	37.987	0.567	3.6	0.1576	0.842	0.1576	0.842	0.1870	58.9	273	331.9	4626.57
37.42	38.113	0.693	3.6	0.1925	0.808	0.1925	0.808	0.2384	59.2	273	332.2	3960.94
37.42	38.254	0.834	3.6	0.2317	0.768	0.2317	0.768	0.3016	59.5	273	332.5	3314.35
37.42	38.396	0.976	3.6	0.2710	0.729	0.2710	0.729	0.3717	59.8	273	332.8	2738.48
37.42	38.555	1.135	3.6	0.3152	0.685	0.3152	0.685	0.4602	60.1	273	333.1	2149.41
37.42	38.718	1.298	3.6	0.3606	0.639	0.3606	0.639	0.5641	60.4	273	333.4	1587.40
37.42	38.892	1.472	3.6	0.4089	0.591	0.4089	0.591	0.6919	60.7	273	333.7	1022.12
37.42	39.073	1.653	3.6	0.4591	0.541	0.4591	0.541	0.8486	61	273	334	455.78

Table A.3: Crocodile IgM data calculated from equations 1 – 5 (Chapter 3). Third replicate.

Fmin	PfLDH IgY Fluoro data	F- F min	Fmax-Fmin	(F-Fmin)/Fmax-Fmin)	1-(F-Fmin)/Fmax-Fmin) (F-Fmin)/Fmax-Fmin)	Therefore Pu is:	Pf	Ku	T		T in kelvin	ΔμG
38.09	38.135	0.045	3.58	0.0125	0.987	0.0125	0.987	0.0127	57.1	273	330.1	11985.93
38.09	38.190	0.1	3.58	0.0280	0.972	0.0280	0.972	0.0288	57.4	273	330.4	9744.79
38.09	38.245	0.155	3.58	0.0433	0.957	0.0433	0.957	0.0452	57.7	273	330.7	8512.23
38.09	38.329	0.239	3.58	0.0667	0.933	0.0667	0.933	0.0714	58	273	331	7263.32
38.09	38.421	0.331	3.58	0.0926	0.907	0.0926	0.907	0.1020	58.3	273	331.3	6287.48
38.09	38.522	0.432	3.58	0.1208	0.879	0.1208	0.879	0.1374	58.6	273	331.6	5473.27
38.09	38.645	0.555	3.58	0.1551	0.845	0.1551	0.845	0.1836	58.9	273	331.9	4677.96
38.09	38.762	0.672	3.58	0.1877	0.812	0.1877	0.812	0.2311	59.2	273	332.2	4046.68
38.09	38.901	0.811	3.58	0.2266	0.773	0.2266	0.773	0.2929	59.5	273	332.5	3394.56
38.09	39.063	0.973	3.58	0.2719	0.728	0.2719	0.728	0.3735	59.8	273	332.8	2725.36
38.09	39.209	1.119	3.58	0.3126	0.687	0.3126	0.687	0.4547	60.1	273	333.1	2182.92
38.09	39.373	1.283	3.58	0.3583	0.642	0.3583	0.642	0.5584	60.4	273	333.4	1615.41
38.09	39.530	1.44	3.58	0.4022	0.598	0.4022	0.598	0.6729	60.7	273	333.7	1099.42
38.09	39.709	1.619	3.58	0.4523	0.548	0.4523	0.548	0.8260	61	273	334	531.01

Table A.4: Crocodile IgY (first transition peak) data calculated from equations 1 – 5 (Chapter 3). First replicate.

Fmin	PfLDH IgY Fluoro data	F- F min	Fmax-Fmin	(F-Fmin)/Fmax-Fmin)	1-(F-Fmin)/Fmax-Fmin) (F-Fmin)/Fmax-Fmin)	Therefore Pu is:	Pf	Ku= (pu/pf)	T		T in kelvin	ΔμG
6.77	6.786	0.016	3.09	0.005	0.995	0.005	0.995	0.005	59.8	273	332.8	14499.20
6.77	6.802	0.032	3.09	0.010	0.990	0.010	0.990	0.010	60.1	273	333.1	12647.19
6.77	6.832	0.062	3.09	0.020	0.980	0.020	0.980	0.020	60.4	273	333.4	10782.89
6.77	6.866	0.096	3.09	0.031	0.969	0.031	0.969	0.032	60.7	273	333.7	9552.47
6.77	6.904	0.134	3.09	0.043	0.957	0.043	0.957	0.045	61	273	334	8591.90
6.77	6.940	0.170	3.09	0.055	0.945	0.055	0.945	0.058	61.3	273	334.3	7905.24
6.77	6.989	0.219	3.09	0.071	0.929	0.071	0.929	0.076	61.6	273	334.6	7165.38
6.77	7.043	0.273	3.09	0.088	0.912	0.088	0.912	0.097	61.9	273	334.9	6503.10
6.77	7.112	0.342	3.09	0.111	0.889	0.111	0.889	0.125	62.2	273	335.2	5804.60
6.77	7.181	0.411	3.09	0.133	0.867	0.133	0.867	0.153	62.5	273	335.5	5231.87
6.77	7.268	0.498	3.09	0.161	0.839	0.161	0.839	0.192	62.8	273	335.8	4608.30
6.77	7.367	0.597	3.09	0.193	0.807	0.193	0.807	0.239	63.1	273	336.1	3995.88
6.77	7.477	0.707	3.09	0.229	0.771	0.229	0.771	0.297	63.4	273	336.4	3397.62
6.77	7.593	0.823	3.09	0.266	0.734	0.266	0.734	0.363	63.7	273	336.7	2836.37
6.77	7.727	0.957	3.09	0.310	0.690	0.310	0.690	0.449	64	273	337	2246.02
6.77	7.876	1.106	3.09	0.358	0.642	0.358	0.642	0.558	64.3	273	337.3	1638.72
6.77	8.031	1.261	3.09	0.408	0.592	0.408	0.592	0.690	64.6	273	337.6	1043.24
6.77	8.184	1.414	3.09	0.458	0.542	0.458	0.542	0.843	64.9	273	337.9	478.58

Table A.5: Crocodile IgY (second transition peak) data calculated from equations 1 – 5 (Chapter 3). Second replicate.

Fmin	PfLDH IgY Fluoro data	F- F min	Fmax-Fmin	(F-Fmin)/Fmax-Fmin)	1-(F-Fmin)/Fmax-Fmin) (F-Fmin)/Fmax-Fmin)	Therefore Pu is:	Pf	Ku= (pu/pf)	T_m		T in kelvin	ΔμG
8.84	8.984	0.144	3.18	0.045	0.955	0.045	0.955	0.047	66.4	273	339.4	8609.66
8.84	9.125	0.285	3.18	0.090	0.910	0.090	0.910	0.098	66.7	273	339.7	6552.13
8.84	9.254	0.414	3.18	0.130	0.870	0.130	0.870	0.150	67	273	340	5370.94
8.84	9.373	0.533	3.18	0.168	0.832	0.168	0.832	0.201	67.3	273	340.3	4534.43
8.84	9.482	0.642	3.18	0.202	0.798	0.202	0.798	0.253	67.6	273	340.6	3892.48
8.84	9.592	0.752	3.18	0.236	0.764	0.236	0.764	0.310	67.9	273	340.9	3322.74
8.84	9.689	0.849	3.18	0.267	0.733	0.267	0.733	0.364	68.2	273	341.2	2864.08
8.84	9.792	0.952	3.18	0.299	0.701	0.299	0.701	0.427	68.5	273	341.5	2415.77
8.84	9.892	1.052	3.18	0.331	0.669	0.331	0.669	0.494	68.8	273	341.8	2001.96
8.84	9.998	1.158	3.18	0.364	0.636	0.364	0.636	0.573	69.1	273	342.1	1583.73
8.84	10.104	1.264	3.18	0.397	0.603	0.397	0.603	0.659	69.4	273	342.4	1186.06
8.84	10.210	1.370	3.18	0.431	0.569	0.431	0.569	0.757	69.7	273	342.7	792.92
8.84	10.323	1.483	3.18	0.466	0.534	0.466	0.534	0.873	70	273	343	386.02

Table A.6: Crocodile IgY (first transition peak) data calculated from equations 1 – 5 (Chapter 3). Third replicate.

Fmin	PfLDH IgY Fluoro data	F- F min	Fmax-Fmin	(F-Fmin)/Fmax-Fmin)	1-(F-Fmin)/Fmax-Fmin) (F-Fmin)/Fmax-Fmin)	Therefore Pu is:	Pf	Ku= (pu/pf)	T	273	T in kelvin	ΔμG
6.97	6.979	0.009	2.7	0.003	0.997	0.003	0.997	0.003	59.8	273	332.8	15872.83
6.97	6.999	0.029	2.7	0.011	0.989	0.011	0.989	0.011	60.1	273	333.1	12500.96
6.97	7.020	0.050	2.7	0.018	0.982	0.018	0.982	0.019	60.4	273	333.4	11023.30
6.97	7.046	0.076	2.7	0.028	0.972	0.028	0.972	0.029	60.7	273	333.7	9813.92
6.97	7.071	0.101	2.7	0.037	0.963	0.037	0.963	0.039	61	273	334	9021.89
6.97	7.101	0.131	2.7	0.048	0.952	0.048	0.952	0.051	61.3	273	334.3	8280.24
6.97	7.138	0.168	2.7	0.062	0.938	0.062	0.938	0.066	61.6	273	334.6	7543.36
6.97	7.190	0.220	2.7	0.082	0.918	0.082	0.918	0.089	61.9	273	334.9	6743.38
6.97	7.246	0.276	2.7	0.102	0.898	0.102	0.898	0.114	62.2	273	335.2	6059.29
6.97	7.308	0.338	2.7	0.125	0.875	0.125	0.875	0.143	62.5	273	335.5	5423.99
6.97	7.383	0.413	2.7	0.153	0.847	0.153	0.847	0.181	62.8	273	335.8	4776.65
6.97	7.465	0.495	2.7	0.183	0.817	0.183	0.817	0.225	63.1	273	336.1	4173.08
6.97	7.557	0.587	2.7	0.217	0.783	0.217	0.783	0.278	63.4	273	336.4	3583.65
6.97	7.661	0.691	2.7	0.256	0.744	0.256	0.744	0.344	63.7	273	336.7	2986.85
6.97	7.775	0.805	2.7	0.298	0.702	0.298	0.702	0.425	64	273	337	2398.68
6.97	7.893	0.923	2.7	0.342	0.658	0.342	0.658	0.520	64.3	273	337.3	1836.64
6.97	8.027	1.057	2.7	0.391	0.609	0.391	0.609	0.643	64.6	273	337.6	1239.05
6.97	8.173	1.203	2.7	0.446	0.554	0.446	0.554	0.804	64.9	273	337.9	613.33

Table A.7: Crocodile IgY (second transition peak) data calculated from equations 1 – 5 (Chapter 3). First replicate.

Fmin	PfLDH IgY Fluoro data	F- F min	Fmax-Fmin	(F-Fmin)/Fmax-Fmin)	1-(F-Fmin)/Fmax-Fmin) (F-Fmin)/Fmax-Fmin)	Therefore Pu is:	Pf	Ku= (pu/pf)	T		T in kelvin	ΔμG
8.62	8.755	0.135	3.16	0.043	0.957	0.043	0.957	0.045	66.1	273	339.1	8767.52
8.62	8.885	0.265	3.16	0.084	0.916	0.084	0.916	0.091	66.4	273	339.4	6751.80
8.62	9.013	0.393	3.16	0.125	0.875	0.125	0.875	0.142	66.7	273	339.7	5508.83
8.62	9.117	0.497	3.16	0.157	0.843	0.157	0.843	0.187	67	273	340	4742.44
8.62	9.222	0.602	3.16	0.191	0.809	0.191	0.809	0.235	67.3	273	340.3	4092.91
8.62	9.327	0.707	3.16	0.224	0.776	0.224	0.776	0.288	67.6	273	340.6	3523.10
8.62	9.427	0.807	3.16	0.256	0.744	0.256	0.744	0.343	67.9	273	340.9	3031.09
8.62	9.522	0.902	3.16	0.285	0.715	0.285	0.715	0.399	68.2	273	341.2	2605.43
8.62	9.617	0.997	3.16	0.315	0.685	0.315	0.685	0.461	68.5	273	341.5	2199.99
8.62	9.716	1.096	3.16	0.347	0.653	0.347	0.653	0.531	68.8	273	341.8	1797.03
8.62	9.818	1.198	3.16	0.379	0.621	0.379	0.621	0.611	69.1	273	342.1	1402.74
8.62	9.915	1.295	3.16	0.410	0.590	0.410	0.590	0.695	69.4	273	342.4	1037.10
8.62	10.005	1.385	3.16	0.438	0.562	0.438	0.562	0.780	69.7	273	342.7	707.10
8.62	10.098	1.478	3.16	0.468	0.532	0.468	0.532	0.879	70	273	343	368.23

Table A.8: Crocodile IgY (first transition peak) data calculated from equations 1 – 5 (Chapter 3). Second replicate.

Fmin	PfLDH IgY Fluoro data	F- F min	Fmax-Fmin	(F-Fmin)/Fmax-Fmin)	1-(F-Fmin)/Fmax-Fmin) (F-Fmin)/Fmax-Fmin)	Therefore Pu is:	Pf	Ku= (pu/pf)	T	273	T in kelvin	ΔμG
6.8	6.808	0.008	2.96	0.003	0.997	0.003	0.997	0.003	59.8	273	332.8	16526.80
6.8	6.830	0.030	2.96	0.010	0.990	0.010	0.990	0.010	60.1	273	333.1	12676.65
6.8	6.847	0.047	2.96	0.016	0.984	0.016	0.984	0.016	60.4	273	333.4	11465.02
6.8	6.875	0.075	2.96	0.025	0.975	0.025	0.975	0.026	60.7	273	333.7	10133.39
6.8	6.909	0.109	2.96	0.037	0.963	0.037	0.963	0.038	61	273	334	9063.88
6.8	6.947	0.147	2.96	0.050	0.950	0.050	0.950	0.052	61.3	273	334.3	8200.34
6.8	6.992	0.192	2.96	0.065	0.935	0.065	0.935	0.069	61.6	273	334.6	7419.59
6.8	7.048	0.248	2.96	0.084	0.916	0.084	0.916	0.091	61.9	273	334.9	6666.97
6.8	7.111	0.311	2.96	0.105	0.895	0.105	0.895	0.117	62.2	273	335.2	5974.05
6.8	7.184	0.384	2.96	0.130	0.870	0.130	0.870	0.149	62.5	273	335.5	5309.29
6.8	7.264	0.464	2.96	0.157	0.843	0.157	0.843	0.186	62.8	273	335.8	4696.00
6.8	7.354	0.554	2.96	0.187	0.813	0.187	0.813	0.230	63.1	273	336.1	4101.44
6.8	7.456	0.656	2.96	0.222	0.778	0.222	0.778	0.285	63.4	273	336.4	3512.30
6.8	7.568	0.768	2.96	0.259	0.741	0.259	0.741	0.350	63.7	273	336.7	2936.30
6.8	7.694	0.894	2.96	0.302	0.698	0.302	0.698	0.432	64	273	337	2349.04
6.8	7.831	1.031	2.96	0.348	0.652	0.348	0.652	0.535	64.3	273	337.3	1756.67
6.8	7.975	1.175	2.96	0.397	0.603	0.397	0.603	0.658	64.6	273	337.6	1173.31
6.8	8.127	1.327	2.96	0.448	0.552	0.448	0.552	0.813	64.9	273	337.9	581.93

Table A.9: Crocodile IgY (second transition peak) data calculated from equations 1 – 5 (Chapter 3). Third replicate.

Fmin	PfLDH IgY Fluoro data	F- F min	Fmax-Fmin	(F-Fmin)/Fmax-Fmin)	1-(F-Fmin)/Fmax-Fmin) (F-Fmin)/Fmax-Fmin)	Therefore Pu is:	Pf	Ku= (pu/pf)	T		T in kelvin	ΔμG
8.73	8.873	0.143	3.14	0.045	0.955	0.045	0.955	0.048	66.4	273	339.4	8589.90
8.73	9.010	0.280	3.14	0.089	0.911	0.089	0.911	0.098	66.7	273	339.7	6561.78
8.73	9.128	0.398	3.14	0.127	0.873	0.127	0.873	0.145	67	273	340	5454.75
8.73	9.244	0.514	3.14	0.164	0.836	0.164	0.836	0.196	67.3	273	340.3	4617.01
8.73	9.355	0.625	3.14	0.199	0.801	0.199	0.801	0.249	67.6	273	340.6	3942.52
8.73	9.466	0.736	3.14	0.235	0.765	0.235	0.765	0.306	67.9	273	340.9	3353.28
8.73	9.573	0.843	3.14	0.268	0.732	0.268	0.732	0.367	68.2	273	341.2	2844.63
8.73	9.671	0.941	3.14	0.300	0.700	0.300	0.700	0.428	68.5	273	341.5	2408.18
8.73	9.775	1.045	3.14	0.333	0.667	0.333	0.667	0.499	68.8	273	341.8	1976.05
8.73	9.882	1.152	3.14	0.367	0.633	0.367	0.633	0.580	69.1	273	342.1	1551.17
8.73	9.988	1.258	3.14	0.401	0.599	0.401	0.599	0.668	69.4	273	342.4	1148.40
8.73	10.098	1.368	3.14	0.436	0.564	0.436	0.564	0.772	69.7	273	342.7	736.46
8.73	10.201	1.471	3.14	0.468	0.532	0.468	0.532	0.881	70	273	343	360.52

Table A.10: Mouse IgG data calculated from equations 1 – 5 (Chapter 3). First replicate.

Fm	PfLDH IgY Fluoro data	F- F min	Fmax-Fmin	(F-Fmin)/Fmax-Fmin)	1-(F-Fmin)/Fmax-Fmin) (F-Fmin)/Fmax-Fmin)	Therefore Pu is:	Pf	Ku= (pu/pf)		T	T in kelvin	ΔGμ
5.101	5.103	0.002	2.986	0.001	0.999	0.001	0.999	0.001	273	57.4	330.4	20638.11
5.101	5.103	0.002	2.986	0.001	0.999	0.001	0.999	0.001	273	57.7	330.7	19508.61
5.101	5.103	0.002	2.986	0.001	0.999	0.001	0.999	0.001	273	58	331	19583.5
5.101	5.103	0.002	2.986	0.001	0.999	0.001	0.999	0.001	273	58.3	331.3	19706.54
5.101	5.108	0.007	2.986	0.002	0.998	0.002	0.998	0.002	273	58.6	331.6	16819.41
5.101	5.110	0.009	2.986	0.003	0.997	0.003	0.997	0.003	273	58.9	331.9	16140.01
5.101	5.108	0.007	2.986	0.002	0.998	0.002	0.998	0.002	273	59.2	332.2	16758.53
5.101	5.109	0.008	2.986	0.003	0.997	0.003	0.997	0.003	273	59.5	332.5	16253.62
5.101	5.101	0.000	2.986	0.000	1.000	0.000	1.000	0.000	273	59.8	332.8	24152.5
5.101	5.106	0.005	2.986	0.002	0.998	0.002	0.998	0.002	273	60.1	333.1	17761.85
5.101	5.109	0.008	2.986	0.003	0.997	0.003	0.997	0.003	273	60.4	333.4	16356.6
5.101	5.116	0.015	2.986	0.005	0.995	0.005	0.995	0.005	273	60.7	333.7	14757.08
5.101	5.121	0.020	2.986	0.007	0.993	0.007	0.993	0.007	273	61	334	13899.81
5.101	5.124	0.023	2.986	0.008	0.992	0.008	0.992	0.008	273	61.3	334.3	13495.53
5.101	5.125	0.024	2.986	0.008	0.992	0.008	0.992	0.008	273	61.6	334.6	13349.32
5.101	5.134	0.033	2.986	0.011	0.989	0.011	0.989	0.011	273	61.9	334.9	12551.5
5.101	5.139	0.038	2.986	0.013	0.987	0.013	0.987	0.013	273	62.2	335.2	12133.92
5.101	5.146	0.045	2.986	0.015	0.985	0.015	0.985	0.015	273	62.5	335.5	11688.54
5.101	5.146	0.045	2.986	0.015	0.985	0.015	0.985	0.015	273	62.8	335.8	11679.64
5.101	5.150	0.049	2.986	0.016	0.984	0.016	0.984	0.017	273	63.1	336.1	11456.79
5.101	5.159	0.058	2.986	0.020	0.980	0.020	0.980	0.020	273	63.4	336.4	10955.03

5.101	5.173	0.072	2.986	0.024	0.976	0.024	0.976	0.025	273	63.7	336.7	10359.52
5.101	5.186	0.085	2.986	0.029	0.971	0.029	0.971	0.029	273	64	337	9885.79
5.101	5.194	0.093	2.986	0.031	0.969	0.031	0.969	0.032	273	64.3	337.3	9638.15
5.101	5.205	0.104	2.986	0.035	0.965	0.035	0.965	0.036	273	64.6	337.6	9338.21
5.101	5.221	0.120	2.986	0.040	0.960	0.040	0.960	0.042	273	64.9	337.9	8927.16
5.101	5.239	0.138	2.986	0.046	0.954	0.046	0.954	0.048	273	65.2	338.2	8519.11
5.101	5.253	0.152	2.986	0.051	0.949	0.051	0.949	0.054	273	65.5	338.5	8232.71
5.101	5.269	0.168	2.986	0.056	0.944	0.056	0.944	0.060	273	65.8	338.8	7943.55
5.101	5.287	0.186	2.986	0.062	0.938	0.062	0.938	0.066	273	66.1	339.1	7644.59
5.101	5.306	0.205	2.986	0.069	0.931	0.069	0.931	0.074	273	66.4	339.4	7363.85
5.101	5.327	0.226	2.986	0.076	0.924	0.076	0.924	0.082	273	66.7	339.7	7072.66
5.101	5.348	0.247	2.986	0.083	0.917	0.083	0.917	0.090	273	67	340	6797.59
5.101	5.369	0.268	2.986	0.090	0.910	0.090	0.910	0.098	273	67.3	340.3	6559.88
5.101	5.402	0.301	2.986	0.101	0.899	0.101	0.899	0.112	273	67.6	340.6	6192.73
5.101	5.439	0.338	2.986	0.113	0.887	0.113	0.887	0.128	273	67.9	340.9	5830.93
5.101	5.475	0.374	2.986	0.125	0.875	0.125	0.875	0.143	273	68.2	341.2	5517.11
5.101	5.516	0.415	2.986	0.139	0.861	0.139	0.861	0.161	273	68.5	341.5	5179.17
5.101	5.563	0.462	2.986	0.155	0.845	0.155	0.845	0.183	273	68.8	341.8	4829.21
5.101	5.614	0.513	2.986	0.172	0.828	0.172	0.828	0.208	273	69.1	342.1	4471.87
5.101	5.671	0.570	2.986	0.191	0.809	0.191	0.809	0.236	273	69.4	342.4	4109.01
5.101	5.723	0.622	2.986	0.208	0.792	0.208	0.792	0.263	273	69.7	342.7	3802.04
5.101	5.775	0.674	2.986	0.226	0.774	0.226	0.774	0.291	273	70	343	3518.08
5.101	5.833	0.732	2.986	0.245	0.755	0.245	0.755	0.325	273	70.3	343.3	3209.13
5.101	5.898	0.797	2.986	0.267	0.733	0.267	0.733	0.364	273	70.6	343.6	2886.60
5.101	5.965	0.864	2.986	0.289	0.711	0.289	0.711	0.407	273	70.9	343.9	2570.57
5.101	6.029	0.928	2.986	0.311	0.689	0.311	0.689	0.451	273	71.2	344.2	2277.53
5.101	6.099	0.998	2.986	0.334	0.666	0.334	0.666	0.502	273	71.5	344.5	1974.48
5.101	6.173	1.072	2.986	0.359	0.641	0.359	0.641	0.560	273	71.8	344.8	1663.81
5.101	6.256	1.155	2.986	0.387	0.613	0.387	0.613	0.631	273	72.1	345.1	1323.34

5.101	6.338	1.237	2.986	0.414	0.586	0.414	0.586	0.708	273	72.4	345.4	993.05
5.101	6.419	1.318	2.986	0.441	0.559	0.441	0.559	0.790	273	72.7	345.7	676.85
5.101	6.506	1.405	2.986	0.471	0.529	0.471	0.529	0.889	273	73	346	338.95

Table A.11: Mouse IgG data calculated from equations 1 – 5 (Chapter 3). Second replicate.

Fm	PfLDH IgY Fluoro data	F- F min	Fmax-Fmin	(F-Fmin)/Fmax-Fmin)	1-(F-Fmin)/Fmax-Fmin) (F-Fmin)/Fmax-Fmin)	Therefore Pu is:	Pf	Ku= (pu/pf)		T	T in kelvin	ΔGμ
5.431	5.433	0.002	2.716	0.001	0.999	0.001	0.999	0.001	273	61.3	334.3	20225.53
5.431	5.434	0.003	2.716	0.001	0.999	0.001	0.999	0.001	273	61.6	334.6	18974.62
5.431	5.443	0.012	2.716	0.005	0.995	0.005	0.995	0.005	273	61.9	334.9	15024.75
5.431	5.450	0.019	2.716	0.007	0.993	0.007	0.993	0.007	273	62.2	335.2	13813.81
5.431	5.451	0.020	2.716	0.007	0.993	0.007	0.993	0.007	273	62.5	335.5	13679.52
5.431	5.458	0.027	2.716	0.010	0.990	0.010	0.990	0.010	273	62.8	335.8	12820.89
5.431	5.473	0.042	2.716	0.015	0.985	0.015	0.985	0.016	273	63.1	336.1	11603.08
5.431	5.483	0.052	2.716	0.019	0.981	0.019	0.981	0.020	273	63.4	336.4	10988.63
5.431	5.490	0.059	2.716	0.022	0.978	0.022	0.978	0.022	273	63.7	336.7	10644.62
5.431	5.496	0.065	2.716	0.024	0.976	0.024	0.976	0.025	273	64	337	10370.96
5.431	5.509	0.078	2.716	0.029	0.971	0.029	0.971	0.029	273	64.3	337.3	9883.54
5.431	5.526	0.095	2.716	0.035	0.965	0.035	0.965	0.036	273	64.6	337.6	9311.31
5.431	5.535	0.104	2.716	0.038	0.962	0.038	0.962	0.040	273	64.9	337.9	9061.43
5.431	5.548	0.117	2.716	0.043	0.957	0.043	0.957	0.045	273	65.2	338.2	8729.47
5.431	5.568	0.137	2.716	0.050	0.950	0.050	0.950	0.053	273	65.5	338.5	8265.57
5.431	5.584	0.153	2.716	0.056	0.944	0.056	0.944	0.060	273	65.8	338.8	7940.90
5.431	5.609	0.178	2.716	0.066	0.934	0.066	0.934	0.070	273	66.1	339.1	7484.58

5.431	5.628	0.197	2.716	0.072	0.928	0.072	0.928	0.078	273	66.4	339.4	7195.66
5.431	5.652	0.221	2.716	0.081	0.919	0.081	0.919	0.089	273	66.7	339.7	6841.96
5.431	5.680	0.249	2.716	0.091	0.909	0.091	0.909	0.101	273	67	340	6489.65
5.431	5.711	0.280	2.716	0.103	0.897	0.103	0.897	0.115	273	67.3	340.3	6116.95
5.431	5.742	0.311	2.716	0.115	0.885	0.115	0.885	0.129	273	67.6	340.6	5791.37
5.431	5.785	0.354	2.716	0.130	0.870	0.130	0.870	0.150	273	67.9	340.9	5379.74
5.431	5.821	0.390	2.716	0.144	0.856	0.144	0.856	0.168	273	68.2	341.2	5067.16
5.431	5.865	0.434	2.716	0.160	0.840	0.160	0.840	0.190	273	68.5	341.5	4716.06
5.431	5.911	0.480	2.716	0.177	0.823	0.177	0.823	0.215	273	68.8	341.8	4373.13
5.431	5.966	0.535	2.716	0.197	0.803	0.197	0.803	0.245	273	69.1	342.1	3998.96
5.431	6.020	0.589	2.716	0.217	0.783	0.217	0.783	0.277	273	69.4	342.4	3655.40
5.431	6.078	0.647	2.716	0.238	0.762	0.238	0.762	0.313	273	69.7	342.7	3313.92
5.431	6.135	0.704	2.716	0.259	0.741	0.259	0.741	0.350	273	70	343	2993.60
5.431	6.196	0.765	2.716	0.282	0.718	0.282	0.718	0.392	273	70.3	343.3	2671.90
5.431	6.265	0.834	2.716	0.307	0.693	0.307	0.693	0.443	273	70.6	343.6	2327.19
5.431	6.331	0.900	2.716	0.331	0.669	0.331	0.669	0.496	273	70.9	343.9	2006.99
5.431	6.395	0.964	2.716	0.355	0.645	0.355	0.645	0.550	273	71.2	344.2	1710.61
5.431	6.465	1.034	2.716	0.381	0.619	0.381	0.619	0.615	273	71.5	344.5	1392.72
5.431	6.539	1.108	2.716	0.408	0.592	0.408	0.592	0.689	273	71.8	344.8	1069.48
5.431	6.617	1.186	2.716	0.437	0.563	0.437	0.563	0.775	273	72.1	345.1	730.46
5.431	6.706	1.275	2.716	0.469	0.531	0.469	0.531	0.885	273	72.4	345.4	351.59

Table A.12: Mouse IgG data calculated from equations 1 – 5 (Chapter 3). Third replicate.

Fm	PfLDH IgY Fluoro data	F- F min	Fmax-Fmin	(F-Fmin)/Fmax-Fmin)	1-(F-Fmin)/Fmax-Fmin) (F-Fmin)/Fmax-Fmin)	Therefore Pu is:	Pf	Ku= (pu/pf)		T	T in kelvin	ΔGμ
5.264	5.264	0.000	3.014	0.000	1.000	0.000	1.000	0.000	273	61.3	334.3	29995.51
5.264	5.269	0.005	3.014	0.002	0.998	0.002	0.998	0.002	273	61.6	334.6	17934.12
5.264	5.275	0.011	3.014	0.004	0.996	0.004	0.996	0.004	273	61.9	334.9	15596.90
5.264	5.279	0.015	3.014	0.005	0.995	0.005	0.995	0.005	273	62.2	335.2	14812.40
5.264	5.290	0.026	3.014	0.009	0.991	0.009	0.991	0.009	273	62.5	335.5	13261.40
5.264	5.297	0.033	3.014	0.011	0.989	0.011	0.989	0.011	273	62.8	335.8	12576.95
5.264	5.301	0.037	3.014	0.012	0.988	0.012	0.988	0.012	273	63.1	336.1	12289.45
5.264	5.310	0.046	3.014	0.015	0.985	0.015	0.985	0.015	273	63.4	336.4	11675.51
5.264	5.315	0.051	3.014	0.017	0.983	0.017	0.983	0.017	273	63.7	336.7	11345.71
5.264	5.326	0.062	3.014	0.020	0.980	0.020	0.980	0.021	273	64	337	10837.75
5.264	5.336	0.072	3.014	0.024	0.976	0.024	0.976	0.024	273	64.3	337.3	10419.54
5.264	5.345	0.081	3.014	0.027	0.973	0.027	0.973	0.028	273	64.6	337.6	10084.07
5.264	5.359	0.095	3.014	0.031	0.969	0.031	0.969	0.033	273	64.9	337.9	9625.64
5.264	5.376	0.112	3.014	0.037	0.963	0.037	0.963	0.039	273	65.2	338.2	9142.06
5.264	5.390	0.126	3.014	0.042	0.958	0.042	0.958	0.044	273	65.5	338.5	8808.36
5.264	5.411	0.147	3.014	0.049	0.951	0.049	0.951	0.051	273	65.8	338.8	8364.85
5.264	5.432	0.168	3.014	0.056	0.944	0.056	0.944	0.059	273	66.1	339.1	7980.64
5.264	5.454	0.190	3.014	0.063	0.937	0.063	0.937	0.067	273	66.4	339.4	7616.73
5.264	5.477	0.213	3.014	0.071	0.929	0.071	0.929	0.076	273	66.7	339.7	7280.82
5.264	5.502	0.238	3.014	0.079	0.921	0.079	0.921	0.086	273	67	340	6942.11
5.264	5.532	0.268	3.014	0.089	0.911	0.089	0.911	0.098	273	67.3	340.3	6586.75

5.264	5.568	0.304	3.014	0.101	0.899	0.101	0.899	0.112	273	67.6	340.6	6196.90
5.264	5.603	0.339	3.014	0.113	0.887	0.113	0.887	0.127	273	67.9	340.9	5851.51
5.264	5.638	0.374	3.014	0.124	0.876	0.124	0.876	0.142	273	68.2	341.2	5540.51
5.264	5.682	0.418	3.014	0.139	0.861	0.139	0.861	0.161	273	68.5	341.5	5183.98
5.264	5.731	0.467	3.014	0.155	0.845	0.155	0.845	0.184	273	68.8	341.8	4818.54
5.264	5.785	0.521	3.014	0.173	0.827	0.173	0.827	0.209	273	69.1	342.1	4456.34
5.264	5.831	0.567	3.014	0.188	0.812	0.188	0.812	0.232	273	69.4	342.4	4161.37
5.264	5.884	0.620	3.014	0.206	0.794	0.206	0.794	0.259	273	69.7	342.7	3850.92
5.264	5.938	0.674	3.014	0.224	0.776	0.224	0.776	0.288	273	70	343	3549.87
5.264	6.002	0.738	3.014	0.245	0.755	0.245	0.755	0.325	273	70.3	343.3	3212.56
5.264	6.067	0.803	3.014	0.266	0.734	0.266	0.734	0.363	273	70.6	343.6	2892.84
5.264	6.134	0.870	3.014	0.289	0.711	0.289	0.711	0.406	273	70.9	343.9	2580.62
5.264	6.199	0.935	3.014	0.310	0.690	0.310	0.690	0.449	273	71.2	344.2	2288.58
5.264	6.276	1.012	3.014	0.336	0.664	0.336	0.664	0.506	273	71.5	344.5	1952.86
5.264	6.349	1.085	3.014	0.360	0.640	0.360	0.640	0.562	273	71.8	344.8	1650.48
5.264	6.430	1.166	3.014	0.387	0.613	0.387	0.613	0.631	273	72.1	345.1	1320.82
5.264	6.511	1.247	3.014	0.414	0.586	0.414	0.586	0.706	273	72.4	345.4	1001.21
5.264	6.597	1.333	3.014	0.442	0.558	0.442	0.558	0.793	273	72.7	345.7	665.28
5.264	6.682	1.418	3.014	0.470	0.530	0.470	0.530	0.888	273	73	346	340.44

Table A.13: Rabbit IgG data calculated from equations 1 – 5 (Chapter 3). First replicate.

Fm	PfLDH IgY Fluoro data	F- F min	Fmax-Fmin	(F-Fmin)/Fmax-Fmin)	1-(F-Fmin)/Fmax-Fmin) (F-Fmin)/Fmax-Fmin)	Therefore Pu is:	Pf	Ku= (pu/pf)		T	T in Kelvin	ΔμG
5.44	5.452	0.012	3.52	0.003	0.997	0.003	0.997	0.004	273	63.7	336.7	15828.71
5.44	5.456	0.016	3.52	0.004	0.996	0.004	0.996	0.005	273	64	337	15137.12
5.44	5.468	0.028	3.52	0.008	0.992	0.008	0.992	0.008	273	64.3	337.3	13494.28
5.44	5.485	0.045	3.52	0.013	0.987	0.013	0.987	0.013	273	64.6	337.6	12212.83
5.44	5.498	0.058	3.52	0.016	0.984	0.016	0.984	0.017	273	64.9	337.9	11490.41
5.44	5.518	0.078	3.52	0.022	0.978	0.022	0.978	0.023	273	65.2	338.2	10663.51
5.44	5.532	0.092	3.52	0.026	0.974	0.026	0.974	0.027	273	65.5	338.5	10196.26
5.44	5.547	0.107	3.52	0.030	0.970	0.030	0.970	0.031	273	65.8	338.8	9760.72
5.44	5.574	0.134	3.52	0.038	0.962	0.038	0.962	0.040	273	66.1	339.1	9101.36
5.44	5.593	0.153	3.52	0.043	0.957	0.043	0.957	0.045	273	66.4	339.4	8723.59
5.44	5.624	0.184	3.52	0.052	0.948	0.052	0.948	0.055	273	66.7	339.7	8181.59
5.44	5.651	0.211	3.52	0.060	0.940	0.060	0.940	0.064	273	67	340	7784.43
5.44	5.680	0.240	3.52	0.068	0.932	0.068	0.932	0.073	273	67.3	340.3	7394.98
5.44	5.714	0.274	3.52	0.078	0.922	0.078	0.922	0.084	273	67.6	340.6	7004.67
5.44	5.754	0.314	3.52	0.089	0.911	0.089	0.911	0.098	273	67.9	340.9	6586.29
5.44	5.791	0.351	3.52	0.100	0.900	0.100	0.900	0.111	273	68.2	341.2	6244.27
5.44	5.833	0.393	3.52	0.112	0.888	0.112	0.888	0.126	273	68.5	341.5	5885.27
5.44	5.875	0.435	3.52	0.124	0.876	0.124	0.876	0.141	273	68.8	341.8	5565.73
5.44	5.931	0.491	3.52	0.140	0.860	0.140	0.860	0.162	273	69.1	342.1	5174.01
5.44	5.983	0.543	3.52	0.154	0.846	0.154	0.846	0.182	273	69.4	342.4	4846.52
5.44	6.040	0.600	3.52	0.171	0.829	0.171	0.829	0.206	273	69.7	342.7	4508.05

5.44	6.099	0.659	3.52	0.187	0.813	0.187	0.813	0.230	273	70	343	4185.45
5.44	6.162	0.722	3.52	0.205	0.795	0.205	0.795	0.258	273	70.3	343.3	3869.22
5.44	6.236	0.796	3.52	0.226	0.774	0.226	0.774	0.292	273	70.6	343.6	3512.66
5.44	6.311	0.871	3.52	0.248	0.752	0.248	0.752	0.329	273	70.9	343.9	3179.23
5.44	6.383	0.943	3.52	0.268	0.732	0.268	0.732	0.366	273	71.2	344.2	2877.04
5.44	6.464	1.024	3.52	0.291	0.709	0.291	0.709	0.411	273	71.5	344.5	2550.48
5.44	6.546	1.106	3.52	0.314	0.686	0.314	0.686	0.458	273	71.8	344.8	2236.35
5.44	6.634	1.194	3.52	0.339	0.661	0.339	0.661	0.514	273	72.1	345.1	1911.96
5.44	6.729	1.289	3.52	0.366	0.634	0.366	0.634	0.578	273	72.4	345.4	1574.98
5.44	6.821	1.381	3.52	0.392	0.608	0.392	0.608	0.646	273	72.7	345.7	1257.87
5.44	6.911	1.471	3.52	0.418	0.582	0.418	0.582	0.718	273	73	346	953.36
5.44	7.002	1.562	3.52	0.444	0.556	0.444	0.556	0.798	273	73.3	346.3	651.20
5.44	7.095	1.655	3.52	0.470	0.530	0.470	0.530	0.887	273	73.6	346.6	345.02

Table A.14: Rabbit IgG data calculated from equations 1 – 5 (Chapter 3). Second replicate.

Fm	PfLDH IgY Fluoro data	F- F min	Fmax-Fmin	(F-Fmin)/Fmax-Fmin)	1-(F-Fmin)/Fmax-Fmin) (F-Fmin)/Fmax-Fmin)	Therefore Pu is:	Pf	Ku= (pu/pf)		T	T in Kelvin	ΔμG
5.74	5.742	0.002	3.54	0.001	0.999	0.001	0.999	0.001	273	60.7	333.7	20409.65
5.74	5.744	0.004	3.54	0.001	0.999	0.001	0.999	0.001	273	61	334	19053.42
5.74	5.747	0.007	3.54	0.002	0.998	0.002	0.998	0.002	273	61.3	334.3	17479.49
5.74	5.754	0.014	3.54	0.004	0.996	0.004	0.996	0.004	273	61.6	334.6	15481.57
5.74	5.764	0.024	3.54	0.007	0.993	0.007	0.993	0.007	273	61.9	334.9	13914.51
5.74	5.774	0.034	3.54	0.010	0.990	0.010	0.990	0.010	273	62.2	335.2	12939.39
5.74	5.775	0.035	3.54	0.010	0.990	0.010	0.990	0.010	273	62.5	335.5	12887.80
5.74	5.781	0.041	3.54	0.011	0.989	0.011	0.989	0.012	273	62.8	335.8	12450.21
5.74	5.790	0.050	3.54	0.014	0.986	0.014	0.986	0.014	273	63.1	336.1	11890.28
5.74	5.793	0.053	3.54	0.015	0.985	0.015	0.985	0.015	273	63.4	336.4	11726.52
5.74	5.798	0.058	3.54	0.016	0.984	0.016	0.984	0.017	273	63.7	336.7	11478.52
5.74	5.804	0.064	3.54	0.018	0.982	0.018	0.982	0.019	273	64	337	11178.54
5.74	5.814	0.074	3.54	0.021	0.979	0.021	0.979	0.021	273	64.3	337.3	10798.25
5.74	5.827	0.087	3.54	0.025	0.975	0.025	0.975	0.025	273	64.6	337.6	10327.69
5.74	5.840	0.100	3.54	0.028	0.972	0.028	0.972	0.029	273	64.9	337.9	9929.60
5.74	5.857	0.117	3.54	0.033	0.967	0.033	0.967	0.034	273	65.2	338.2	9499.54
5.74	5.876	0.136	3.54	0.038	0.962	0.038	0.962	0.040	273	65.5	338.5	9069.67
5.74	5.897	0.157	3.54	0.044	0.956	0.044	0.956	0.046	273	65.8	338.8	8649.49
5.74	5.915	0.175	3.54	0.049	0.951	0.049	0.951	0.052	273	66.1	339.1	8337.94

5.74	5.941	0.201	3.54	0.057	0.943	0.057	0.943	0.060	273	66.4	339.4	7933.63
5.74	5.967	0.227	3.54	0.064	0.936	0.064	0.936	0.068	273	66.7	339.7	7573.41
5.74	5.993	0.253	3.54	0.071	0.929	0.071	0.929	0.077	273	67	340	7253.92
5.74	6.016	0.276	3.54	0.078	0.922	0.078	0.922	0.084	273	67.3	340.3	6994.51
5.74	6.052	0.312	3.54	0.088	0.912	0.088	0.912	0.097	273	67.6	340.6	6613.91
5.74	6.083	0.343	3.54	0.097	0.903	0.097	0.903	0.107	273	67.9	340.9	6322.93
5.74	6.123	0.383	3.54	0.108	0.892	0.108	0.892	0.121	273	68.2	341.2	5987.75
5.74	6.166	0.426	3.54	0.120	0.880	0.120	0.880	0.137	273	68.5	341.5	5651.71
5.74	6.212	0.472	3.54	0.133	0.867	0.133	0.867	0.154	273	68.8	341.8	5319.69
5.74	6.263	0.523	3.54	0.148	0.852	0.148	0.852	0.173	273	69.1	342.1	4985.08
5.74	6.325	0.585	3.54	0.165	0.835	0.165	0.835	0.198	273	69.4	342.4	4613.96
5.74	6.376	0.636	3.54	0.180	0.820	0.180	0.820	0.219	273	69.7	342.7	4328.08
5.74	6.441	0.701	3.54	0.198	0.802	0.198	0.802	0.247	273	70	343	3990.74
5.74	6.507	0.767	3.54	0.217	0.783	0.217	0.783	0.277	273	70.3	343.3	3667.46
5.74	6.571	0.831	3.54	0.235	0.765	0.235	0.765	0.307	273	70.6	343.6	3374.10
5.74	6.648	0.908	3.54	0.256	0.744	0.256	0.744	0.345	273	70.9	343.9	3045.12
5.74	6.724	0.984	3.54	0.278	0.722	0.278	0.722	0.385	273	71.2	344.2	2733.41
5.74	6.797	1.057	3.54	0.299	0.701	0.299	0.701	0.426	273	71.5	344.5	2446.30
5.74	6.878	1.138	3.54	0.321	0.679	0.321	0.679	0.474	273	71.8	344.8	2142.56
5.74	6.961	1.221	3.54	0.345	0.655	0.345	0.655	0.527	273	72.1	345.1	1839.75
5.74	7.049	1.309	3.54	0.370	0.630	0.370	0.630	0.587	273	72.4	345.4	1532.13
5.74	7.139	1.399	3.54	0.395	0.605	0.395	0.605	0.653	273	72.7	345.7	1224.70
5.74	7.224	1.484	3.54	0.419	0.581	0.419	0.581	0.722	273	73	346	936.97
5.74	7.311	1.571	3.54	0.444	0.556	0.444	0.556	0.798	273	73.3	346.3	651.05
5.74	7.407	1.667	3.54	0.471	0.529	0.471	0.529	0.890	273	73.6	346.6	335.03

Table A.15: Rabbit IgG data calculated from equations 1 – 5 (Chapter 3). Third replicate.

Fm	PfLDH IgY Fluoro data	F- F min	Fmax- Fmin	(F- Fmin)/Fmax- Fmin)	1-(F- Fmin)/Fmax- Fmin) (F- Fmin)/Fmax- Fmin)	Therefore Pu is:	Pf	Ku= (pu/pf)		T	T in Kelvin	ΔμG
5.75	5.756	0.006	3.18	0.002	0.998	0.002	0.998	0.002	273	60.7	333.7	17632.25
5.75	5.756	0.006	3.18	0.002	0.998	0.002	0.998	0.002	273	61	334	17525.28
5.75	5.764	0.014	3.18	0.004	0.996	0.004	0.996	0.004	273	61.3	334.3	15151.17
5.75	5.766	0.016	3.18	0.005	0.995	0.005	0.995	0.005	273	61.6	334.6	14703.43
5.75	5.772	0.022	3.18	0.007	0.993	0.007	0.993	0.007	273	61.9	334.9	13831.49
5.75	5.781	0.031	3.18	0.010	0.990	0.010	0.990	0.010	273	62.2	335.2	12907.33
5.75	5.783	0.033	3.18	0.010	0.990	0.010	0.990	0.010	273	62.5	335.5	12721.49
5.75	5.789	0.039	3.18	0.012	0.988	0.012	0.988	0.012	273	62.8	335.8	12274.51
5.75	5.793	0.043	3.18	0.014	0.986	0.014	0.986	0.014	273	63.1	336.1	11985.81
5.75	5.799	0.049	3.18	0.015	0.985	0.015	0.985	0.016	273	63.4	336.4	11629.60
5.75	5.802	0.052	3.18	0.016	0.984	0.016	0.984	0.017	273	63.7	336.7	11463.10
5.75	5.811	0.061	3.18	0.019	0.981	0.019	0.981	0.020	273	64	337	11019.13
5.75	5.820	0.070	3.18	0.022	0.978	0.022	0.978	0.023	273	64.3	337.3	10628.54
5.75	5.830	0.080	3.18	0.025	0.975	0.025	0.975	0.026	273	64.6	337.6	10257.72
5.75	5.846	0.096	3.18	0.030	0.970	0.030	0.970	0.031	273	64.9	337.9	9755.56
5.75	5.861	0.111	3.18	0.035	0.965	0.035	0.965	0.036	273	65.2	338.2	9347.88
5.75	5.871	0.121	3.18	0.038	0.962	0.038	0.962	0.040	273	65.5	338.5	9080.29
5.75	5.885	0.135	3.18	0.043	0.957	0.043	0.957	0.044	273	65.8	338.8	8769.49
5.75	5.903	0.153	3.18	0.048	0.952	0.048	0.952	0.050	273	66.1	339.1	8420.43
5.75	5.922	0.172	3.18	0.054	0.946	0.054	0.946	0.057	273	66.4	339.4	8082.70

5.75	5.950	0.200	3.18	0.063	0.937	0.063	0.937	0.067	273	66.7	339.7	7637.07
5.75	5.967	0.217	3.18	0.068	0.932	0.068	0.932	0.073	273	67	340	7387.80
5.75	5.995	0.245	3.18	0.077	0.923	0.077	0.923	0.083	273	67.3	340.3	7029.90
5.75	6.029	0.279	3.18	0.088	0.912	0.088	0.912	0.096	273	67.6	340.6	6626.99
5.75	6.066	0.316	3.18	0.099	0.901	0.099	0.901	0.110	273	67.9	340.9	6249.18
5.75	6.104	0.354	3.18	0.111	0.889	0.111	0.889	0.125	273	68.2	341.2	5892.34
5.75	6.145	0.395	3.18	0.124	0.876	0.124	0.876	0.142	273	68.5	341.5	5545.69
5.75	6.181	0.431	3.18	0.135	0.865	0.135	0.865	0.157	273	68.8	341.8	5268.82
5.75	6.224	0.474	3.18	0.149	0.851	0.149	0.851	0.175	273	69.1	342.1	4952.57
5.75	6.263	0.513	3.18	0.161	0.839	0.161	0.839	0.193	273	69.4	342.4	4690.98
5.75	6.309	0.559	3.18	0.176	0.824	0.176	0.824	0.213	273	69.7	342.7	4401.65
5.75	6.359	0.609	3.18	0.192	0.808	0.192	0.808	0.237	273	70	343	4106.04
5.75	6.413	0.663	3.18	0.209	0.791	0.209	0.791	0.263	273	70.3	343.3	3807.27
5.75	6.471	0.721	3.18	0.227	0.773	0.227	0.773	0.293	273	70.6	343.6	3503.69
5.75	6.542	0.792	3.18	0.249	0.751	0.249	0.751	0.332	273	70.9	343.9	3156.37
5.75	6.610	0.860	3.18	0.270	0.730	0.270	0.730	0.371	273	71.2	344.2	2841.40
5.75	6.691	0.941	3.18	0.296	0.704	0.296	0.704	0.420	273	71.5	344.5	2483.32
5.75	6.767	1.017	3.18	0.320	0.680	0.320	0.680	0.470	273	71.8	344.8	2164.64
5.75	6.843	1.093	3.18	0.344	0.656	0.344	0.656	0.524	273	72.1	345.1	1855.33
5.75	6.926	1.176	3.18	0.370	0.630	0.370	0.630	0.587	273	72.4	345.4	1529.07
5.75	7.010	1.260	3.18	0.396	0.604	0.396	0.604	0.656	273	72.7	345.7	1211.05
5.75	7.089	1.339	3.18	0.421	0.579	0.421	0.579	0.728	273	73	346	914.28
5.75	7.166	1.416	3.18	0.445	0.555	0.445	0.555	0.803	273	73.3	346.3	631.67
5.75	7.251	1.501	3.18	0.472	0.528	0.472	0.528	0.894	273	73.6	346.6	322.48

Table A.16: Chicken IgY data calculated from equations 1 – 5 (Chapter 3). First replicate.

Fmin	PfLDH IgY Fluoro data	F- F min	Fmax-Fmin	(F-Fmin)/Fmax-Fmin)	1-(F-Fmin)/Fmax-Fmin) (F-Fmin)/Fmax-Fmin)	Therefore Pu is:	Pf	Ku= (pu/pf)	T		T in kelvin	ΔGμ
9.37	9.401	0.031	19.5	0.002	0.998	0.002	0.998	0.002	62.2	273	335.2	17995.27
9.37	9.421	0.051	19.5	0.003	0.997	0.003	0.997	0.003	62.5	273	335.5	16595.49
9.37	9.438	0.068	19.5	0.003	0.997	0.003	0.997	0.003	62.8	273	335.8	15806.05
9.37	9.438	0.068	19.5	0.003	0.997	0.003	0.997	0.004	63.1	273	336.1	15800.20
9.37	9.447	0.077	19.5	0.004	0.996	0.004	0.996	0.004	63.4	273	336.4	15464.12
9.37	9.483	0.113	19.5	0.006	0.994	0.006	0.994	0.006	63.7	273	336.7	14407.64
9.37	9.540	0.170	19.5	0.009	0.991	0.009	0.991	0.009	64	273	337	13268.15
9.37	9.559	0.189	19.5	0.010	0.990	0.010	0.990	0.010	64.3	273	337.3	12983.31
9.37	9.588	0.218	19.5	0.011	0.989	0.011	0.989	0.011	64.6	273	337.6	12584.07
9.37	9.620	0.250	19.5	0.013	0.987	0.013	0.987	0.013	64.9	273	337.9	12205.67
9.37	9.690	0.320	19.5	0.016	0.984	0.016	0.984	0.017	65.2	273	338.2	11506.95
9.37	9.747	0.377	19.5	0.019	0.981	0.019	0.981	0.020	65.5	273	338.5	11048.33
9.37	9.815	0.445	19.5	0.023	0.977	0.023	0.977	0.023	65.8	273	338.8	10581.70
9.37	9.879	0.509	19.5	0.026	0.974	0.026	0.974	0.027	66.1	273	339.1	10205.95
9.37	9.956	0.586	19.5	0.030	0.970	0.030	0.970	0.031	66.4	273	339.4	9804.58
9.37	10.054	0.684	19.5	0.035	0.965	0.035	0.965	0.036	66.7	273	339.7	9362.35
9.37	10.165	0.795	19.5	0.041	0.959	0.041	0.959	0.042	67	273	340	8930.28
9.37	10.271	0.901	19.5	0.046	0.954	0.046	0.954	0.048	67.3	273	340.3	8564.89
9.37	10.389	1.019	19.5	0.052	0.948	0.052	0.948	0.055	67.6	273	340.6	8205.98
9.37	10.541	1.171	19.5	0.060	0.940	0.060	0.940	0.064	67.9	273	340.9	7795.89
9.37	10.721	1.351	19.5	0.069	0.931	0.069	0.931	0.074	68.2	273	341.2	7369.27

9.37	10.912	1.542	19.5	0.079	0.921	0.079	0.921	0.086	68.5	273	341.5	6970.61
9.37	11.133	1.763	19.5	0.090	0.910	0.090	0.910	0.099	68.8	273	341.8	6561.05
9.37	11.380	2.010	19.5	0.103	0.897	0.103	0.897	0.115	69.1	273	342.1	6154.68
9.37	11.629	2.259	19.5	0.116	0.884	0.116	0.884	0.131	69.4	273	342.4	5786.90
9.37	11.940	2.570	19.5	0.132	0.868	0.132	0.868	0.152	69.7	273	342.7	5371.51
9.37	12.276	2.906	19.5	0.149	0.851	0.149	0.851	0.175	70	273	343	4968.97
9.37	12.664	3.294	19.5	0.169	0.831	0.169	0.831	0.203	70.3	273	343.3	4547.67
9.37	13.056	3.686	19.5	0.189	0.811	0.189	0.811	0.233	70.6	273	343.6	4161.13
9.37	13.477	4.107	19.5	0.211	0.789	0.211	0.789	0.267	70.9	273	343.9	3778.32
9.37	13.975	4.605	19.5	0.236	0.764	0.236	0.764	0.309	71.2	273	344.2	3359.37
9.37	14.487	5.117	19.5	0.262	0.738	0.262	0.738	0.356	71.5	273	344.5	2960.62
9.37	15.074	5.704	19.5	0.293	0.707	0.293	0.707	0.413	71.8	273	344.8	2532.08
9.37	15.650	6.280	19.5	0.322	0.678	0.322	0.678	0.475	72.1	273	345.1	2136.04
9.37	16.286	6.916	19.5	0.355	0.645	0.355	0.645	0.550	72.4	273	345.4	1719.30
9.37	16.939	7.569	19.5	0.388	0.612	0.388	0.612	0.634	72.7	273	345.7	1308.42
9.37	17.647	8.277	19.5	0.424	0.576	0.424	0.576	0.738	73	273	346	875.79
9.37	18.361	8.991	19.5	0.461	0.539	0.461	0.539	0.856	73.3	273	346.3	449.35

Table A.17: Chicken IgY data calculated from equations 1 – 5 (Chapter 3). Second replicate.

Fmin	PfLDH IgY Fluoro data	F- F min	Fmax-Fmin	(F-Fmin)/Fmax-Fmin)	1-(F-Fmin)/Fmax-Fmin) (F-Fmin)/Fmax-Fmin)	Therefore Pu is:	Pf	Ku= (pu/pf)	T	273	T in kelvin	ΔGμ
9.53	9.548	0.018	20.2	0.001	0.999	0.001	0.999	0.001	62.2	273	335.2	19599.96
9.53	9.571	0.041	20.2	0.002	0.998	0.002	0.998	0.002	62.5	273	335.5	17263.14
9.53	9.581	0.051	20.2	0.003	0.997	0.003	0.997	0.003	62.8	273	335.8	16683.62
9.53	9.595	0.065	20.2	0.003	0.997	0.003	0.997	0.003	63.1	273	336.1	16035.19
9.53	9.600	0.070	20.2	0.003	0.997	0.003	0.997	0.003	63.4	273	336.4	15849.90
9.53	9.631	0.101	20.2	0.005	0.995	0.005	0.995	0.005	63.7	273	336.7	14830.50
9.53	9.663	0.133	20.2	0.007	0.993	0.007	0.993	0.007	64	273	337	14050.04
9.53	9.698	0.168	20.2	0.008	0.992	0.008	0.992	0.008	64.3	273	337.3	13404.81
9.53	9.741	0.211	20.2	0.010	0.990	0.010	0.990	0.011	64.6	273	337.6	12771.38
9.53	9.781	0.251	20.2	0.012	0.988	0.012	0.988	0.013	64.9	273	337.9	12294.20
9.53	9.827	0.297	20.2	0.015	0.985	0.015	0.985	0.015	65.2	273	338.2	11827.09
9.53	9.898	0.368	20.2	0.018	0.982	0.018	0.982	0.019	65.5	273	338.5	11222.87
9.53	9.962	0.432	20.2	0.021	0.979	0.021	0.979	0.022	65.8	273	338.8	10774.15
9.53	10.041	0.511	20.2	0.025	0.975	0.025	0.975	0.026	66.1	273	339.1	10297.03
9.53	10.111	0.581	20.2	0.029	0.971	0.029	0.971	0.030	66.4	273	339.4	9931.03
9.53	10.200	0.670	20.2	0.033	0.967	0.033	0.967	0.034	66.7	273	339.7	9524.37
9.53	10.306	0.776	20.2	0.038	0.962	0.038	0.962	0.040	67	273	340	9105.01
9.53	10.419	0.889	20.2	0.044	0.956	0.044	0.956	0.046	67.3	273	340.3	8709.33
9.53	10.548	1.018	20.2	0.050	0.950	0.050	0.950	0.053	67.6	273	340.6	8315.97
9.53	10.706	1.176	20.2	0.058	0.942	0.058	0.942	0.062	67.9	273	340.9	7891.38

9.53	10.889	1.359	20.2	0.067	0.933	0.067	0.933	0.072	68.2	273	341.2	7459.16
9.53	11.105	1.575	20.2	0.078	0.922	0.078	0.922	0.085	68.5	273	341.5	7013.71
9.53	11.329	1.799	20.2	0.089	0.911	0.089	0.911	0.098	68.8	273	341.8	6608.48
9.53	11.548	2.018	20.2	0.100	0.900	0.100	0.900	0.111	69.1	273	342.1	6252.90
9.53	11.815	2.285	20.2	0.113	0.887	0.113	0.887	0.128	69.4	273	342.4	5863.04
9.53	12.121	2.591	20.2	0.128	0.872	0.128	0.872	0.147	69.7	273	342.7	5460.51
9.53	12.488	2.958	20.2	0.146	0.854	0.146	0.854	0.172	70	273	343	5027.80
9.53	12.860	3.330	20.2	0.165	0.835	0.165	0.835	0.197	70.3	273	343.3	4631.40
9.53	13.278	3.748	20.2	0.186	0.814	0.186	0.814	0.228	70.6	273	343.6	4226.58
9.53	13.738	4.208	20.2	0.208	0.792	0.208	0.792	0.263	70.9	273	343.9	3817.65
9.53	14.243	4.713	20.2	0.233	0.767	0.233	0.767	0.304	71.2	273	344.2	3404.90
9.53	14.790	5.260	20.2	0.260	0.740	0.260	0.740	0.352	71.5	273	344.5	2989.99
9.53	15.394	5.864	20.2	0.290	0.710	0.290	0.710	0.409	71.8	273	344.8	2562.99
9.53	16.022	6.492	20.2	0.321	0.679	0.321	0.679	0.474	72.1	273	345.1	2144.72
9.53	16.689	7.159	20.2	0.354	0.646	0.354	0.646	0.549	72.4	273	345.4	1722.64
9.53	17.375	7.845	20.2	0.388	0.612	0.388	0.612	0.635	72.7	273	345.7	1305.65
9.53	18.120	8.590	20.2	0.425	0.575	0.425	0.575	0.740	73	273	346	866.63
9.53	18.864	9.334	20.2	0.462	0.538	0.462	0.538	0.859	73.3	273	346.3	437.51

Table A. 18: Chicken IgY data calculated from equations 1 – 5 (Chapter 3). Third replicate.

Fmin	PfLDH IgY Fluoro data	F- F min	Fmax-Fmin	(F-Fmin)/Fmax-Fmin)	1-(F-Fmin)/Fmax-Fmin) (F-Fmin)/Fmax-Fmin)	Therefore Pu is:	Pf	Ku= (pu/pf)	T		T in kelvin	ΔGμ
11.13	11.152	0.022	19.4	0.001	0.999	0.001	0.999	0.001	63.1	273	336.1	18902.25
11.13	11.181	0.051	19.4	0.003	0.997	0.003	0.997	0.003	63.4	273	336.4	16614.64
11.13	11.230	0.100	19.4	0.005	0.995	0.005	0.995	0.005	63.7	273	336.7	14719.80
11.13	11.252	0.122	19.4	0.006	0.994	0.006	0.994	0.006	64	273	337	14197.38
11.13	11.253	0.123	19.4	0.006	0.994	0.006	0.994	0.006	64.3	273	337.3	14178.97
11.13	11.275	0.145	19.4	0.007	0.993	0.007	0.993	0.008	64.6	273	337.6	13715.68
11.13	11.296	0.166	19.4	0.009	0.991	0.009	0.991	0.009	64.9	273	337.9	13347.54
11.13	11.356	0.226	19.4	0.012	0.988	0.012	0.988	0.012	65.2	273	338.2	12483.13
11.13	11.398	0.268	19.4	0.014	0.986	0.014	0.986	0.014	65.5	273	338.5	12013.85
11.13	11.460	0.330	19.4	0.017	0.983	0.017	0.983	0.017	65.8	273	338.8	11431.31
11.13	11.530	0.400	19.4	0.021	0.979	0.021	0.979	0.021	66.1	273	339.1	10887.30
11.13	11.609	0.479	19.4	0.025	0.975	0.025	0.975	0.025	66.4	273	339.4	10376.75
11.13	11.692	0.562	19.4	0.029	0.971	0.029	0.971	0.030	66.7	273	339.7	9921.81
11.13	11.765	0.635	19.4	0.033	0.967	0.033	0.967	0.034	67	273	340	9570.68
11.13	11.895	0.765	19.4	0.039	0.961	0.039	0.961	0.041	67.3	273	340.3	9033.02
11.13	12.030	0.900	19.4	0.046	0.954	0.046	0.954	0.049	67.6	273	340.6	8563.31
11.13	12.202	1.072	19.4	0.055	0.945	0.055	0.945	0.058	67.9	273	340.9	8047.12
11.13	12.354	1.224	19.4	0.063	0.937	0.063	0.937	0.067	68.2	273	341.2	7655.31
11.13	12.552	1.422	19.4	0.073	0.927	0.073	0.927	0.079	68.5	273	341.5	7203.88
11.13	12.751	1.621	19.4	0.084	0.916	0.084	0.916	0.091	68.8	273	341.8	6805.92
11.13	12.977	1.847	19.4	0.095	0.905	0.095	0.905	0.105	69.1	273	342.1	6404.62

11.13	13.226	2.096	19.4	0.108	0.892	0.108	0.892	0.121	69.4	273	342.4	6010.44
11.13	13.529	2.399	19.4	0.124	0.876	0.124	0.876	0.141	69.7	273	342.7	5580.65
11.13	13.854	2.724	19.4	0.140	0.860	0.140	0.860	0.163	70	273	343	5167.04
11.13	14.247	3.117	19.4	0.161	0.839	0.161	0.839	0.191	70.3	273	343.3	4719.52
11.13	14.631	3.501	19.4	0.180	0.820	0.180	0.820	0.220	70.6	273	343.6	4322.99
11.13	15.081	3.951	19.4	0.204	0.796	0.204	0.796	0.256	70.9	273	343.9	3899.17
11.13	15.559	4.429	19.4	0.228	0.772	0.228	0.772	0.296	71.2	273	344.2	3485.95
11.13	16.117	4.987	19.4	0.257	0.743	0.257	0.743	0.346	71.5	273	344.5	3039.84
11.13	16.695	5.565	19.4	0.287	0.713	0.287	0.713	0.402	71.8	273	344.8	2611.26
11.13	17.300	6.170	19.4	0.318	0.682	0.318	0.682	0.466	72.1	273	345.1	2188.64
11.13	17.938	6.808	19.4	0.351	0.649	0.351	0.649	0.541	72.4	273	345.4	1766.05
11.13	18.616	7.486	19.4	0.386	0.614	0.386	0.614	0.628	72.7	273	345.7	1335.45
11.13	19.333	8.203	19.4	0.423	0.577	0.423	0.577	0.733	73	273	346	895.23
11.13	20.067	8.937	19.4	0.461	0.539	0.461	0.539	0.854	73.3	273	346.3	454.10